Empirical Validations of Shading/Daylighting/Load Interactions in Building Energy Simulation Tools

A Report for the International Energy Agency's
SHC Task 34/ ECBCS Annex 43 Project C
August 2007

Written by
Peter Loutzenhiser and Heinrich Manz
Laboratory for Building Technologies
Swiss Federal Laboratories for Materials Testing and Research
and
Gregory Maxwell
Department of Mechanical Engineering
Iowa State University

EMPA
Materials Science & Technology

IOWA ENERGY CENTER

SHC
SOLAR HEATING & COOLING PROGRAMME
INTERNATIONAL ENERGY AGENCY

International Energy Agency
Energy Conservation in Buildings and Community Systems Programme

Using Contributions from

S. Carl, T. Frank, and R. Bundi
Laboratory for Building Technologies
Swiss Federal Laboratories for Materials Testing and Research

P. Strachan
Department of Mechanical Engineering
Strathclyde University

C. Felsmann
Institute of Thermodynamics and Building Systems Engineering
Technical University of Dresden

S. Moosberger and G. Zweifel
Department of Architecture and Technology
University of Applied Science of Central Switzerland

J. L'Hoest, P. Andre, and C. Adam
Department des Sciences et Gestion de l'Environnement
University of Liege

P. Oelhafen,G. Reber, and R. Steiner
Institut für Physik
Universität Basel

ACKNOWLEDGEMENTS

For the Swiss Federal Laboratories for Materials Testing and Research (EMPA) portion of the project, we would like to gratefully acknowledge the financial support of the Swiss Federal Office of Energy (BFE) for building the test facility and funding our participation in the International Energy Agency's (IEA) Task 34/Annex 43, especially M. Zimmerman, C. Filleux, and A. Eckmanns.

During the course of this project, many companies generously donated materials for this project, which included: Glas Trösch with the glazing unit, Griesser with the exterior shading screen and Venetian blind assembly, Nysan Shading Systems Inc. with the interior shading screen, and 4B Bachmann with the window.

Many thanks to our colleagues at EMPA, including: M. Amberg, B. Binder, R. Blessing, M. Camenzind, M. Christenson, K. Meyer, T. Nussbaumer, H. Simmler, and R. Vonbank, and our colleagues from IEA Task 34/Annex 43 including: J. Neymark, R. Judkoff, and P. Heiselberg for their help.

For the Energy Resource Station (ERS) portion of the project, we would like to gratefully acknowledge the financial support of the Iowa Energy Center under Grant 9608. We would also like to thank the people at the Wisconsin Energy Center for providing the windows and the people at Nysan Shading Systems Inc. for the shading screens. We would like to acknowledge Som Shrestha for his hard work designing and implemented the motorized blind controls. We would also like to recognize the staff at the ERS for their assistance in setting up and running these experiments. The people specifically involved in this endeavor included: C. Klaassen, D. Perry, X. Hui Zhou, and E. Kadic.

Finally, we would like to thank S. Vardeman and M. Morris from Iowa State University for their valuable direction in the formulating the statistical and sensitivity analyses.

PREFACE

This report is a product of a joint effort between International Energy Agency (IEA) Solar Heating and Cooling (SHC) and Energy Conservation in Buildings and Community Systems (ECBCS) Programmes. SHC monitors this work as Task 34 and ECBCS monitors this work as Annex 43. Ron Judkoff of the National Renewable Energy Laboratory (NREL) was the Operating Agent for IEA SHC 34/ECBCS 43 on behalf of the United States Department of Energy.

International Energy Agency

The International Energy Agency (IEA) was established in 1974 within the framework of the Organisation for Economic Co-operation and Development (OECD) to implement an international energy programme. A basic aim of the IEA is to foster co-operation among the twenty-four IEA participating countries and to increase energy security through energy conservation, development of alternative energy sources and energy research, development and demonstration (RD&D).

Solar Heating and Cooling Programme

The Solar Heating and Cooling Programme was one of the first IEA Implementing Agreements to be established. Since 1977, its members have been collaborating to advance active solar and passive solar technologies and their application in buildings and other areas, such as agriculture and industry. Current members are:

Australia	Finland	Portugal
Austria	France	Spain
Belgium	Italy	Sweden
Canada	Mexico	Switzerland
Denmark	Netherlands	United States
European Commission	New Zealand	
Germany	Norway	

A total of 39 Tasks have been initiated, 30 of which have been completed. Each Task is managed by an Operating Agent from one of the participating countries. Overall control of the program rests with an Executive Committee comprised of one representative from each contracting party to the Implementing Agreement. In addition to the Task work, a number of special activities—Memorandum of Understanding with solar thermal trade organizations, statistics collection and analysis, conferences and workshops—have been undertaken.

The Tasks of the IEA Solar Heating and Cooling Programme, both underway and completed are as follows:

Current Tasks:

Task 32	Advanced Storage Concepts for Solar and Low Energy Buildings
Task 33	Solar Heat for Industrial Processes
Task 34	Testing and Validation of Building Energy Simulation Tools
Task 35	PV/Thermal Solar Systems
Task 36	Solar Resource Knowledge Management
Task 37	Advanced Housing Renovation with Solar & Conservation
Task 38	Solar Assisted Cooling Systems
Task 39	Polymeric Materials for Solar Thermal Applications

Completed Tasks:

Task 1	Investigation of the Performance of Solar Heating and Cooling Systems
Task 2	Coordination of Solar Heating and Cooling R&D

Task 3	Performance Testing of Solar Collectors
Task 4	Development of an Insolation Handbook and Instrument Package
Task 5	Use of Existing Meteorological Information for Solar Energy Application
Task 6	Performance of Solar Systems Using Evacuated Collectors
Task 7	Central Solar Heating Plants with Seasonal Storage
Task 8	Passive and Hybrid Solar Low Energy Buildings
Task 9	Solar Radiation and Pyranometry Studies
Task 10	Solar Materials R&D
Task 11	Passive and Hybrid Solar Commercial Buildings
Task 12	Building Energy Analysis and Design Tools for Solar Applications
Task 13	Advance Solar Low Energy Buildings
Task 14	Advance Active Solar Energy Systems
Task 16	Photovoltaics in Buildings
Task 17	Measuring and Modeling Spectral Radiation
Task 18	Advanced Glazing and Associated Materials for Solar and Building Applications
Task 19	Solar Air Systems
Task 20	Solar Energy in Building Renovation
Task 21	Daylight in Buildings
Task 23	Optimization of Solar Energy Use in Large Buildings
Task 22	Building Energy Analysis Tools
Task 24	Solar Procurement
Task 25	Solar Assisted Air Conditioning of Buildings
Task 26	Solar Combisystems
Task 28	Solar Sustainable Housing
Task 27	Performance of Solar Facade Components
Task 29	Solar Crop Drying
Task 31	Daylighting Buildings in the 21st Century

Completed Working Groups:

CSHPSS, ISOLDE, Materials in Solar Thermal Collectors, and the Evaluation of Task 13 Houses

To find more IEA Solar Heating and Cooling Programme publications or learn about the Programme visit our Internet site at **www.iea-shc.org** or contact the SHC Executive Secretary, Pamela Murphy, e-mail: pmurphy@MorseAssociatesInc.com.

Energy Conservation in Buildings and Community Systems

Overall control of the program is maintained by an Executive Committee, which not only monitors existing projects but also identifies new areas where collaborative effort may be beneficial. To date the following projects have been initiated by the executive committee on Energy Conservation in Buildings and Community Systems (completed projects are identified by (*)):

Annex 1:	Load Energy Determination of Buildings (*)
Annex 2:	Ekistics and Advanced Community Energy Systems (*)
Annex 3:	Energy Conservation in Residential Buildings (*)
Annex 4:	Glasgow Commercial Building Monitoring (*)
Annex 5:	Air Infiltration and Ventilation Centre
Annex 6:	Energy Systems and Design of Communities (*)
Annex 7:	Local Government Energy Planning (*)
Annex 8:	Inhabitants Behaviour with Regard to Ventilation (*)
Annex 9:	Minimum Ventilation Rates (*)
Annex 10:	Building HVAC System Simulation (*)
Annex 11:	Energy Auditing (*)

Annex 12: Windows and Fenestration (*)
Annex 13: Energy Management in Hospitals (*)
Annex 14: Condensation and Energy (*)
Annex 15: Energy Efficiency in Schools (*)
Annex 16: BEMS 1- User Interfaces and System Integration (*)
Annex 17: BEMS 2- Evaluation and Emulation Techniques (*)
Annex 18: Demand Controlled Ventilation Systems (*)
Annex 19: Low Slope Roof Systems (*)
Annex 20: Air Flow Patterns within Buildings (*)
Annex 21: Thermal Modelling (*)
Annex 22: Energy Efficient Communities (*)
Annex 23: Multi Zone Air Flow Modelling (COMIS) (*)
Annex 24: Heat, Air and Moisture Transfer in Envelopes (*)
Annex 25: Real time HEVAC Simulation (*)
Annex 26: Energy Efficient Ventilation of Large Enclosures (*)
Annex 27: Evaluation and Demonstration of Domestic Ventilation Systems (*)
Annex 28: Low Energy Cooling Systems (*)
Annex 29: Daylight in Buildings (*)
Annex 30: Bringing Simulation to Application (*)
Annex 31: Energy-Related Environmental Impact of Buildings (*)
Annex 32: Integral Building Envelope Performance Assessment (*)
Annex 33: Advanced Local Energy Planning (*)
Annex 34: Computer-Aided Evaluation of HVAC System Performance (*)
Annex 35: Design of Energy Efficient Hybrid Ventilation (HYBVENT) (*)
Annex 36: Retrofitting of Educational Buildings (*)
Annex 37: Low Exergy Systems for Heating and Cooling of Buildings (LowEx) (*)
Annex 38: Solar Sustainable Housing (*)
Annex 39: High Performance Insulation Systems (*)
Annex 40: Building Commissioning to Improve Energy Performance (*)
Annex 41: Whole Building Heat, Air and Moisture Response (MOIST-ENG)
Annex 42: The Simulation of Building-Integrated Fuel Cell and Other Cogeneration Systems (FC+COGEN-SIM)
Annex 43: Testing and Validation of Building Energy Simulation Tools
Annex 44: Integrating Environmentally Responsive Elements in Buildings
Annex 45: Energy Efficient Electric Lighting for Buildings
Annex 46: Holistic Assessment Tool-kit on Energy Efficient Retrofit Measures for Government Buildings (EnERGo)
Annex 47: Cost-Effective Commissioning for Existing and Low Energy Buildings
Annex 48: Heat Pumping and Reversible Air Conditioning
Annex 49: Low Exergy Systems for High Performance Built Environments and Communities
Annex 50: Prefabricated Systems for Low Energy / High Comfort Building Renewal

Working Group - Energy Efficiency in Educational Buildings (*)
Working Group - Indicators of Energy Efficiency in Cold Climate Buildings (*)
Working Group - Annex 36 Extension: The Energy Concept Adviser (*)
(*) – Completed

Participating countries in ECBCS:

Australia, Belgium, CEC, Canada, Czech Republic, Denmark, Finland, France, Germany, Greece, Israel, Italy, Japan, the Netherlands, New Zealand, Norway, Poland, Portugal, Sweden, Switzerland, Turkey, United Kingdom and the United States of America.

SHC Task 34 / ECBCS Annex 43: Testing and Validation of Building Energy Simulation Tools

Goal and Objectives

The goal of this Task/Annex is to undertake pre-normative research to develop a comprehensive and integrated suite of building energy analysis tool tests involving analytical, comparative, and empirical methods. These methods will provide for quality assurance of software, and some of the methods will be enacted by codes and standards bodies to certify software used for showing compliance to building energy standards. This goal will be pursued by accomplishing the following objectives:

- Create and make widely available a comprehensive and integrated suite of IEA Building Energy Simulation Test (BESTEST) cases for evaluating, diagnosing, and correcting building energy simulation software. Tests will address modeling of the building thermal fabric and building mechanical equipment systems in the context of innovative low energy buildings.
- Maintain and expand as appropriate analytical solutions for building energy analysis tool evaluation.
- Create and make widely available high quality empirical validation data sets, including detailed and unambiguous documentation of the input data required for validating software, for a selected number of representative design conditions.

Scope

This Task/Annex investigates the availability and accuracy of building energy analysis tools and engineering models to evaluate the performance of innovative low-energy buildings. Innovative low-energy buildings attempt to be highly energy efficient through use of advanced energy-efficiency technologies or a combination of energy efficiency and solar energy technologies. To be useful in a practical sense such tools must also be capable of modeling conventional buildings. The scope of the Task is limited to building energy simulation tools, including emerging modular type tools, and to widely used innovative low-energy design concepts. Activities will include development of analytical, comparative and empirical methods for evaluating, diagnosing, and correcting errors in building energy simulation software.

The audience for the results of the Task/Annex is building energy simulation tool developers, and codes and standards (normes) organizations that need methods for certifying software. However, tool users, such as architects, engineers, energy consultants, product manufacturers, and building owners and managers, are the ultimate beneficiaries of the research, and will be informed through targeted reports and articles.

Means

The objectives are to be achieved by the Participants in the following Projects.

Comparative and Analytical Verification Tests:

Project A: Ground-Coupled Heat Transfer with respect to Floor Slab and Basement Constructions

Project B: Multi-Zone Buildings and Air Flow

Empirical Validation and Comparative Tests:
Project C: Shading/Daylighting/Load Interaction
Project D: Mechanical Equipment and Controls
Project E: Buildings with Double-Skin Facades
Other:
Project G: Web Site for Consolidation of Tool Evaluation Tests

Participants

The participants in the task are Australia, Belgium, Canada, Czech Republic, Denmark, France, Germany, Japan, the Netherlands, Spain, Sweden, Switzerland, the United Kingdom, and the United States. The United States served as the Operating Agent for this Task, with Ron Judkoff of the National Renewable Energy Laboratory providing Operating Agent services on behalf of the U.S. Department of Energy.

This report documents work carried out under Project C: Shading/Daylighting/Load Interaction

TABLE OF CONTENTS

LIST OF FIGURES

LIST OF TABLES

EXECUTIVE SUMMARY

Buildings with highly glazed façades are becoming increasingly popular around the world. Shading devices are vital components for preventing overheating in buildings during the summer and reducing and/or eliminating the need for active cooling. Building energy simulation programs are tools which can be used to predict and optimize energy performance in buildings. The integral approach, by which all relevant energy transport paths are simultaneously processed, makes these programs essential for designing modern buildings. However, successful application of a program requires careful and thorough validations. This is especially true when assessing solar gain and daylighting models. Even now, there are still very few high-quality data sets for empirical validation of solar gain and daylighting models currently available.

Therefore, the purpose of this project was to create data sets for use when evaluating the accuracies of models for glazing units and windows with and without shading devices. Program outputs were compared with experiments performed at two research facilities designed for these types of studies. The two facilities included: 1) an outdoor test cell located on the Swiss Federal Laboratories for Materials Testing and Research (EMPA) in Duebendorf, Switzerland and 2) the Energy Resource Station (ERS) located in Ankeny, Iowa USA.

A series of eight experiments that subsequently increased in complexity was performed in an outdoor test cell. The test cell was designed for calorimetric measurements and equipped with guard zones. The experimental series consisted of two characterization experiments and six experiments with solar gains.

Particular emphasis was placed on accurately determining the test cell characteristics. The first two experiments were run without solar gains to specify the thermophysical properties, including the thermal bridges, of the test cell. The first experiment was a steady-state experiment that was used in conjunction with a three-dimensional heat transfer simulation to quantify the thermal bridges. In the second experiment, the air temperature inside the test cell was allowed to float in response to a pseudo-random heat input. This experiment was simulated by seven building energy simulation programs and results from the programs were used to conclude that test cell specifications were very accurate for empirical validation.

Prior to the solar gain experiments, a preliminary exercise was performed to identify the most accurate tilted surface radiation model in each program. A series of experiments was then carried out to evaluate solar gain models in building energy simulation programs starting with the simplest case and increasing in complexity with each experiment. A solar selective glazing unit without shading, with external and internal diffuse shading screens, an external Venetian blind assembly, and internal mini-blind assembly were employed. A final experiment with a window (i.e. glazing unit with frame) was performed. Increasing the complexities of subsequent experiments allowed for careful assessments and diagnoses of the results. In these experiments, the heating/cooling powers in the test cell were adjusted to maintain a nearly constant test cell air temperature.

Robust experimental and sensitivity analyses were used to assess the impact of uncertainties of the measurands and program inputs. A set of comprehensive statistical parameters was employed to compare results of building energy simulation programs with the experiments applying 95% level of significance to determine whether the programs were validated or not. Up to seven programs were evaluated for each experiment, including: HELIOS, EnergyPlus, DOE-2.1E, ESP-r, TRNSYS-TUD, IDA-ICE, and TRNSYS-ULg. The impact of these validation exercises is already being realized. So far, several program errors and deficiencies in the programs have been identified with respect to solar radiation, glazing, shading, and surface heat transfer. These results also show that this is a high-quality data set.

Two additional experiments were performed at the ERS. For these studies, various windows and interior and exterior shading combinations were tested to evaluate daylighting algorithms and the associated interactions in building energy simulation tools and subsidiary software. Analyses were then performed to assess the overall performance of the programs. For this study, two building energy simulation programs were used, including: EnergyPlus and DOE-2.1E. Various

parameters were compared at the zone level, including: reheat coil power, airflow rate, air temperatures, daylight illuminance at the reference points, and light power.

These studies are believed to be some of the most detailed empirical validations of solar gain models implemented in building energy simulation programs ever performed. The authors' intention is that the data are widely used by program developers and modelers for future validation efforts.

CHAPTER 1: INTRODUCTION

The validation of building energy simulation programs is an important component in the development and refinement of models and algorithms implemented in the software. Numerous efforts within the framework of the International Energy Agency's (IEA) Solar Heating and Cooling (SHC) Tasks and Energy Conservation in Building Community Systems Annexes (ECBCS) have dealt with many facets of program validations. Judkoff [1] discusses the three different types of validation used in building energy simulation software which include: 1) analytical validation (comparing program results to an analytical solution), 2) comparative validation (program-to-program comparisons), and 3) empirical validation (comparing results with an actual experiment). Each of these validation methodologies has its own advantages and disadvantages. For analytical comparisons, the advantages include: no input uncertainty, exact truth standard, and inexpensive to perform; however, the primary disadvantage is that there are limited numbers of cases for which analytical solutions can be derived. The advantages for the comparative comparisons are that there are no input uncertainties, not limited to simple cases, and quick and inexpensive to perform. The primary disadvantage to these types of comparisons is that there is no truth standard. This research focuses on the third type of validation—empirical validation. The advantages of empirical validation include: an approximate truth standard within uncertainties in the instrumentation and data acquisition system and that there are no limitations due to the complexity of the cases. The disadvantages are that measurements involve some degree of experimental uncertainty, detailed high quality measurements are very expensive and time-consuming to perform, and there are a limited number of data sites where this is economically practical.

Empirical validations can be performed at various levels including: structure, systems and equipment, and whole building, which combines and integrates the first two levels of empirical validation into an additional level.

Building energy simulation programs are now being used by engineers and architects more than ever to simulate new highly glazed facades around the world. Therefore, robust empirical validations of solar gain and daylighting algorithms and the associated interactions are necessary endeavors to provide confidence that these programs simulate reality. Thus, the motivation for this study was to provide high-quality data sets and an evaluation methodology for empirical validation of solar gain and daylighting algorithms in building energy simulation programs and subsidiary software. The specific focus of this research was to assess the performance of various building energy simulation programs when modeling a glazing unit with and without various shading devices, windows, daylighting, and associated interactions; however, results from the experiments are now available for use in assessing the performance of future releases of current and future building energy simulation programs.

CHAPTER 2: EXPERIMENTS, VALIDATION EXERCISES, METHODOLOGY, AND PARTICIPANTS

A suite of experiments was performed in the Swiss Federal Laboratories for Materials Testing and Research (EMPA) outdoor test facility in Duebendorf, Switzerland (described in Chapter 3) that focused on evaluating solar gain modeling, and two experiments were performed at the Energy Resource Station (ERS) test facility in Ankeny, Iowa USA (Chapter 4) to evaluate daylighting models and associated zone interactions. Results from the experiments were used to carry out empirical validation exercises in building energy simulation programs. To assess the performance of the various building energy simulation programs and make detailed comparisons with the experiments, a methodology, factoring in experimental uncertainties in input and output parameters, was designed for evaluating program performances. Descriptions of the experiments, validation exercises, methodologies, and a list of participants are described in subsequent sections of this chapter.

2.1. EMPA Experiments

Eight experiments were performed for empirical validations of building energy software in conjunction with the IEA Task 34/Annex 34 Project C. The experiments were designed to start very simply and subsequently increase in complexity and are listed as:

1. steady-state test cell characterization,
2. transient test cell characterization,
3. glazing unit only,
4. glazing unit with an external shading screen,
5. glazing unit with an internal shading screen,
6. glazing unit with an external Venetian blind assembly,
7. glazing unit with an internal mini-blind assembly, and
8. window (glazing unit with a frame).

2.2. EMPA Validations Exercises

Eight validation exercises were performed that started simple and progressively increased in complexity and are listed below:

1. test cell transient characterization (Experiment 2),
2. evaluation of irradiation models on tilted facades (Experiment 3),
3. glazing unit only (Experiment 3),
4. glazing unit with external shading screen (Experiment 4),
5. glazing unit with internal shading screen (Experiment 5),
6. glazing unit with external Venetian blinds (Experiment 6),
7. glazing unit with internal mini-blinds (Experiment 7), and
8. window (i.e. glazing unit with a window frame) (Experiment 8).

After completion of the test cell characterization experiments (Experiments 1 and 2), subsequent tests used “constant” temperatures within the test cell and the guard zone. For all exercises except Exercise 2, measured hourly outer surface temperatures for the test cell construction element surfaces adjacent to the guard zone and internal loads were used as boundary conditions inputs to the programs.

Additionally, for the solar gain exercises (Exercises 3-8), measured weather data (in both hourly and sub-hourly increments depending on the capacities of the programs) and hourly average air temperatures inside the test cell were used as program inputs. The experiments were run during periods when there was no snow on the ground in order to accurately account for ground reflectance. Before each solar gain experiment, highly reflective insulation material was fixed over the outside of the glazing unit shown in Figure 2.1. This was accounted for in the weather data by

setting the irradiance values to zero for these hours. In comparisons between program predictions and experimental results of cooling power, the first 120 h were removed; so each period consisted of 480 h (20 days). Long periods of time were chosen to run the experiment to ensure diverse atmospheric conditions (both sunny and cloudy days).

Figure 2.1. Photograph of the test cell during the preconditioning phase.

2.3. ERS Experiments

Two experiments were performed at the ERS that assessed the performance of daylight algorithms implemented into building energy simulation programs. Exterior test rooms were used to investigate program performance with different window/shading combinations. A general layout of the facility showing the exterior test rooms is given in Figure 2.2.

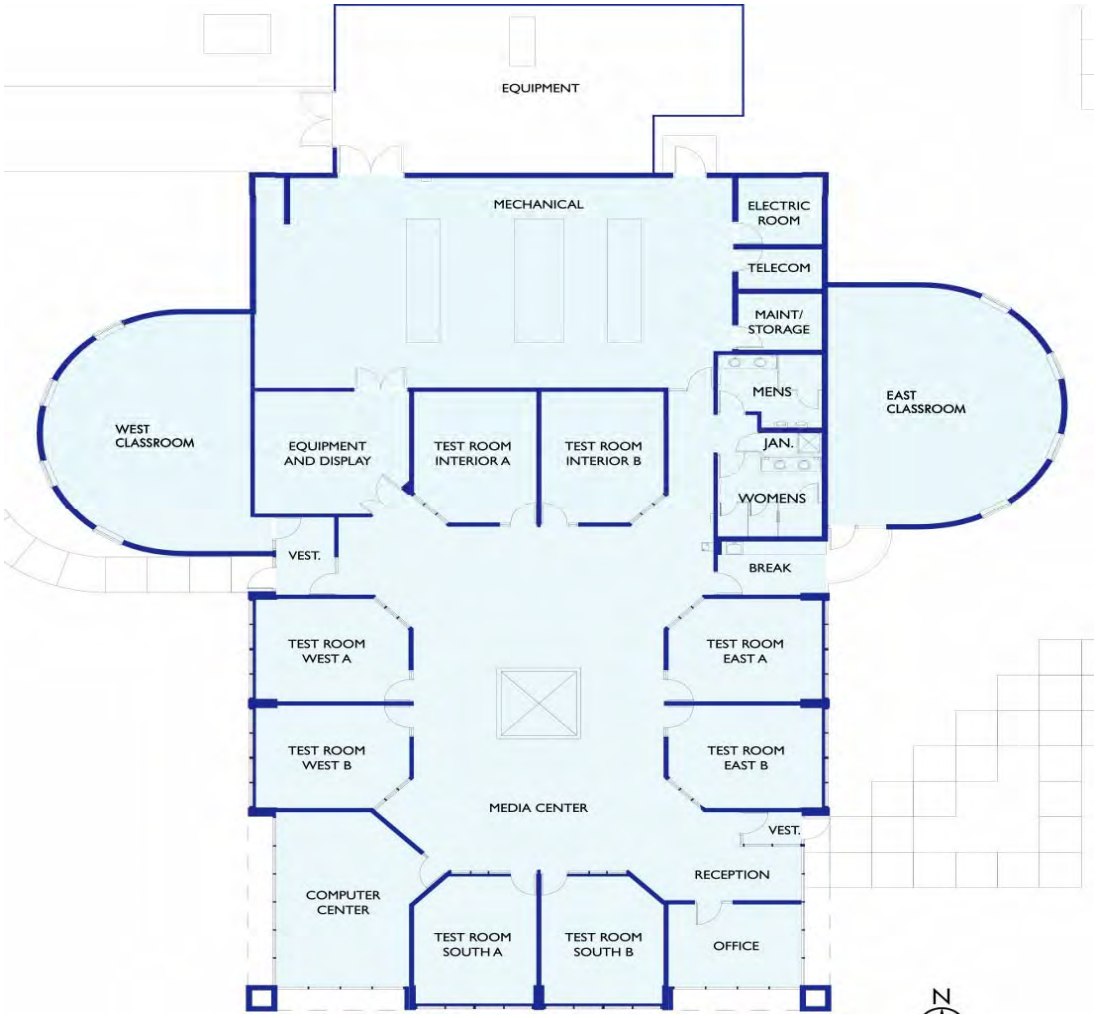

Figure 2.2. A floor plan of the Energy Resource Station.

The first experiment examined three types of windows in combination with three window shading devices. These experiments were performed in the exterior test rooms (Figure 2.2) and the various permutations of windows and shading devices are shown in Table 2.1. For the ERS validations, each experiment was used to perform a simulation exercise; therefore, no distinctions will be made between simulation exercises and experiments.

Table 2.1. ERS Test rooms shading and window configurations for Experiment 1.

Test Room	**Window Type**	**Interior Window Treatment**	**Exterior Window Treatment**
East A	25.2 mm Low-E#3 Glazing System	Motorized Mini-blinds	none
East B	25.2 mm Low-E#3 Glazing System	Fixed Slat Angle Horizontal Mini-blinds	none
South A	25.2 mm Clear Glass Glazing System	Nysan Shading Screens	none
South B	25.2 mm Clear Glass Glazing System	Fixed Slat Angle Horizontal Mini-blinds	none
West A	25.2 mm Low-E#2 Glazing System	Nysan Shading Screens	Exterior Fins
West B	25.2 mm Low-E#2 Glazing System	none	Exterior Fins

The second experiment used only two types of windows in combination with three window shading devices shown in Table 2.2.

Table 2.2. ERS Test rooms shading and window configurations for Experiment 2.

Test Room	Window Type	Interior Window Treatment	Exterior Window Treatment
East A	25.2 mm Low-E#3 Glazing System	Nysan Superweave 1000 (10% open) White Fabric	none
East B	25.2 mm Low-E#2 Glazing System	White Muslin Fabric	none
South A	25.2 mm Low-E#3 Glazing System	Nysan Superweave 1000 (10% open) White Fabric	Exterior Fins
South B	25.2 mm Low-E#2 Glazing System	White Muslin Fabric	Exterior Fins
West A	25.2 mm Low-E#3 Glazing System	Nysan Superweave 1000 (10% open) White Fabric	none
West B	25.2 mm Low-E#2 Glazing System	White Muslin Fabric	none

The results presented focused on comparisons in the exterior test rooms. The specific parameters compared were the zone reheat coil powers, zone temperatures, daylight illuminance at the reference point, and light powers. For consistency, all results were compared in hourly increments. More detailed information about the ERS testing facility is provided in Chapter 13.

2.4. Empirical Validation Methodology

A consistent methodology was used to compare the performances of each building energy simulation program for all experiments. In order to carefully evaluate each program, experimental uncertainties of output parameters and detailed sensitivity studies were conducted to quantify the impact of uncertainties in program input parameters propagating through the program and affecting prediction outputs. These uncertainties were evaluated at a 95% significance level and used as a guide for program validation. When the programs were within these overlapping 95% credible limits, they were considered validated. Figure 2.3 contains a flowchart diagramming the methodology.

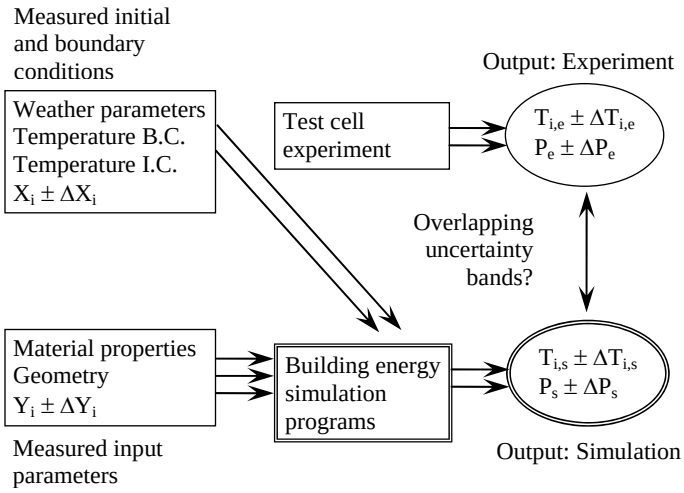

Figure 2.3. Methodology for empirical validation of building energy simulation programs.

Many simulators chose to use weather data that were in sub-hourly time intervals; however, all results were then provided and evaluated for 1 hour time intervals to provide consistent comparisons between different program outputs because hourly outputs were the smallest increments currently available for all of the programs. A number of different measures were used to quantify the observed relationships between measured and simulated results. These were based on the basic statistical summary measures: the sample mean, $\bar{x}$, the sample maximum, x_{max}, and minimum, x_{min}, values, and sample standard deviation, s.

To compare each simulation to the experiment, differences between experimental and corresponding simulated values, D_i (where the index i hour of the experiment), were first computed. The arithmetic mean, $\overline{D}$ and absolute maximum, $|D_{max}|$ and minimum, $|D_{min}|$ differences were then determined for each simulated quantity. Further, the average absolute difference, $\overline{|D|}$, was computed using Equation 2.1.

$$\overline{|D|} = \frac{1}{n}\sum_{i=1}^{n}|D_i| \tag{2.1}$$

This is one possible quantification of the overall magnitude of disagreement between the simulations and the experiment. Another is the root mean squared difference, D_{rms}, defined in Equation 2.2.

$$D_{rms} = \sqrt{\frac{1}{n}\sum_{i=1}^{n}D_i^2} \tag{2.2}$$

It is an algebraic fact that this quantity is related to the sample mean and sample standard deviation of differences by Equation 2.3.

$$D_{rms} = \sqrt{\frac{n-1}{n}S_D^2 + \overline{D}^2} \tag{2.3}$$

For additional comparisons, the 95% quantiles (the upper 5% points of the sample distributions) for the absolute differences, $|D|_{95\%}$, were computed for all simulations. Uncertainties associated with the average temperature calculated by summing the sample variance with the propagated error squared. The cooling power uncertainties were computed assuming Bayesian errors. Ninety-five percent credible limits were computed for all experiments at each hour, $OU_{i,Exp}$, and the average uncertainty, $\overline{OU}$, was reported in the summary tables under the experiment column. All of these calculations were performed neglecting time-series serial correlations (which could also impact the overall uncertainty).

Additional uncertainty analysis was performed in EnergyPlus, using a Monte Carlo Analysis (MCA) to quantify overall output uncertainty for the building energy simulation programs due to uncertainties in input parameters. Ninety-five percent credible limits $OU_{i,EnergyPlus}$, for each hour were also calculated and the mean quantity, $\overline{OU}$, are reported in the statistical analyses under the EnergyPlus column. N-way factorial analyses were also performed for each experiment to assess the sensitivity of all input uncertainties on the output. An in-depth description providing background information and implementation of the MCA and N-way factorial analysis (for the EMPA Experiments) in EnergyPlus is given by Loutzenhiser et al [2].

To compare the performance of the individual building energy simulation programs, the uncertainty ratio, UR_i, was devised to compare hourly differences with experimental and input errors and is shown in Equation 2.4. When the quantity is less than or equal to unity, the results were considered validated within 95% credible limits.

$$UR_i = \frac{|D_i|}{OU_{i,Exp} + OU_{i,EnergyPlus}} \tag{2.4}$$

For the ERS experiments, it was not possible to compare several of the parameters during certain times of the day (i.e. light power). Therefore, a criterion for evaluating the uncertainty ratio was implemented and described in a subsequent chapter. When employed, there were several parameters from the ERS experiments that used a truncated number of results from each array. The number of comparisons from each array, N, is also provided in the statistical analyses.

2.5. Participating Organizations and Simulation Tools

Numerous organizations performed the empirical validations at various levels using numerous building energy simulation programs. A list of participants in the EMPA and ERS studies are given

in Tables 2.3 and 2.4, respectively.

Table 2.3. List of participants, building energy simulation programs, and level of participation for the EMPA experiments.

Institution	Modeler(s)	Building Energy Simulation Program	Header Name	Level of Participation
EMPA	S. Carl and T. Frank	HELIOS	HELIOS	All exercises
EMPA/Iowa State University (ISU)	P. Loutzenhiser	EnergyPlus	EnergyPlus	All exercises
EMPA/Iowa State University (ISU)	P. Loutzenhiser	DOE-2.1E	DOE-2.1E	Exercises 1-5 and 8
Strathclyde University	P. Strachan	ESP-r	ESP-r	Exercises 1-5
Technical University of Dresden	C. Felsmann	TRNSYS-TUD	TRNSYS-TUD	Exercises 1-5
University of Applied Science of Central Switzerland (HTAL)	S. Moosberger and G. Zweifel	IDA-ICE	IDA-ICE	Exercises 1- 2
University of Applied Science of Central Switzerland (HTAL)	S. Moosberger and G. Zweifel	IDA-ICE with Parasol for a window model with a 1st parameter guess	IDA-PAR	Exercise 3
University of Applied Science of Central Switzerland (HTAL)	S. Moosberger and G. Zweifel	IDA-ICE with existing model and 2nd parameter guess	IDA-SIA	Exercises 3-5
University of Applied Science of Central Switzerland (HTAL)	S. Moosberger and G. Zweifel	IDA-ICE with a new window model	IDA-Detwind	Exercise 3 and 8
University of Liege (ULg)	Julien L'Hoest	TRNSYS	TRNSYS-ULg	All Exercises

Table 2.4. List of participants, building energy simulation programs, and level of participation for the ERS experiments.

Institution	Modeler(s)	Building Energy Simulation Program(s)	Level of Participation
ISU/EMPA	P. Loutzenhiser and G Maxwell	EnergyPlus	Both Exercises
ISU/EMPA	P. Loutzenhiser and G Maxwell	DOE-2.1E	Both Exercises

CHAPTER 3: EMPA FACILITY DESCRIPTION

The outdoor test facility is located on the EMPA campus in Duebendorf, Switzerland. The test facility is comprised of two identical test cells, where five of six faces in each test cell are adjacent to guard zones allowing for more precise determination of boundary conditions. The test cells and guard zones each have their own air conditioning unit. According to Strachan [3], test cells offer an economical and practical alternative between full-scale modeling of an actual building and the laboratory; test cell also provide the best environment for generating high-quality data sets for whole building empirical validations.

The air in the test cell was distributed near the floor by two textile ducts and extracted near the ceiling through metal ducts. Despite large air changes in the test cell, measurements taken near the wall with a hotwire anemometer revealed very small velocities. Air temperatures within the space were measured with 18 double shielding thermocouples, which divide the test cell into 18 equal parts for the solar gain experiments. An illustration of the test cell setup is shown in Figure 3.1.

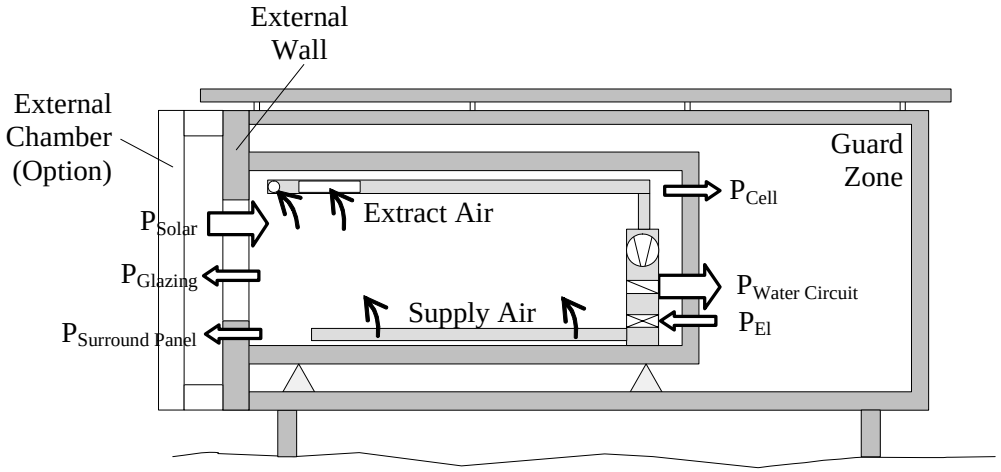

Figure 3.1. EMPA test cell schematic.

Additional characterizations of the test cell are described in this section, including:

- test cell location and dimension,
- thermal bridge quantification,
- thermal mass and air-tightness,
- thermophysical properties,
- sensors,
- ground reflectance, and
- explanation of experimental data.

3.1. Test Cell Location and Dimensions

The test cell is located on the EMPA campus in Duebendorf, Switzerland. Table 3.1 contains information regarding the global location, time zone, and orientation of the test cell.

Table 3.1. Location of the EMPA test cell.

Degrees of longitude	8.6° East
Degrees of latitude	47.7° North
Altitude above sea-level	430 m
Time Zone	Central European Time (GMT + 1 h)
Orientation of external wall	29° (south = 0°, west =90°)

The internal dimensions of the test cell are shown in Table 3.2.

Table 3.2. Dimensions of the test cell.

Internal height	2.360 m
Internal width	2.850 m
Internal length	4.626 m
Area of the north/south wall	6.726 m^2
Area of the east/west wall	10.917 m^2
Area of the floor/ceiling	13.184 m^2
Internal volume	31.114 m^3

3.2. Thermal Bridge Quantification

According to Moinard and Guyon [4], determining the overall thermal test cell characteristics is imperative for empirical validations. Thermal bridges are usually more important in test cells than in real buildings because the dimensions are smaller and conduction through the walls is the only heat loss mechanism. Therefore, the total thermal losses─including those at edges, door, sealing at external wall and intersections of pipes or flexes with the test cell envelope─were computed using TRISCO software [5]. This program allowed for a three dimensional steady-state analysis of heat transfer processes. For this exercise, a combined heat transfer coefficient was chosen that factored in radiation and convection. Equivalent thermal conductivities of cavities were calculated according to prEN ISO 10077-2 [6]. The final model of the test cell employed $5.6 \cdot 10^6$ nodes. The results of these simulations are shown in Figures 3.2a and 3.2b. The results in Figure 3.2a were generated for a 1 K temperature difference between the test cell air and the guard zone. High heat fluxes were seen at the sealing of the door and at the sealing between test cell and removable external wall. Figure 3.2c shows an image of the test cell taken by an infrared camera of the thermal bridges at the door. The picture was taken for a 20 K temperature difference between the test cell air and the guard zone.

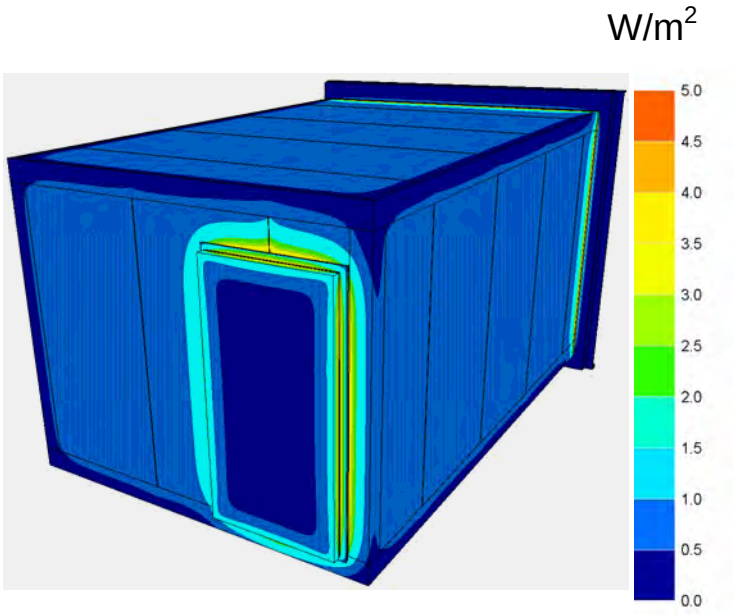

Figure 3.2a. Computed heat fluxes at the outer surfaces of the test cell.

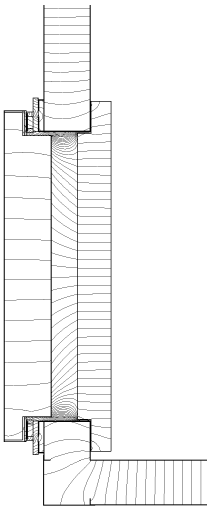

Figure 3.2b. Computed heat fluxes for a horizontal cross-section of the door.

Figure 3.2c. Infrared picture of the test cell door.

Table 3.3 contain the steady-state properties at for an inside air temperature at 20°C for the thermal transmittances. This parameter refers to the heat flow between the test cell air and the outer surface of the test cell envelope.

Table 3.3. Steady-state heat transfer characteristics of the test cell.

	Area m^2	One-dimensional thermal transmittance W/m^2-K	One-dimensional overall thermal transmittance W/K	Three-dimensional overall thermal transmittance (including edge effects and thermal bridges) W/K	Thermal bridges and edge effects W/K
Ceiling	13.184	0.155	2.040	3.170	1.130
North Wall	6.726	0.155	1.041	1.941	0.901
East Wall	6.726	0.258	1.733	1.850	0.117
South Wall	10.917	0.155	1.689	2.530	0.841
West Wall	10.917	0.155	1.689	2.491	0.802
Floor	13.184	0.147	1.935	3.180	1.245
Total			10.127	15.162	5.036

The thermal conductance from a TRISCO software simulation of the entire cell envelope (from inside the cell to the outer surfaces, including thermal bridges) at inside test cell air temperatures 0°C and 20°C (and guard zone temperatures of -1°C and 19°C, respectively) were calculated to be 13.539 W/K and 14.721 W/K, respectively.

The thermal conductance as a function of mean wall temperature for the guard zone and the

exterior wall are given in Equations 3.1 and 3.2, respectively.

Guard zone: $H_{GZ}(\theta) = 11.877 + 0.0534 \cdot \theta$ (W/K) (3.1)

Exterior wall: $H_{EW}(\theta) = 1.662 + 0.0057 \cdot \theta$ (W/K) (3.2)

where

θ is the mean wall temperature in °C.

A steady-state experiment (Experiment 1) was also performed and results were used to assess the computation of the thermal conductances from the 3-D simulation. An external chamber was mounted over the external facade of the test cell, and the boundary conditions were kept as close to constant values as possible. Two phases of the experiment with different sets of boundary conditions were performed. The steady-state time-averaged conditions for both phases of the experiment are given in Table 3.4. These calculations were performed using the mean wall temperatures for the exterior wall and guard zone of 36.6°C and 31.6°C, respectively. Applying an energy balance to the test cell for each phase of the experiment and solving both equations simultaneously resulted in overall thermal conductances for the construction elements adjacent to external chamber (external wall) and guard zones were 2.12 ± 0.59 W/K and 12.23 ± 0.53 W/K, respectively. A comparison between the overall thermal conductance from the steady-state experiment and the conductance computed from TRISCO as a function of temperatures (Equations 2.1 and 2.2) with uncertainties is shown in Figure 3.3.

Table 3.4. Steady-state experiment: time-averaged values and uncertainties for thermal conductance calculations.

	Test cell heat input	**Air temperature in the test cell**	**Temperature in the guarded zone**	**Temperature in the external chamber**
Phase 1	282.26 ± 4 W	43.13 ± 0.5°C	23.50 ± 0.5°C	23.24 ± 0.5°C
Phase 2	145.04 ± 3 W	36.45 ± 0.5°C	23.33 ± 0.5°C	43.74 ± 0.5°C

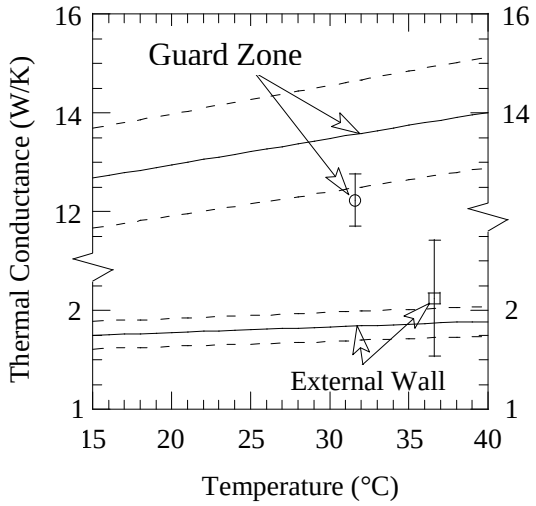

Figure 3.3. Comparison of thermal conductances of the external wall and guard zone as function of temperature found by simulation and the steady-state experiment.

3.3. Thermal Mass and Air-tightness

The internal mass of the technical equipment positioned in the test cell, which consisted of metallic ducts, grills, fans, a heat exchanger apparatus inside a metal casing, an electrical cabinet, etc. was estimated to be 200 KJ/K. Because the steel sheets were a major component in the thermal mass, the thermal response was assumed to be fast compared to the test cell envelope. The impact of this mass on the overall transient thermal behavior of the test cell was rather small.

To ensure the test cell was airtight, gaps between the steel sheets used for test cell construction were sealed with silicon. Two stage rubber seals were installed and the door and the external walls to eliminate air leaks. The infiltration was tested using the blower door method. When the test cell was pressurized to 50 Pa, the air exchange rate was found to be 0.2 h^{-1}. The assumption was then made that zone infiltration was negligible.

3.4. Thermophysical and Optical Properties

The thermophysical properties of the test cell were obtained from measurements, literature, product specification, a three dimensional whole test cell simulation, and a steady-state experiment used for overall thermal characterization of the test cell. Tables 3.5 to 3.7 show layer sequences, thicknesses and thermophysical properties for all layers of the test cell envelope. Layer Number 1 denotes the outside layer of the test cell. In the case of the thermal conductivity for the insulation and plywood layers, the quantities are based on a linear regression analysis calculated as a function of the average temperature of the material. Because not all building energy simulation programs can account for temperature-dependent thermophysical properties, the mean construction element temperature averaged over time was computed and, for each exercise requiring the modeling the test cell, temperature-dependent thermal conductivities were fixed accordingly.

Table 3.5. Layer properties of the ceiling, north (incl. door), east and west wall.

Layer number	Material	Thickness mm	Thermal conductivity W/m-K	Density kg/m^3	Specific heat J/kg-K
1	Sheet steel	0.7	53.62	7837	460.8
2	PU foam	138.6	$0.01921 + 0.000137 \cdot \theta$	30	1800
3	Sheet steel	0.7	53.62	7837	460.8

where θ is temperature in °C.

Table 3.6. Layer properties of the floor.

Layer number	Material	Thickness mm	Thermal conductivity W/m-K	Density kg/m^3	Specific heat J/kg-K
1	Sheet steel	0.7	53.62	7837	460.8
2	PU foam	140	$0.01921 + 0.000137 \cdot \theta$	30	1800
3	PU foam (higher density)	20	0.070	45	1800
4	Sheet steel with surface structure	2.5	53.62	7837	460.8

Table 3.7. Layer properties of the external wall.

Layer number	Material	Thickness Mm	Thermal conductivity W/m-K	Density kg/m^3	Specific heat J/kg-K
1	Plywood	10	$0.136359 + 0.000175 \cdot \theta$	850	1605
2	EPS foam	130	$0.03356 + 0.000127 \cdot \theta$	28	1460
3	Plywood	10	$0.136359 + 0.000175 \cdot \theta$	850	1605

The optical properties of the test cell surfaces were also measured and are shown in Table 3.8. The solar reflectance was computed according to European Standard EN 410 [7] using Glad Software [8], and the hemispherical emittance was measured with an emissometer based on a calorimetric method.

Table 3.8. Optical properties of test cell surfaces.

Surface element	Solar reflectance, %	Hemispherical emittance, %
Inner surfaces of walls and ceiling	75.7	92
Inner surface of floor	24.6	96
Outer / inner surfaces of south wall	76.6	93

3.5. Sensors

The sensors used in the test facility were periodically calibrated according an EMPA quality assurance system. Nearly 150 parameters were measured every six minutes (four minutes for Experiment 1 and 2). After each full hour, average values were computed from the last hour of data acquisition. Table 3.9 contains a list of all the metrological equipment and accuracies used at the facility. In Table 3.10, specifications for the most important parameters in the test cell and external chamber in the guard zone are shown and with their respective accuracies.

Table 3.9. Weather data parameters and equipment.

Parameter	Unit	Type of sensor / measurement	Number of sensors	Accuracy
Solar global irradiance, façade plane	W/m^2	Pyranometer (Kipp & Zonen CM 21)	1	± 2 %
Solar global horizontal irradiance	W/m^2	Pyranometer (Kipp & Zonen CM 21)	1	± 2 %
Solar diffuse horizontal irradiance	W/m^2	Pyranometer, mounted under the shading ball of a tracker (Kipp & Zonen CM 11)	1	± 3 %
Direct-normal irradiance	W/m^2	Pyrheliometer, mounted in an automatic sun-following tracker (Kipp & Zonen CH 1)	1	± 2 %
Infrared irradiance, façade plane	W/m^2	Pyrgeometers (Kipp & Zonen CG 4)	1	± 2 %
Outside air temperature, in front of façade	°C	Radiation shielded, mechanically ventilated thermocouples	2	± 0.5 K
Wind speed, in front of façade	m/s	Ultrasonic anemometer (WindMaster)	1	± 1.5 %
Horizontal illuminance	Lx	Luxmeter (Kipp & Zonen LuxLite, Minolta T-10W)	2	± 3 %
Pressure	hPa	Barometric Pressure Measuring Device (Vaisala PTA 427)	1	± 0.5 hPa
Relative humidity	%	Humidity Transmitter (Vaisala HMP 130Y Series)	1	± 1% (0-90%) ± 2% (90-100%)

Table 3.10. Parameters measured in the test cell, the external chamber and the guard zone and approximate accuracies according to manufacturer specifications.

Parameter	Unit	Type of sensor / measurement	Number of sensors	Accuracy
Air temperatures, inside test cell	°C	Thermocouple, radiation shielded by two cylinders	18	± 0.3 K
Air temperatures, in external chamber	°C	Thermocouple, radiation shielded by two cylinders	5	± 0.3 K
Air temperatures, in guard zone, 0.1 m in front of cell surface	°C	Thermocouple, radiation shielded by two cylinders	25	± 0.3 K
Surface temperatures, inner surface of cell envelope	°C	Thermocouple	30	± 0.3 K
Surface temperatures, outer surface of cell envelope	°C	Thermocouple	30	± 0.3 K
Heating power, inside test cell	W	Electric power (Infratek 106A)	1	± 0.1 %
Cooling power, inside test cell	W	Electromagnetic flowmeter (Endress+Hauser Promag 53H) and temperature difference measurement (PT100)	3	± 2 %
Illuminance, horizontal inside cell	Lux	Luxmeter (Minolta T-1H)	3	± 2 %

3.6. Ground Reflectance Measurement

Artificial green turf was installed in front of the test cell to represent a typical outdoor surface. Hemispherical-hemispherical reflectance at each wavelength was determined by using angular

dependent model for absorptance, $\alpha(\theta)$, [9] for incident angles between 0° and 80°, and a linear model between 80° and 90°. This piecewise function is shown in Equation 3.3. Equation 3.4 was used to calculate the hemispherical-hemispherical reflectance, ρ_{hem} [10]. This integral was evaluated numerically using Engineering Equation Solver [11]. Directional-hemispherical reflectance at a normal incident angle was measured. Solar reflectance was determined according to European Standard EN 410 [7] by means of GLAD software [8] and the directional-hemispherical reflectance at a normal angle of incidence is provided in Table 3.11. A photograph of the artificial turf is shown in Figure 3.4. The specular components of the reflectance were measured at Basel University by Professor Peter Oelhafen and his research group for incident angles of 20°, 40°, and 60° and found to be less than 1%; therefore the surface was considered a Lambert surface [9].

$$\frac{\alpha(\theta)}{\alpha_n} = \begin{cases} 1 + 2.0345\times10^{-3}\theta - 1.99\times10^{-4}\theta^2 + 5.324\times10^{-6}\theta^3 - 4.799\times10^{-8}\theta^4 & 0^\circ \le \theta \le 80^\circ \\ -0.064\theta + 5.76 & 80^\circ \le \theta \le 90^\circ \end{cases} \quad (3.3)$$

where

θ is the angle of incidence in ° and
α_n is the normal absorptance.

$$\rho_{hem} = 2\int_0^{90} (1-\alpha(\theta))\sin(\theta)\cos(\theta)d\theta \quad (3.4)$$

Table 3.11. Ground reflectance.

	Hemispherical reflectance, %	Normal incident reflectance, %
Solar	14.8	8.8

3.7. Explanation of Experimental Data

The purpose of this series of experiments was to provide a well-documented description of the experiments and experimental data inputs and outputs that could be used to empirically validate building energy simulation programs. A description of the experiments and results from many building energy simulation programs are described in subsequent chapters of this report. However, the required inputs for simulating the exercises and the outputs used for comparisons are contained in Excel files that are described in Appendix A; the combined results and data from this report can be extremely useful for developers and modelers wishing to validate their own building energy simulation programs.

CHAPTER 4: EMPA TRANSIENT CHARACTERIZATION EXPERIMENT (EXERCISE 1)

An experiment designed to evaluate the transient characteristics of the test cell was performed. Details concerning the test cell, thermophysical properties, experimental setup, and results are provided.

4.1. Test Cell

An external chamber (Figure 4.1a) was mounted over the exterior wall with no window (Figure 4.1b) for climate control. The air temperatures in the guard zone and the external chamber were maintained near 23°C, and the air inside the guarded cell was re-circulated and stirred to reduce thermal stratification. During the test, the re-circulating fans operated constantly and added an internal heat load of ~77 W. After an initial preconditioning phase of 50 hours, a pseudo-random heat source of ~196 W was turned on and off to provide an additional internal load. The heat source was located inside the test cell's re-circulation/conditioning apparatus and can, therefore, be considered purely convective.

Figure 4.1a. Photograph of test toom with external chamber.

Figure 4.1b. Outdoor test facility with removable façade element.

4.2. Thermophysical Properties

Temperature-dependent thermophysical properties were evaluated at the mean temperature of the construction elements averaged over time for the entire experiment; the mean temperature was computed as 28.38°C. Tables 4.1a to 4.1c contain fixed thermophysical properties for each construction element.

Table 4.1a. Ceiling, north, east and west wall construction evaluated at 28.38°C.

Layer number	Material	Thickness mm	Thermal conductivity W/m-K	Density kg/m^3	Specific heat J/kg-K
1	Sheet steel	0.7	53.62	7837	460.8
2	PU foam	139	0.023098	30	1800
3	Sheet steel	0.7	53.62	7837	460.8

Table 4.1b. Floor construction evaluated at 28.38°C.

Layer number	Material	Thickness mm	Thermal conductivity W/m-K	Density kg/m^3	Specific heat J/kg-K
1	Sheet steel	0.7	53.62	7837	460.8
2	PU foam	140	0.023098	30	1800
3	PU foam (higher density)	20	0.070	45	1800
4	Sheet steel with surface structure	2.5	53.62	7837	460.8

Table 4.1c. South wall construction evaluated at 28.38°C.

Layer number	Material	Thickness mm	Thermal conductivity W/m-K	Density kg/m^3	Specific heat J/kg-K
1	Plywood	10	0.14133	850	1605
2	EPS foam	130	0.03716	28	1460
3	Plywood	10	0.14133	850	1605

4.3. Experimental Setup

Hourly averaged values (where 1 corresponds to a time from 0:00 to 1:00) for the measured mean surface temperatures (boundary conditions), test cell air temperatures and internal loads were used as inputs to the building energy simulation programs. Figure 4.2 shows the locations of the temperature sensors in test cell. Additional double-shielded thermocouples were added for subsequent experiments.

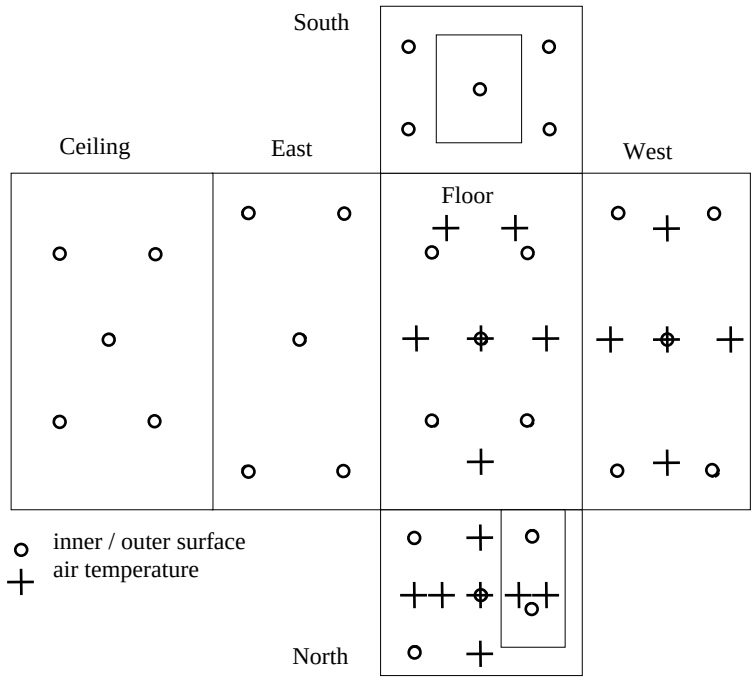

Figure 4.2. Location of temperature sensors.

Figure 4.3 contains a plot of the results for the experiment. Included in the plot are the mean test cell air temperature, mean surface temperatures, and the additional internal load introduced into the space.

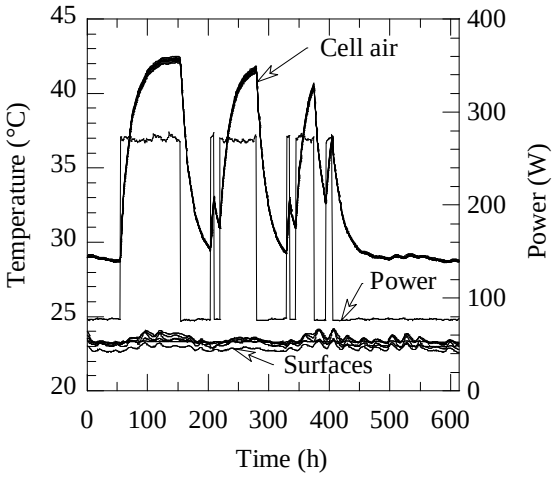

Figure 4.3. Measured pseudo-random heating power and temperatures.

4.4. Results

Test cell air temperature comparisons from the experiment and each building energy simulation program are contained in this section as well as the results from a comprehensive set of statistical analysis.

The measured and predicted test cell air temperatures from HELIOS, EnergyPlus, DOE-2.1E, ESP-r, TRNSYS-TUD, IDA-ICE, and TRNSYS-ULg are shown in Figures 4.4a to 4.4g, respectively. Other parameters used for diagnostic purposes that were not included were convective heat transfer coefficients and inner surface temperatures for all construction elements.

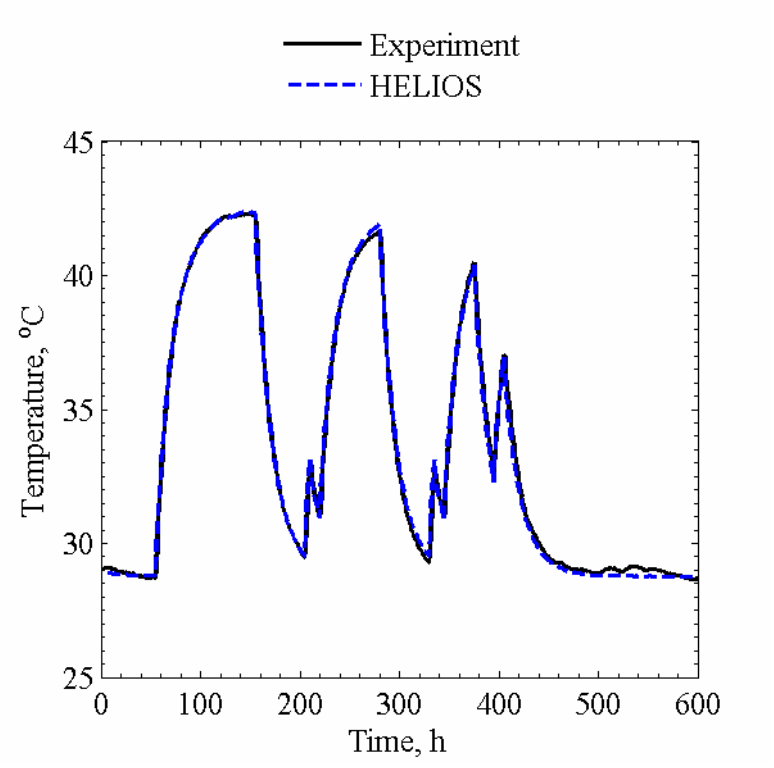

Figures 4.4a. Test cell air temperature comparisons for HELIOS.

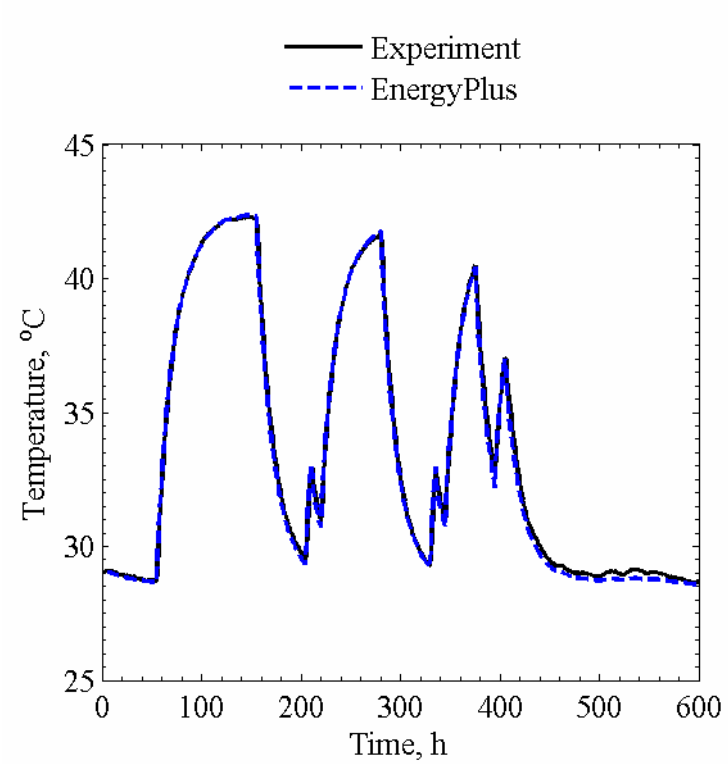

Figures 4.4b. Test cell air temperature comparisons for EnergyPlus.

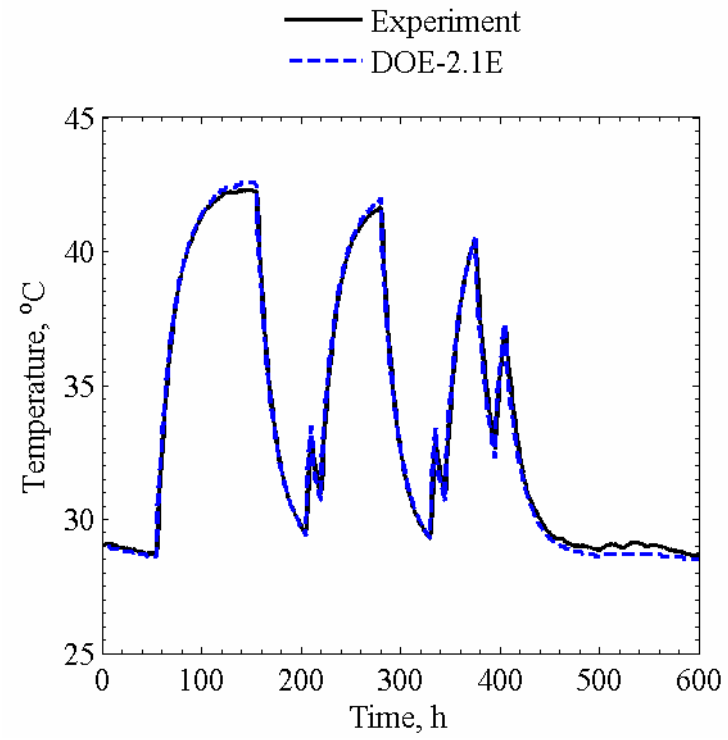

Figures 4.4c. Test cell air temperature comparisons for DOE-2.1E.

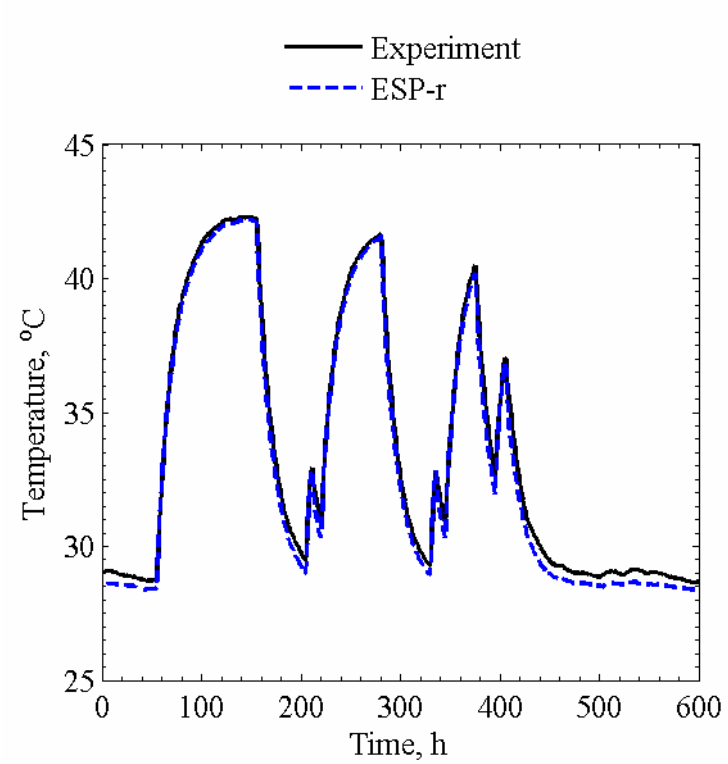

Figures 4.4d. Test cell air temperature comparisons for ESP-r.

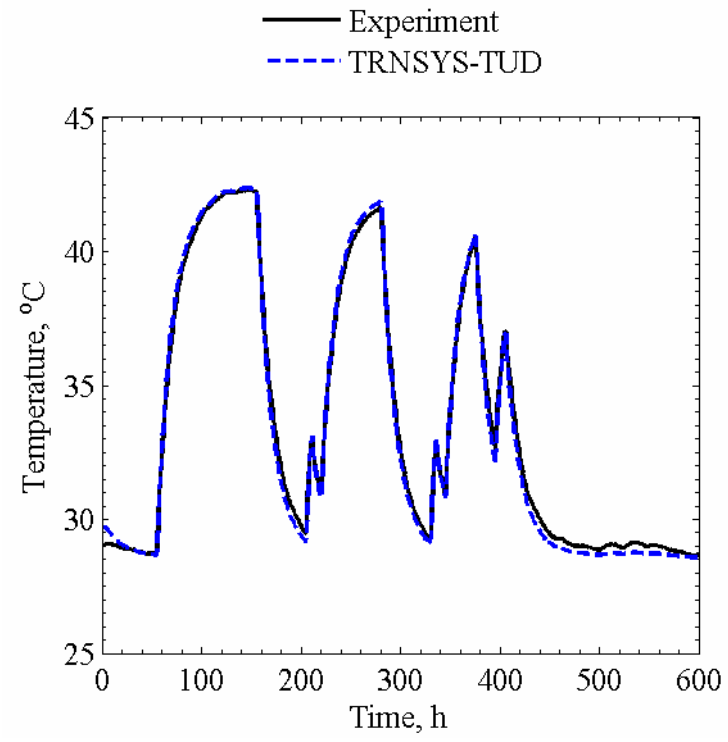

Figures 4.4e. Test cell air temperature comparisons for TRNSYS-TUD.

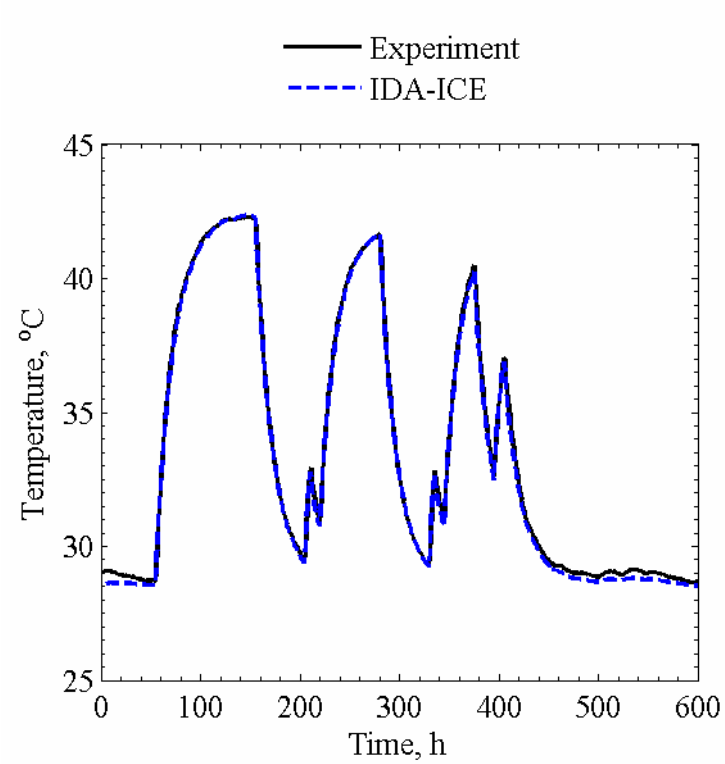

Figures 4.4f. Test cell air temperature comparisons for IDA-ICE.

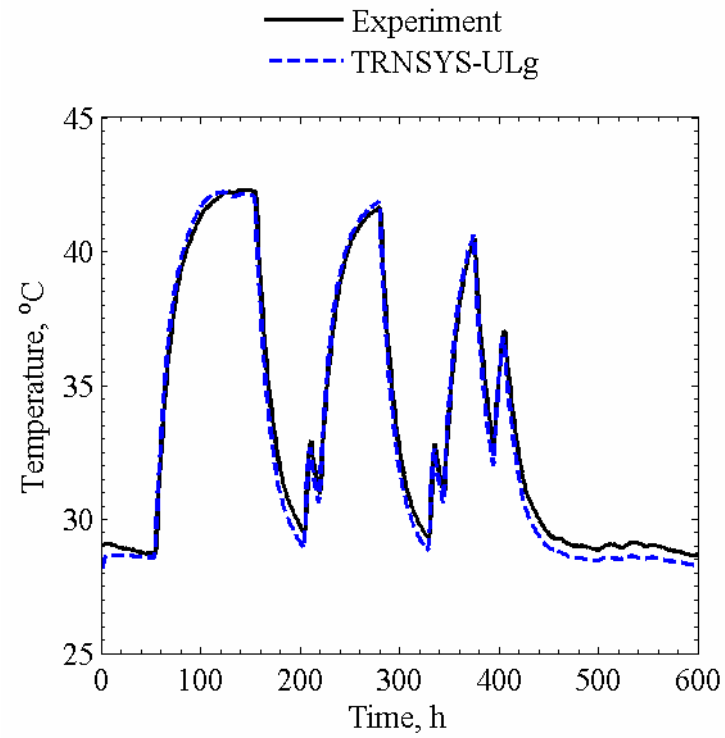

Figures 4.4g. Test cell air temperature comparisons for TRNSYS-ULg.

The MCA was performed in EnergyPlus for all hours of the experiment along with an assessment of experimental uncertainties for the test cell air temperatures. The hourly 95% credible limits for MCA, experiment, and sum are shown in Figure 4.5. An n-way factorial analysis was used to assess the sensitivity of the output test cell air temperature to uncertainties of input parameters. The 10 most influential parameters averaged over the experiment that impacted the predicted air temperatures are shown in Table 4.2; these results include n-way factorial analysis for

both forward and backward differencing. Statistical comparisons were performed employing the methodology described in Chapter 2 for all programs, and the results are displayed in Table 4.3.

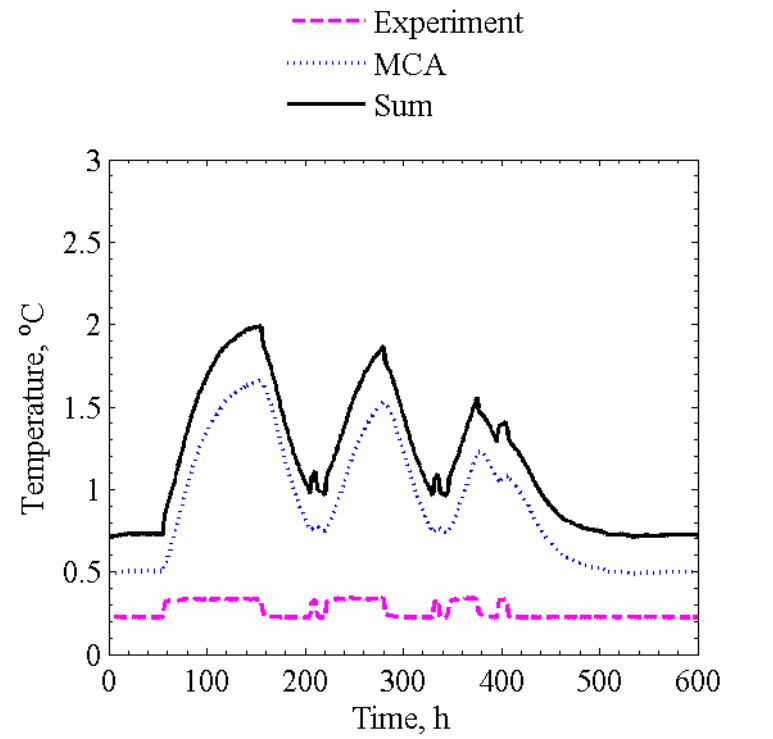

Figure 4.5. Experimental uncertainty, uncertainty of simulation results due to uncertainty in input parameters and total uncertainty.

Table 4.2. Average overall uncertainty and 10 most influential parameter uncertainties that impacted the cell air temperature predictions in K.

Parameter	Forward	Backward
Overall uncertainty	0.454	0.481
Thermal bridge	-0.321	0.344
PU foam conductivity	-0.269	0.287
PU foam floor conductivity	-0.075	0.077
South wall surface temperature	0.057	-0.057
Ceiling surface temperature	0.055	-0.055
Floor surface temperature	0.053	-0.053
West wall surface temperature	0.046	-0.046
East wall surface temperature	0.046	-0.046
North wall surface temperature	0.044	-0.044
EPS foam conductivity	-0.042	0.043

Table 4.3. Statistical analysis for the test cell air temperature.

Parameter	Experiment	HELIOS	EnergyPlus	DOE-2.1E	ESP-r	TRNSYS-TUD	IDA-ICE	TRNSYS-Ulg
$\bar{x}$	33.5 °C	33.5 °C	33.4 °C	33.5 °C	33.2 °C	33.4 °C	33.4 °C	33.3 °C
s	4.9 K	4.9 K	4.9 K	5.0 K	5.0 K	5.0 K	4.9 K	5.1 K
x_{max}	42.3 °C	42.4 °C	42.4 °C	42.6 °C	42.2 °C	42.4 °C	42.4 °C	42.2 °C
x_{min}	28.7 °C	28.7 °C	28.6 °C	28.5 °C	28.4 °C	28.6 °C	28.5 °C	28.0 °C
$\overline{D}$	-	0.0 K	0.1 K	0.1 K	0.4 K	0.1 K	0.1 K	0.3 K
$\overline{\lvert D \rvert}$	-	0.2 K	0.2 K	0.3 K	0.4 K	0.2 K	0.2 K	0.5 K
$\lvert D_{max} \rvert$	-	1.0 K	0.7 K	1.2 K	0.9 K	0.7 K	0.6 K	1.1 K
$\lvert D_{min} \rvert$	-	0.0 K	0.0 K	0.0 K	0.0 K	0.0 K	0.0 K	0.0 K
D_{rms}	-	0.2 K	0.2 K	0.3 K	0.4 K	0.3 K	0.2 K	0.5 K
$\lvert D \rvert_{95\%}$	-	0.5 K	0.5 K	0.7 K	0.7 K	0.5 K	0.4 K	0.9 K
$\overline{OU}$	0.3 K	-	0.9 K	-	-	-	-	-
$\overline{UR}$	-	0.2	0.2	0.2	0.4	0.2	0.2	0.4
UR_{max}	-	1.1	0.8	1.4	0.7	0.9	0.7	1.4
UR_{min}	-	0.0	0.0	0.0	0.0	0.0	0.0	0.0
$\overline{\lvert D \rvert} / \bar{x} \times 100\%$	-	0.5%	0.5%	0.8%	1.1%	0.7%	0.5%	1.4%
$\overline{D} / \bar{x} \times 100\%$	-	0.1%	0.4%	0.2%	1.1%	0.3%	0.4%	0.8%

Based on these results, the conclusion was reached that the thermal bridges and thermophysical and optical properties in the test cell were well-described; these results provided a foundation for proceeding to experiments in this test cell that focused on the impact of solar gains with and without shading devices. Further analysis and discussion of the experiment and results is provided by Manz et al. [12].

CHAPTER 5: EMPA EVALUATION OF IRRADIATION MODELS ON TILTED FACADES (EXERCISE 2)

In preparation for the solar gain experiments, a preliminary exercise was designed to ascertain the accuracies of tilted surface radiation models from each building energy simulation. The experiment was performed from October 2 to October 26, 2004 at the EMPA outdoor test cell; the purpose of this exercise was to take two of three radiation measurement (direct-normal irradiance, diffuse irradiance, or global horizontal irradiance) along with the measured ground reflectance (quantified in Chapter 3) and predict the incident radiation (or global vertical irradiance) on the southwest façade.

The validation for this exercise focused on comparing measured global vertical solar irradiance on the exterior façade with predictions from each building energy simulation program. An assessment of the three components of solar irradiance (direct-normal, global horizontal, and diffuse horizontal) and the formulation of the various titled radiation models are described by Loutzenhiser et al. [2]. Plots for measured and prediction global vertical irradiance on the vertical façade are listed with corresponding figures as:

- HELIOS Perez 1987 (Figure 5.1a),
- EnergyPlus Perez 1990 (Figure 5.1b),
- DOE-2.1E Perez 1990 (Figure 5.1c),
- ESP-r Isotropic (Figure 5.1d),
- ESP-r Klucher (Figure 5.1e),
- ESP-R Muneer (Figure 5.1f),
- ESP-r Perez 1987 (Figure 5.1g),
- ESP-r Perez 1990 (Figure 5.1h),
- TRNSYS-TUD Hay Davies (Figure 5.1i),
- TRNSYS-TUD Isotropic (Figure 5.1j),
- TRNSYS-TUD Perez 1990 (Figure 5.1k),
- TRNSYS-TUD Reindl (Figure 5.1l),
- IDA-ICE Perez 1990 (Figure 5.1m),
- TRNSYS-Ulg Hay Davies (Figure 5.1n),
- TRNSYS-Ulg Isotropic (Figure 5.1o),
- TRNSYS-Ulg Perez 1990 (Figure 5.1p), and
- TRNSYS-Ulg Reindl (Figure 5.1q).

Each figure contains two plots; the plot on the left are measurements of the vertical solar irradiance on the outside facade compared with predicted results from the building energy simulation program and 95% credible limits from both the experiment and the MCA, all averaged over each hour of the day for the duration of the experiment. The plot on the right contains maximum, minimum, and mean absolute differences between measured and predicted global vertical solar irradiances for a given hour of the day over the entire experiment. The same type of plot was used for comparing cooling powers for the solar gain experiments discussed in subsequent chapters.

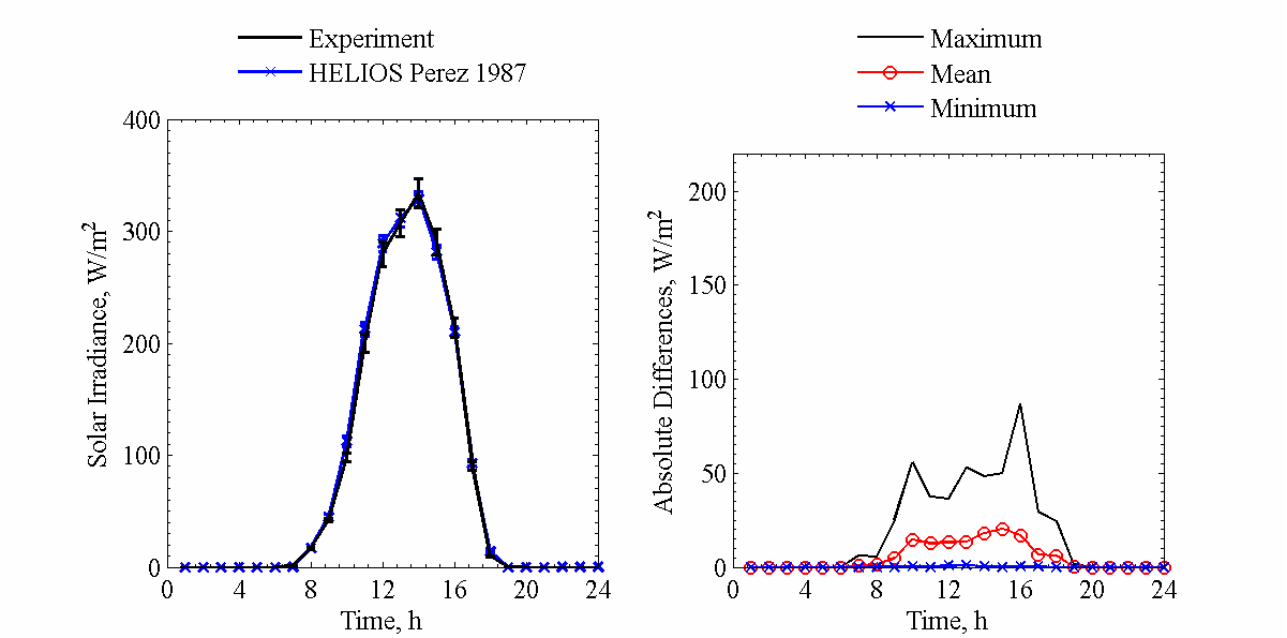

Figure 5.1a. Global vertical solar irradiance comparisons for HELIOS Perez 1987 averaged over each given hour of the day (left) and absolute maximum, mean, and minimum differences for a given hour of the day (right).

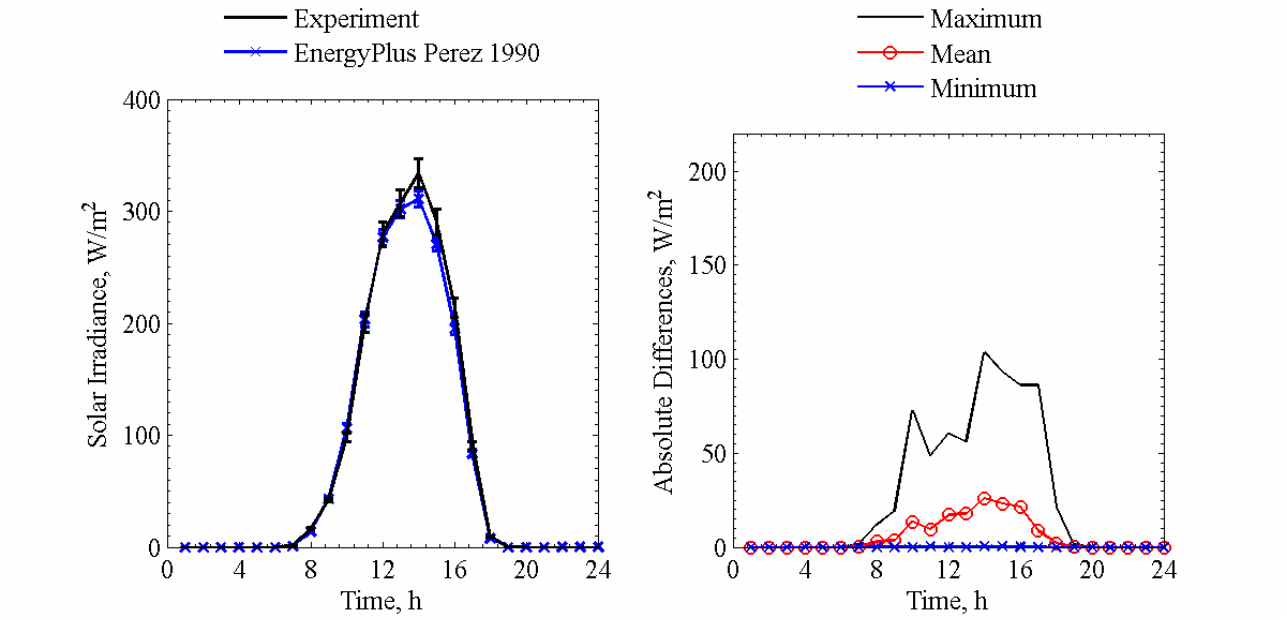

Figure 5.1b. Global vertical solar irradiance comparisons for EnergyPlus Perez 1990 averaged over each given hour of the day (left) and absolute maximum, mean, and minimum differences for a given hour of the day (right).

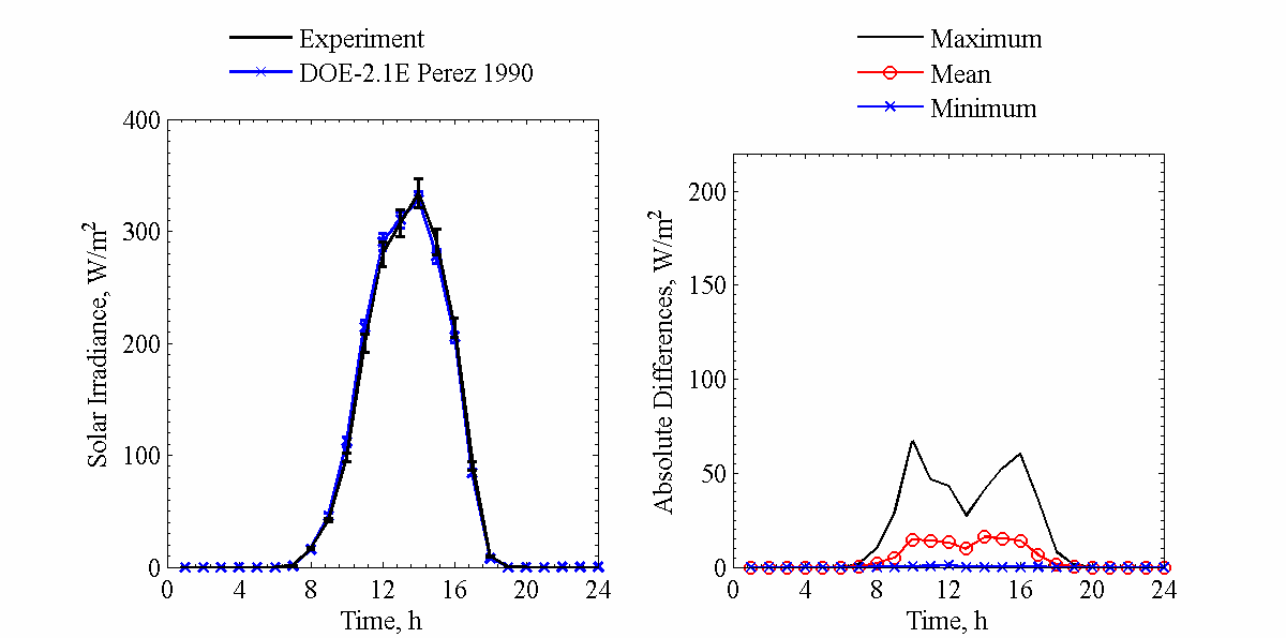

Figure 5.1c. Global vertical solar irradiance comparisons for DOE-2.1E Perez 1990 averaged over each given hour of the day (left) and absolute maximum, mean, and minimum differences for a given hour of the day (right).

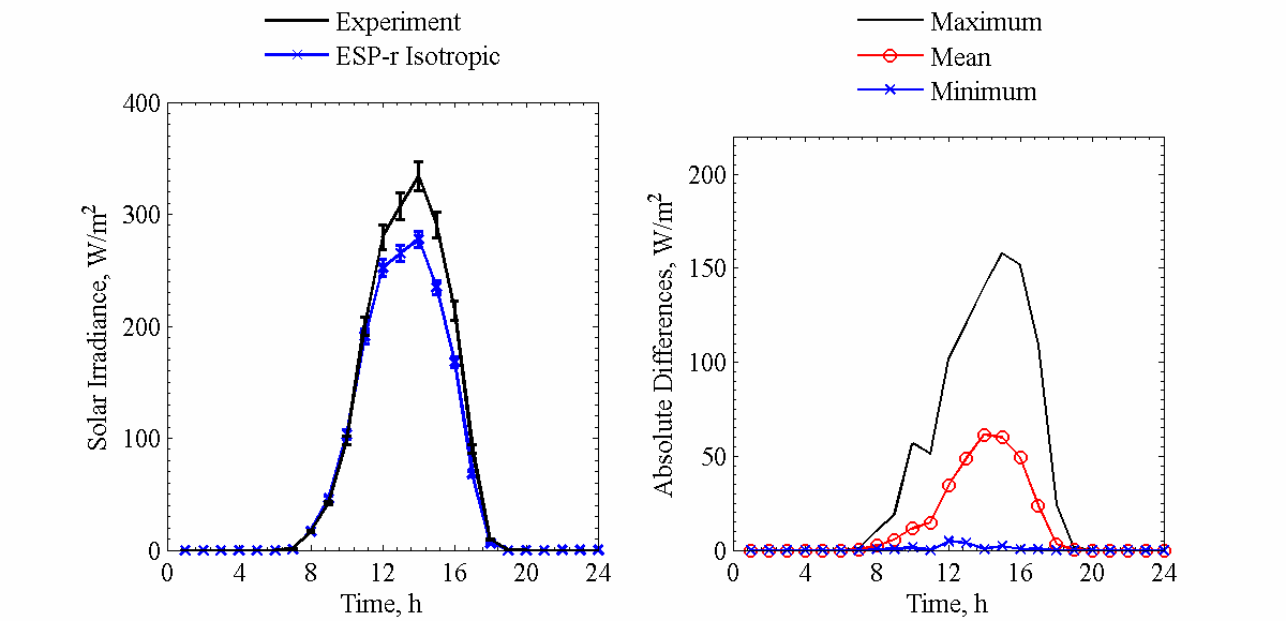

Figure 5.1d. Global vertical solar irradiance comparisons for ESP-r Isotropic averaged over each given hour of the day (left) and absolute maximum, mean, and minimum differences for a given hour of the day (right).

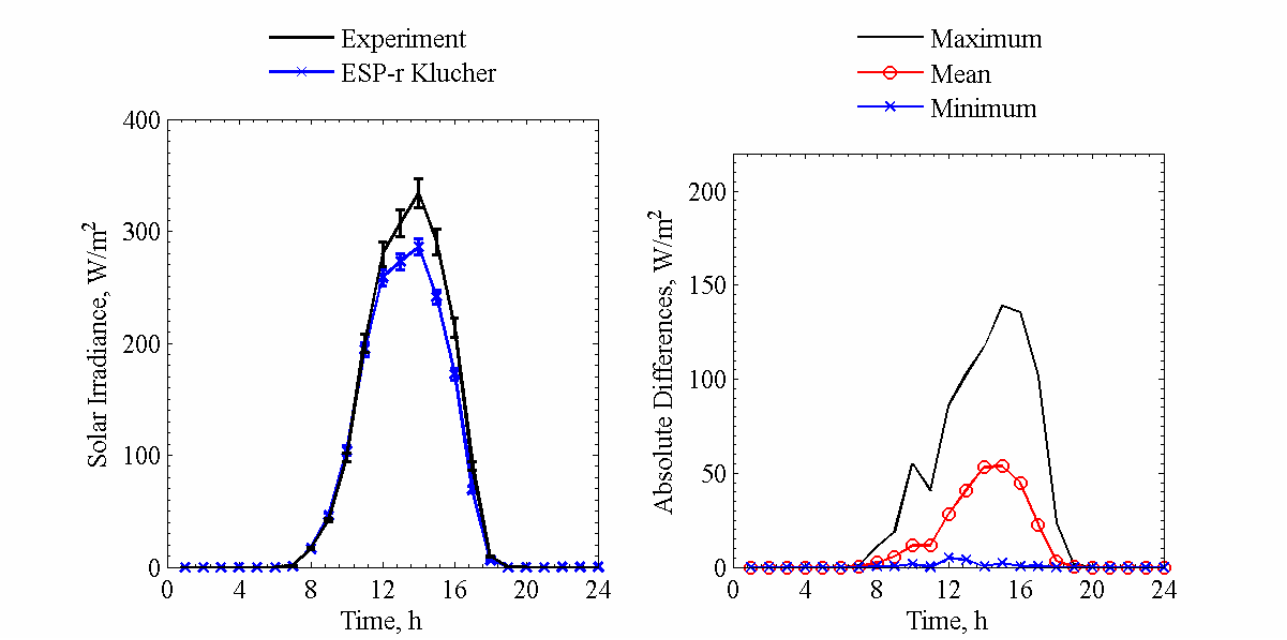

Figure 5.1e. Global vertical solar irradiance comparisons for ESP-r Klucher averaged over each given hour of the day (left) and absolute maximum, mean, and minimum differences for a given hour of the day (right).

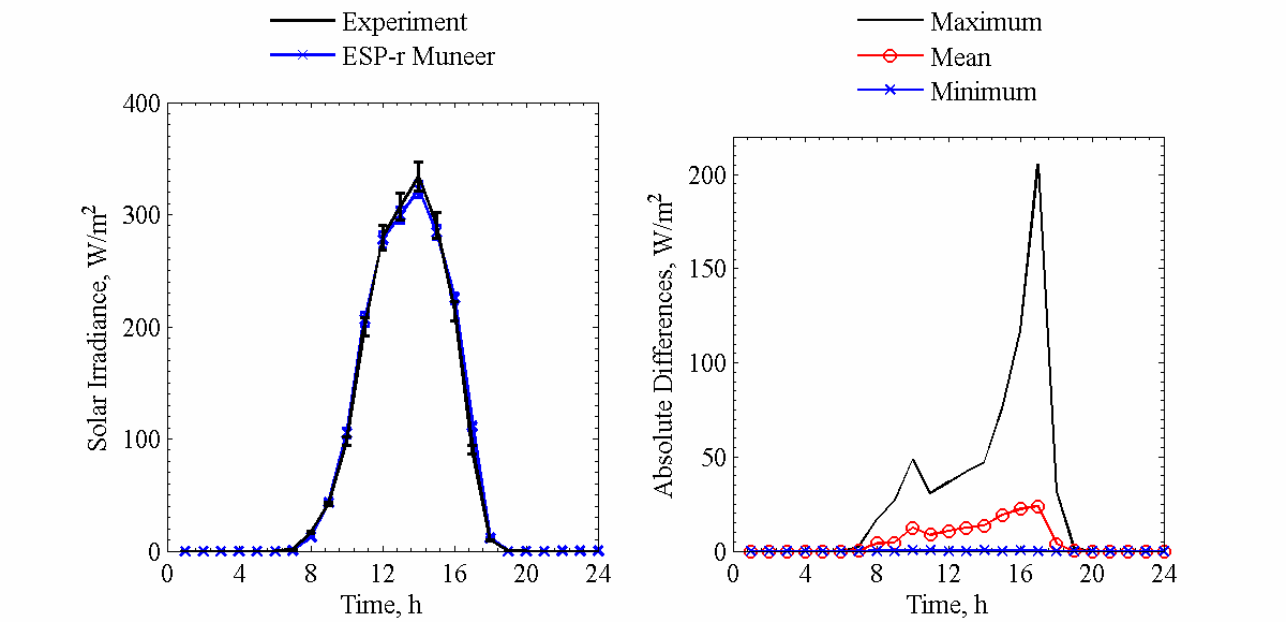

Figure 5.1f. Global vertical solar irradiance comparisons for ESP-r Muneer averaged over each given hour of the day (left) and absolute maximum, mean, and minimum differences for a given hour of the day (right).

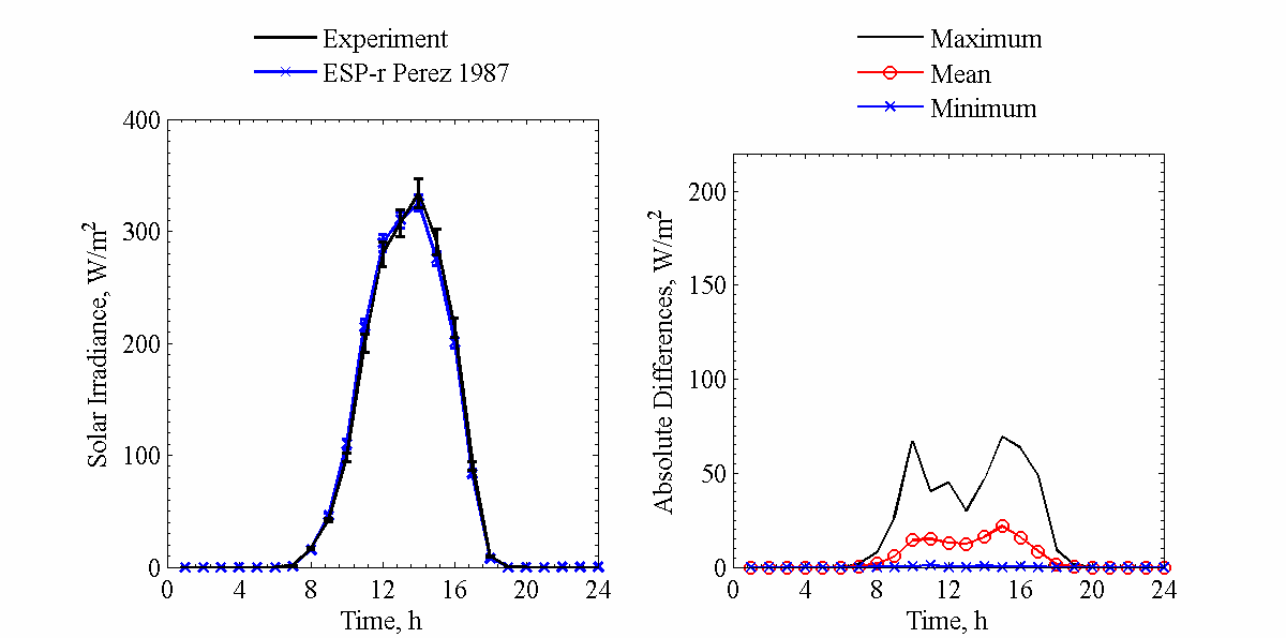

Figure 5.1g. Global vertical solar irradiance comparisons for ESP-r Perez 1987 averaged over each given hour of the day (left) and absolute maximum, mean, and minimum differences for a given hour of the day (right).

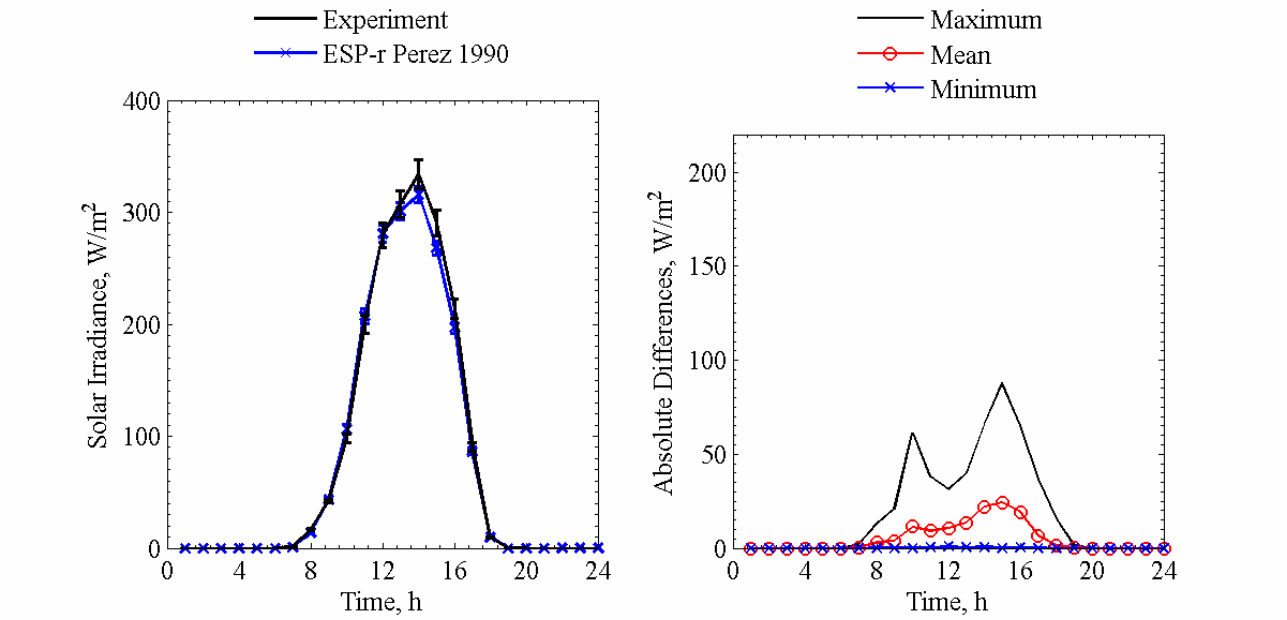

Figure 5.1h. Global vertical solar irradiance comparisons for ESP-r Perez 1990 averaged over each given hour of the day (left) and absolute maximum, mean, and minimum differences for a given hour of the day (right).

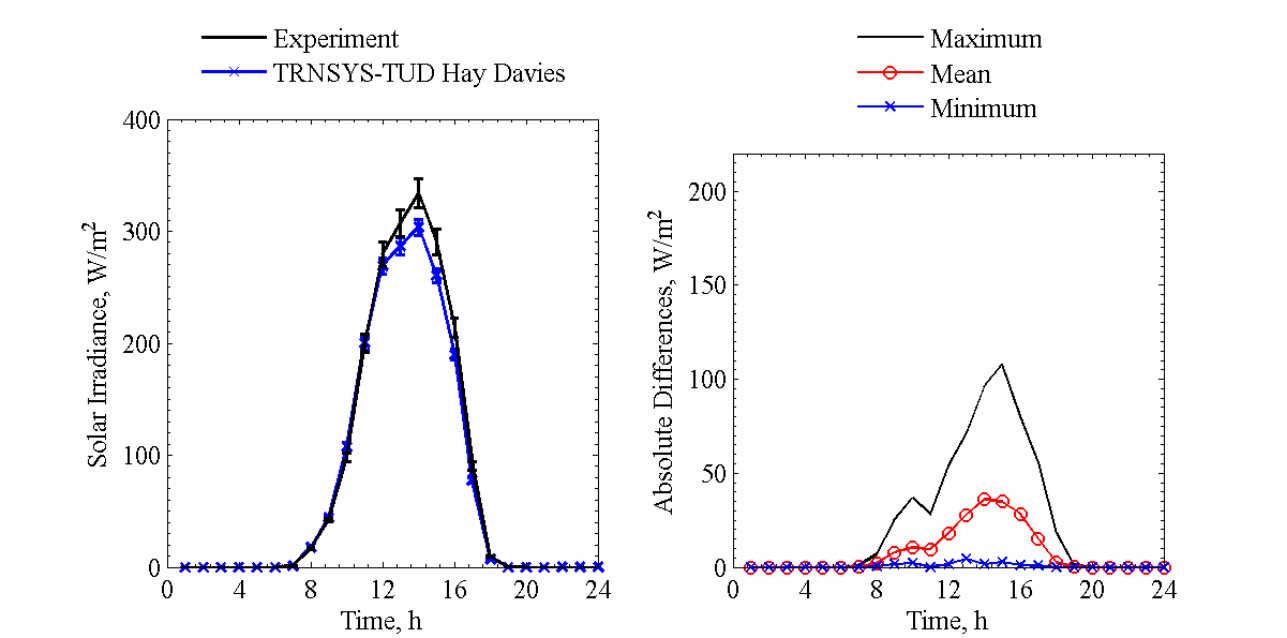

Figure 5.1i. Global vertical solar irradiance comparisons for TRNSYS-TUD Hay Davies averaged over each given hour of the day (left) and absolute maximum, mean, and minimum differences for a given hour of the day (right).

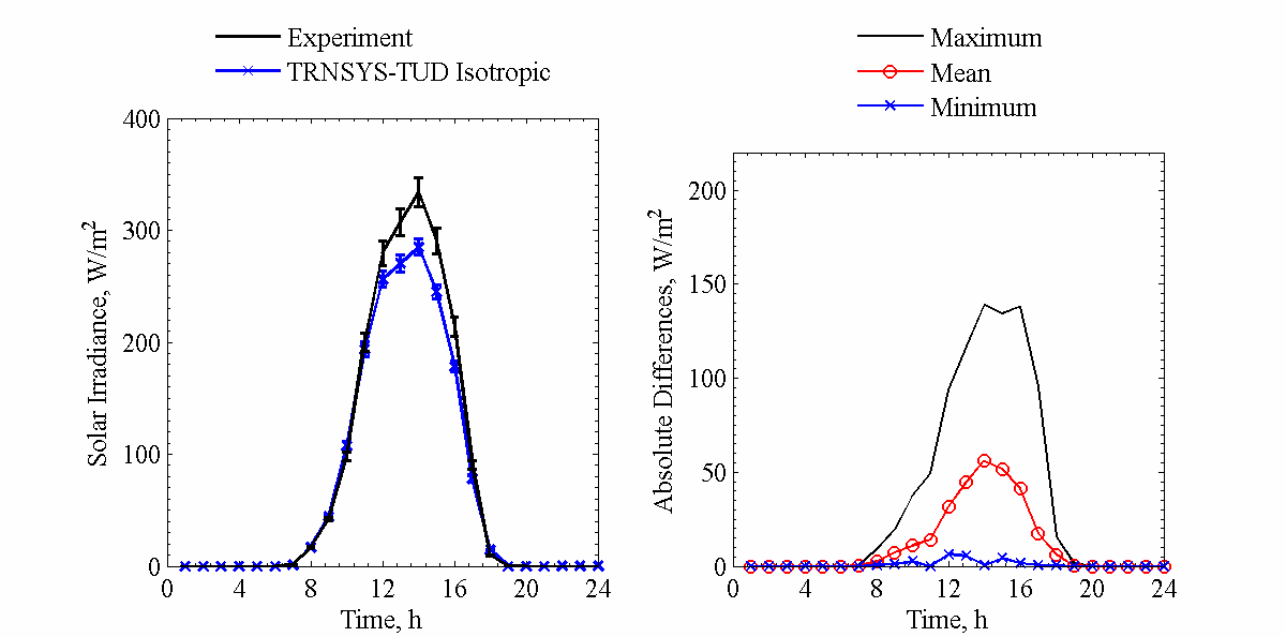

Figure 5.1j. Global vertical solar irradiance comparisons for TRNSYS-TUD Isotropic averaged over each given hour of the day (left) and absolute maximum, mean, and minimum differences for a given hour of the day (right).

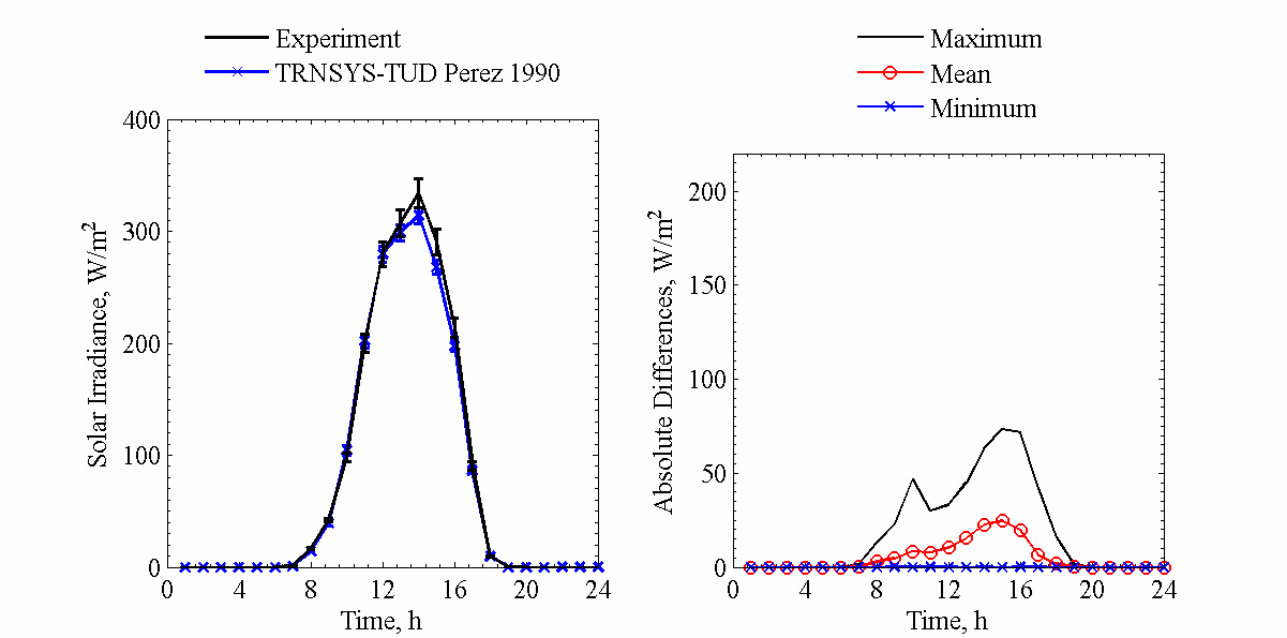

Figure 5.1k. Global vertical solar irradiance comparisons for TRNSYS-TUD Perez 1990 averaged over each given hour of the day (left) and absolute maximum, mean, and minimum differences for a given hour of the day (right).

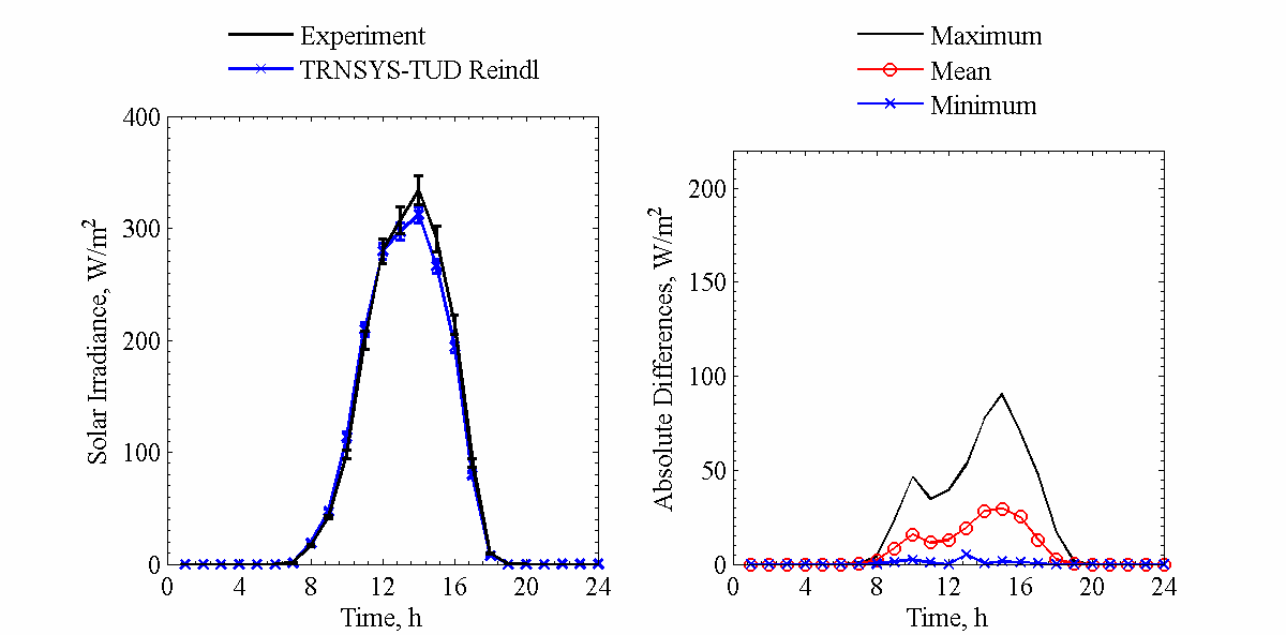

Figure 5.1l. Global vertical solar irradiance comparisons for TRNSYS-TUD Reindl averaged over each given hour of the day (left) and absolute maximum, mean, and minimum differences for a given hour of the day (right).

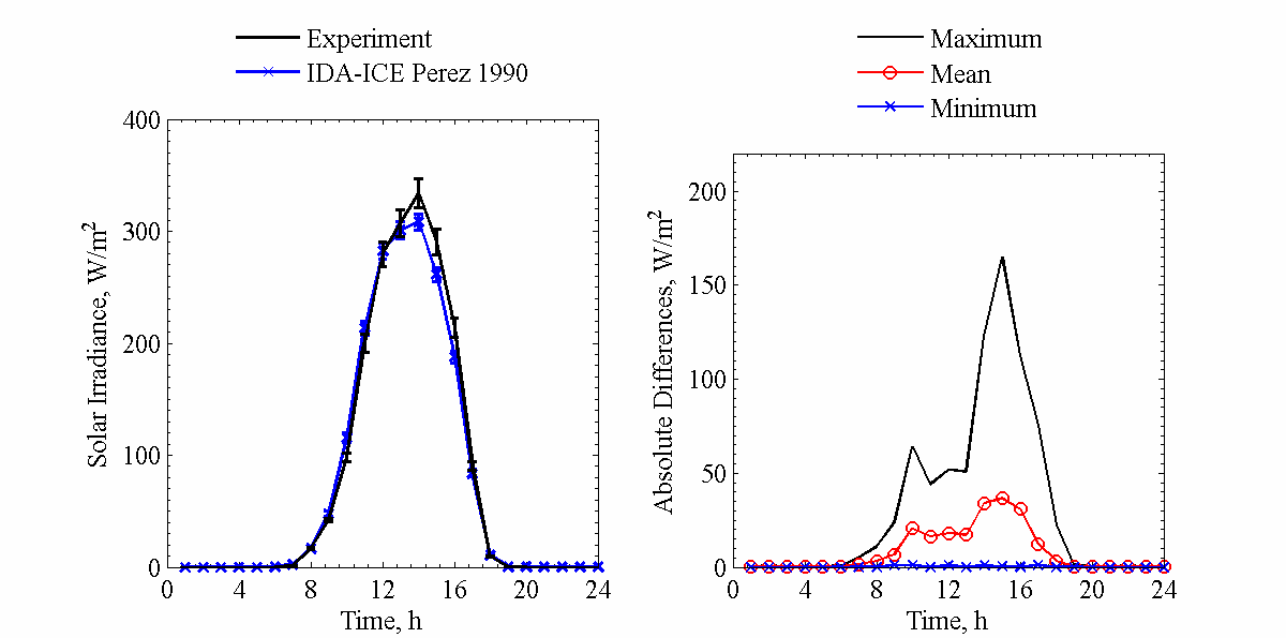

Figure 5.1m. Global vertical solar irradiance comparisons for IDA-ICE Perez 1990 averaged over each given hour of the day (left) and absolute maximum, mean, and minimum differences for a given hour of the day (right).

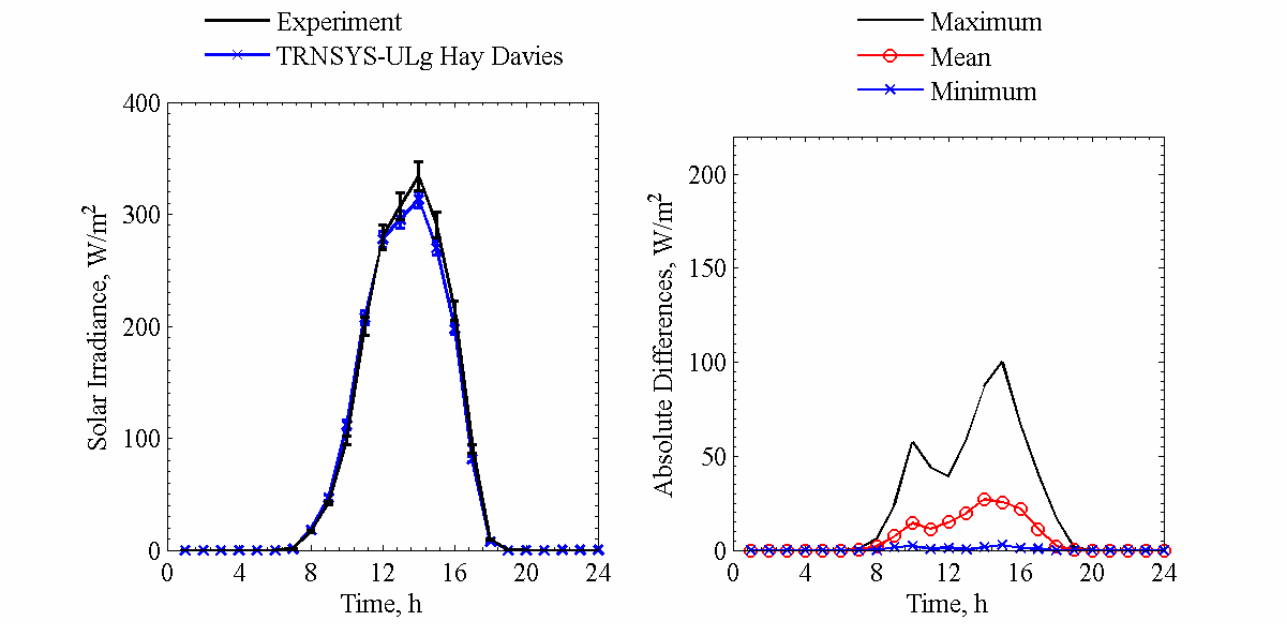

Figure 5.1n. Global vertical solar irradiance comparisons for TRNSYS-ULg Hay Davies averaged over each given hour of the day (left) and absolute maximum, mean, and minimum differences for a given hour of the day (right).

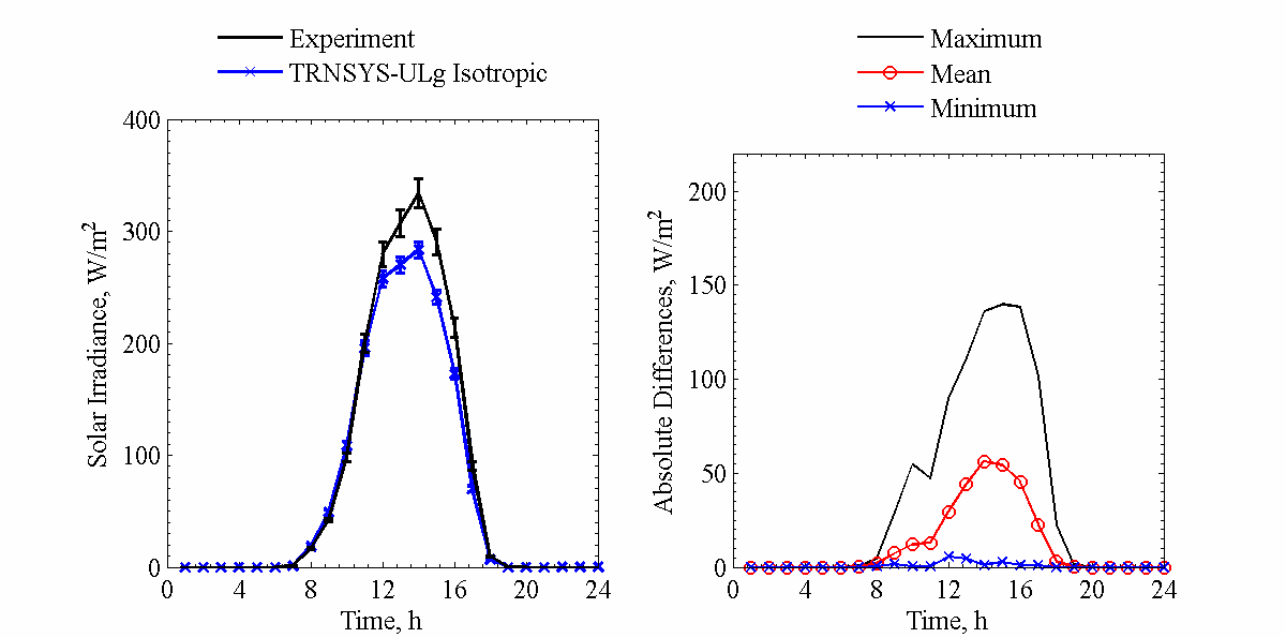

Figure 5.1o. Global vertical solar irradiance comparisons for TRNSYS-ULg Isotropic averaged over each given hour of the day (left) and absolute maximum, mean, and minimum differences for a given hour of the day (right).

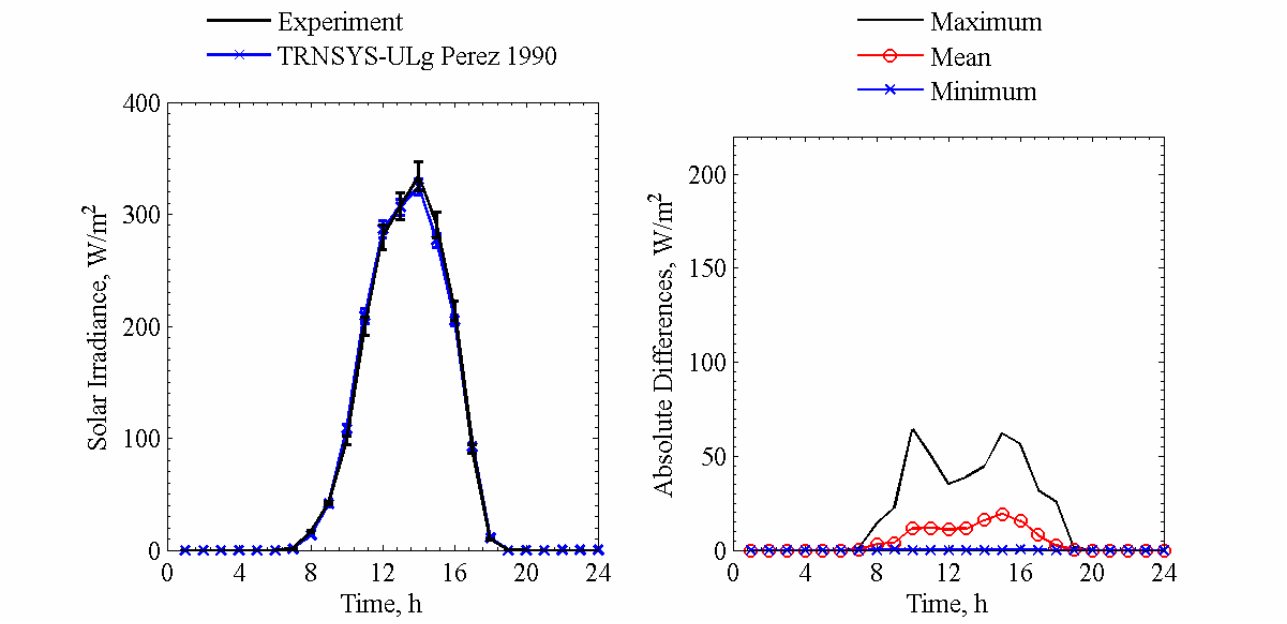

Figure 5.1p. Global vertical solar irradiance comparisons for TRNSYS-ULg Perez 1990 averaged over each given hour of the day (left) and absolute maximum, mean, and minimum differences for a given hour of the day (right).

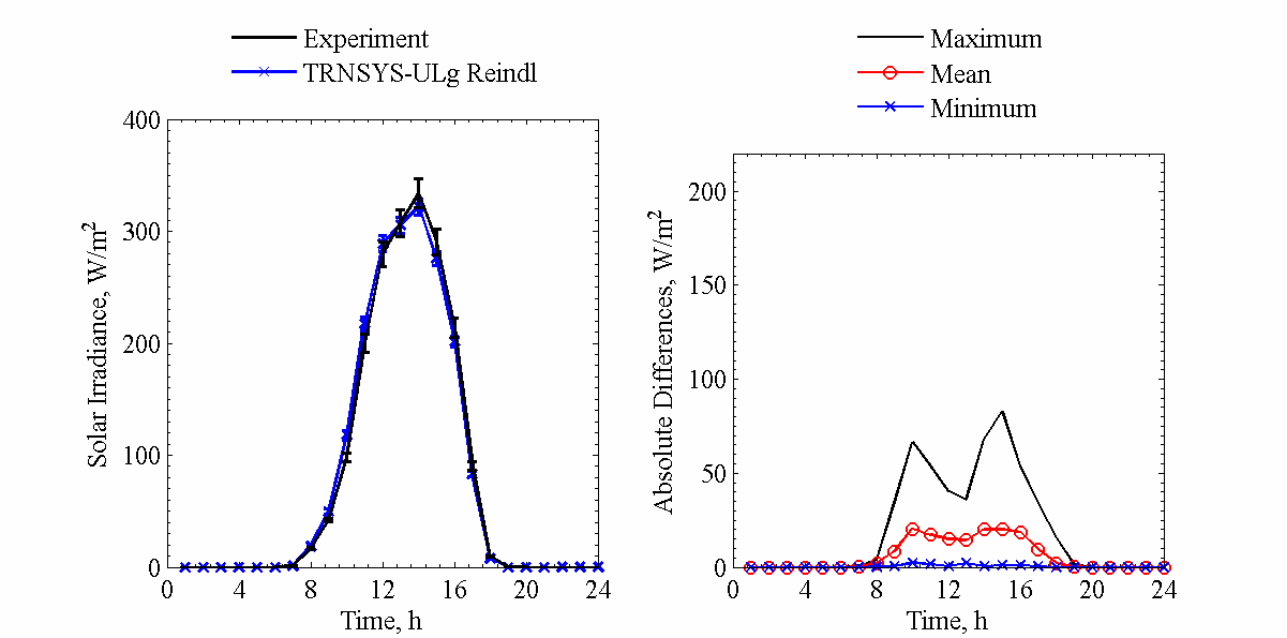

Figure 5.1q. Global vertical solar irradiance comparisons for TRNSYS-ULg Reindl averaged over each given hour of the day (left) and absolute maximum, mean, and minimum differences for a given hour of the day (right).

Table 5.1 contains overall, individual, and associated interactions from input uncertainties that impacted the global vertical solar irradiance predictions taken from the n-way factorial analysis averaged over the entire experiment. Statistical comparisons are contained in Table 5.2; the results were only analyzed when the solar altitude was greater than zero (when the sun was up).

Table 5.1. N-way factorial analyses to evaluate the sensitivities of outputs on input uncertainties.

Factorial analyses	**Forward differencing W/m^2**	**Backward differencing W/m^2**
Direct-normal solar irradiance	1.13	-1.10
Diffuse horizontal solar irradiance	1.37	-1.28
Ground reflectance	0.357	-0.357
Building azimuth	-0.499	0.500
Interactions between direct-normal and diffuse horizontal solar irradiance	-0.0560	-0.0831
Interaction between direct-normal solar irradiance and ground reflectance	0.00155	0.00158
Interaction between direct-normal solar irradiance and building azimuth	-0.00464	-0.00464
Interactions between diffuse horizontal solar irradiance and ground reflectance	0.00352	0.00380
Interactions between diffuse horizontal solar irradiance and building azimuth	-0.00267	-0.00264
Interactions between ground reflectance and building azimuth	No Interactions	No Interactions
Average overall uncertainty	2.40	2.40

Table 5.2. Statistical comparisons for Exercise 2.

Parameter	Experiment	HELIOS Perez 1987	EnergyPlus Perez 1990	DOE-2.1E Perez 1990	ESP-r Isotropic	ESP-r Klucher	ESP-r Muneer
$\bar{x}$	176.1 W/m^2	179.2 W/m^2	169.7 W/m^2	177.2 W/m^2	152.5 W/m^2	156.1 W/m^2	177.8 W/m^2
s	223.8 W/m^2	216.7 W/m^2	211.8 W/m^2	218.6 W/m^2	185.1 W/m^2	190.2 W/m^2	228.5 W/m^2
x_{max}	856.8 W/m^2	812.0 W/m^2	817.8 W/m^2	820.4 W/m^2	728.8 W/m^2	743.5 W/m^2	915.7 W/m^2
x_{min}	0.2 W/m^2	0.0 W/m^2	0.3 W/m^2	0.0 W/m^2	0.4 W/m^2	0.4 W/m^2	0.3 W/m^2
$\overline{D}$	-	-3.0 W/m^2	6.4 W/m^2	-1.1 W/m^2	23.6 W/m^2	20.0 W/m^2	-1.7 W/m^2
$\overline{\lvert D \rvert}$	-	12.0 W/m^2	13.7 W/m^2	10.5 W/m^2	29.5 W/m^2	26.0 W/m^2	12.7 W/m^2
$\lvert D_{max} \rvert$	-	87.0 W/m^2	103.5 W/m^2	67.1 W/m^2	157.7 W/m^2	139.1 W/m^2	205.5 W/m^2
$\lvert D_{min} \rvert$	-	0.0 W/m^2	0.0 W/m^2	0.0 W/m^2	0.0 W/m^2	0.0 W/m^2	0.0 W/m^2
D_{rms}	-	18.7 W/m^2	24.2 W/m^2	17.0 W/m^2	51.1 W/m^2	44.8 W/m^2	25.3 W/m^2
$\lvert D \rvert_{95\%}$	-	44.8 W/m^2	56.4 W/m^2	40.3 W/m^2	132.0 W/m^2	115.8 W/m^2	47.4 W/m^2
$\overline{OU}$	6.9 W/m^2	-	4.6 W/m^2	-	-	-	-
$\overline{UR}$	-	2.4	1.3	1.3	2.5	2.4	1.4
UR_{max}	-	71.3	12.4	20.4	17.0	17.0	10.9
UR_{min}	-	0.0	0.0	0.0	0.0	0.0	0.0
$\overline{\lvert D \rvert} / \bar{x} \times 100\%$	-	6.8%	7.8%	5.9%	16.7%	14.8%	7.2%
$\overline{D} / \bar{x} \times 100\%$	-	-1.7%	3.7%	-0.6%	13.4%	11.3%	-1.0%

Table 5.2. Statistical comparisons for Exercise 2 (Continued).

Parameter	Experiment	ESP-r Perez 1987	ESP-r Perez 1990	TRNSYS-TUD Hay Davies	TRNSYS-TUD Isotropic	TRNSYS-TUD Perez 1990	TRNSYS-TUD Reindl
$\bar{x}$	176.1 W/m^2	175.9 W/m^2	171.3 W/m^2	179.8 W/m^2	169.7 W/m^2	177.2 W/m^2	170.9 W/m^2
s	223.8 W/m^2	215.7 W/m^2	212.2 W/m^2	211.2 W/m^2	211.8 W/m^2	218.6 W/m^2	209.4 W/m^2
x_{max}	856.8 W/m^2	806.7 W/m^2	804.7 W/m^2	781.4 W/m^2	817.8 W/m^2	820.4 W/m^2	810.4 W/m^2
x_{min}	0.2 W/m^2	0.1 W/m^2	0.3 W/m^2	0.5 W/m^2	0.3 W/m^2	0.0 W/m^2	0.4 W/m^2
$\overline{D}$	-	0.2 W/m^2	4.8 W/m^2	-3.7 W/m^2	6.4 W/m^2	-1.1 W/m^2	5.2 W/m^2
$\overline{\lvert D \rvert}$	-	11.7 W/m^2	11.7 W/m^2	22.2 W/m^2	13.7 W/m^2	10.5 W/m^2	15.7 W/m^2
$\lvert D_{max} \rvert$	-	69.3 W/m^2	87.7 W/m^2	101.3 W/m^2	103.5 W/m^2	67.1 W/m^2	90.4 W/m^2
$\lvert D_{min} \rvert$	-	0.0 W/m^2	0.0 W/m^2	0.0 W/m^2	0.0 W/m^2	0.0 W/m^2	0.0 W/m^2
D_{rms}	-	18.9 W/m^2	20.4 W/m^2	33.6 W/m^2	24.2 W/m^2	17.0 W/m^2	24.0 W/m^2
$\lvert D \rvert_{95\%}$	-	45.6 W/m^2	50.9 W/m^2	81.4 W/m^2	56.4 W/m^2	40.3 W/m^2	56.3 W/m^2
$\overline{OU}$	6.9 W/m^2	-	-	-	4.6 W/m^2	-	-
$\overline{UR}$	-	1.3	1.2	3.2	1.3	1.3	2.3
UR_{max}	-	12.1	11.2	39.0	12.4	20.4	20.4
UR_{min}	-	0.0	0.0	0.0	0.0	0.0	0.0
$\overline{\lvert D \rvert} / \bar{x} \times 100\%$	-	6.7%	6.7%	12.6%	7.8%	5.9%	8.9%
$\overline{D} / \bar{x} \times 100\%$	-	0.1%	2.7%	-2.1%	3.7%	-0.6%	3.0%

Table 5.2. Statistical comparisons for Exercise 2 (Continued).

Parameter	Experiment	IDA-ICE Perez 1990	TRNSYS-ULg Hay Davies	TRNSYS-ULg Isotropic	TRNSYS-ULg Perez 1990	TRNSYS-ULg Reindl
$\bar{x}$	176.1 W/m^2	156.1 W/m^2	170.9 W/m^2	156.5 W/m^2	175.6 W/m^2	176.7 W/m^2
s	223.8 W/m^2	190.2 W/m^2	214.3 W/m^2	189.9 W/m^2	217.7 W/m^2	218.7 W/m^2
x_{max}	856.8 W/m^2	743.5 W/m^2	838.5 W/m^2	748.2 W/m^2	820.9 W/m^2	848.4 W/m^2
x_{min}	0.2 W/m^2	0.4 W/m^2	0.4 W/m^2	0.4 W/m^2	0.4 W/m^2	0.4 W/m^2
$\overline{D}$	-	20.0 W/m^2	5.2 W/m^2	19.6 W/m^2	0.6 W/m^2	-0.6 W/m^2
$\overline{\lvert D \rvert}$	-	26.0 W/m^2	14.7 W/m^2	27.1 W/m^2	10.7 W/m^2	13.8 W/m^2
$\lvert D_{max} \rvert$	-	139.1 W/m^2	100.2 W/m^2	139.7 W/m^2	64.3 W/m^2	82.7 W/m^2
$\lvert D_{min} \rvert$	-	0.0 W/m^2	0.0 W/m^2	0.0 W/m^2	0.0 W/m^2	0.0 W/m^2
D_{rms}	-	44.8 W/m^2	23.3 W/m^2	46.2 W/m^2	17.5 W/m^2	20.5 W/m^2
$\lvert D \rvert_{95\%}$	-	115.8 W/m^2	57.4 W/m^2	121.9 W/m^2	43.2 W/m^2	46.3 W/m^2
$\overline{OU}$	6.9 W/m^2	-	-	-	-	-
$\overline{UR}$	-	2.4	2.2	2.6	1.2	2.3
UR_{max}	-	17.0	20.6	20.6	20.6	20.6
UR_{min}	-	0.0	0.0	0.0	0.0	0.0
$\overline{\lvert D \rvert} / \bar{x} \times 100\%$	-	14.8%	8.4%	15.4%	6.1%	7.8%
$\overline{D} / \bar{x} \times 100\%$	-	11.3%	3.0%	11.1%	0.3%	-0.4%

These results were used to identify the existing tilted surface radiation model that performed best in each building energy simulation program or to implement a different tilted surface radiation model into the program(s). This was also a vital step for identifying discrepancies in the solar gain experiments. In-depth analyses and discussion of these results are provided by Loutzenhiser et al. [2]. The uncertainty ratio provides guidance for identifying which model performed best. This quantity factored in the 95% credible limits with instantaneous comparisons of the models compared with the measurands for each hour. The average uncertainty ratio was used to rank the models over the given period and is useful in subsequent exercises.

CHAPTER 6: EMPA GLAZING UNIT ONLY (EXERCISE 3)

An experiment was performed in the test cell from October 2 to October 26, 2004 to evaluate the impact of solar gains through a glazing unit. Information about the glazing unit, thermophysical properties evaluated at mean envelope temperatures, the linear thermal transmittance of the glazing unit, and results are provided in subsequent sections.

6.1. Description of the Experiment

This section contains specific information about the experiment, including the following information:

- the mounting and properties of the glazing.
- a two-dimensional steady-state heat transfer simulation and calorimetric measurements used to calculate the linear thermal transmittance of the mounting and spacer,
- a description of the equipment used to measure the weather data, and
- thermophysical properties of the test cell envelope.

A photograph of the test cell taken during the experiment is shown in Figure 6.1.

Figure 6.1. A photograph of the test cell.

6.1.1. Glazing Unit Properties

The glazing unit for this experiment was mounted in the southwest exterior construction element of the test cell. The glazing properties from measured data are listed in Table 6.1. Measured optical properties for each glass pane as a function of wavelength from 250 nm to 2500 nm are contained in "Experiment 3.xls". Properties of the individual panes are described in Table 6.2. The integral inside and outside solar reflectances and solar transmittance were calculated according to European Standard EN 410 [7] in GLAD software [8]. The thermal transmittance due to the space and mounting was calculated from simulation and a calorimetric experiment and is described in a later section. For the individual panes of glass, the emittance was measured using an emissometer based on a calorimetric method. A dimensioned drawing of the exterior construction element as seen from this inside of the test cell showing the position of the glazing is presented in Figure 6.2. The dimensions, in meters, of the glazing in the figure correspond to the aperture height and width.

Table 6.1. Glazing unit properties.

Parameter	Quantity
Normal solar transmittance	42.9%
Normal solar exterior reflectance	25.2%
Normal solar interior reflectance	21.4%
Center-pane thermal transmittance	1.144 W/m^2-K
Aperture glazing width	1.17 m
Aperture glazing height	1.42 m
Aperture glazing area	1.66 m^2
Aperture perimeter length	5.18 m

Table 6.2a. Optical properties for the outer pane of glass (solar control Low-E).

Parameter	Quantity
Normal solar transmittance, %	50.9
Normal solar exterior reflectance, %	28.5
Normal solar interior reflectance, %	29.6
Outer emittance, %	89.4
Inner emittance, %	9.7

Table 6.2b. Optical properties for the inner pane of glass (clear float glass).

Parameter	Quantity
Normal solar transmittance, %	80.8
Normal solar exterior reflectance, %	7.6
Normal solar interior reflectance, %	7.6
Outer emittance, %	87.8
Inner emittance, %	88.7

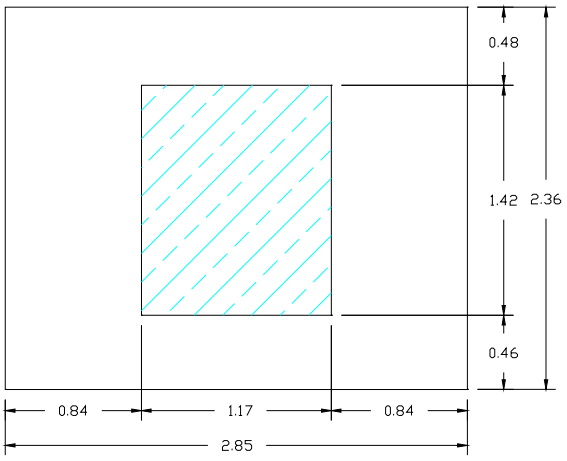

Figure 6.2. Position of the glazing in the exterior wall in meters seen from the inside of the test cell.

In addition to normal optical properties, angular dependent front reflectance, back reflectance, and transmittance were measured at various angles of incidents for the glazing unit from 300 nm to 1650 nm (properties from 1650 nm to 2500 nm were estimated using the value at 1650 nm) at the University of Basel. The properties were integrated over the solar spectrum using European Standard EN 410 [7] in GLAD software [8] and are shown in Tables 6.3.

Table 6.3. Optical properties as a function of incident angle.

Incident angle, °	**0**	**15**	**30**	**45**	**50**	**55**	**60**	**65**	**67.5**	**70**	**72.5**	**75**
Solar transmittance, %	42.1	41.7	40.9	38.9	37.6	35.8	33.2	29.5	27.2	24.6	21.6	18.4
Solar reflectance (front), %	-	26.7	26.6	27.6	28.4	30.0	32.3	35.9	38.5	41.6	45.0	49.4
Solar reflectance (back), %	-	24.6	24.7	26.2	27.3	29.3	32.2	36.7	39.7	43.4	47.4	52.6

6.1.2. Linear Thermal Transmittance

The impact of the window spacer and construction used to mount the glazing in the test cell was simulated using a two-dimensional steady-state heat transfer software package called BISCO [13]. To simulate the aluminum spacer, a dimensioned cross-section of the aluminum spacer provided by the manufacturer was used. Figure 6.3 shows a dimensioned drawing, in millimeters, of the spacer, the mounting construction and a portion of the exterior window and wall. BISCO simulation results coupled with calorimetric measurements [14] were used to quantify the impact of the spacer and the frame. From these results, the linear thermal transmittance was then computed.

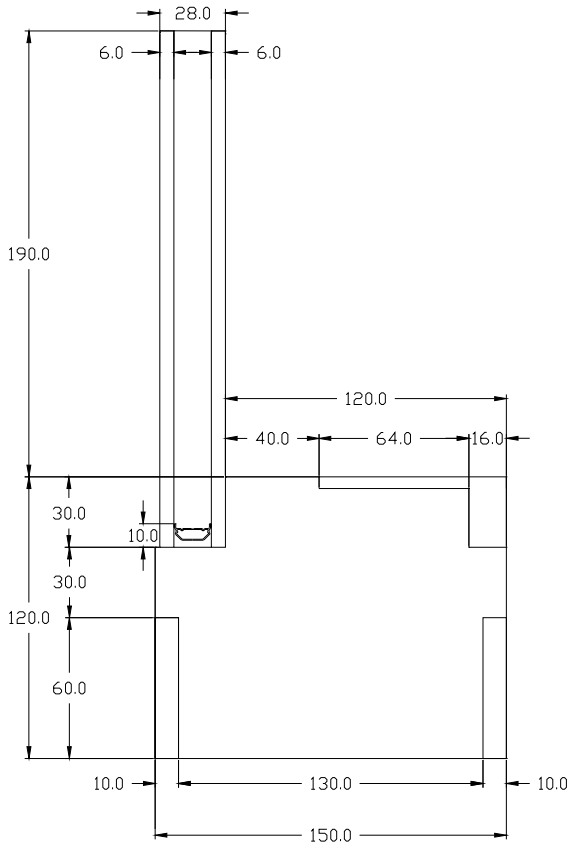

Figure 6.3. Dimensioned drawing of the spacer and frame in millimeters.

The thermal conductivities of the construction materials were required to perform the simulation. These properties were taken from literature, calculation, and in-house measurements. For temperature-dependent properties, the thermal conductivity was evaluated at a mean envelope temperature of 10°C. Table 6.4 provides a list of the quantities and color-coding of the materials and their respective thermal conductivities. An iterative procedure using the simulation results and the calorimetric measurements was employed to calculate the equivalent thermal conductivity for the argon cavity space—which factored in the impact of conduction, radiation, and convection. The procedure simulated the spacer, calculated the linear thermal transmittance, and then recalculated a center-pane thermal transmittance.

Table 6.4. List of materials and their respective thermal conductivities.

Material	Thermal conductivity, W/m-K	Color-coding
Desiccant	0.130	
Aluminum	220.0	
Polyisobutylene	0.220	
Polysulfid	0.400	
Argon 90%/air 10%	0.02313	
Glass	1.0	
Plywood	0.1381	
Wood	0.110	
EPS Foam	0.03483	

The specified properties for the boundary conditions included the temperature and the heat transfer coefficients for the outside and inside of the frame; these values were taken from prEN ISO 10077-2 [6]. These results, as well as the color-coding, are presented in Table 6.5.

Table 6.5. Boundary condition properties.

Boundary condition	Temperature, °C	Heat transfer coefficient, W/m^2-K	Color-coding
Inside air	20	7.7	
Outside air	0	25.0	

The bitmap of the cross-section of the glazing unit, spacer, and mounting used for the BISCO simulation of the frame and glazing construction and the spacer are shown in Figures 6.4a and 6.4b.

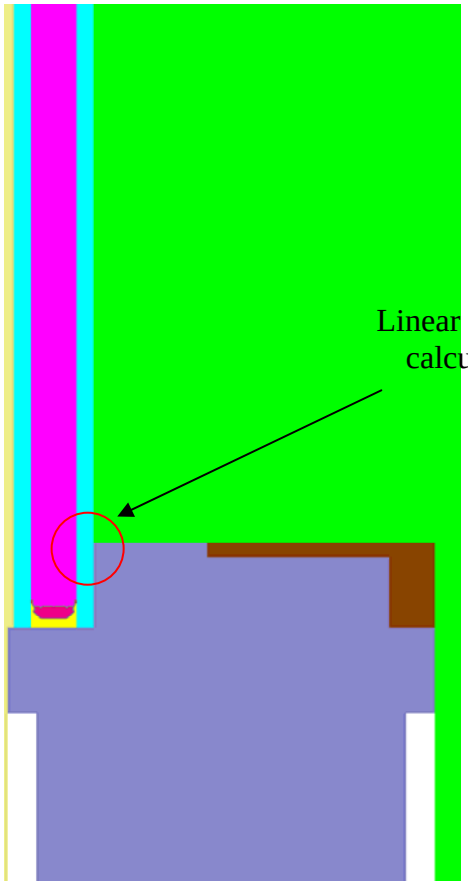

Figure 6.4a. Cross-section of the glazing and frame.

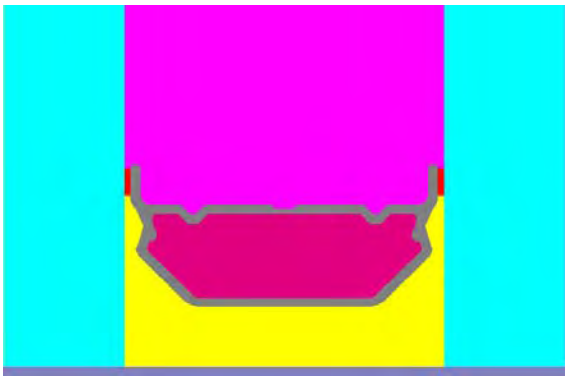

Figure 6.4b. Cross-section of the aluminum spacer.

For the BISCO simulation, the bitmap was divided up into 243,205 nodes and the heat transfer through the element was calculated as 6.72 W/m. Isotherm and heat flow line illustrations are shown in Figures 6.5a and 6.5b to help visualize the two-dimensional heat flow path.

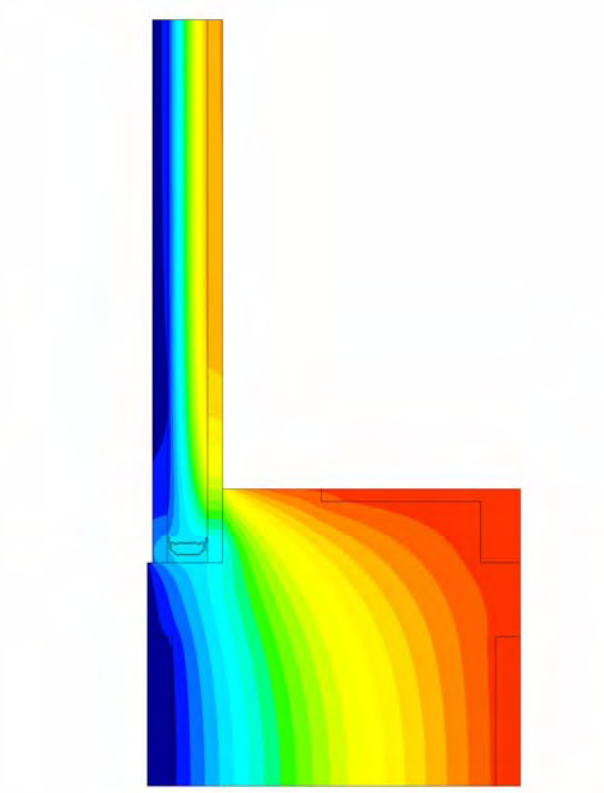

Figure 6.5a. Isotherm illustration from the BISCO simulation.

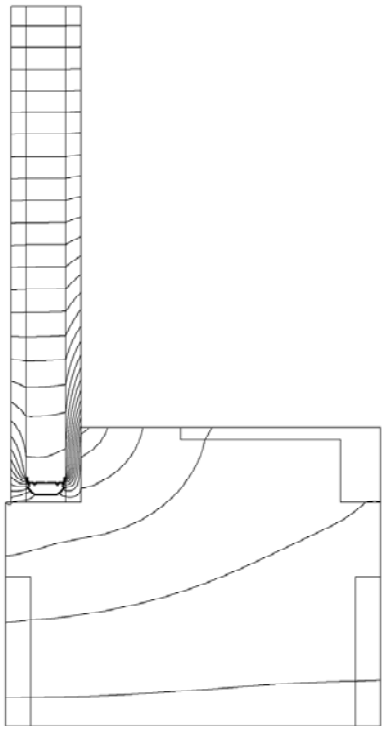

Figure 6.5b. Heat flow line illustration from the BISCO simulation.

One-dimensional heat transfer was calculated using Equation 6.1. A list of the additional parameters used for this calculation is shown in Table 6.6.

$$Q'_{1-D} = \left\{ L_g U_g + \frac{L_w}{\left(\frac{1}{h_i} + \frac{2d_{ply}}{\lambda_{ply}} + \frac{d_{eps}}{\lambda_{eps}} + \frac{1}{h_o} \right)} \right\} (\theta_i - \theta_o) \qquad (6.1)$$

where

L_g is the length of the glazing used from the simulation,
U_g is the center pane thermal transmittance of the glazing,
L_w is the length of the wall from the simulation,
h_i is the inside heat transfer coefficient,
d_{ply} is the width of the plywood,
λ_{ply} is the thermal conductivity of the plywood,
d_{eps} is the width of the eps foam,
λ_{eps} is the thermal conductivity of the eps foam,
h_o is the outside heat transfer coefficient,
θ_I is the inside temperature, and
θ_o is the outside temperature.

Table 6.6. Values of the variables used for the 1-D heat transfer calculation.

Parameter	Quantity
L_g	0.190 m
U_g	1.144 W/m^2-K
L_w	0.120 m
d_{ply}	0.01 m
d_{eps}	0.130 m

Using the simulation conditions, the one-dimensional heat transfer was calculated to be 4.94 W/m. The linear thermal transmittance, ψ, was calculated using Equation 6.2 to be 0.08899 W/m-K.

$$\psi = \frac{Q'_{BISCO} - Q'_{1-D}}{\theta_i - \theta_o} \tag{6.2}$$

where

Q'_{BISCO} is the heat transfer from the BISCO simulation.

6.1.3. Thermophysical Properties of the Test Cell Envelope

The mean temperatures of the construction elements are shown in Table 6.7. The thermophysical properties, fixed at the mean temperatures, are contained in Tables 6.8a to 6.8c.

Table 6.7. Mean temperatures for of the construction element during experiment.

Construction element	Mean temperature, °C
Ceiling, east, west, and north walls	22.78
Floor	22.72
South wall	17.49

Table 6.8a. Ceiling, north, east and west wall construction evaluated at 22.78°C.

Layer number	Material	Thickness mm	Thermal conductivity W/m-K	Density kg/m^3	Specific heat J/kg-K
1	Sheet steel	0.7	53.62	7837	460.8
2	PU foam	139	0.02233	30	1800
3	Sheet steel	0.7	53.62	7837	460.8

Table 6.8b. Floor construction evaluated at 22.72°C.

Layer number	Material	Thickness mm	Thermal conductivity W/m-K	Density kg/m^3	Specific heat J/kg-K
1	Sheet steel	0.7	53.62	7837	460.8
2	PU foam	140	0.02232	30	1800
3	PU foam (higher density)	20	0.070	45	1800
4	Sheet steel with surface structure	2.5	53.62	7837	460.8

Table 6.8c. South wall construction evaluated at 17.49°C.

Layer number	Material	Thickness mm	Thermal conductivity W/m-K	Density kg/m^3	Specific heat J/kg-K
1	Plywood	10	0.1394	850	1605
2	EPS foam	130	0.03578	28	1460
3	Plywood	10	0.1394	850	1605

6.2. Results

The empirical validation for this exercise focused on comparing cooling power. Plots for cooling powers from HELIOS, EnergyPlus, DOE-2.1E, ESP-r, TRNSYS-TUD, IDA-PAR, IDA-SIA, IDA-Detwind, and TRNSYS-ULg are shown in Figures 6.6a to 6.61, respectively. Table 6.9 contains overall and 10 most influential input uncertainties averaged over the experiment that impacted the cooling power predictions taken from the n-way factorial analysis. A summary of the statistical comparisons is contained in Table 6.10.

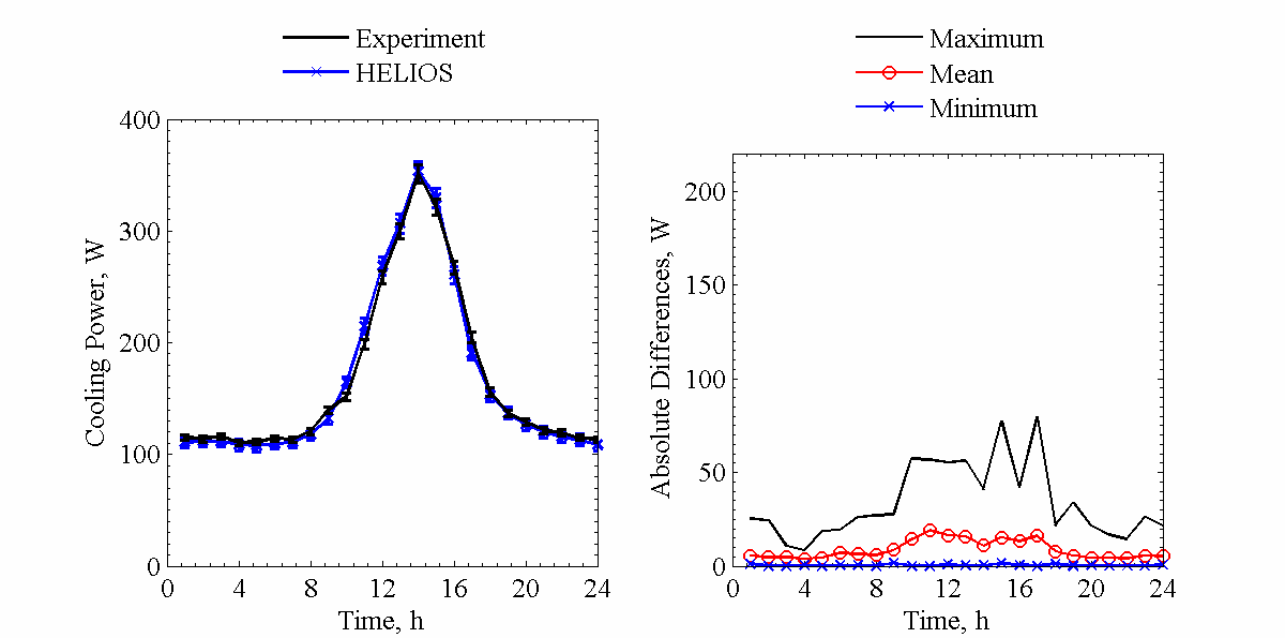

Figure 6.6a. Cooling power comparisons for HELIOS averaged over each given hour of the day (left) and absolute maximum, mean, and minimum differences for a given hour of the day (right).

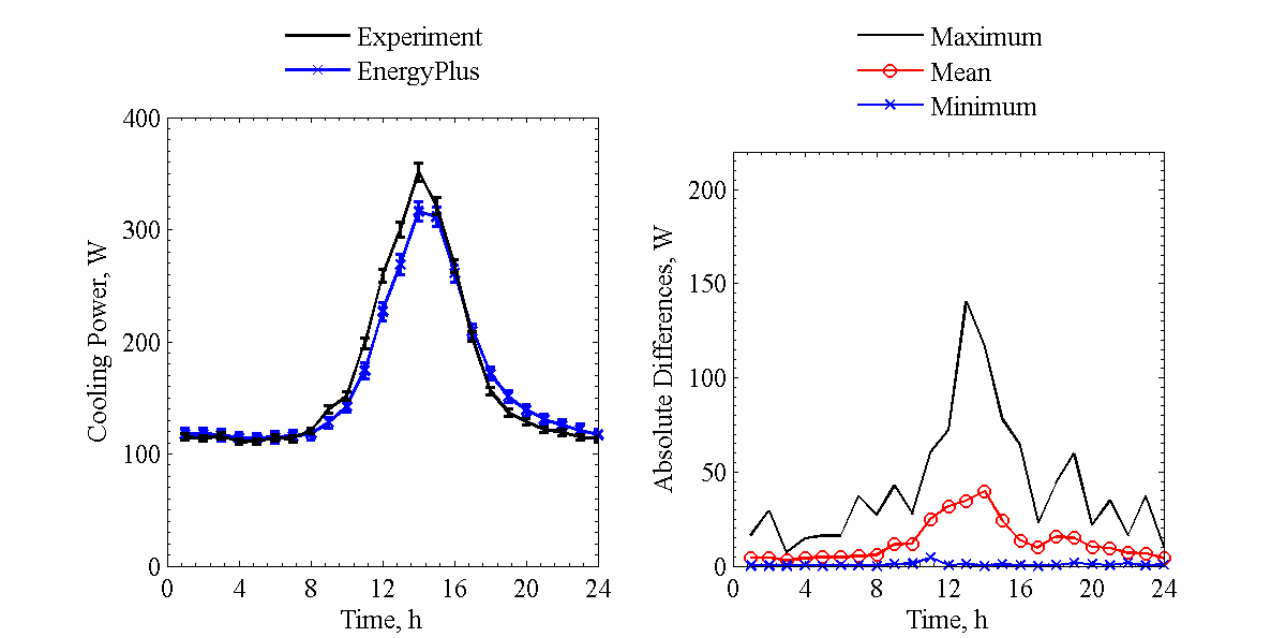

Figure 6.6b. Cooling power comparisons for EnergyPlus averaged over each given hour of the day (left) and absolute maximum, mean, and minimum differences for a given hour of the day (right).

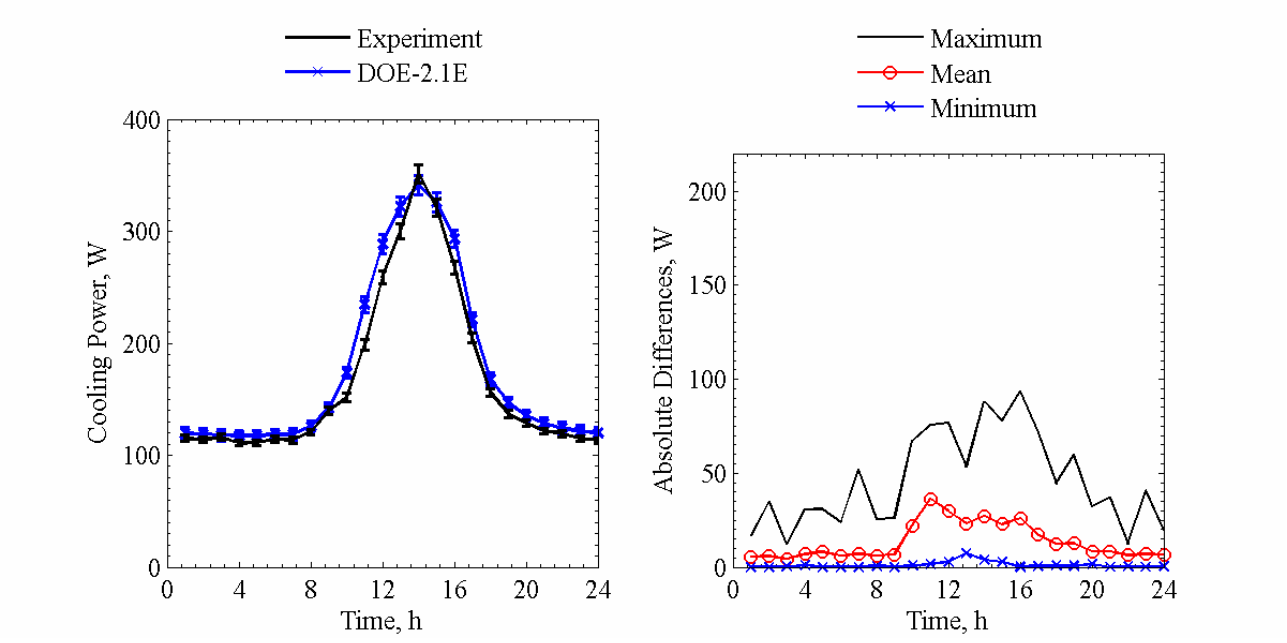

Figure 6.6c. Cooling power comparisons for DOE-2.1E averaged over each given hour of the day (left) and absolute maximum, mean, and minimum differences for a given hour of the day (right).

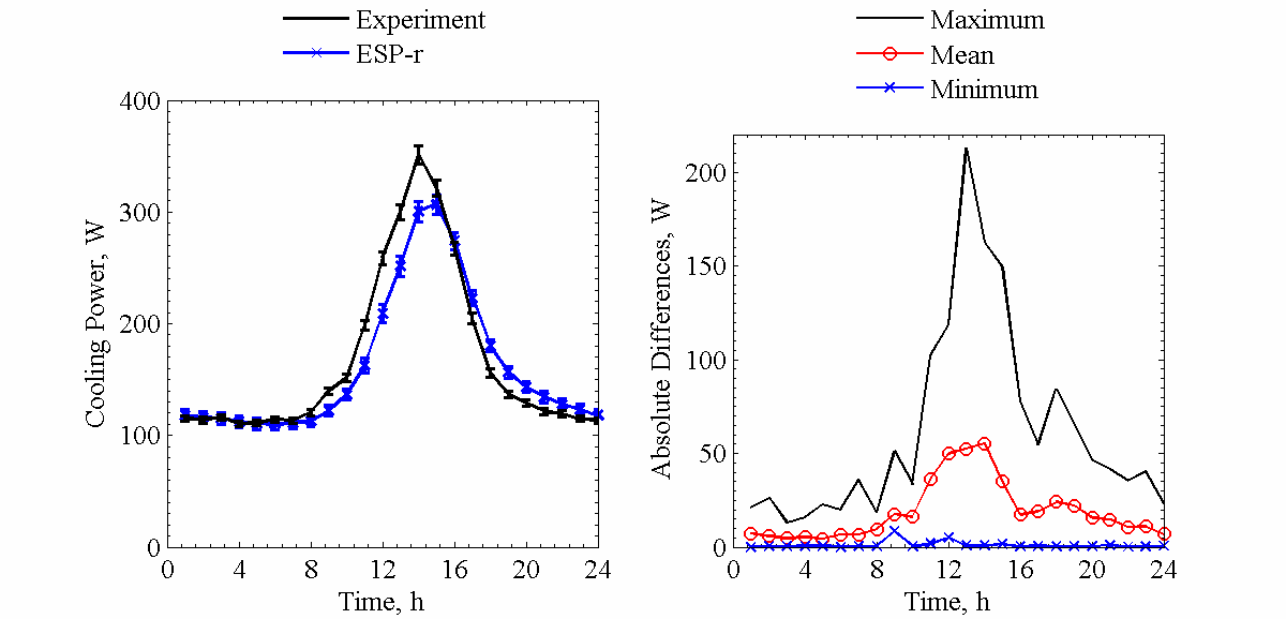

Figure 6.6d. Cooling power comparisons for ESP-r averaged over each given hour of the day (left) and absolute maximum, mean, and minimum differences for a given hour of the day (right).

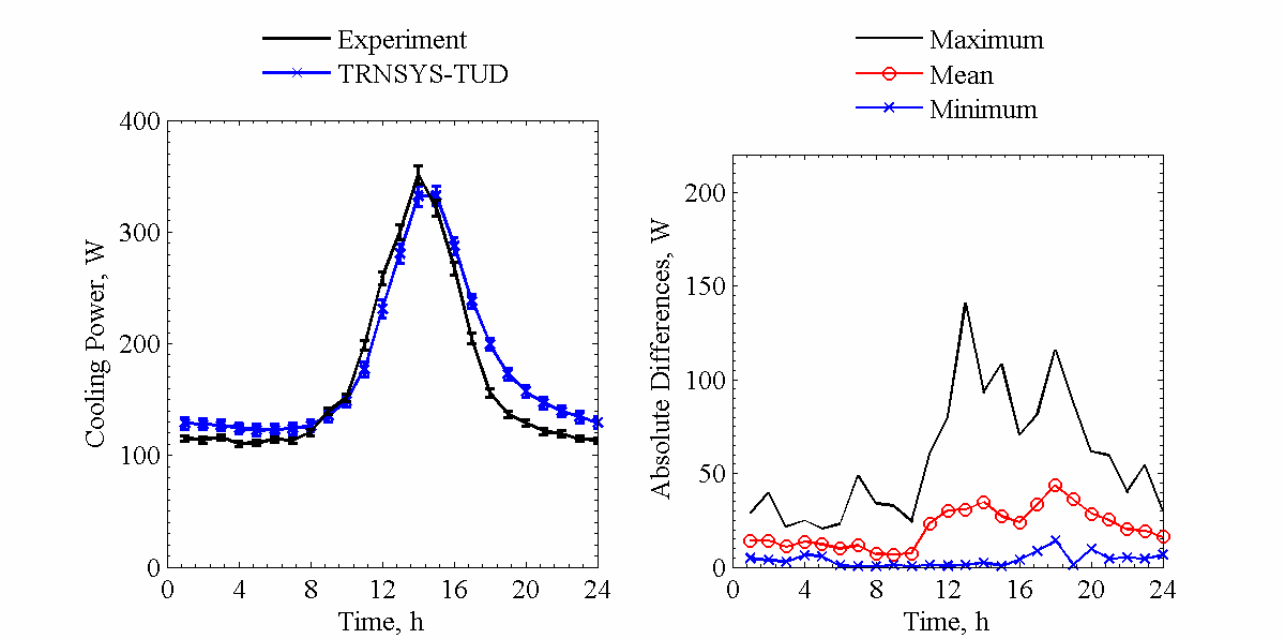

Figure 6.6d. Cooling power comparisons for TRNSYS-TUD averaged over each given hour of the day (left) and absolute maximum, mean, and minimum differences for a given hour of the day (right).

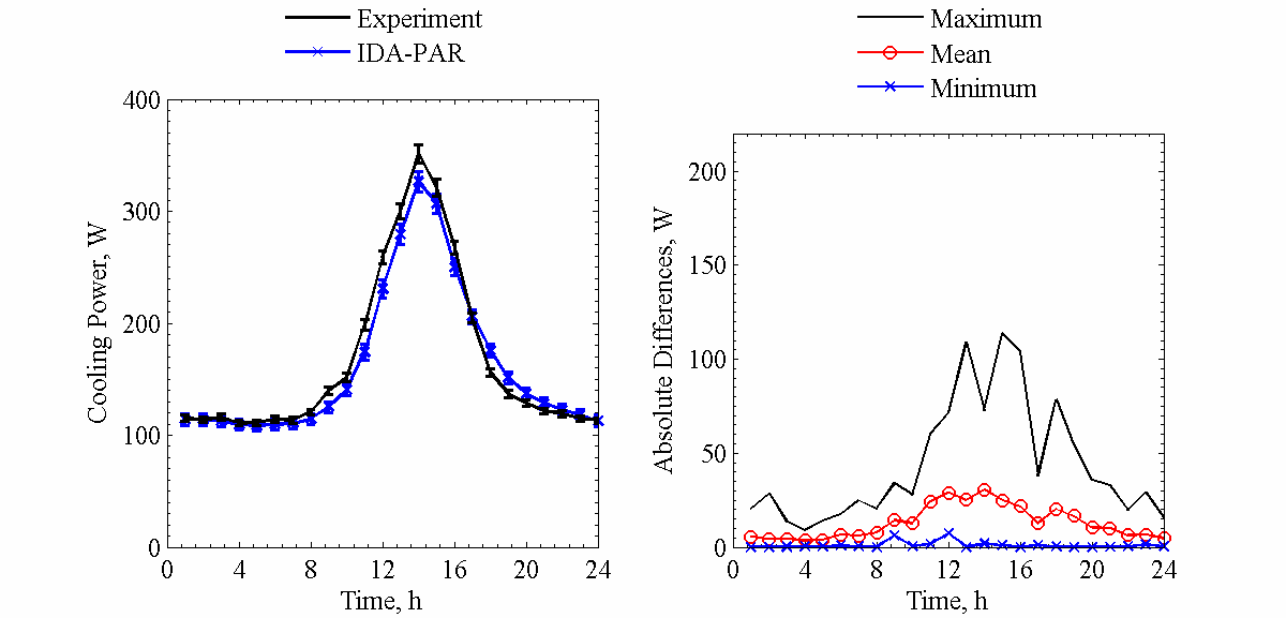

Figure 6.6e. Cooling power comparisons for IDA-PAR averaged over each given hour of the day (left) and absolute maximum, mean, and minimum differences for a given hour of the day (right).

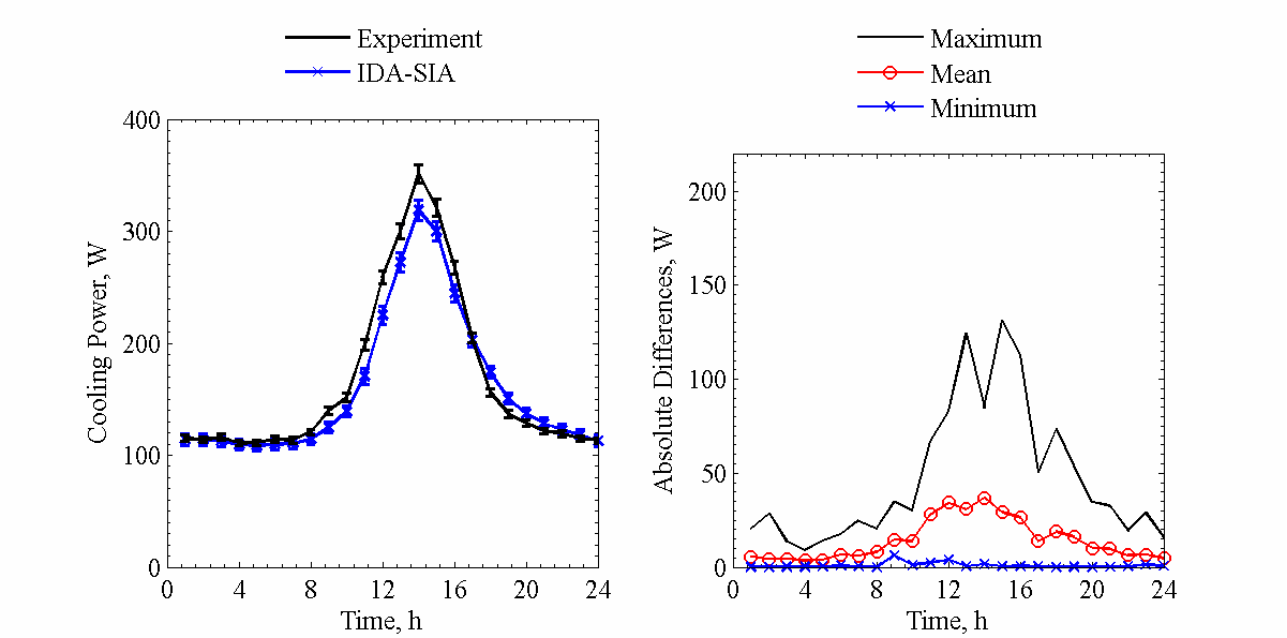

Figure 6.6f. Cooling power comparisons for IDA-SIA averaged over each given hour of the day (left) and absolute maximum, mean, and minimum differences for a given hour of the day (right).

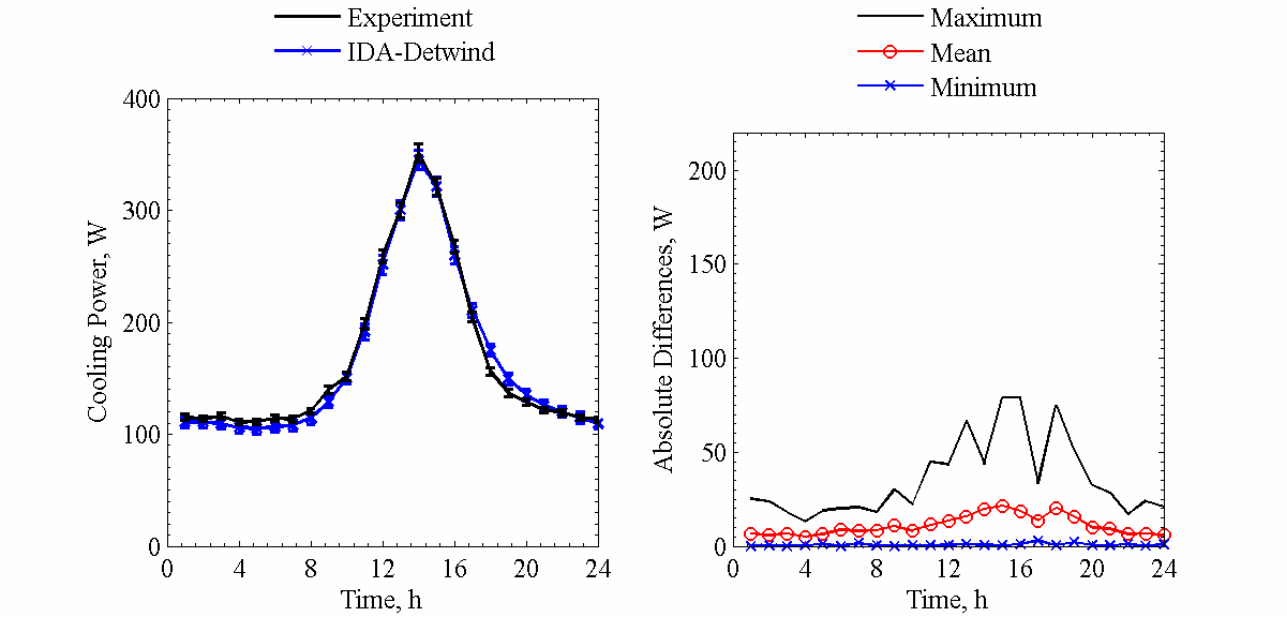

Figure 6.6g. Cooling power comparisons for IDA-Detwind averaged over each given hour of the day (left) and absolute maximum, mean, and minimum differences for a given hour of the day (right).

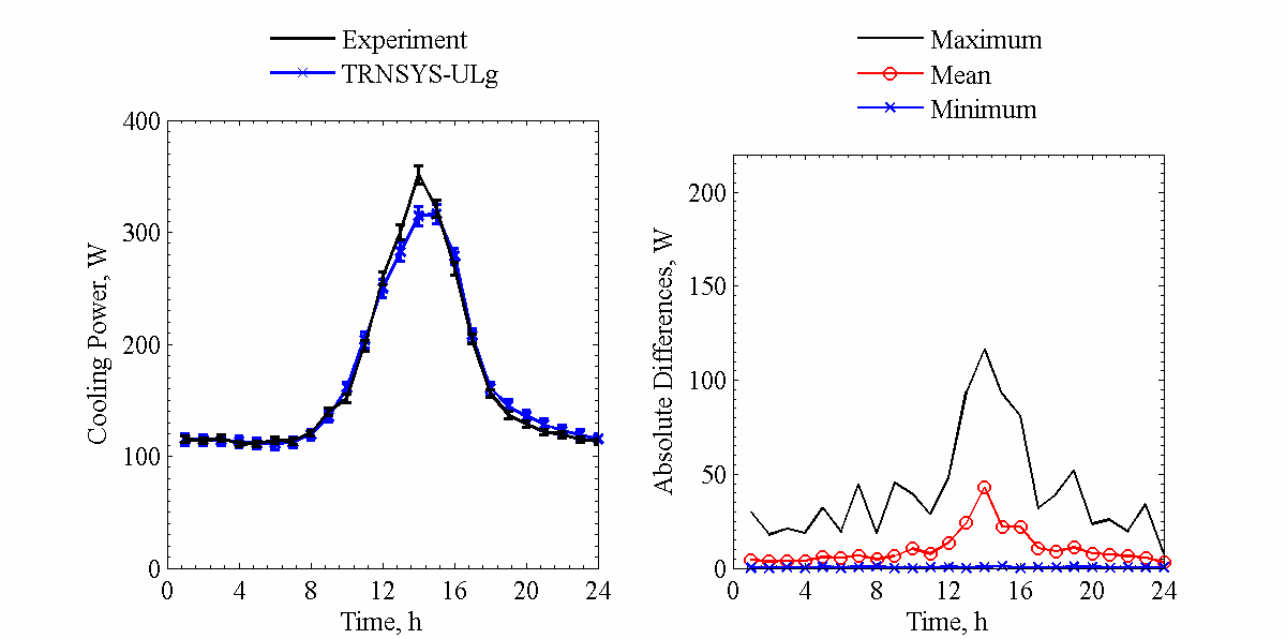

Figure 6.6h. Cooling power comparisons for TRNSYS-ULg averaged over each given hour of the day (left) and absolute maximum, mean, and minimum differences for a given hour of the day (right).

Table 6.9. Average overall uncertainty and 10 most influential input parameters from the n-way factorial analyses in Watts.

Parameter	**Forward**	**Backward**
Overall uncertainty	3.08	3.06
Average inside air temperature	-1.82	1.82
Floor surface temperature	0.92	-0.92
Fan power	0.92	-0.92
Outside air temperature	0.82	-0.82
Ceiling surface temperature	0.73	-0.73
North wall surface temperature	0.52	-0.52
East wall surface temperature	0.46	-0.46
Outer pane transmittance	0.39	-0.39
Diffuse horizontal solar irradiance	0.39	-0.36
West wall surface temperature	0.38	-0.38

Table 6.10. Statistical comparisons for cooling power in Exercise 3.

Parameter	Experiment	HELIOS	EnergyPlus	DOE-2.1E	ESP-r	TRNSYS-TUD	IDA-PAR	IDA-SIA	IDA-Detwind	TRNSYS-ULg
$\bar{x}$	166.6 W	166.0 W	163.4 W	176.6 W	161.4 W	176.9 W	161.6 W	159.8 W	164.9 W	166.1 W
s	116.1 W	119.3 W	101.5 W	117.7 W	99.0 W	106.2 W	105.4 W	101.4 W	112.3 W	107.0 W
x_{max}	847.9 W	845.5 W	767.5 W	780.0 W	750.2 W	816.1 W	816.8 W	792.8 W	829.1 W	797.9 W
x_{min}	54.1 W	67.8 W	83.5 W	106.0 W	82.3 W	93.2 W	73.9 W	73.8 W	68.8 W	84.6 W
$\overline{D}$	-	0.7 W	3.2 W	-10.0 W	5.2 W	-10.3 W	5.0 W	6.8 W	1.7 W	0.5 W
$\overline{\lvert D \rvert}$	-	8.7 W	12.8 W	13.5 W	19.0 W	20.8 W	13.1 W	14.3 W	11.0 W	10.4 W
$\lvert D_{max} \rvert$	-	79.6 W	140.5 W	93.6 W	213.1 W	140.7 W	114.0 W	131.4 W	79.0 W	116.2 W
$\lvert D_{min} \rvert$	-	0.0 W	0.1 W	0.0 W	0.0 W	0.2 W	0.0 W	0.0 W	0.1 W	0.0 W
D_{rms}	-	14.3 W	22.2 W	21.6 W	33.4 W	28.2 W	21.0 W	23.9 W	16.0 W	19.4 W
$\lvert D \rvert_{95\%}$	-	33.0 W	52.3 W	54.6 W	79.1 W	60.3 W	47.2 W	56.5 W	37.1 W	39.4 W
$\overline{OU}$	3.8 W	-	5.9 W	-	-	-	-	-	-	-
$\overline{UR}$	-	0.8	1.1	1.3	1.6	2.1	1.2	1.3	1.1	0.9
UR_{max}	-	6.1	9.3	9.3	10.4	13.8	8.5	8.4	8.0	8.1
UR_{min}	-	0.0	0.0	0.0	0.0	0.0	0.0	0.0	0.0	0.0
$\overline{\lvert D \rvert} / \bar{x} \times 100\%$	-	5.2%	7.7%	8.1%	11.4%	12.5%	7.8%	8.6%	6.6%	6.2%
$\overline{D} / \bar{x} \times 100\%$	-	0.4%	1.9%	-6.0%	3.1%	-6.2%	3.0%	4.1%	1.0%	0.3%

Program-to-program comparisons were also used to try to diagnose differences between the programs. One of these parameters, useful in assessing solar gain models, was the transmitted solar power through the glazing unit. Figure 6.7 contains a plot of the transmitted solar power averaged over each given hour of the day through the glazing unit for all programs.

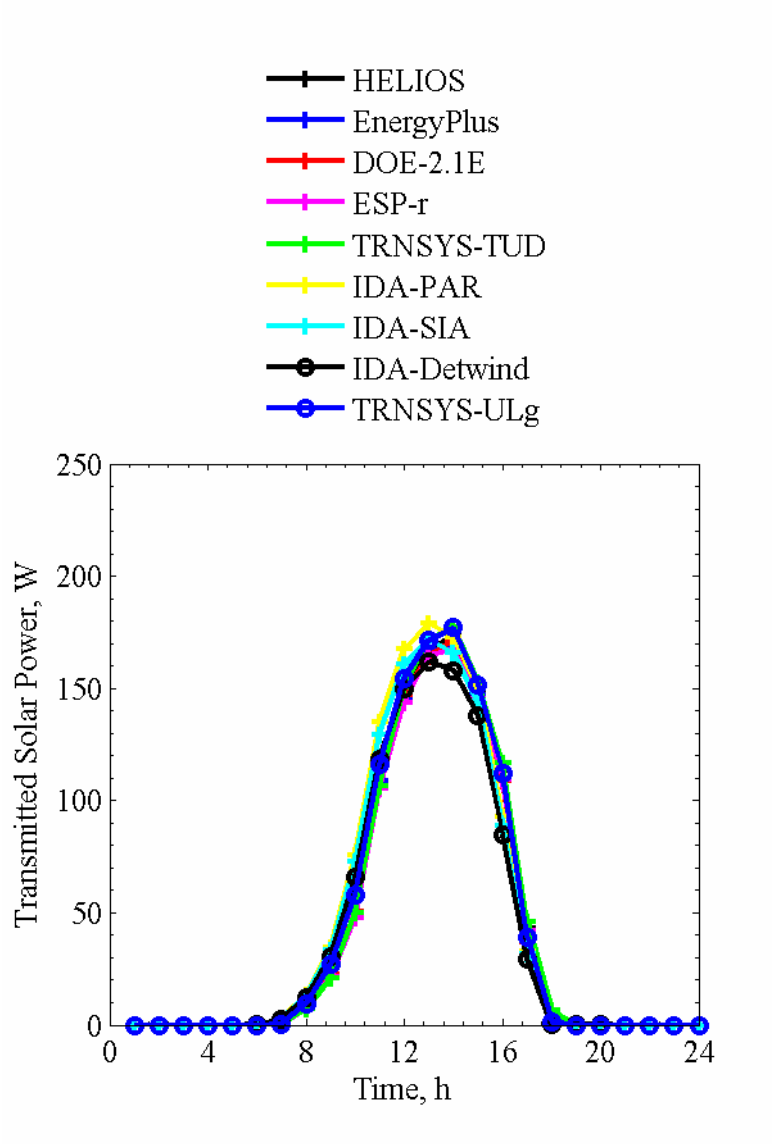

Figure 6.7. Transmitted solar power averaged over each given hour of the day.

Small differences were seen in the transmitted solar power which indicated that the window models were very similar. Therefore, many of the discrepancies in the predicted cooling powers from each simulation are a result of variations in internal and external heat transfer from convection and long-wave radiation and the modeling of internal short-wave radiation. In-depth analyses and discussion of these results are provided by Loutzenhiser et al. [15].

CHAPTER 7: EMPA GLAZING UNIT WITH EXTERIOR SHADING SCREEN (EXERCISE 4)

An experiment designed to evaluate the impact of solar gains through a glazing unit with a diffuse, exterior shading screen was run in the test cell from March 23 to April 16, 2005. Information concerning the properties and mounting of the exterior shading screen is provided.

7.1. Description of the Experiment

This section contains specific information about the experiment including the following information:

- geometry and optical properties of the exterior shading screen and
- thermophysical properties of test cell envelope.

7.1.1. Geometry and Optical Properties of the Exterior Shade Screen

For this experiment, an exterior shading screen was installed 10 cm from the glazing and is pictured in Figure 7.1. The shade was mounted to allow air to flow between gap of the external shade and the glazing; a dimensioned drawing of the shade position relative to the glazing is shown in Figure 7.2.

Figure 7.1. Photograph of the exterior shade mounted on the test cell.

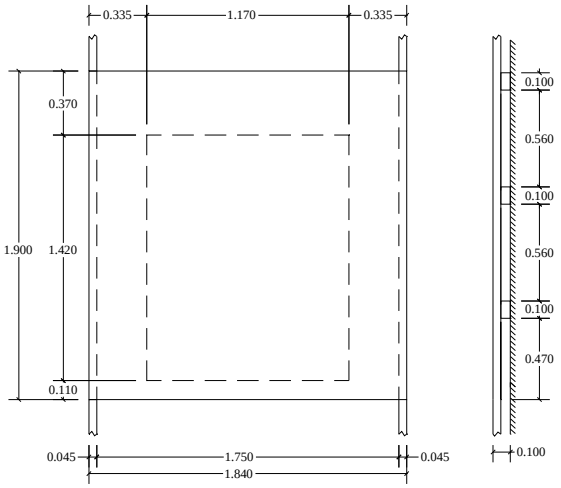

Figure 7.2. Dimensioned drawing of the external shade, in meters, relative to the glazing unit.

The optical properties of the shading screen were measured at normal incident angles using a spectrometer. The transmittance and reflectance as a function of wavelength from 250 nm to 2500 nm are contained in "Experiment 4.xls". The optical properties integrated over the solar spectrum for the shading screen were computed according to European Standard EN 410 [7] using GLAD software [8] and are shown in Table 7.1.

Table 7.1. Optical properties of the exterior shade.

Property	Quantity
Normal solar transmittance, %	21.5
Normal solar reflectance, %	59.6

7.1.2. Thermophysical Properties of the Test Cell Envelope

The mean envelope temperatures of the construction elements are shown in Table 7.2. The thermophysical properties, fixed at the mean construction element temperatures, are contained in Tables 7.3a to 7.3c.

Table 7.2. Mean temperatures for of the construction element during experiment.

Construction element	Mean temperature, °C
Ceiling, east, west, and north walls	22.58
Floor	22.34
South wall	16.34

Table 7.3a. Ceiling, north, east and west wall construction evaluated at 22.58°C.

Layer number	Material	Thickness mm	Thermal conductivity W/m-K	Density kg/m^3	Specific heat J/kg-K
1	Sheet steel	0.7	53.62	7837	460.8
2	PU foam	139	0.02230	30	1800
3	Sheet steel	0.7	53.62	7837	460.8

Table 7.3b. Floor construction evaluated at 22.34°C.

Layer number	Material	Thickness mm	Thermal conductivity W/m-K	Density kg/m^3	Specific heat J/kg-K
1	Sheet steel	0.7	53.62	7837	460.8
2	PU foam	140	0.02227	30	1800
3	PU foam (higher density)	20	0.070	45	1800
4	Sheet steel with surface structure	2.5	53.62	7837	460.8

Table 7.3c. South wall construction evaluated at 16.34°C.

Layer number	Material	Thickness mm	Thermal conductivity W/m-K	Density kg/m^3	Specific heat J/kg-K
1	Plywood	10	0.1384	850	1605
2	EPS foam	130	0.03564	28	1460
3	Plywood	10	0.1384	850	1605

7.2. Results

The empirical validation for this exercise focused on comparing cooling power. Plots for cooling power from HELIOS, EnergyPlus, DOE-2.1E, ESP-r, TRNSYS-TUD, IDA-SIA, and TRNSYS-ULg are shown in Figures 7.3a to 7.3g, respectively. Two plots are contained in each figure. Table 7.4 contains the overall and 10 most influential input uncertainties, averaged over the experiment, which impacted the cooling power predictions taken from the n-way factorial analysis. A summary of the statistical comparisons is contained in Table 7.5.

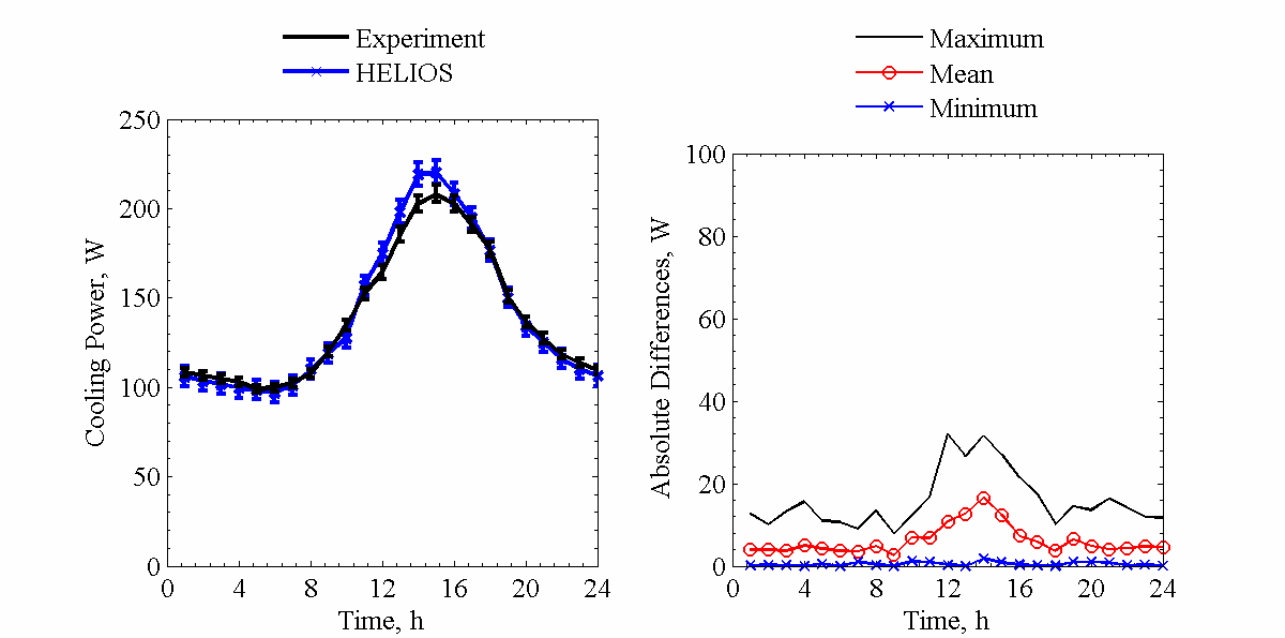

Figure 7.3a. Cooling power comparisons for HELIOS averaged over each given hour of the day (left) and absolute maximum, mean, and minimum differences for a given hour of the day (right).

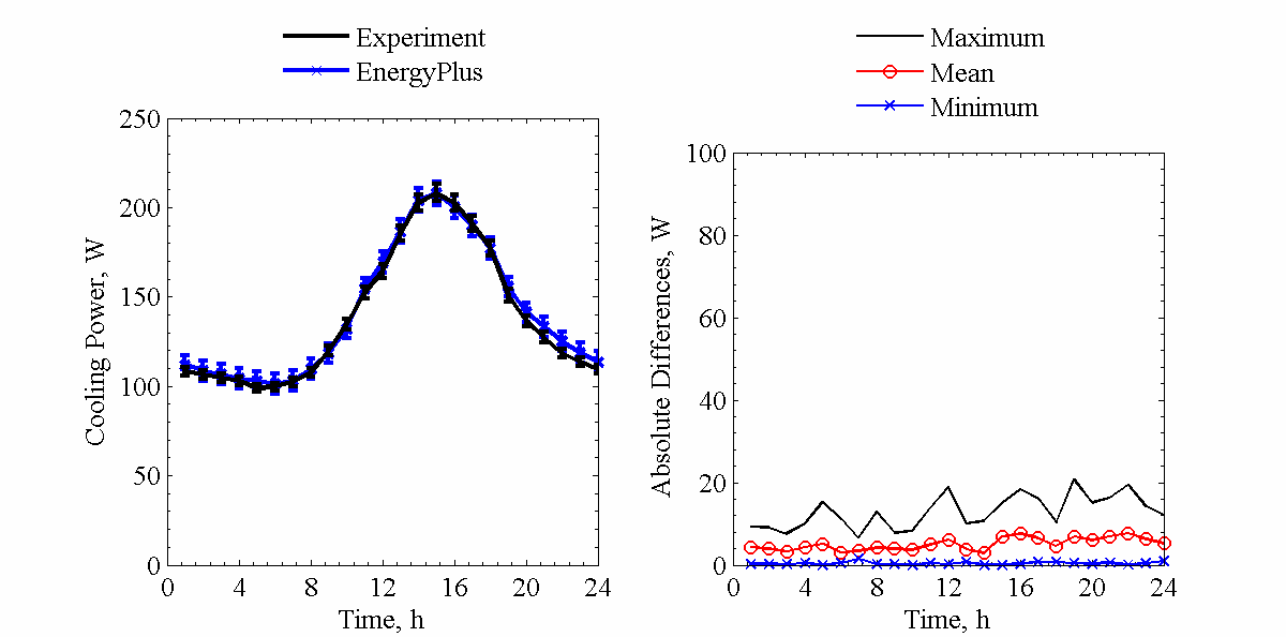

Figure 7.3b. Cooling power comparisons for EnergyPlus averaged over each given hour of the day (left) and absolute maximum, mean, and minimum differences for a given hour of the day (right).

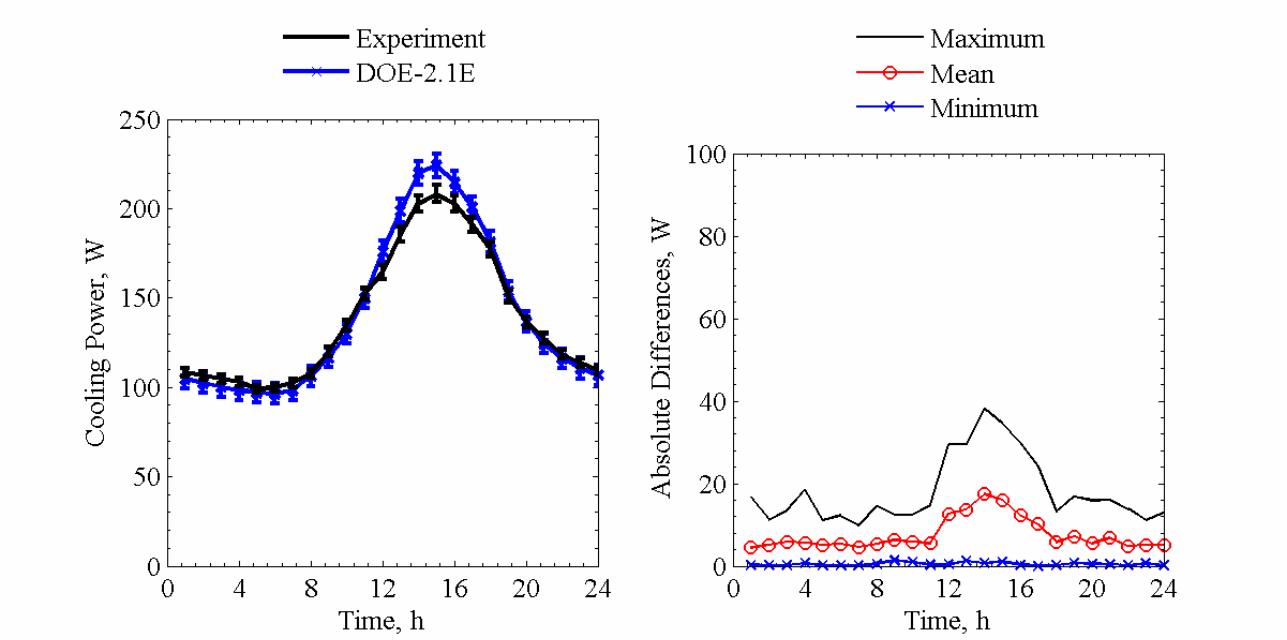

Figure 7.3c. Cooling power comparisons for DOE-2.1E averaged over each given hour of the day (left) and absolute maximum, mean, and minimum differences for a given hour of the day (right).

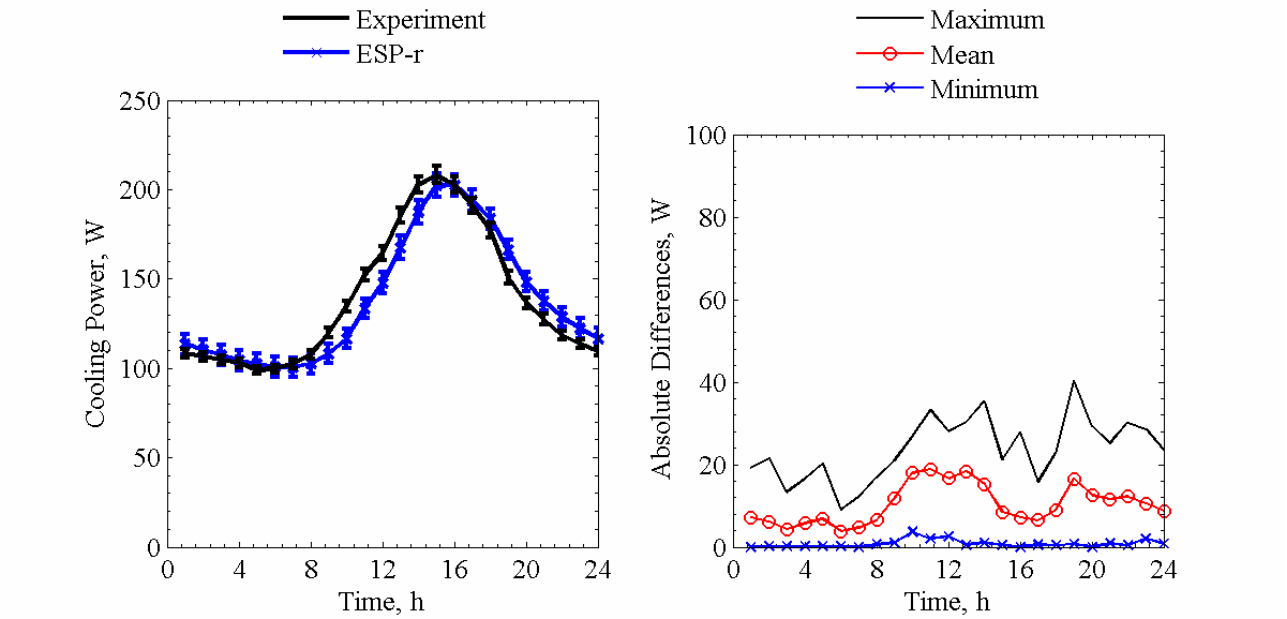

Figure 7.3d. Cooling power comparisons for ESP-r averaged over each given hour of the day (left) and absolute maximum, mean, and minimum differences for a given hour of the day (right).

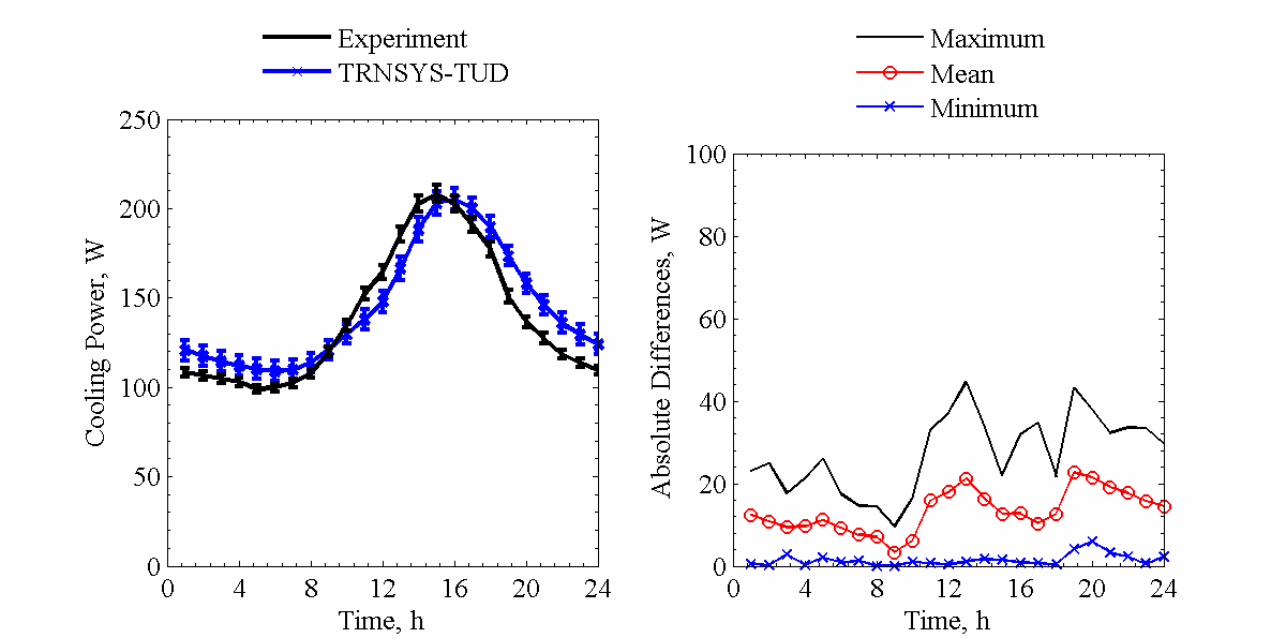

Figure 7.3e. Cooling power comparisons for TRNSYS-TUD averaged over each given hour of the day (left) and absolute maximum, mean, and minimum differences for a given hour of the day (right).

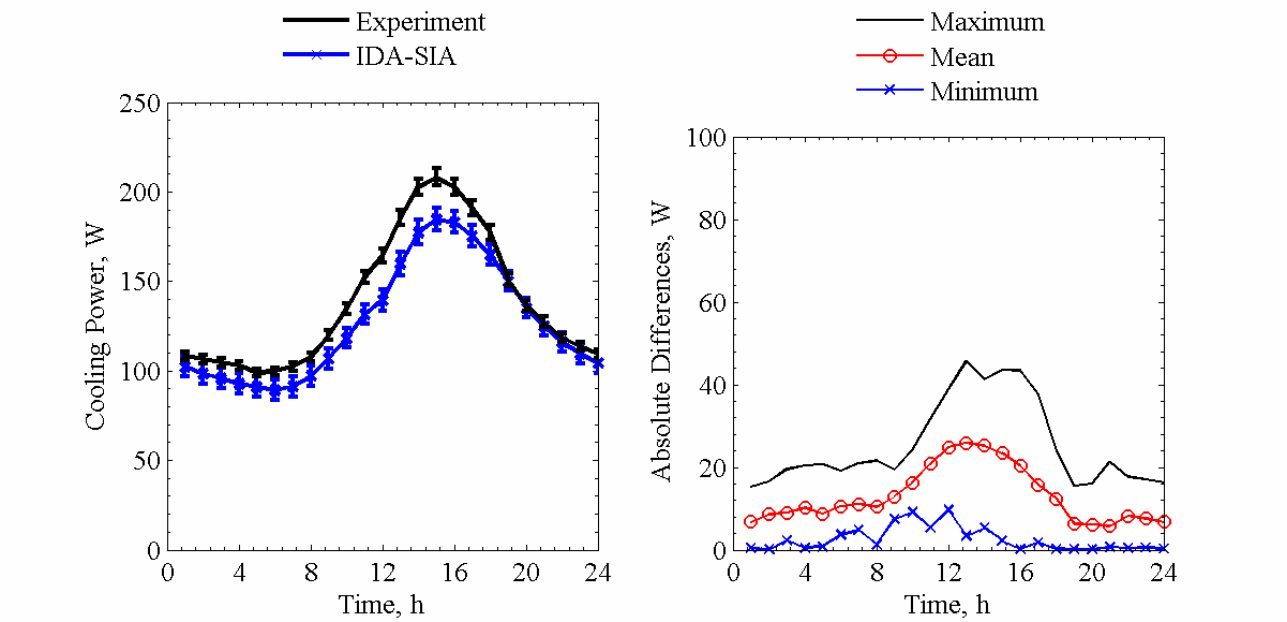

Figure 7.3f. Cooling power comparisons for IDA-SIA averaged over each given hour of the day (left) and absolute maximum, mean, and minimum differences for a given hour of the day (right).

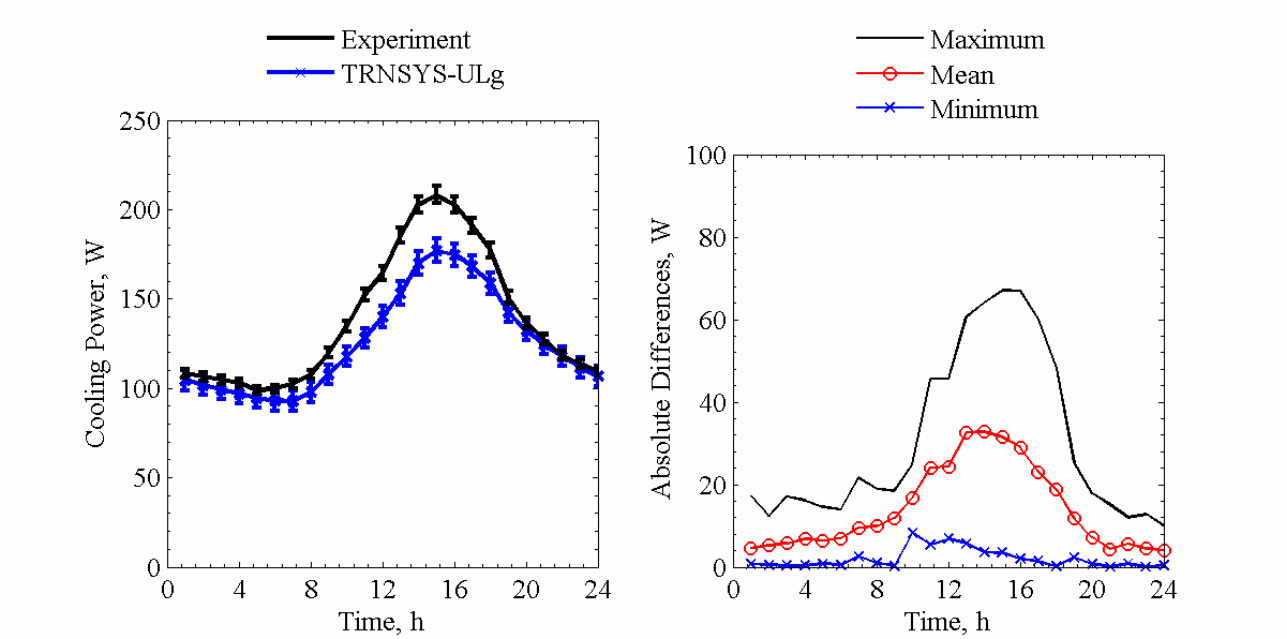

Figure 7.3g. Cooling power comparisons for TRNSYS-ULg averaged over each given hour of the day (left) and absolute maximum, mean, and minimum differences for a given hour of the day (right).

Table 7.4. Average overall uncertainty and 10 most influential input parameters from the n-way factorial analyses in Watts.

Parameter	**Forward**	**Backward**
Overall uncertainty	3.04	3.04
Average room air temperature	-1.83	1.83
Floor surface temperature	1.29	-1.30
Ceiling surface temperature	1.02	-1.02
Fan power	0.91	-0.91
Outside air temperature	0.89	-0.89
East wall surface temperature	0.68	-0.68
North wall surface temperature	0.50	-0.50
West wall surface temperature	0.37	-0.37
Transmittance of the outer glazing	0.18	-0.19
Diffuse horizontal solar irradiance	0.17	-0.18

Table 7.5. Statistical comparisons for cooling power in Exercise 4.

Parameter	Experiment	HELIOS	EnergyPlus	DOE-2.1E	ESP-r	TRNSYS-TUD	IDA-SIA	TRNSYS-ULg
$\bar{x}$	138.6 W	139.7 W	140.7 W	140.1 W	137.6 W	144.3 W	126.6 W	125.5 W
s	50.4 W	55.4 W	48.1 W	57.1 W	48.7 W	44.5 W	44.4 W	37.3 W
x_{max}	317.4 W	332.6 W	303.4 W	337.0 W	310.2 W	301.4 W	277.4 W	252.4 W
x_{min}	73.2 W	78.2 W	84.5 W	83.0 W	82.0 W	90.7 W	65.1 W	67.2 W
$\overline{D}$	-	-1.2 W	-2.1 W	-1.6 W	0.9 W	-5.7 W	11.9 W	13.1 W
$\overline{\lvert D \rvert}$	-	6.2 W	5.1 W	7.6 W	10.3 W	13.3 W	13.1 W	14.1 W
$\lvert D_{max} \rvert$	-	32.0 W	20.7 W	38.1 W	40.4 W	44.6 W	45.6 W	67.0 W
$\lvert D_{min} \rvert$	-	0.0 W	0.0 W	0.1 W	0.0 W	0.1 W	0.1 W	0.0 W
D_{rms}	-	8.6 W	6.5 W	10.3 W	13.3 W	16.3 W	16.5 W	20.7 W
$\lvert D \rvert_{95\%}$	-	19.2 W	13.3 W	23.9 W	26.8 W	32.0 W	36.6 W	54.7 W
$\overline{OU}$	3.1 W	-	5.8 W	-	-	-	-	-
$\overline{UR}$	-	0.6	0.6	0.8	1.1	1.5	1.4	1.4
UR_{max}	-	2.9	2.6	2.8	4.1	4.6	3.8	5.0
UR_{min}	-	0.0	0.0	0.0	0.0	0.0	0.0	0.0
$\overline{\lvert D \rvert} / \bar{x} \times 100\%$	-	4.4%	3.7%	5.5%	7.5%	9.6%	9.5%	10.1%
$\overline{D} / \bar{x} \times 100\%$	-	-0.9%	-1.5%	-1.1%	0.7%	-4.1%	8.6%	9.4%

Figure 7.4 contains a plot of the transmitted solar power for each given hour of the day through the glazing unit and exterior shading screen for all programs.

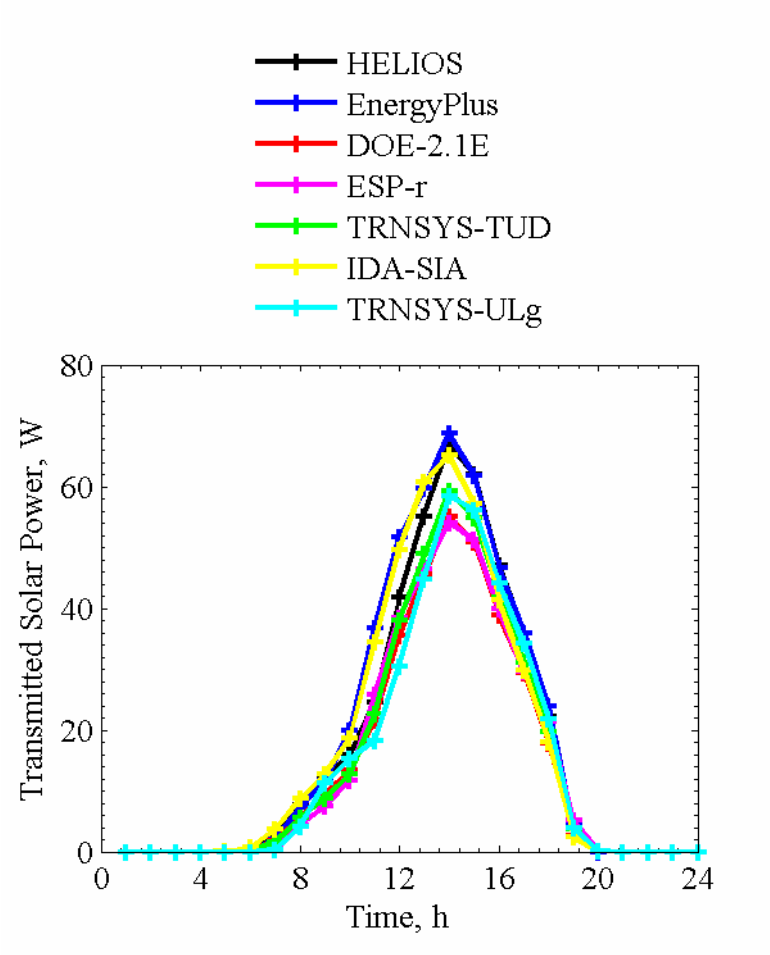

Figure 7.4. Transmitted solar power averaged over each given hour of the day.

The optical models used in each building energy simulation program used different assumptions to account for the shading screen; this in conjunction with modeling of the air gap and associated long-wave radiation exchange caused additional differences in predicted cooling power. However, the magnitude of the transmitted solar power was significantly reduced compared with the glazing only experiment resulting in closer cooling power predictions. In-depth analyses and discussion of these results are provided by Loutzenhiser et al. [16].

CHAPTER 8: EMPA GLAZING UNIT WITH AN INTERIOR SHADING SCREEN (EXERCISE 5)

An experiment designed to evaluate the impact of solar gains through a glazing with a diffuse, interior shading screen was run from June 8 to July 2, 2005. Information about the mounting of the interior shade and other parameters are provided in this chapter.

8.1. Description of the Experiment

This section contains specific information about the experiment, which includes the following information:

- geometry and optical properties of the interior shading screen and
- thermophysical properties of the test cell envelope.

8.1.1. Geometry and Optical Properties of the Interior Shade Screen

For this experiment, an interior shading screen was installed 16 cm from the glazing and is pictured in Figure 8.1. The shade was mounted to allow air to flow between gap of the interior shade and the glazing unit; a dimensioned drawing of the shade position relative to the glazing is shown in Figure 8.2.

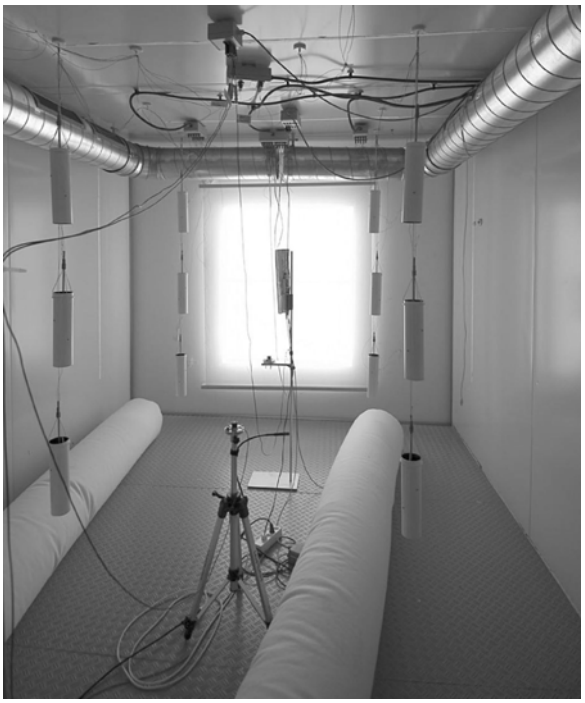

Figure 8.1. Photograph of the interior shade mounted on the test cell.

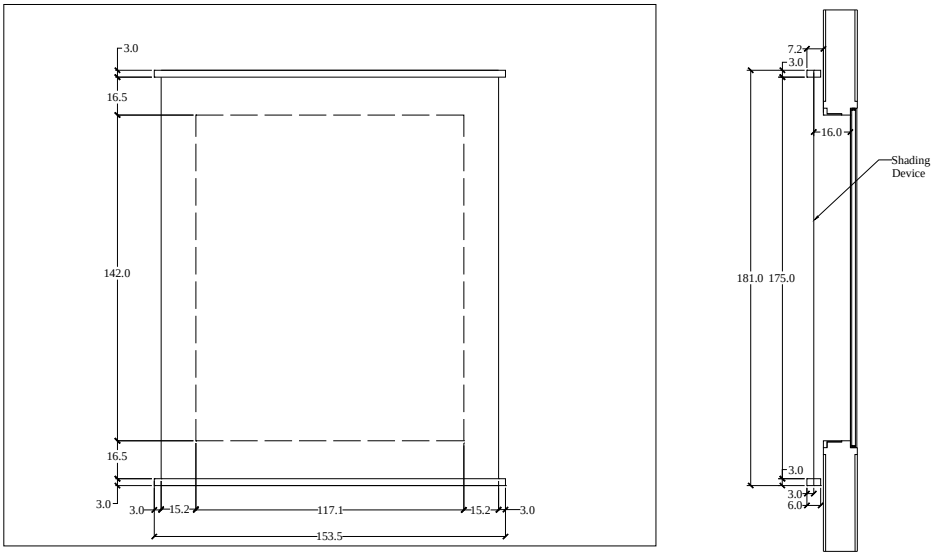

Figure 8.2. Dimensioned drawing of the interior shade, in centimeters, relative to the glazing.

The optical properties of the shade were measured at normal incident angles using a spectrometer. The transmittance and reflectance as a function of wavelength from 250 nm to 2500 nm are contained in "Experiment 5.xls". The optical properties for the interior shade were integrated over the solar spectrum according to EN 410 [7] using GLAD software [8] and are shown in Table 8.1.

Table 8.1. Optical properties of the interior shading screen.

Property	**Quantity**
Normal solar transmittance, %	30.4
Normal solar reflectance, %	59.4

8.1.2. Thermophysical Properties of the Test Cell Envelope

The mean envelope temperatures of the construction elements are shown in Table 8.2. The thermophysical properties, fixed at the mean construction element temperatures, are contained in Tables 8.3a to 8.3c.

Table 8.2. Mean temperatures for of the construction element during experiment.

Construction element	**Mean temperature, °C**
Ceiling, east, west, and north walls	22.83
Floor	22.75
South wall	20.91

Table 8.3a. Ceiling, north, east and west wall construction evaluated at 22.83°C.

Layer number	**Material**	**Thickness mm**	**Thermal conductivity W/m-K**	**Density Kg/m^3**	**Specific heat J/kg-K**
1	Sheet steel	0.7	53.62	7837	460.8
2	PU foam	139	0.02234	30	1800
3	Sheet steel	0.7	53.62	7837	460.8

Table 8.3b. Floor construction evaluated at 22.75°C.

Layer number	**Material**	**Thickness mm**	**Thermal conductivity W/m-K**	**Density kg/m^3**	**Specific heat J/kg-K**
1	Sheet steel	0.7	53.62	7837	460.8
2	PU foam	140	0.02233	30	1800
3	PU foam (higher density)	20	0.070	45	1800
4	Sheet steel with surface Structure	2.5	53.62	7837	460.8

Table 8.3c. South wall construction evaluated at 20.91°C.

Layer number	Material	Thickness mm	Thermal conductivity W/m-K	Density Kg/m^3	Specific heat J/kg-K
1	Plywood	10	0.1404	850	1605
2	EPS foam	130	0.03622	28	1460
3	Plywood	10	0.1404	850	1605

8.2. Results

The empirical validation for this exercise focused on comparing cooling power. Plots for cooling power from HELIOS, EnergyPlus, DOE-2.1E, ESP-r, TRNSYS-TUD, IDA-SIA, and TRNSYS-ULg are shown in Figures 8.3a to 8.3d, respectively. Table 8.4 contains the average overall and 10 most influential input uncertainties that impacted the cooling power predictions taken from the n-way factorial analysis. A summary of the statistical comparisons is contained in Table 8.5.

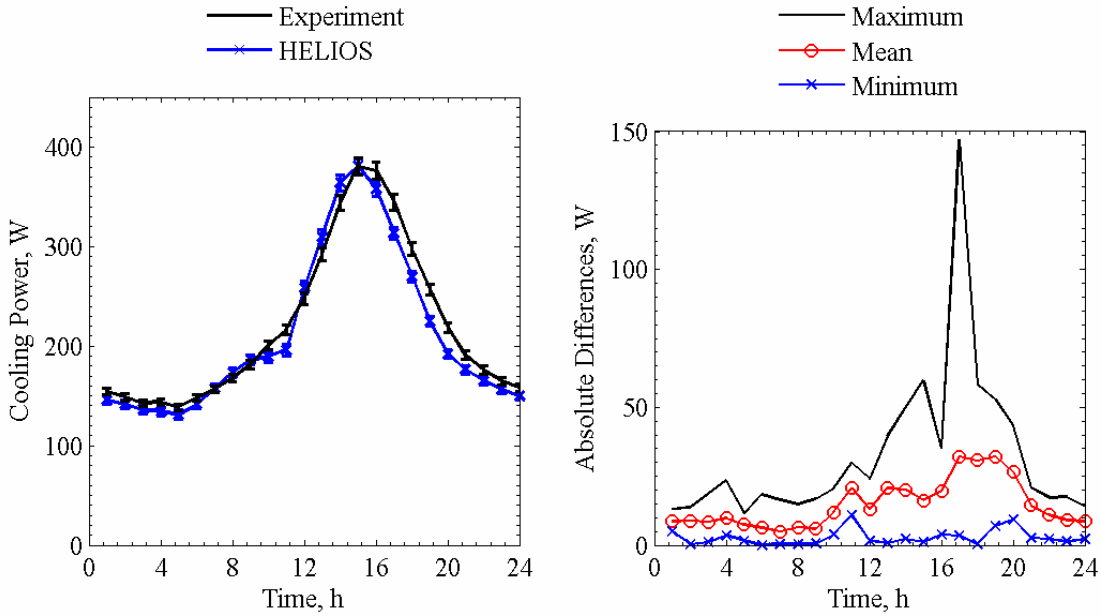

Figure 8.3a. Cooling power comparisons for HELIOS averaged over each given hour of the day (left) and absolute maximum, mean, and minimum differences for a given hour of the day (right).

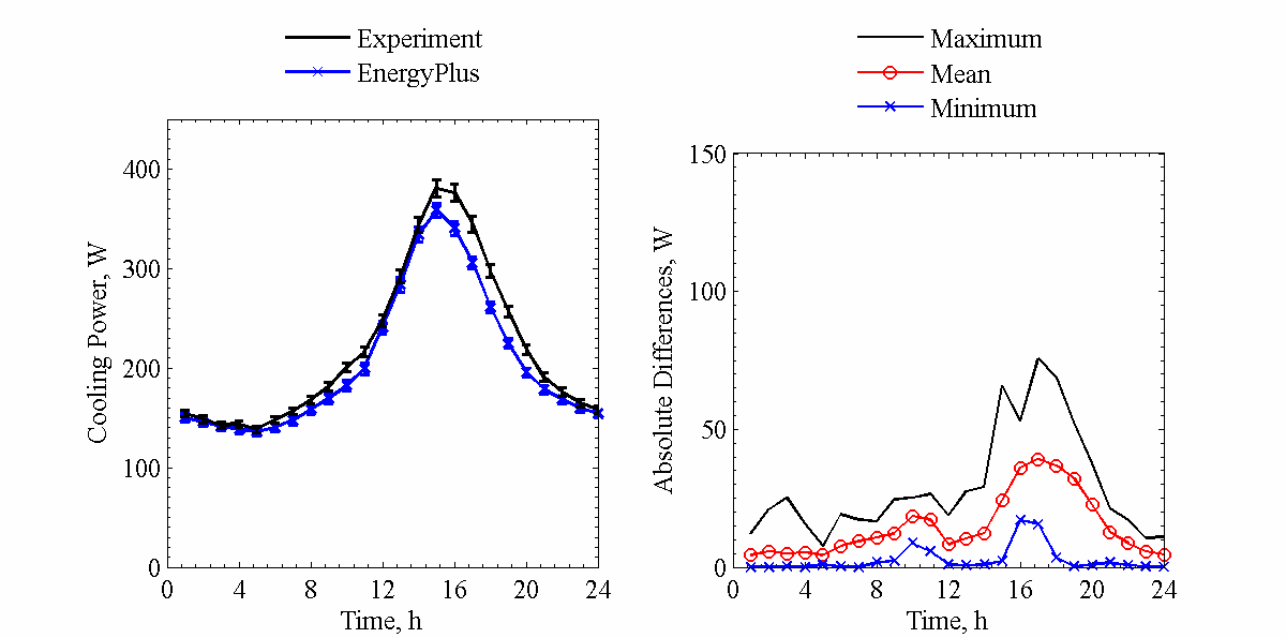

Figure 8.3b. Cooling power comparisons for EnergyPlus averaged over each given hour of the day (left) and absolute maximum, mean, and minimum differences for a given hour of the day (right).

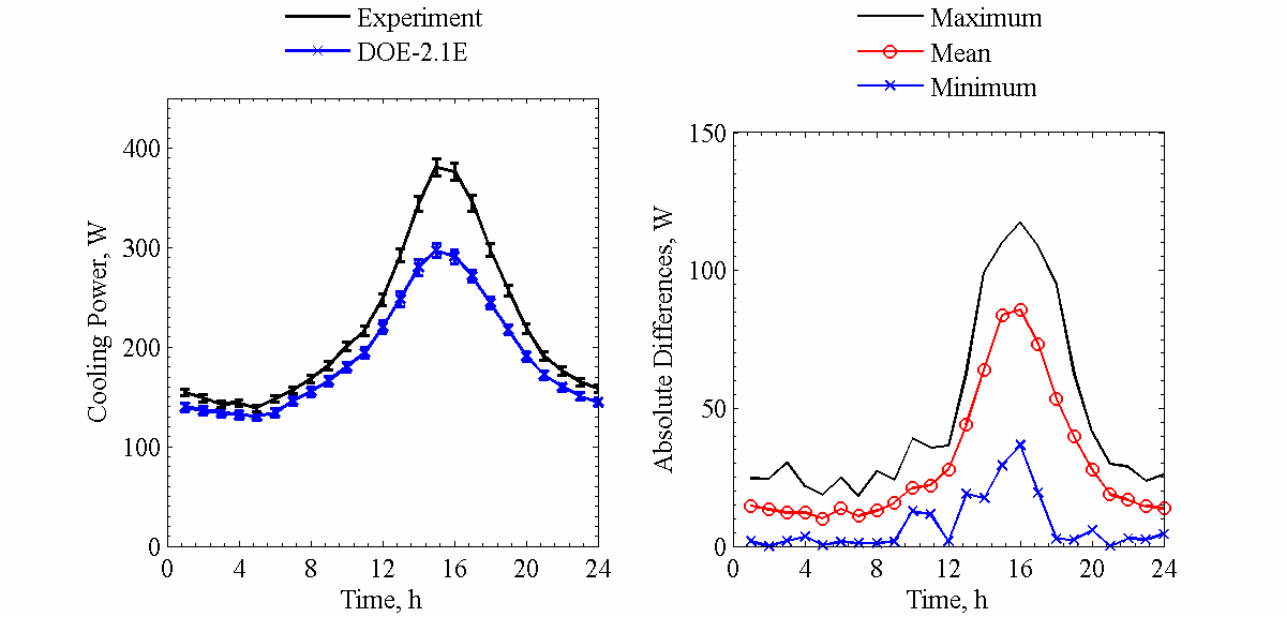

Figure 8.3c. Cooling power comparisons for DOE-2.1E averaged over each given hour of the day (left) and absolute maximum, mean, and minimum differences for a given hour of the day (right).

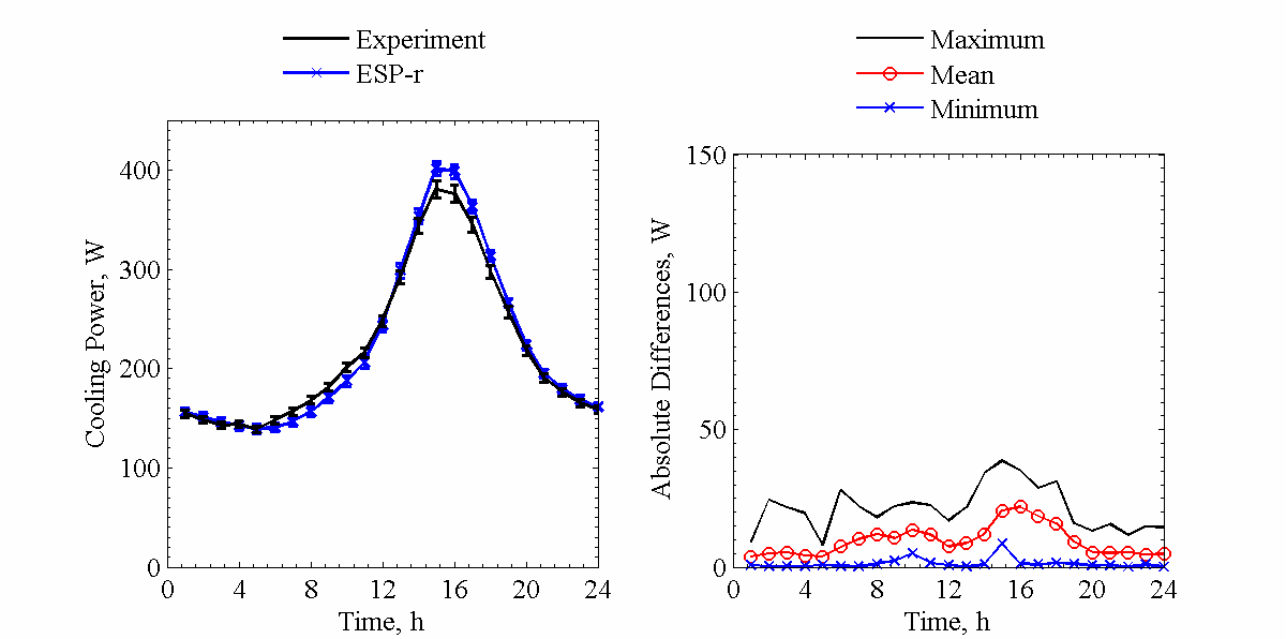

Figure 8.3d. Cooling power comparisons for ESP-r averaged over each given hour of the day (left) and absolute maximum, mean, and minimum differences for a given hour of the day (right).

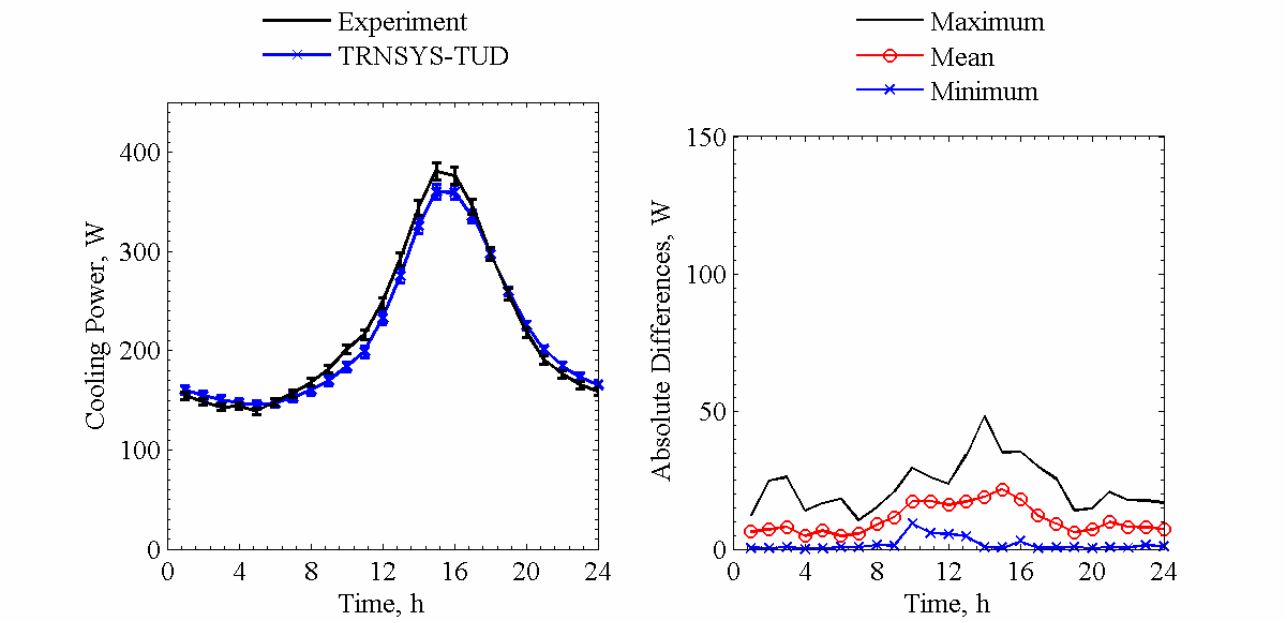

Figure 8.3e. Cooling power comparisons for TRNSYS-TUD averaged over each given hour of the day (left) and absolute maximum, mean, and minimum differences for a given hour of the day (right).

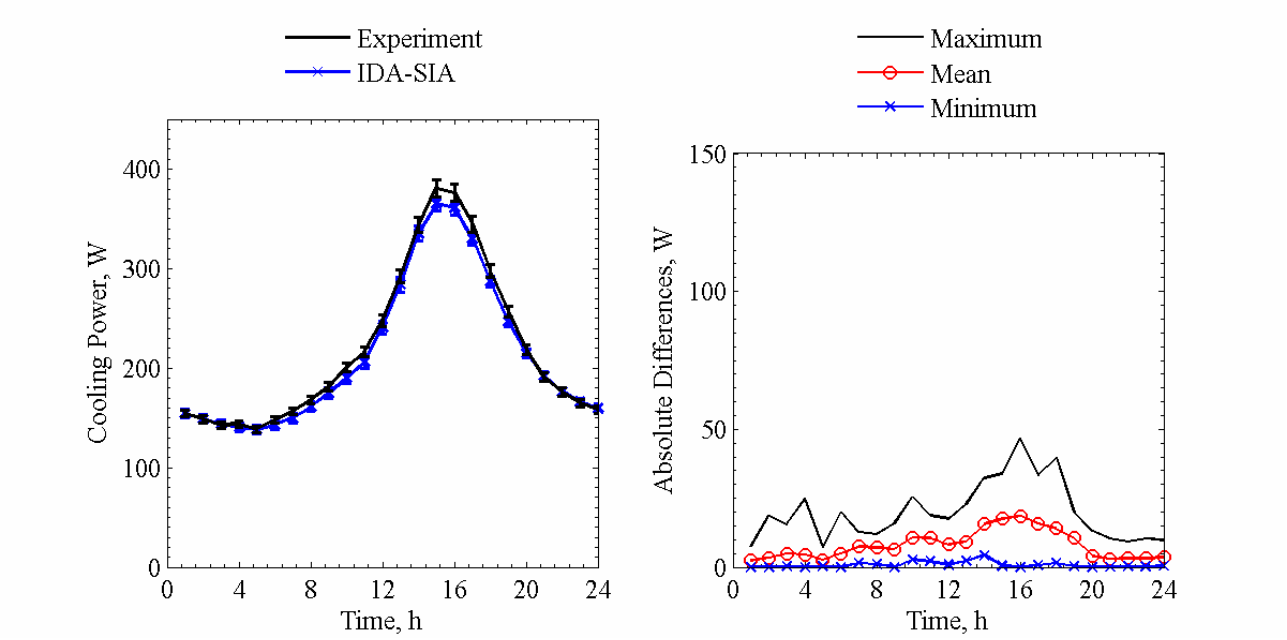

Figure 8.3f. Cooling power comparisons for IDA-SIA averaged over each given hour of the day (left) and absolute maximum, mean, and minimum differences for a given hour of the day (right).

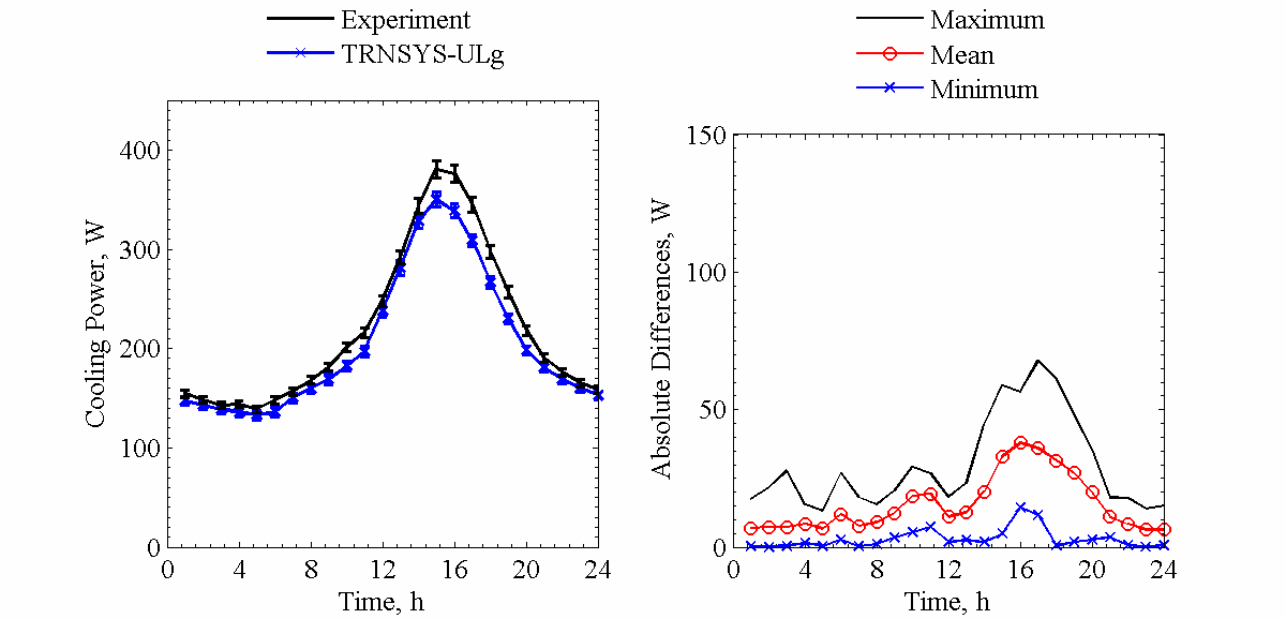

Figure 8.3g. Cooling power comparisons for TRNSYS-ULg averaged over each given hour of the day (left) and absolute maximum, mean, and minimum differences for a given hour of the day (right).

Table 8.4. Average overall uncertainty and 10 most influential input parameters from the n-way factorial analyses in Watts.

Parameter	**Forward**	**Backward**
Overall uncertainty	2.66	2.63
Average room air temperature	-1.39	1.40
Fan power	0.89	-0.89
Outside air temperature	0.88	-0.87
North wall surface temperature	0.71	-0.71
Ceiling surface temperature	0.60	-0.60
West wall surface temperature	0.48	-0.48
Floor surface temperature	0.40	-0.39
Inner glazing front reflectance	-0.37	0.29
Transmittance of the outer glazing	0.36	-0.32
Diffuse horizontal solar irradiance	0.34	-0.34

Table 8.5. Statistical comparisons for cooling power in Exercise 5.

Parameter	**Experiment**	**HELIOS**	**EnergyPlus**	**DOE-2.1E**	**ESP-r**	**TRNSYS-TUD**	**IDA-SIA**	**TRNSYS-ULg**
$\bar{x}$	218.7 W	210.4 W	204.8 W	188.9 W	221.2 W	215.0 W	212.9 W	203.9 W
s	85.2 W	85.3 W	76.5 W	58.8 W	92.1 W	77.2 W	79.6 W	75.3 W
x_{max}	459.4 W	441.5 W	419.5 W	342.0 W	477.4 W	435.8 W	431.7 W	411.4 W
x_{min}	100.6 W	107.3 W	119.9 W	119.0 W	116.7 W	124.5 W	111.5 W	115.8 W
$\overline{D}$	-	8.2 W	13.9 W	29.7 W	-2.5 W	3.7 W	5.8 W	14.8 W
$\overline{\lvert D \rvert}$	-	14.8 W	14.7 W	30.1 W	9.4 W	10.8 W	8.0 W	15.7 W
$\lvert D_{max} \rvert$	-	146.9 W	75.7 W	117.4 W	38.7 W	48.2 W	46.7 W	67.7 W
$\lvert D_{min} \rvert$	-	0.1 W	0.1 W	0.0 W	0.0 W	0.1 W	0.0 W	0.0 W
D_{rms}	-	19.9 W	20.2 W	40.6 W	12.3 W	13.5 W	11.1 W	20.5 W
$\lvert D \rvert_{95\%}$	-	40.6 W	44.0 W	94.8 W	25.7 W	26.5 W	24.7 W	43.8 W
$\overline{OU}$	4.9 W	-	5.2 W	-	-	-	-	-
$\overline{UR}$	-	1.4	1.3	2.6	0.9	1.0	0.7	1.4
UR_{max}	-	11.3	5.8	7.7	3.5	3.7	3.2	5.2
UR_{min}	-	0.0	0.0	0.0	0.0	0.0	0.0	0.0
$\overline{\lvert D \rvert} / \bar{x} \times 100\%$	-	6.7%	6.7%	13.8%	4.3%	4.9%	3.7%	7.2%
$\overline{D} / \bar{x} \times 100\%$	-	3.8%	6.4%	13.6%	-1.1%	1.7%	2.6%	6.8%

Figure 8.4 contains a plot of the transmitted solar power for a given hour of the day through the glazing unit and interior shading screen for all programs.

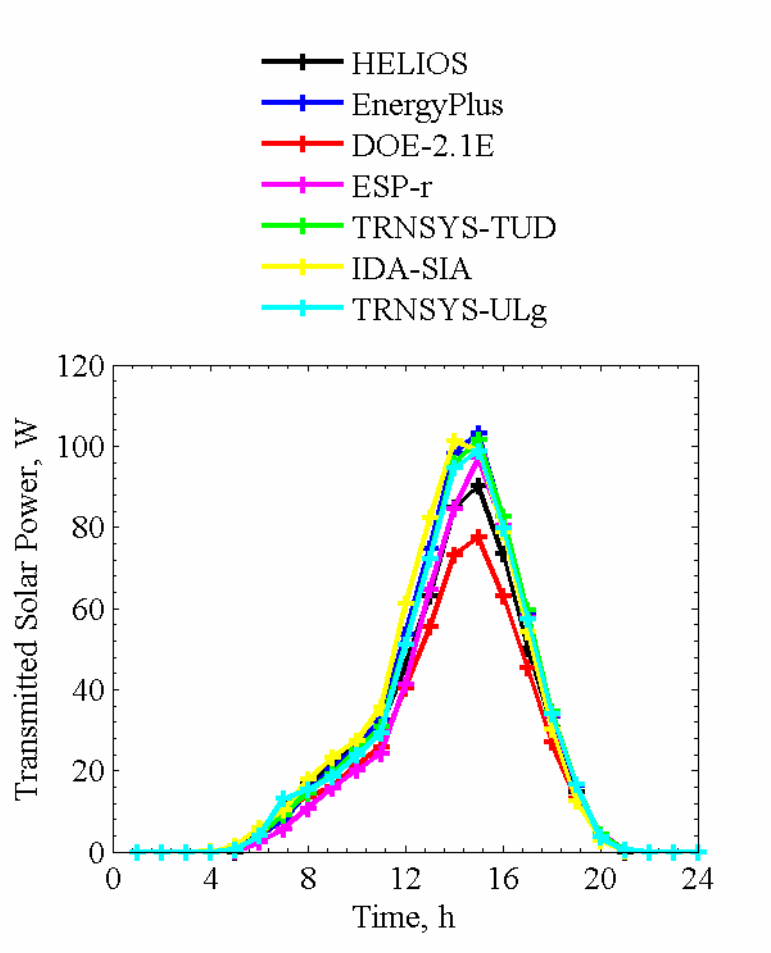

Figure 8.4. Transmitted solar power averaged over each given hour of the day.

Many of the same modeling challenges and differences in the optical model from the exterior shading screen exercise were also apparent in this simulation exercise. In-depth analyses and discussion of these results are provided by Loutzenhiser et al. [16].

CHAPTER 9: GLAZING UNIT WITH EXTERIOR VENETIAN BLIND (EXERCISE 6)

An experiment designed to evaluate the impact of solar gains through a glazing unit with an exterior Venetian blind assembly was run in the EMPA test cell from July 16 to September 5, 2005. The first part of the experiment was performed with the slats in the horizontal position, and the second part was with the outer slat blade (farthest from the glazing unit) tilted downward toward the ground at a 45° angle; the slat position was changed on August 16, 2005 at 7:00 AM. Information about exterior Venetian blind mounting and the results from this exercise are provided.

9.1. Description of the Experiment

This section contains specific information about the experiment, which includes the following information:

- geometry and optical properties of the exterior Venetian blind assembly and
- thermophysical properties of the test cell envelope.

9.1.1. Geometry and Optical Properties of the Exterior Venetian Blind Assembly

For this experiment, an exterior Venetian blind assembly was installed 1.0 cm from the exterior glazing surface and is pictured in Figure 9.1. A dimensioned drawing of the blind position relative to the glazing unit and the geometry of the blind slat are shown in Figures 9.2 and 9.3, respectively.

Figure 9.1. Photograph of the exterior blind mounted in front of the test cell.

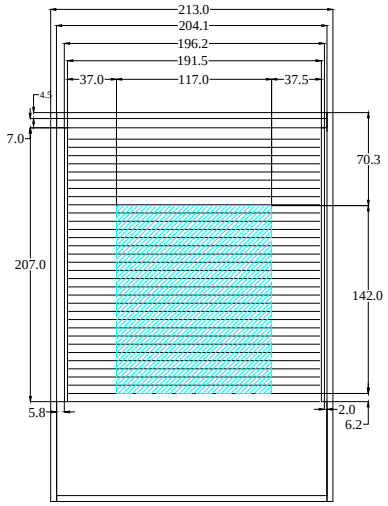

Figure 9.2. Dimensioned drawing of the exterior Venetian blind, in centimeters, relative to the glazing.

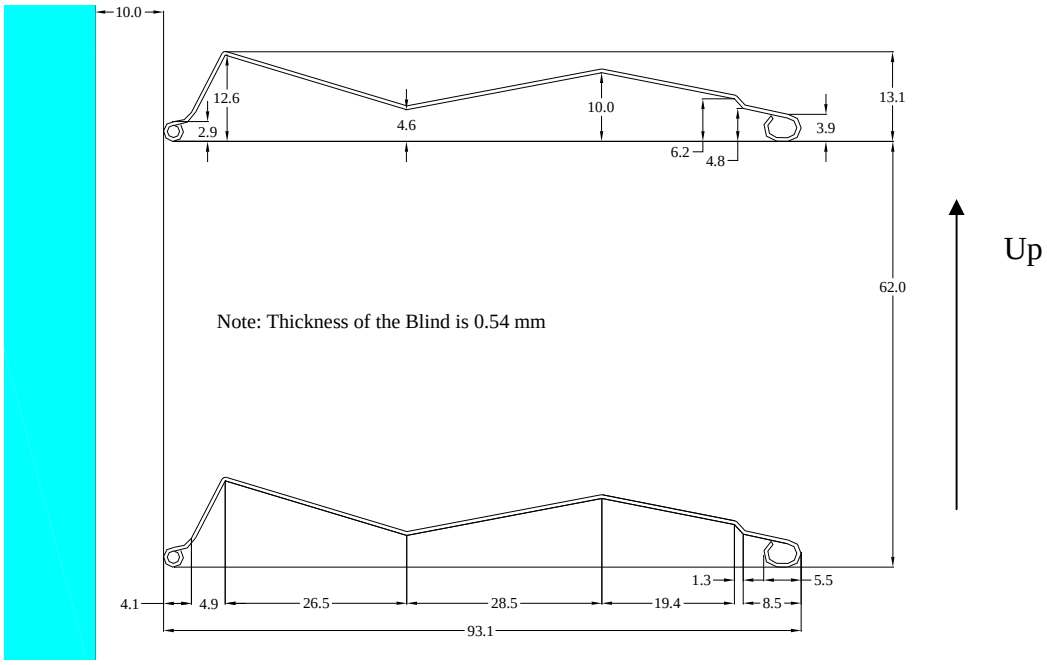

Figure 9.3. Dimensioned cross-section of the blind slats positions relative to the glazing unit in millimeters.

The optical properties of the exterior blind were measured at normal incident angles using a spectrometer. The transmittance and reflectance as a function of wavelength from 250 nm to 2500 nm can be found in "Experiment 6.xls". The solar reflectance, computed according to European Standard EN 410 [7] using GLAD software [8], and hemispherical emittance, measured with an emissometer based on a calorimetric method, are shown in Table 9.1.

Table 9.1. Optical properties of the slat surfaces.

Property	**Quantity**
Normal solar reflectance, %	44.1
Hemispherical emittance, %	86.2

9.1.2. Thermophysical Properties of the Test Cell Envelope

Table 9.2 contains the mean envelope temperatures for both blind slat positions. The thermophysical properties evaluated at these mean construction element temperatures are contained in Tables 9.3a to 9.3c for the Venetian blinds horizontally positioned and Tables 9.4a to 9.4c when tilted downward 45°.

Table 9.2. Mean temperatures for of the construction element during experiment.

Construction element	**Mean temperature, °C**	
	Horizontal	**45° Downward**
Ceiling, east, west, and north walls	22.72	20.83
Floor	22.72	20.83
South wall	20.82	20.90

Table 9.3a. Ceiling, north, east and west wall construction evaluated at 22.72°C.

Layer number	**Material**	**Thickness mm**	**Thermal conductivity W/m-K**	**Density kg/m^3**	**Specific heat J/kg-K**
1	Sheet steel	0.7	53.62	7837	460.8
2	PU foam	139	0.02232	30	1800
3	Sheet steel	0.7	53.62	7837	460.8

Table 9.3b. Floor construction evaluated at 22.72°C.

Layer number	Material	Thickness mm	Thermal conductivity W/m-K	Density kg/m^3	Specific heat J/kg-K
1	Sheet steel	0.7	53.62	7837	460.8
2	PU foam	140	0.02232	30	1800
3	PU foam (higher density)	20	0.070	45	1800
4	Sheet steel with surface structure	2.5	53.62	7837	460.8

Table 9.3c. South wall construction evaluated at 20.82°C.

Layer number	Material	Thickness mm	Thermal conductivity W/m-K	Density kg/m^3	Specific heat J/kg-K
1	Plywood	10	0.1400	850	1605
2	EPS foam	130	0.03620	28	1460
3	Plywood	10	0.1400	850	1605

Table 9.4a. Ceiling, north, east and west wall construction evaluated at 22.83°C.

Layer number	Material	Thickness mm	Thermal conductivity W/m-K	Density kg/m^3	Specific heat J/kg-K
1	Sheet steel	0.7	53.62	7837	460.8
2	PU foam	139	0.02234	30	1800
3	Sheet steel	0.7	53.62	7837	460.8

Table 9.4b. Floor construction evaluated at 22.83°C.

Layer number	Material	Thickness mm	Thermal conductivity W/m-K	Density kg/m^3	Specific heat J/kg-K
1	Sheet steel	0.7	53.62	7837	460.8
2	PU foam	140	0.02232	30	1800
3	PU foam (higher density)	20	0.070	45	1800
4	Sheet steel with surface structure	2.5	53.62	7837	460.8

Table 9.4c. South wall construction evaluated at 20.90°C.

Layer number	Material	Thickness mm	Thermal conductivity W/m-K	Density kg/m^3	Specific heat J/kg-K
1	Plywood	10	0.1400	850	1605
2	EPS foam	130	0.03621	28	1460
3	Plywood	10	0.1400	850	1605

9.2. Results

The empirical validation for this exercise focused on comparing the measured cooling power in the test cell during the experiment with the predicted cooling powers from each building energy simulation program. Results are provided in two sections to reflect and assess the performances of the building energy simulation programs for both Venetian blind slat positions.

9.2.1. Horizontally Positioned Venetian Blind Slat Position

Plots for cooling power from HELIOS, EnergyPlus, TRNSYS-TUD, and TRNSYS-ULg are shown in Figures 9.4a and 9.4d, respectively. Comparisons were made for a 20 day period from July 24 to August 12, 2005. Two plots are contained in each figure. Table 9.5 contains the average overall and the 10 most influential input uncertainties that impacted the cooling power predictions taken from the n-way factorial analysis. A summary of the statistical comparisons is contained in Table 9.6.

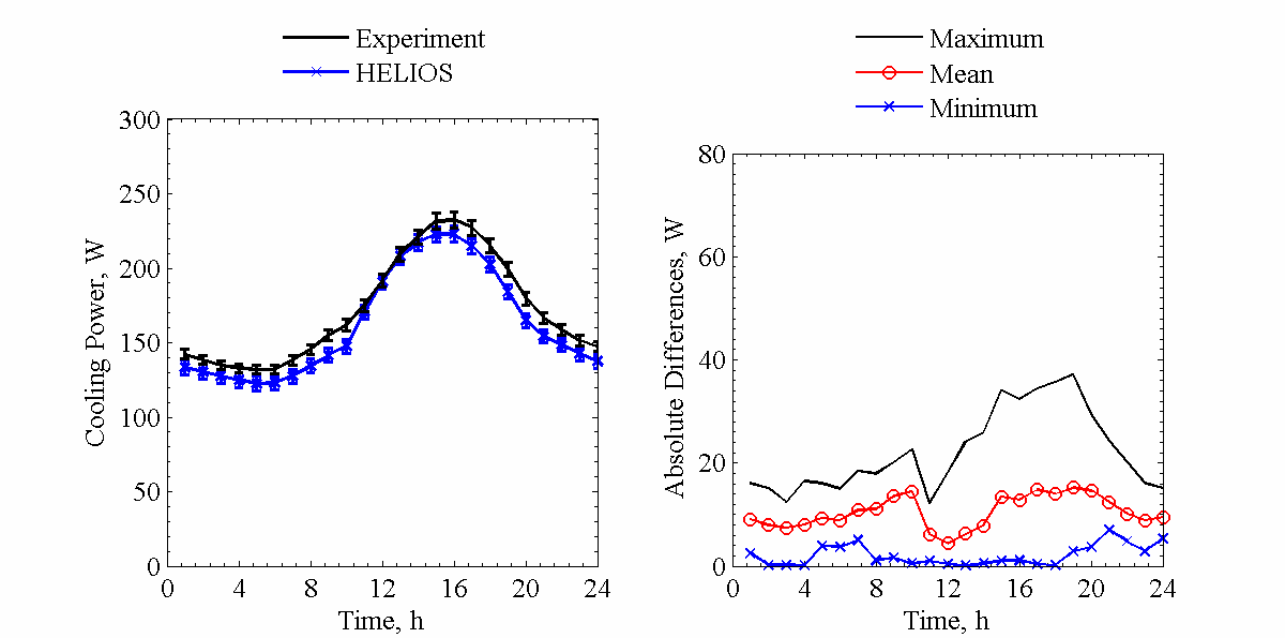

Figure 9.4a. Cooling power comparisons for HELIOS averaged over each given hour of the day (left) and absolute maximum, mean, and minimum differences for a given hour of the day (right).

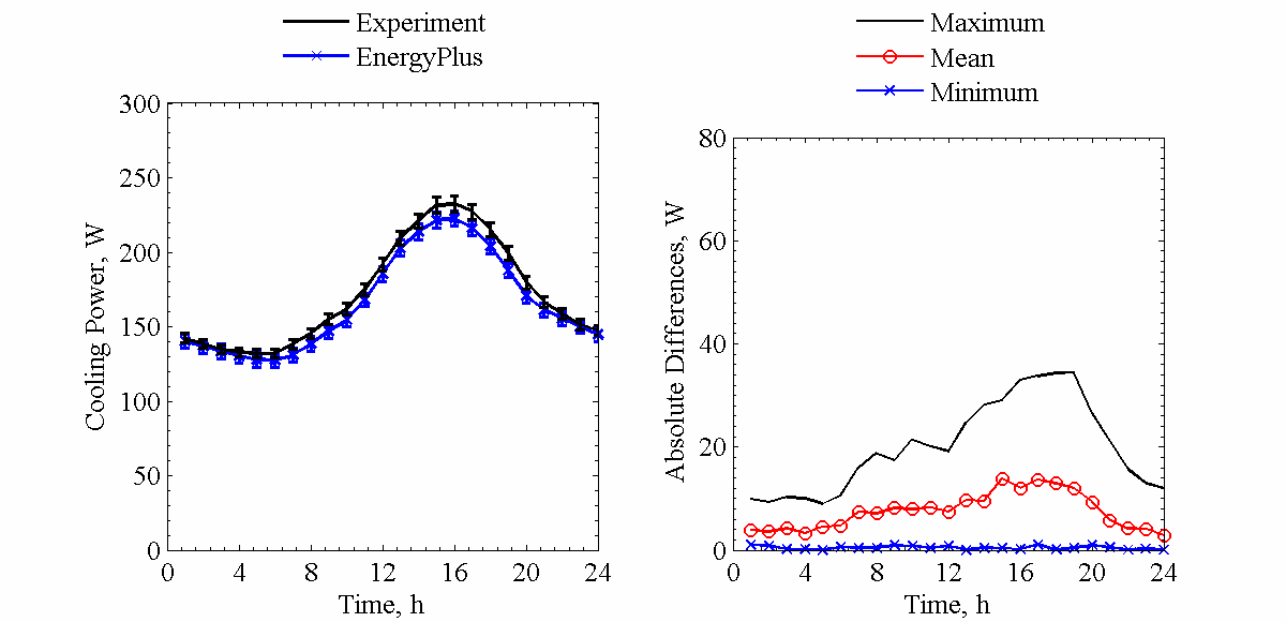

Figure 9.4b. Cooling power comparisons for EnergyPlus averaged over each given hour of the day (left) and absolute maximum, mean, and minimum differences for a given hour of the day (right).

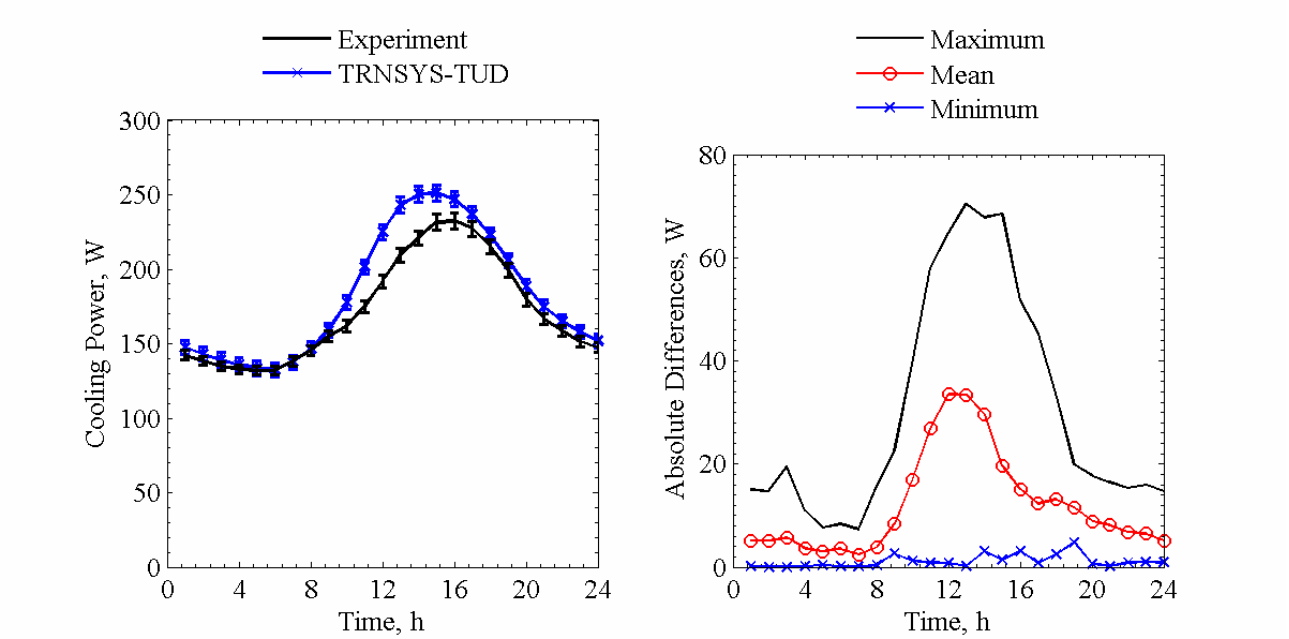

Figure 9.4c. Cooling power comparisons for TRNSYS-TUD averaged over each given hour of the day (left) and absolute maximum, mean, and minimum differences for a given hour of the day (right).

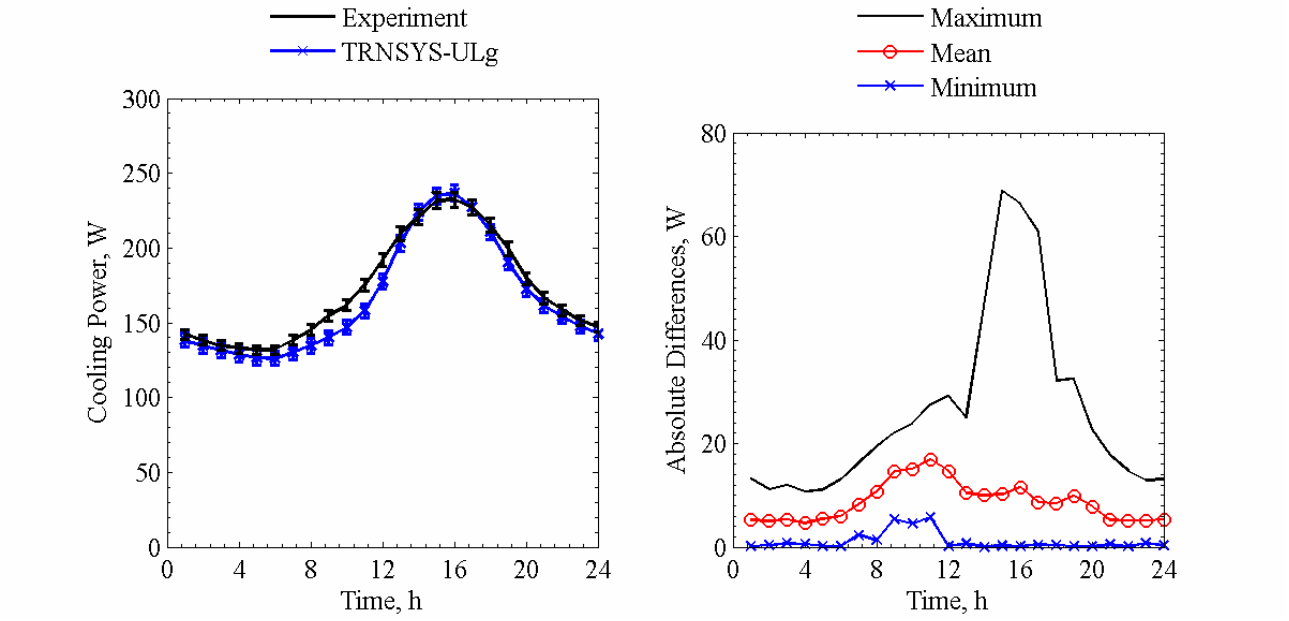

Figure 9.4d. Cooling power comparisons for TRNSYS-ULg averaged over each given hour of the day (left) and absolute maximum, mean, and minimum differences for a given hour of the day (right).

Table 9.5. Average overall uncertainty and 10 most influential input parameters from the n-way factorial analyses in Watts.

Parameter	**Forward**	**Backward**
Overall uncertainty	2.28	2.28
Average inside air temperature	-1.36	1.37
Fan power	0.89	-0.89
Outside air temperature	0.82	-0.82
North wall temperature	0.71	-0.71
Ceiling temperature	0.60	-0.60
West wall surface temperature	0.47	-0.47
Floor surface temperature	0.39	-0.39
East wall surface temperature	0.32	-0.32
Diffuse horizontal solar irradiance	0.23	-0.22
Global horizontal infrared irradiance	0.18	-0.18

Table 9.6. Statistical comparisons for cooling power in Exercise 6 with slats horizontally positioned.

Parameter	**Experiment**	**HELIOS**	**EnergyPlus**	**TRNSYS-TUD**	**TRNSYS-ULg**
$\bar{x}$	171.6 W	162.3 W	165.4 W	182.3 W	165.8 W
s	43.2 W	41.8 W	38.5 W	49.8 W	44.7 W
x_{max}	330.4 W	298.1 W	297.4 W	328.5 W	314.5 W
x_{min}	102.4 W	95.5 W	102.8 W	112.0 W	101.9 W
$\overline{D}$	-	9.4 W	6.2 W	-10.6 W	5.9 W
$\overline{\lvert D \rvert}$	-	10.5 W	7.5 W	12.0 W	8.7 W
$\lvert D_{max} \rvert$	-	37.2 W	34.4 W	70.5 W	68.8 W
$\lvert D_{min} \rvert$	-	0.1 W	0.0 W	0.0 W	0.0 W
D_{rms}	-	12.4 W	10.4 W	17.9 W	11.9 W
$\lvert D \rvert_{95\%}$	-	22.7 W	22.8 W	42.6 W	23.0 W
$\overline{OU}$	3.9 W	-	4.8 W	-	-
$\overline{UR}$	-	1.2	0.8	1.3	1.0
UR_{max}	-	3.2	3.0	7.4	6.5
UR_{min}	-	0.0	0.0	0.0	0.0
$\overline{\lvert D \rvert} / \bar{x} \times 100\%$	-	6.1%	4.4%	7.0%	5.1%
$\overline{D} / \bar{x} \times 100\%$	-	5.5%	3.6%	-6.2%	3.4%

Figure 9.5 contains a plot of the transmitted solar power for each given hour of the day through the glazing unit and horizontally positioned exterior Venetian blind slats for all programs.

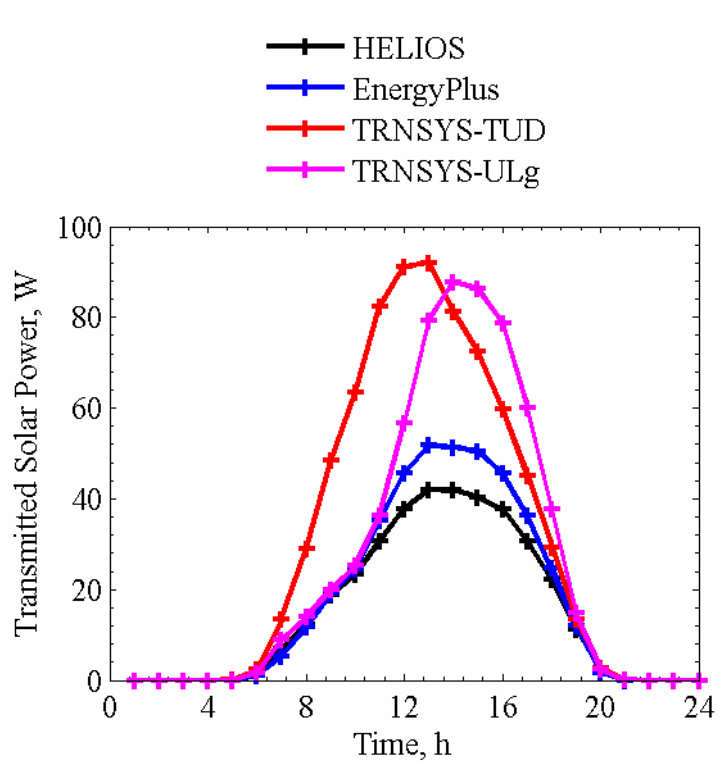

Figure 9.5. Transmitted solar power averaged over each given hour of the day.

9.2.2. Tilted 45° Downward Venetian Blind Slat Position

Plots for cooling power from HELIOS, EnergyPlus, TRNSYS-TUD, and TRNSYS-ULg are shown in Figures 9.6a and 9.6d, respectively. To account for the change in slat blade angle, comparisons were made for a 20 day period from August 17 to September 5, 2005. Table 9.7 contains average overall and 10 most influential input uncertainties that impacted the cooling power predictions taken from the n-way factorial analysis. A summary of the statistical comparisons is contained in Table 9.8.

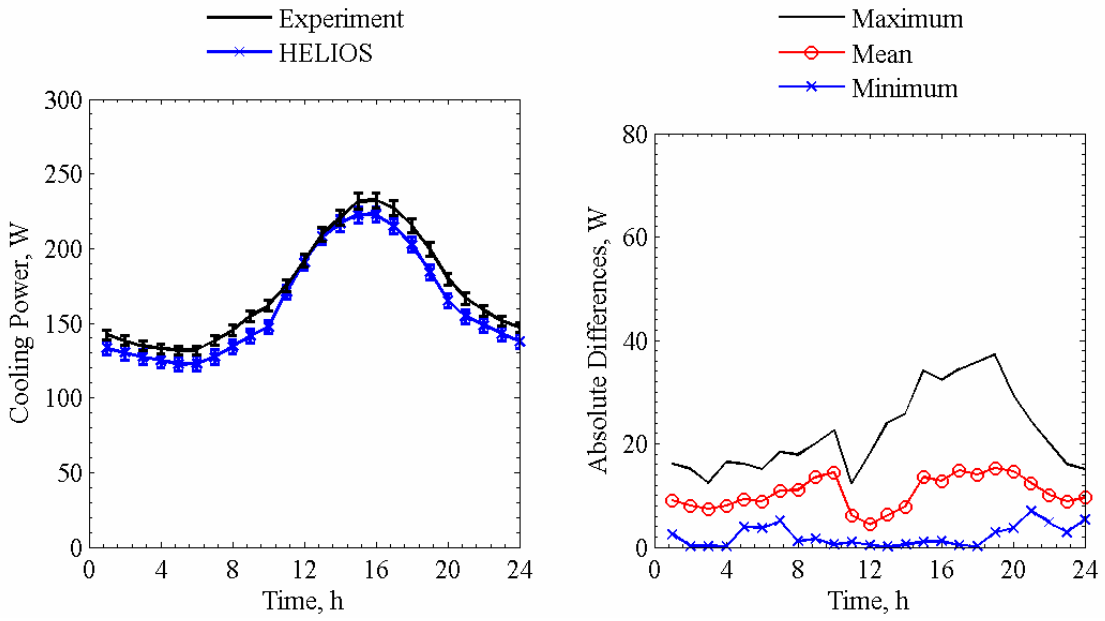

Figure 9.6a. Cooling power comparisons for HELIOS averaged over each given hour of the day (left) and absolute maximum, mean, and minimum differences for a given hour of the day (right).

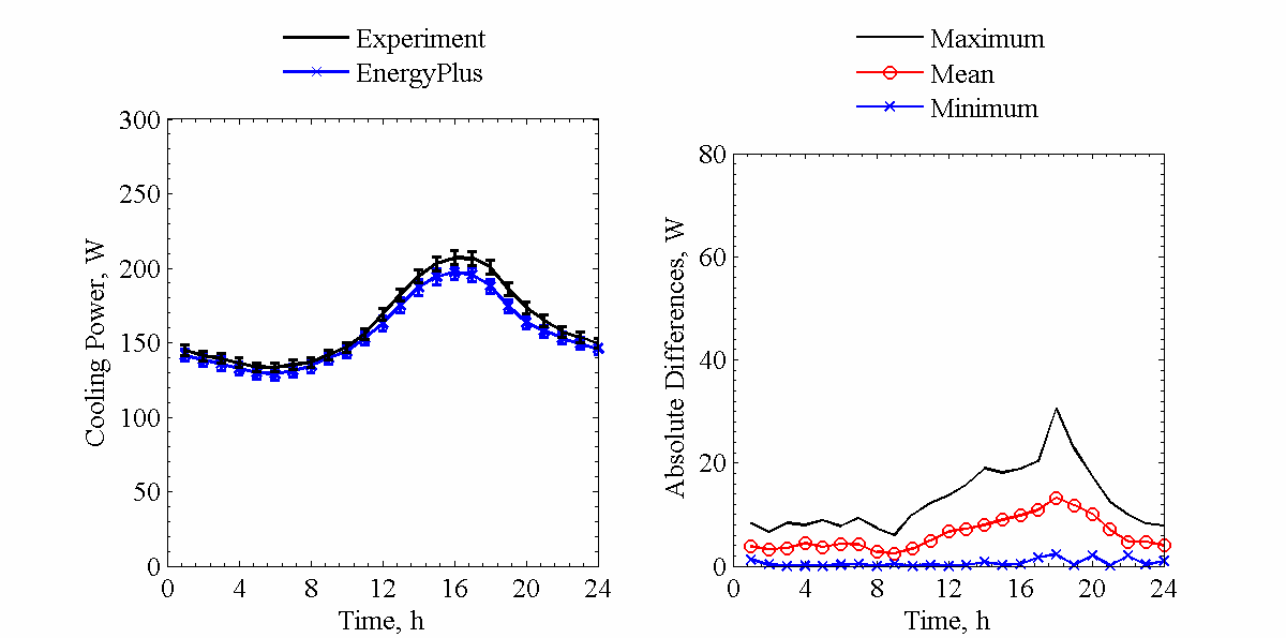

Figure 9.6b. Cooling power comparisons for EnergyPlus averaged over each given hour of the day (left) and absolute maximum, mean, and minimum differences for a given hour of the day (right).

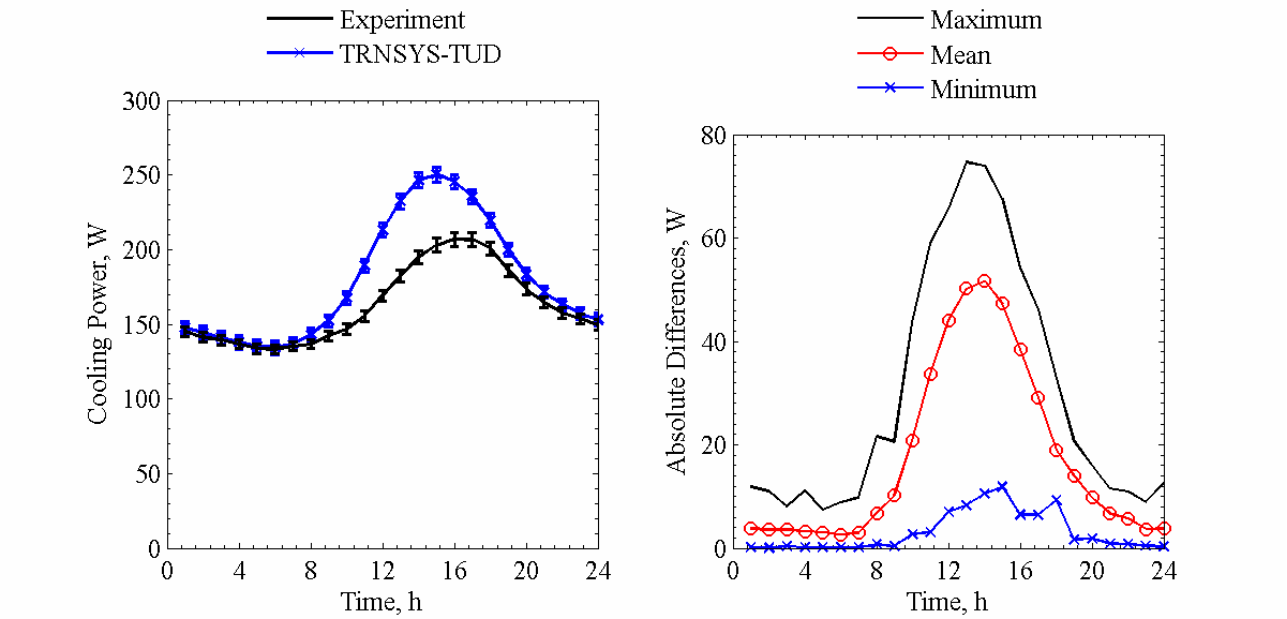

Figure 9.6c. Cooling power comparisons for TRNSYS-TUD averaged over each given hour of the day (left) and absolute maximum, mean, and minimum differences for a given hour of the day (right).

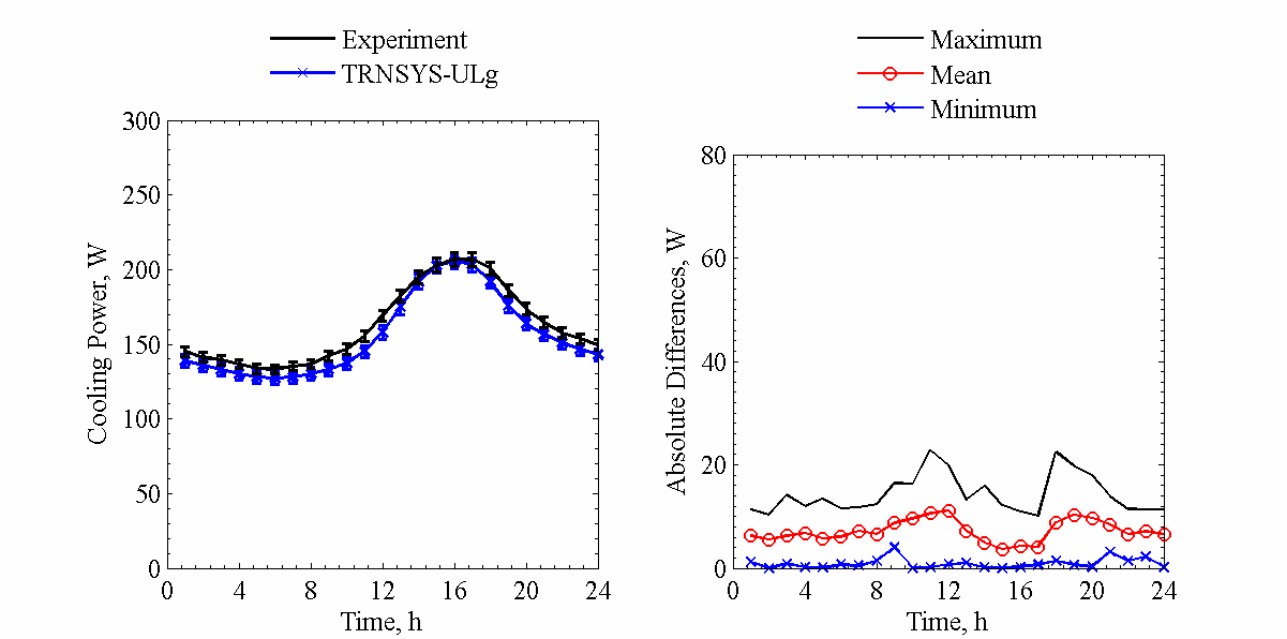

Figure 9.6d. Cooling power comparisons for TRNSYS-ULg averaged over each given hour of the day (left) and absolute maximum, mean, and minimum differences for a given hour of the day (right).

Table 9.7. Average overall uncertainty and 10 most influential input parameters from the n-way factorial analyses in Watts.

Parameter	**Forward**	**Backward**
Overall uncertainty	2.22	2.22
Average inside air temperature	-1.36	1.36
Fan power	0.893	-0.893
Outside air temperature	0.824	-0.821
North wall surface temperature	0.708	-0.708
Ceiling surface temperature	0.598	-0.596
West wall temperature	0.471	-0.470
Floor surface temperature	0.388	-0.388
East wall surface temperature	0.315	-0.315
Global horizontal infrared irradiance	0.144	-0.143
Ground reflectance	0.125	-0.123

Table 9.8. Statistical comparisons for cooling power in Exercise 6 with slats tilted 45° downward.

Parameter	Experiment	HELIOS	EnergyPlus	TRNSYS-TUD	TRNSYS-ULg
$\bar{x}$	162.2 W	157.4 W	156.4 W	179.2 W	155.4 W
s	32.2 W	36.1 W	28.1 W	47.4	32.6 W
x_{max}	260.6 W	253.9 W	242.7 W	295.9 W	258.7 W
x_{min}	112.7 W	100.2 W	107.8 W	117.9 W	110.1 W
$\overline{D}$	-	4.8 W	5.8 W	-17.0 W	6.8 W
$\overline{\lvert D \rvert}$	-	9.5 W	6.2 W	17.4 W	7.2 W
$\lvert D_{max} \rvert$	-	35.5 W	30.5 W	74.7 W	22.8 W
$\lvert D_{min} \rvert$	-	0.0 W	0.0 W	0.1 W	0.0 W
D_{rms}	-	11.0 W	7.9 W	26.1 W	8.4 W
$\lvert D \rvert_{95\%}$	-	19.8 W	16.5 W	59.6 W	16.1 W
$\overline{OU}$	3.7 W	-	4.4 W	-	-
$\overline{UR}$	-	1.2	0.7	2.0	0.9
UR_{max}	-	3.7	3.1	8.0	2.6
UR_{min}	-	0.0	0.0	0.0	0.0
$\overline{\lvert D \rvert} / \bar{x} \times 100\%$	-	5.8%	3.8%	10.7%	4.4%
$\overline{D} / \bar{x} \times 100\%$	-	3.0%	3.6%	-10.5%	4.2%

Figure 9.7 contains a plot of the transmitted solar power for each given hour of the day through the glazing unit and 45° downward positioned exterior Venetian blind slats for all programs.

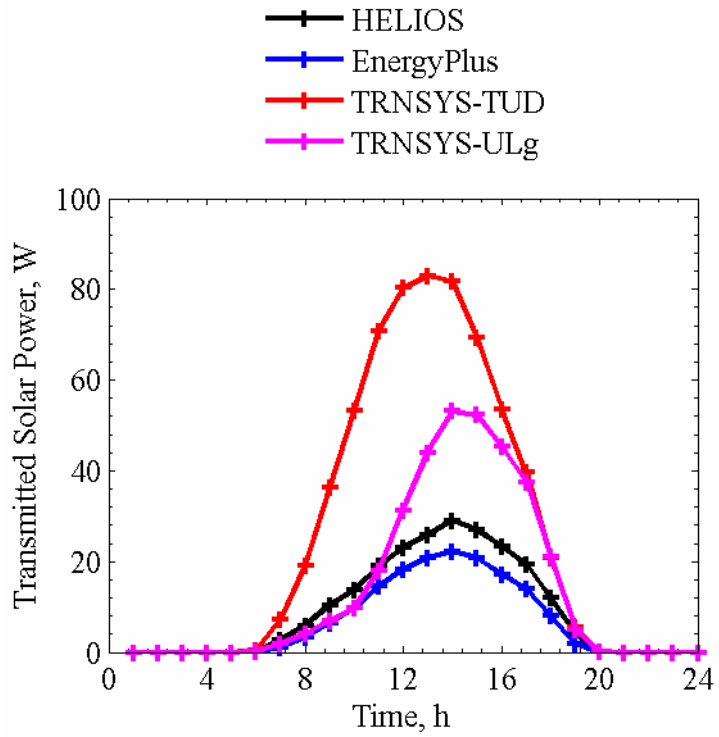

Figure 9.7. Transmitted solar power averaged over each given hour of the day.

Because of the complexities associated with modeling blind assemblies, not all participants simulated this exercise. Overall, the magnitude of the transmitted solar power into the test cell was

quite low but not uniform from program to program. Different assumptions for modeling the blind assembly discussed in the modelers' reports provide additional insight into this discrepancy. In-depth analyses and discussion of these results are provided by Loutzenhiser et al. [18].

CHAPTER 10: GLAZING UNIT WITH INTERIOR MINI-BLIND (EXERCISE 7)

Two components of an experiment were run in the EMPA test cell designed to evaluate the impact of solar gains through a glazing unit with mini-blinds at two different slat positions. The first component was performed with the slats in the horizontal position and was run from October 10, 2005 to November 11, 2005 and the second component, with the outer blind slats (closest to the window) tilted downward at a 45° angle, was run from March 27, 2006 to May 20, 2006.

10.1. Description of the Experiment

This section contains specific information about the experiment, which includes the following information:

- geometry of interior mini-blind assembly and blind slat optical properties and
- thermophysical properties of the test cell envelope.

10.1.1. Geometry of Interior Mini-blind Assembly and Blind Slat Optical Properties

For this experiment, an interior mini-blind assembly was installed and the dimensions relative to the glazing unit and the blind slats are shown in Figures 10.1 and 10.2, respectively.

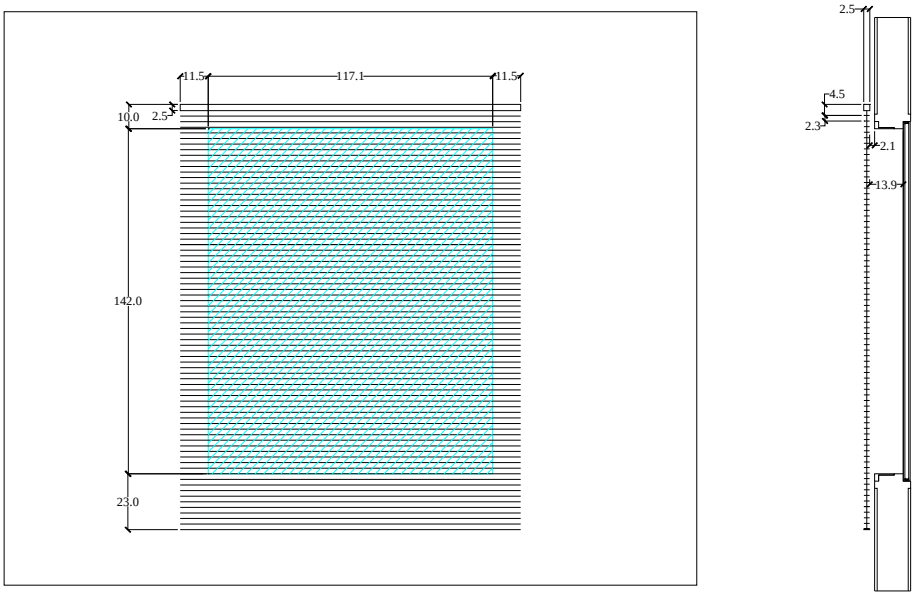

Figure 10.1. Dimensioned drawing of the internal mini-blinds, in centimeters, relative to the glazing.

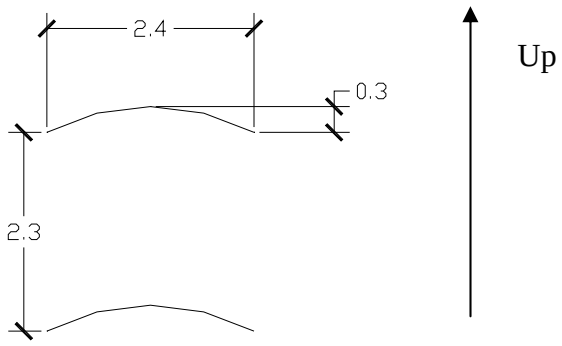

Figure 10.2. Dimensioned cross-section of the internal mini-blinds.

The optical properties of the interior mini-blind slats were measured at normal incident angles

using a spectrometer. The reflectance as a function of wavelength from 250 nm to 2500 nm can be found in "Experiment 7a.xls" and "Experiment 7b.xls". The solar reflectance, computed according to EN 410 [7] using GLAD software [8] and hemispherical emittance, measured with an emissometer based on a calorimetric method, are shown in Table 10.1.

Table 10.1. Optical properties of the slat surfaces.

Property	**Quantity**
Normal solar reflectance, %	63.9
Hemispherical emittance, %	72.1

10.1.2. Thermophysical Properties of the Test Cell Envelope

The mean envelope temperatures of the construction elements for both experiments are shown in Table 10.2. The thermophysical properties, evaluated at the mean construction element temperatures, are contained in Tables 10.3a to 10.3c for the mini-blind assembly horizontally positioned and Tables 10.4a to 10.4c when tilted downward 45°.

Table 10.2. Mean temperatures for of the construction element during experiment.

Construction element	**Mean temperature, °C**	
	Horizontal	**45° Downward**
Ceiling, east, west, and north walls	22.58	22.94
Floor	22.58	22.94
South wall	16.96	15.52

Table 10.3a. Ceiling, north, east and west wall construction evaluated at 22.58°C.

Layer number	**Material**	**Thickness mm**	**Thermal conductivity W/m-K**	**Density kg/m^3**	**Specific heat J/kg-K**
1	Sheet steel	0.7	53.62	7837	460.8
2	PU foam	139	0.02230	30	1800
3	Sheet steel	0.7	53.62	7837	460.8

Table 10.3b. Floor construction evaluated at 22.72°C.

Layer number	**Material**	**Thickness mm**	**Thermal conductivity W/m-K**	**Density kg/m^3**	**Specific heat J/kg-K**
1	Sheet steel	0.7	53.62	7837	460.8
2	PU foam	140	0.02230	30	1800
3	PU foam (higher density)	20	0.070	45	1800
4	Sheet steel with surface Structure	2.5	53.62	7837	460.8

Table 10.3c. South wall construction evaluated at 16.96°C.

Layer number	**Material**	**Thickness mm**	**Thermal conductivity W/m-K**	**Density kg/m^3**	**Specific heat J/kg-K**
1	Plywood	10	0.1393	850	1605
2	EPS foam	130	0.03571	28	1460
3	Plywood	10	0.1393	850	1605

Table 10.4a. Ceiling, north, east and west wall construction evaluated at 22.94°C.

Layer number	**Material**	**Thickness mm**	**Thermal conductivity W/m-K**	**Density kg/m^3**	**Specific heat J/kg-K**
1	Sheet steel	0.7	53.62	7837	460.8
2	PU foam	139	0.02235	30	1800
3	Sheet steel	0.7	53.62	7837	460.8

Table 10.4b. Floor construction evaluated at 22.94°C.

Layer number	Material	Thickness mm	Thermal conductivity W/m-K	Density kg/m^3	Specific heat J/kg-K
1	Sheet steel	0.7	53.62	7837	460.8
2	PU foam	140	0.02235	30	1800
3	PU foam (higher density)	20	0.070	45	1800
4	Sheet steel with surface structure	2.5	53.62	7837	460.8

Table 10.4c. South wall construction evaluated at 15.52°C.

Layer number	Material	Thickness mm	Thermal conductivity W/m-K	Density kg/m^3	Specific heat J/kg-K
1	Plywood	10	0.1391	850	1605
2	EPS foam	130	0.03553	28	1460
3	Plywood	10	0.1391	850	1605

10.2. Results

Results for cooling power are provided in two sections to assess the performances of the building energy simulation programs for both mini-blind slat positions.

10.2.1. Horizontally Positioned Mini-Blind Slat Position

Plots for cooling power from HELIOS, EnergyPlus, and TRNSYS-ULg are shown in Figures 10.3a to 10.3c, respectively. Two plots are contained in each figure. Table 10.5 contains average overall and 10 most influential input uncertainties that impacted the cooling power predictions taken from the n-way factorial analysis. A summary of the statistical comparisons is contained in Table 10.6.

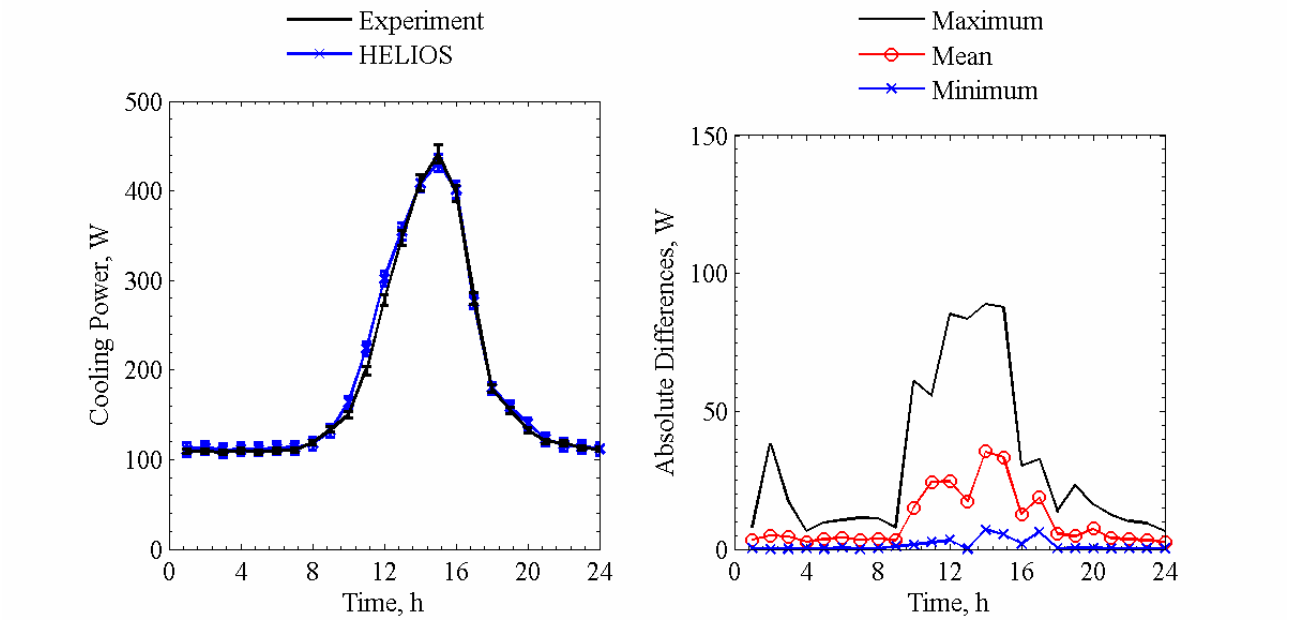

Figure 10.3a. Cooling power comparisons for HELIOS averaged over each given hour of the day (left) and absolute maximum, mean, and minimum differences for a given hour of the day (right).

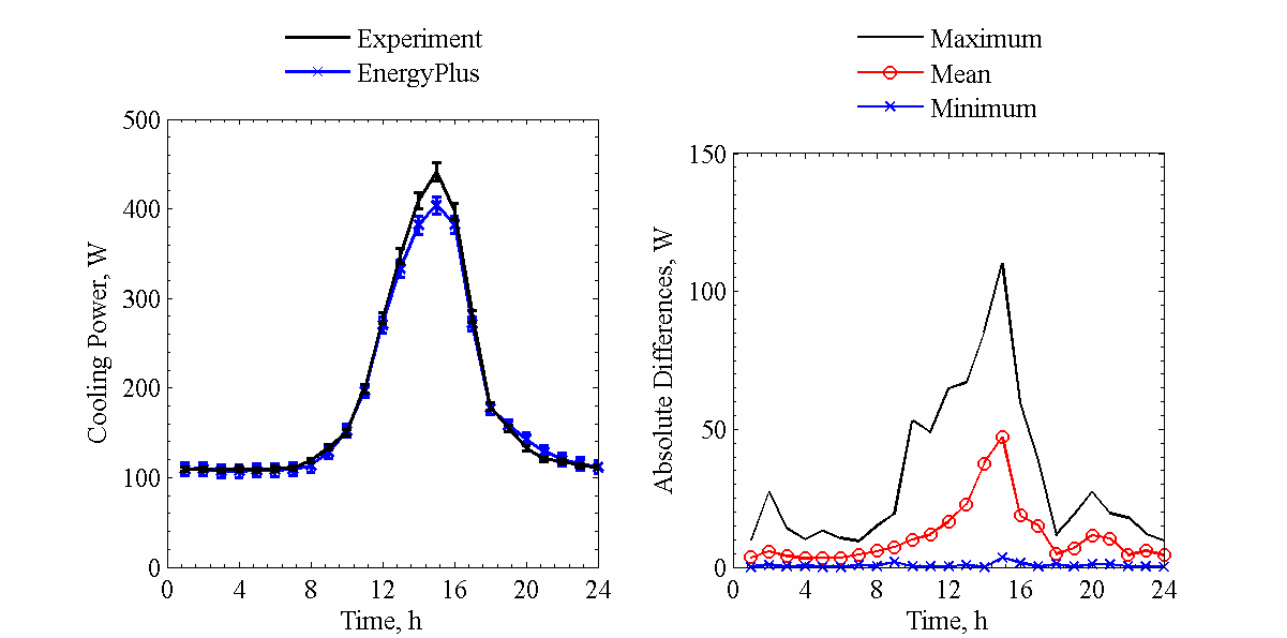

Figure 10.3b. Cooling power comparisons for EnergyPlus averaged over each given hour of the day (left) and absolute maximum, mean, and minimum differences for a given hour of the day (right).

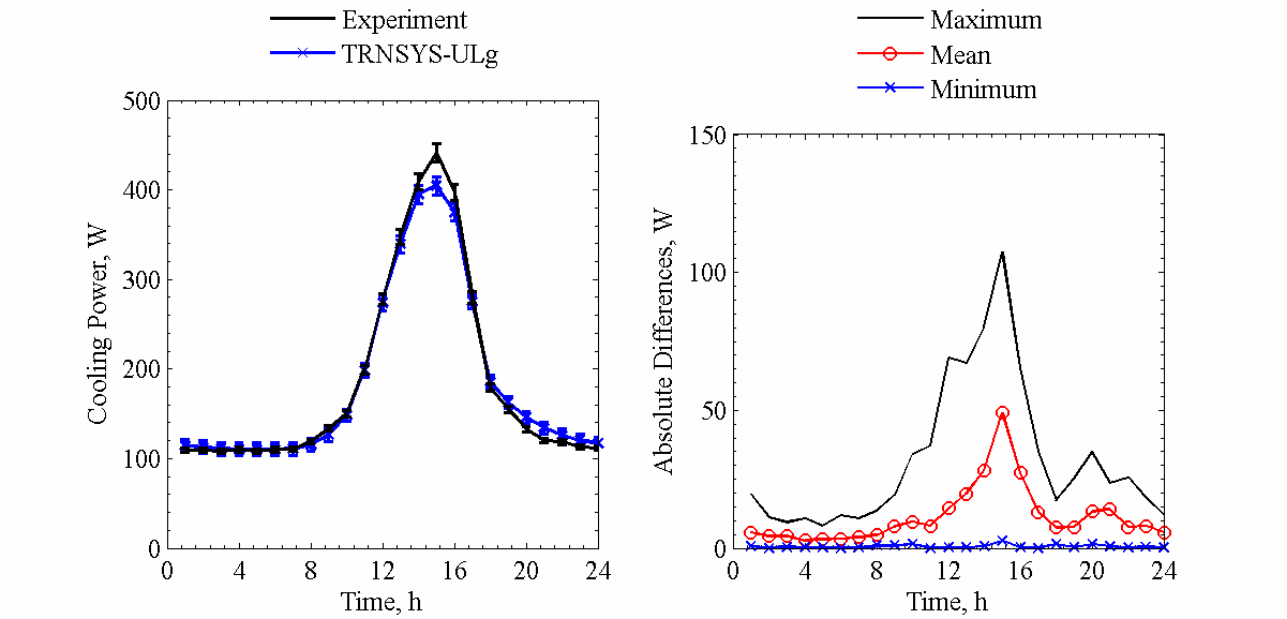

Figure 10.3c. Cooling power comparisons for TRNSYS-ULg averaged over each given hour of the day (left) and absolute maximum, mean, and minimum differences for a given hour of the day (right).

Table 10.5. Average overall uncertainty and 10 most influential input parameters from the n-way factorial analyses in Watts.

Parameter	**Forward**	**Backward**
Overall uncertainty	4.20	4.10
West wall surface temperature	2.13	-2.13
Floor surface temperature	1.78	-1.78
Average air temperature	-1.68	1.68
East wall surface temperature	1.04	-1.04
Fan power	0.90	-0.90
Ceiling surface temperature	0.82	-0.82
Outside air temperature	0.71	-0.71
North wall surface temperature	0.66	-0.66
Global horizontal infrared irradiance	0.47	-0.48
Front reflectance of inner glass pane	-0.44	0.15

Table 10.6. Statistical comparisons for cooling power in Exercise 7 with slats horizontally positioned.

Parameter	**Experiment**	**HELIOS**	**EnergyPlus**	**TRNSYS-ULg**
$\overline{x}$	185.4 W	189.1 W	181.2 W	184.4 W
s	138.0 W	135.4 W	127.5 W	126.0 W
x_{max}	747.0 W	723.2 W	676.2 W	669.9 W
x_{min}	79.8 W	82.5 W	80.7 W	92.0 W
$\overline{D}$	-	-3.7 W	4.2 W	1.0 W
$\overline{\lvert D \rvert}$	-	10.3 W	11.2 W	11.4 W
$\lvert D_{max} \rvert$	-	89.0 W	110.1 W	107.6 W
$\lvert D_{min} \rvert$	-	0.1 W	0.0 W	0.0 W
D_{rms}	-	17.5 W	20.2 W	19.7 W
$\lvert D \rvert_{95\%}$	-	38.1 W	51.4 W	41.8 W
$\overline{OU}$	4.2 W	-	7.6 W	-
$\overline{UR}$	-	0.8	0.8	0.8
UR_{max}	-	5.4	5.0	4.8
UR_{min}	-	0.0	0.0	0.0
$\overline{\lvert D \rvert} / \overline{x} \times 100\%$	-	5.5%	6.1%	6.2%
$\overline{D} / \overline{x} \times 100\%$	-	-2.0%	2.3%	0.6%

Figure 10.4 contains a plot of the transmitted solar power for each given hour of the day through the glazing unit and horizontally positioned interior mini-blind slats for all programs.

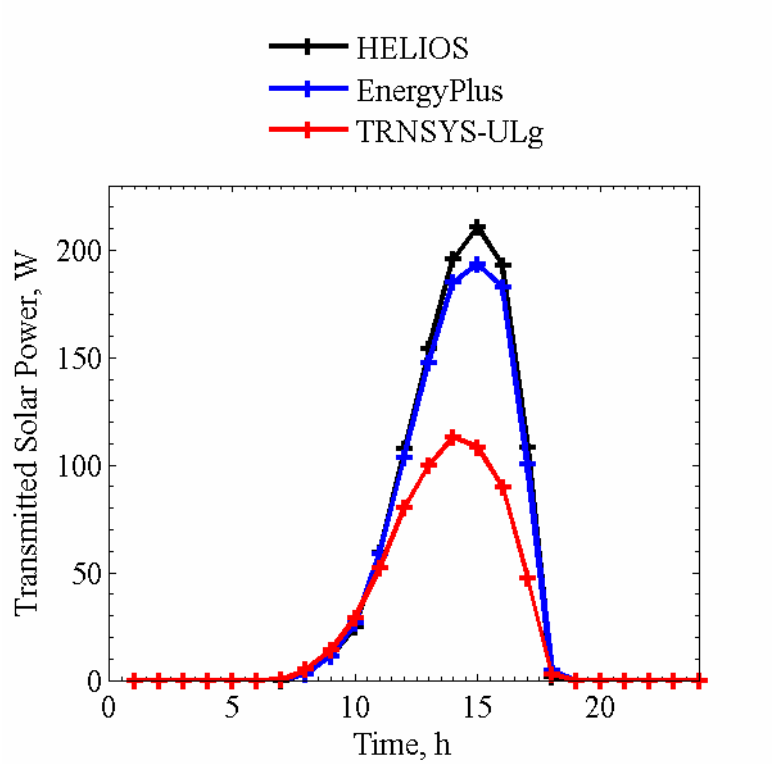

Figure 10.4. Transmitted solar power averaged over each given hour of the day.

10.2.2. Tilted 45° Downward Mini-Blind Slat Position

Plots for cooling power from HELIOS, EnergyPlus and TRNSYS-ULg are shown in Figures 10.5a to 10.5c, respectively. Table 10.7 contains average overall and the 10 most influential input uncertainties that impacted the cooling power predictions taken from the n-way factorial analysis. A summary of the statistical comparisons is contained in Table 10.8.

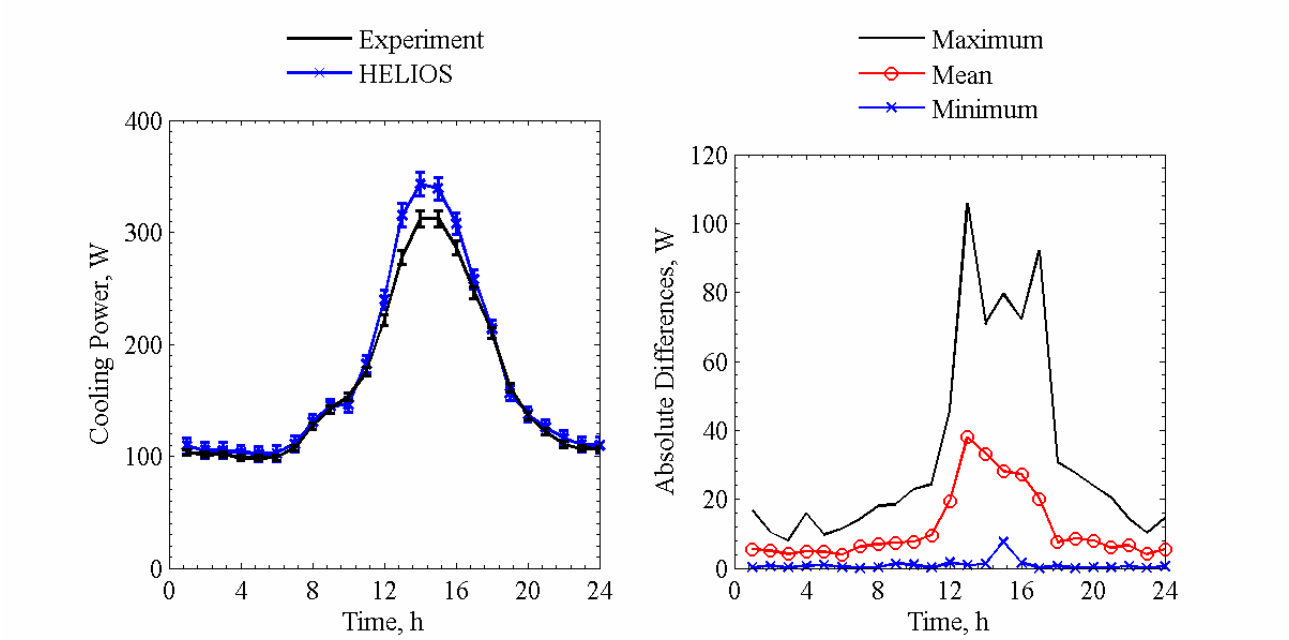

Figure 10.5a. Cooling power comparisons for HELIOS averaged over each given hour of the day (left) and absolute maximum, mean, and minimum differences for a given hour of the day (right).

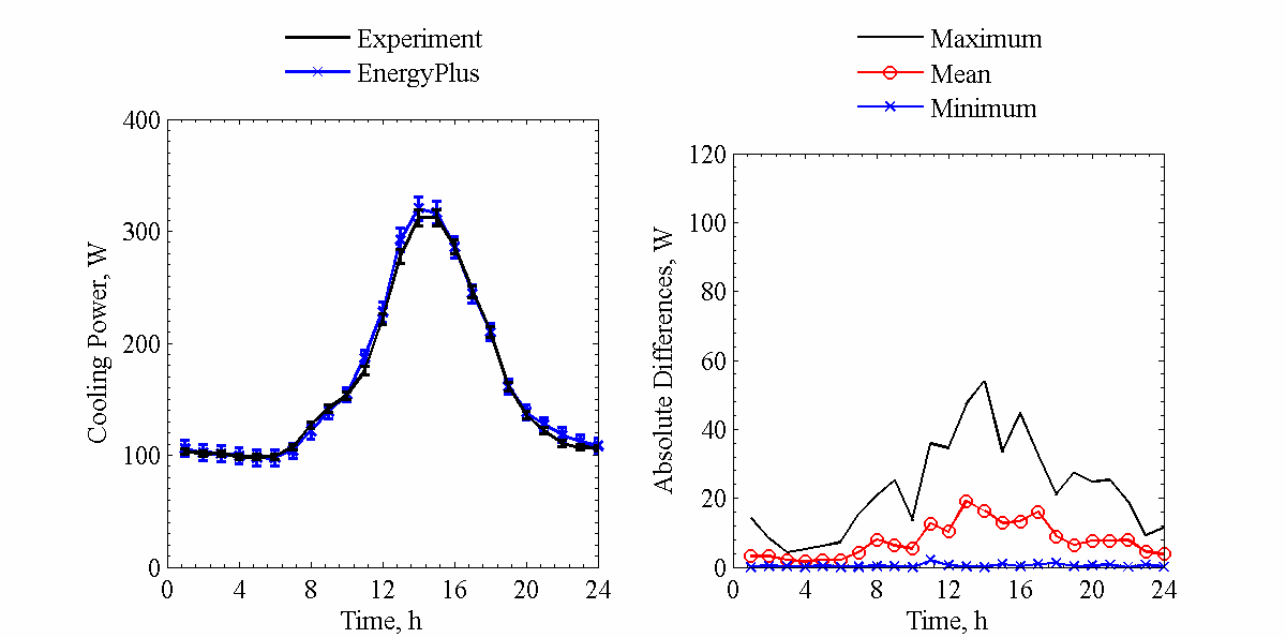

Figure 10.5b. Cooling power comparisons for EnergyPlus averaged over each given hour of the day (left) and absolute maximum, mean, and minimum differences for a given hour of the day (right).

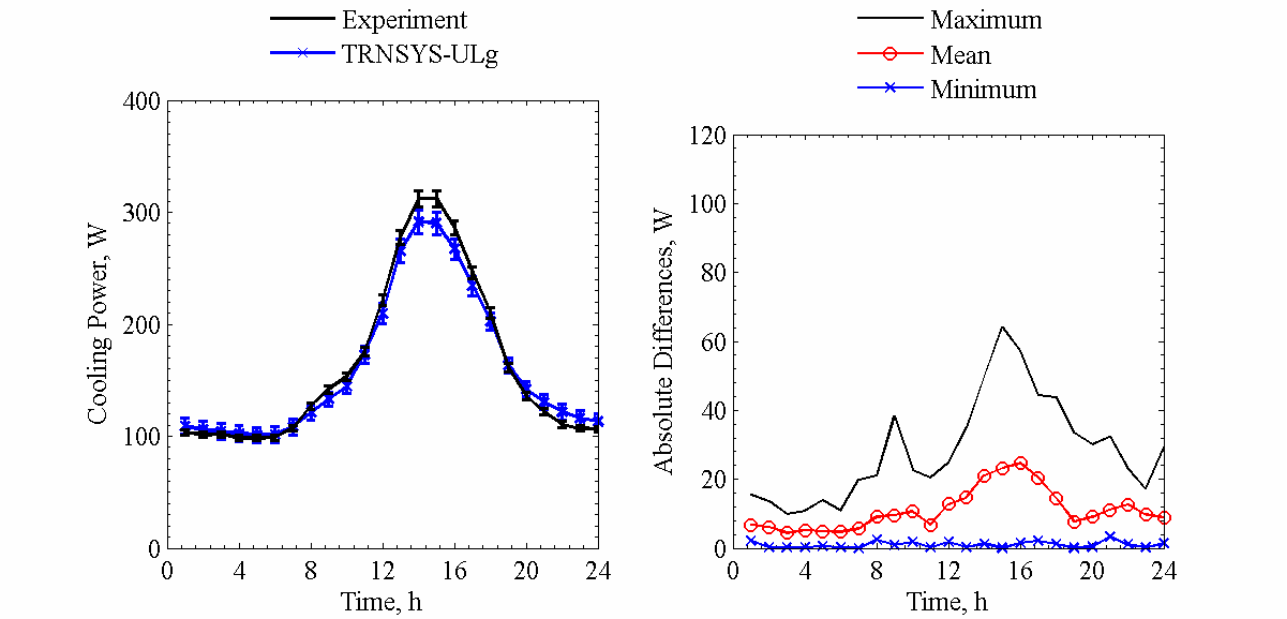

Figure 10.5c. Cooling power comparisons for TRNSYS-ULg averaged over each given hour of the day (left) and absolute maximum, mean, and minimum differences for a given hour of the day (right).

Table 10.7. Average overall uncertainty and 10 most influential input parameters from the n-way factorial analyses in Watts.

Parameter	**Forward**	**Backward**
Overall uncertainty	4.27	4.11
West wall surface temperature	2.13	-2.13
Floor surface temperature	1.77	-1.77
Average air temperature	-1.68	1.68
East wall surface temperature	1.04	-1.03
Fan power	0.87	-0.87
Ceiling surface temperature	0.82	-0.82
Outside air temperature	0.74	-0.74
North wall surface temperature	0.66	-0.66
Front reflectance of inner glass pane	-0.50	0.10
Global horizontal infrared irradiance	0.43	-0.43

Table 10.8. Statistical comparisons for cooling power in Exercise 7 with slats tilted 45° downward.

Parameter	**Experiment**	**HELIOS**	**EnergyPlus**	**TRNSYS-ULg**
$\bar{x}$	163.1 W	171.4 W	165.4 W	160.4 W
s	97.8 W	108.5 W	100.6 W	86.9 W
x_{max}	519.9 W	577.9 W	546.0 W	477.6 W
x_{min}	66.7 W	77.4 W	66.4 W	70.9 W
$\overline{D}$	-	-8.2 W	-2.3 W	2.7 W
$\overline{\lvert D \rvert}$	-	11.6 W	7.8 W	11.0 W
$\lvert D_{max} \rvert$	-	105.9 W	53.8 W	64.1 W
$\lvert D_{min} \rvert$	-	0.0 W	0.0 W	0.0 W
D_{rms}	-	19.1 W	11.9 W	15.5 W
$\lvert D \rvert_{95\%}$	-	45.8 W	28.7 W	36.2 W
$\overline{OU}$	3.7 W	-	7.6 W	-
$\overline{UR}$	-	0.9	0.6	0.9
UR_{max}	-	6.9	3.1	4.0
UR_{min}	-	0.0	0.0	0.0
$\overline{\lvert D \rvert} / \bar{x} \times 100\%$	-	7.1%	4.8%	6.8%
$\overline{D} / \bar{x} \times 100\%$	-	-5.1%	-1.4%	1.7%

Figure 10.6 contains a plot of the transmitted solar power for each given hour of the day through the glazing unit and 45° downward positioned exterior Venetian blind slats for all programs.

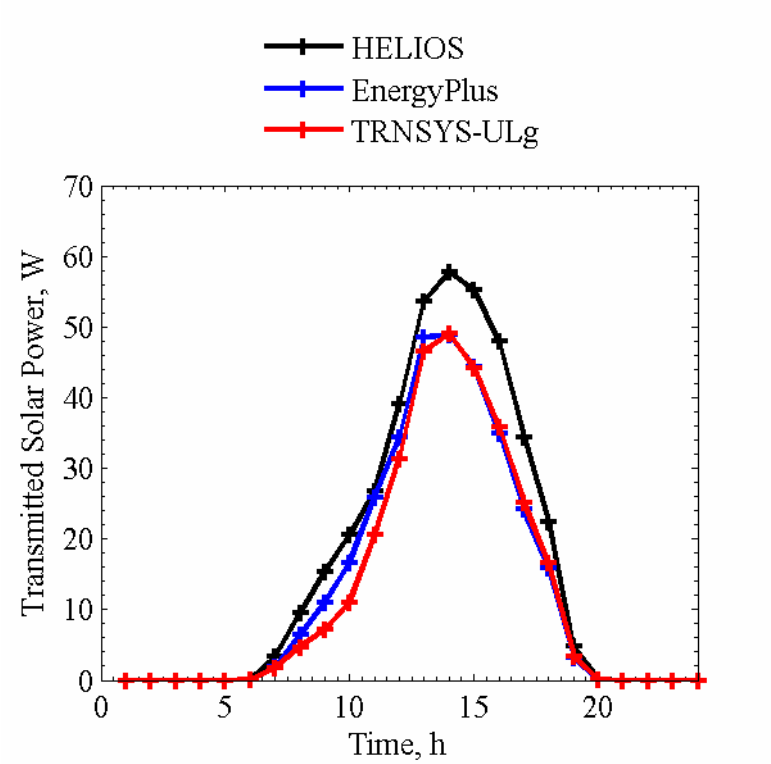

Figure 10.6. Transmitted solar power averaged over each given hour of the day.

Differences like those seen for the exterior blind assembly exercise were also apparent for this exercise. In-depth analyses and discussion of these results are provided by Loutzenhiser et al. [18].

CHAPTER 11: WINDOW (EXERCISE 8)

An experiment was run from June 25 to July 19, 2006 in the EMPA test cell that was designed to evaluate the impact of solar gains through a window (i.e. glazing unit and window frame). Information about the window, thermophysical properties evaluated at mean envelope temperatures, thermal bridges, and results from various programs are provided in this chapter. This exercise differs from Exercise 3 in that the window frame must also now be accounted for in the simulation programs.

11.1. Description of the Experiment

This section contains specific information about the experiment, which includes the following information:

- the placement and properties of the window,
- a two-dimensional steady-state heat transfer simulation and hotbox measurements used to calculate the thermal bridges, and
- thermophysical properties of the test cell envelope.

A photograph of the test cell during the experiment is shown in Figure 11.1.

Figure 11.1. A photograph of the test cell.

11.1.1. Window Properties

For this experiment, a window was mounted in the southwest exterior wall of the test cell. The glazing properties from measurands are listed in Table 11.1. Additional measurements for the individual panes of glass, as a function of wavelength, are provided in "Experiment 8.xls". Properties of the individual panes are described in Table 11.2. The inside and outside solar reflectance and transmittance were calculated using European Standard EN 410 [7] with GLAD software [8]. For the individual panes of glass, the emittances were measured using an emissometer based on a calorimetric method. A dimensioned drawing of the exterior wall as seen from this inside of the test cell showing the position of the glazing is presented in Figure 11.2. The dimensions, in meters, of the glazing in the figure correspond to the aperture height and width. The window frame was painted white and the solar reflectance and emittance of the frame were approximated with the same optical properties of the exterior surface of 76.6% and 93%, respectively.

Table 11.1. Window optical properties.

Parameter	Quantity
Normal solar transmittance	53.7%
Normal solar exterior reflectance	23.3%
Normal solar interior reflectance	22.4%

Table 11.2a. Optical properties for the outer pane of glass (Clear Float Glass).

Parameter	Quantity
Normal solar transmittance	83.6%
Normal solar exterior reflectance	7.8%
Normal solar interior reflectance	7.7%
Outer emittance	85.3%
Inner emittance	87.3%

Table 11.2b. Optical properties for the inner pane of glass (Low-E Pro).

Parameter	Quantity
Normal solar transmittance	62.5%
Normal solar exterior reflectance	24.9%
Normal solar interior reflectance	20.0%
Outer emittance	8.5%
Inner emittance	87.3%

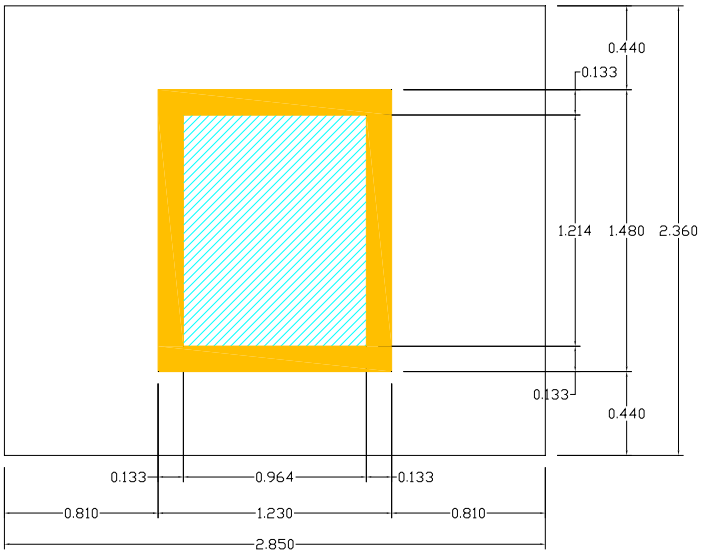

Figure 11.2. Position of the glazing in the exterior wall in meters (inside view).

11.1.2. Thermal Transmittances and Bridges

The impact of the thermal bridges due to the spacer, window frame, and mounting were all computed. The calculations for the linear thermal transmittances for the spacer and mounting and the overall thermal conductance of the window frame are described in this section using a two-dimensional software package called BISCO [13] and calorimetric measurements from the hotbox [18]. The results from the thermal bridge calculations and center-pane thermal transmittance and conductance of the window described in this section are summarized in Table 11.3. Preliminary quantities used for computing these properties are provided in subsequent sections.

Table 11.3. Summary of computed and measured thermal bridge properties and center-pane glazing properties.

Description	Symbol	Quantity
Center-pane thermal transmittance of the glazing unit	U_C	1.163 W/m^2-K
Center-pane thermal conductance of the glazing unit	Λ_C	1.449 W/m^2-K
Linear thermal transmittance for the spacer	ψ_{sp}	0.073 W/m-K
Thermal conductance of the window frame	Λ_{WF}	1.643 W/m^2-K
Linear thermal transmittance for the mounting	ψ_M	-0.028 W/m-K

A dimensioned drawing of a cross section of the glazing unit, window frame, and mounting is shown in Figure 11.3. Table 11.4 contains a list of the materials used in the simulation, thermal conductivities, and coloring coding that correspond to Figure 11.3. The thermal conductivities were taken from literature and in-house measurements; temperature dependent thermophysical properties were fixed as the average between the outer and inner air temperatures for the south wall.

Table 11.4. Materials and thermal conductivities

Material	Thermal Conductivity, W/m-K	Color-coding
Desiccant	0.130	
Aluminum	220.0	
Steel	50.0	
Stainless steel (spacer)	17.0	
Polyisobutylene	0.200	
Butyl	0.240	
Argon 90%/Air 10%	0.029	
Glass	1.0	
Frame	0.110	
Plywood	0.1381	
EPS foam	0.03483	
Soft rubber	0.100	
Weather stripping	0.050	
Insulation panel (Figure 11.4 right)	0.0409	

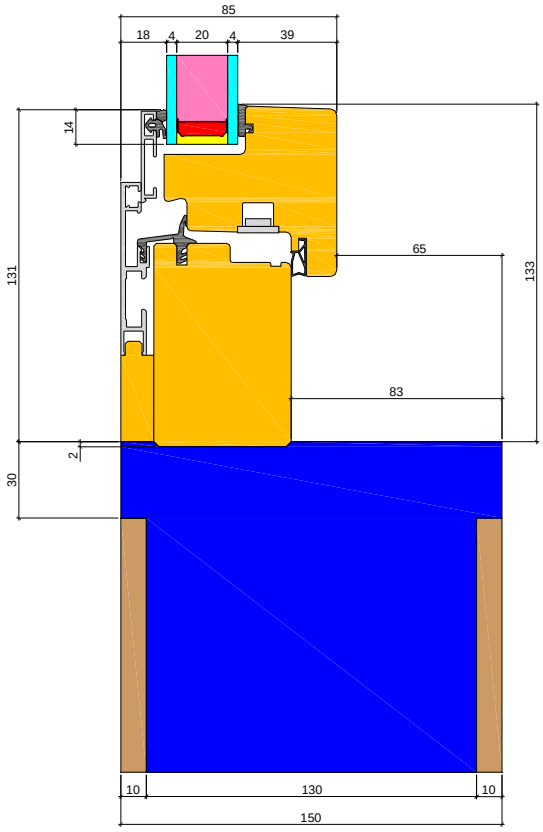

Figure 11.3. Drawing of the spacer and frame in millimeters.

11.1.2.1. Linear Thermal Transmittance of the Spacer

The impact of the spacer was calculated using a two-dimensional drawing of the spacer/frame assembly. The linear thermal transmittance of the spacer was evaluated according to preEN ISO 10077-2 [6]. During the hotbox measurements, the heat flux through the center of the window pane was measured and a center pane thermal transmittance was computed. From this measurement, an equivalent conductivity was computed in the argon filled glazing cavity that factored in the impact of conduction, convection, and radiation. The thermal transmittance was also used to compute an equivalent thermal conductivity of the insulation panel for replacing the glazing unit in the frame as (which deviates slightly from standard which specifies a fixed equivalent thermal conductivity). Figures 11.4 show the bitmaps used for the simulations. Equivalent thermal conductivities of the air cavities were calculated according to preEN ISO 10077-2. The linear thermal transmittance due to the spacer, ψ_{sp}, was computed using Equation 11.1 with results from the BISCO simulations.

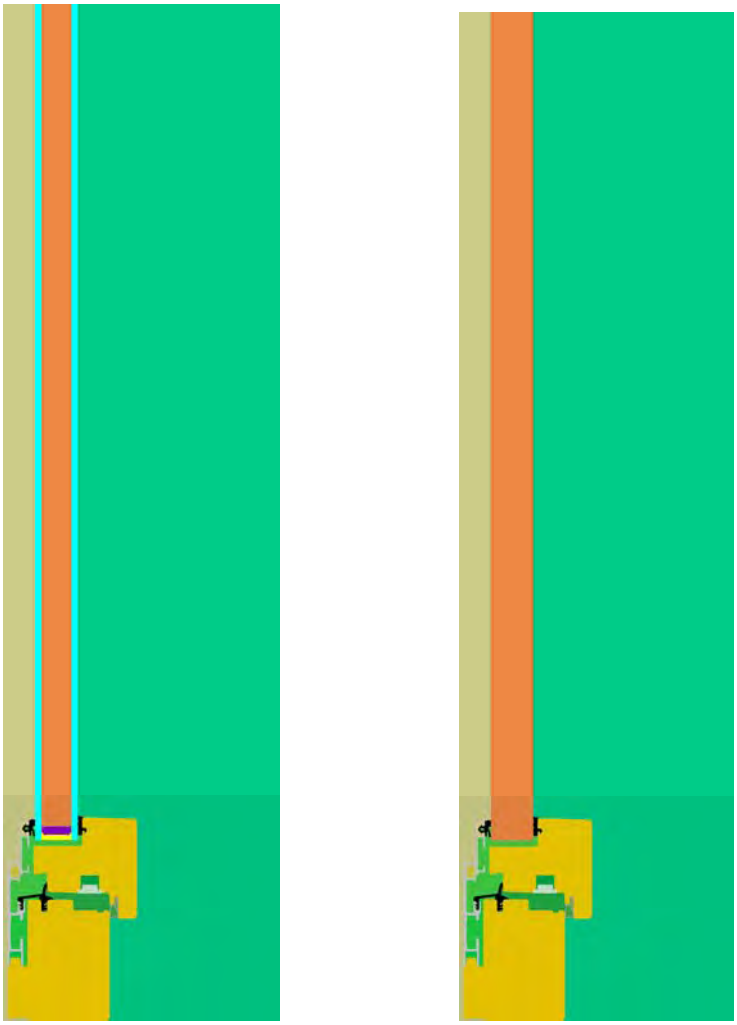

Figure 11.4. Bitmaps for the BISCO calculation with glazing unit (left) and insulation panel (right).

$$\psi_{sp} = \frac{Q'_{sp} - Q'_{ins}}{\theta_i - \theta_o} \qquad (11.1)$$

where

Q'_{sp} is the heat flow per unit length from the BISCO simulation through the glazing unit and window frame,

Q'_{ins} is the heat flow per unit length from the BISCO simulation through the insulation panel and window frame,

θ_i is the inside air temperature, and

θ_i is the outside air temperature.

11.1.2.2. Thermal Conductance of the Window Frame

The thermal transmittance of the window frame was computed by using the BISCO simulation and the results from the linear thermal transmittance for the spacer and the one-dimensional heat transfer assumed by the building energy simulation programs. For this calculation, the window frame was assumed to have fixed height. Linear temperature profiles were assumed across the window frame for the steady one-dimensional heat transfer calculation. The thermal conductance (note this is not thermal transmittance because it does not include heat transfer coefficients) of the frame, Λ_{WF}, was calculated using Equation 11.2.

$$\Lambda_{WF} = \left[\frac{L_{WF}}{\frac{Q'_{sp}}{\theta_i - \theta_o} - \psi_{sp} - L_{GL}U_c} - \frac{1}{h_i} - \frac{1}{h_o} \right]^{-1} \tag{11.2}$$

where

L_{WF} is the height of the window frame for the simulation,
L_{GL} is the height the glazing unit extends out past the frame in the two-dimensional simulation,
h_i is the inside combined heat transfer coefficient, and
h_o is the outside combined heat transfer coefficient.

11.1.2.3. Linear Thermal Transmittance Due to Mounting

A linear thermal transmittance due to the mounting of the window in the frame was computed by coupling BISCO simulation results with hotbox measurements. Therefore, the results for the calculation also included thermal bridges from the spacer and frame {non-homogeneities (i.e. screws, and frames) and corner effects from the window frame and the spacer}. For this calculation, an assumption was made that the outer wall was composed entirely of homogeneous layered material specified for the building energy simulation programs; however, this is not the case because an additional 30 mm of insulation was added near the edge of the window opening for mounting the window. This additional thermal resistance is also included in the linear thermal transmittance computation to quantify mounting effects. The hotbox measurements were also considered quasi-steady state and a linear temperature profiles across each material were assumed for the one-dimensional calculations. Measured film coefficients from the experiment were used for computing this quantity instead of the combined heat transfer coefficients used in the simulations. Equation 11.3 was used to calculate the one-dimensional thermal transmittance, UA_{1D}, through the window frame, outside wall, and the glazing unit. Temperature dependent thermophysical properties were fixed at the mean temperature of the hot and cold chambers.

$$UA_{1D} = A_{wall}\left(R_C + \frac{2d_p}{\lambda_p} + \frac{d_e}{\lambda_e} + R_H \right)^{-1} + A_{WF}\left(R_C + \frac{1}{\Lambda_{WF}} + R_H \right)^{-1} + A_{GL}\left(R_C + \frac{1}{\Lambda_C} + R_H \right)^{-1} \tag{11.3}$$

where

A_{wall} is the area of the outside wall in the hotbox,
R_C is the measured film resistance of the air in the cold chamber,
R_H is the measured film resistance of the air in the hot chamber,
d_p is the width of the plywood,
λ_p is the thermal conductivity of the plywood,
d_e is the width of the eps foam,
λ_e is the thermal conductivity of the eps foam,
A_{WF} is the area of the window frame, and
A_{GL} is the exposed area of the glazing unit.

The linear thermal transmittance of the mounting, ψ_M, was calculated using Equation 11.4. The quantity computed from Equation 11.4 was negative (Table 11.4), indicating that the thermal resistance in one-dimension plus the additional thermal bridging from the spacer and frame was less than the measurements.

$$\psi_M = \frac{\frac{Q_{HB}}{\theta_H - \theta_C} - UA_{1D} - \psi_{SP} P_{SP}}{P_M} \qquad (11.4)$$

where

Q_{HB} is the total heat transfer through the construction element,
θ_H is the temperature of the hot chamber of the hot box,
θ_C is the temperature of the cold chamber of the hot box,
P_{SP} is the perimeter of the exposed glazing unit, and
P_M is the outer perimeter of the window frame.

A BISCO simulation was also run to examine the heat flow and a frame, mounting, and spacer with heat flow lines are shown in Figure 11.5.

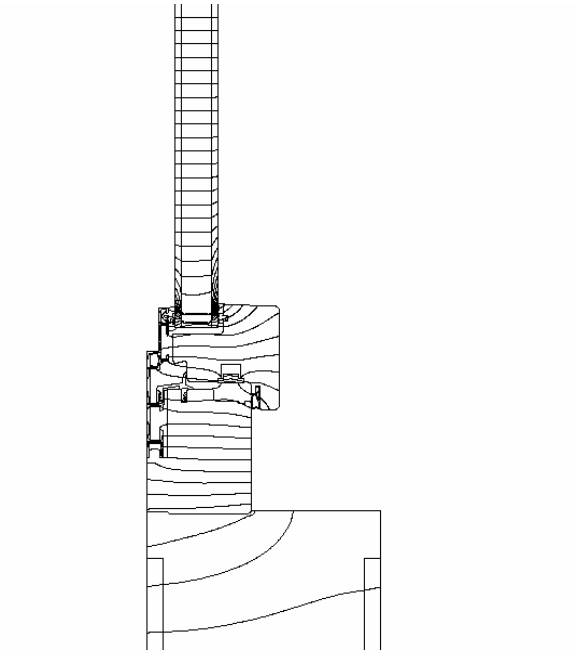

Figure 11.5. Heat flow lines from the BISCO simulation.

11.1.2.4. Quantities Used for the Calculations

The quantities used for computing the impact of the thermal bridges from the simulation and the hotbox measurements are contained in Tables 11.5a and 11.5b, respectively.

Table 11.5a. Values used for the BISCO simulations.

Description	**Symbol**	**Quantity**
Width of the eps foam	d_e	0.130 m
Width of the plywood	d_p	0.010 m
Inside combined heat transfer coefficient for the simulation	h_i	7.7 W/m^2-K
Outside combined heat transfer coefficient for the simulation	h_o	25.0 W/m^2-K
Height of the window frame for the simulation	L_{WF}	0.133 m
Height the glazing unit extends out past the frame in the two-dimensional simulation	L_{GL}	0.55 m
Inside air temperature	θ_i	20.0 °C
Outside air temperature	θ_o	0.0 °C
Heat flow per unit length from the BISCO simulation through the glazing unit and window frame	Q'_{sp}	17.67 W/m
Heat flow per unit length from the BISCO simulation through the insulation panel and window frame	Q'_{ins}	16.21 W/m

Table 11.5b. Measurements from the hotbox.

Description	Symbol	Quantity
Area of the wall	A_{wall}	3.196 m^2
Area of the glazing	A_{GL}	1.170 m^2
Area of the window frame	A_{WF}	0.650 m^2
Width of the eps foam	d_e	0.130 m
Width of the plywood	d_p	0.010 m
Perimeter of the exposed glazing unit	P_{SP}	4.356 m
Outer perimeter of the window frame	P_M	5.420 m
Measured film resistance of the air in the cold chamber	R_C	0.057 m^2-K/W
Measured film resistance of the air in the hot chamber	R_H	0.134 m^2-K/W
Thermal conductivity of the plywood for the experiment	λ_p	0.1385 W/m-K
Thermal conductivity of the eps foam for the experiment	λ_e	0.03509 W/m-K
Total heat transfer through the construction element	Q_{HB}	62.19 W
Air temperature of the hot chamber of the hot box	θ_H	22.08 °C
Air temperature of the cold chamber of the hot box	θ_C	2.01 °C
Baffle temperature of the hot chamber of the hotbox	θ_{BH}	21.66 °C
Baffle temperature of the cold chamber of the hotbox	θ_{BC}	2.06 °C

11.1.3. Thermophysical Properties of the Test Cell Envelope

The mean envelope temperatures for the construction elements are shown in Table 11.6. The thermophysical properties, evaluated at the mean construction element temperatures, are contained in Tables 11.7a to 11.7c.

Table 11.6. Mean temperatures for of the construction element during experiment.

Construction element	Mean temperature, °C
Ceiling, east, west, and north walls	22.75
Floor	22.98
South wall	22.04

Table 11.7a. Ceiling, north, east and west wall constructions evaluated at 22.75°C.

Layer number	Material	Thickness mm	Thermal conductivity W/m-K	Density kg/m^3	Specific heat J/kg-K
1	Sheet steel	0.7	53.62	7837	460.8
2	PU foam	139	0.02237	30	1800
3	Sheet steel	0.7	53.62	7837	460.8

Table 11.7b. Floor construction evaluated at 22.98°C.

Layer number	Material	Thickness mm	Thermal conductivity W/m-K	Density kg/m^3	Specific heat J/kg-K
1	Sheet steel	0.7	53.62	7837	460.8
2	PU foam	140	0.02237	30	1800
3	PU foam (higher density)	20	0.070	45	1800
4	Sheet steel with surface Structure	2.5	53.62	7837	460.8

Table 11.7c. South wall construction elements evaluated at 22.04°C.

Layer number	Material	Thickness mm	Thermal conductivity W/m-K	Density kg/m^3	Specific heat J/kg-K
1	Plywood	10	0.1403	850	1605
2	EPS foam	130	0.03645	28	1460
3	Plywood	10	0.1403	850	1605

11.2. Results

The empirical validation for this exercise focused on comparing cooling power. Plots for cooling power from HELIOS, EnergyPlus, DOE-2.1E, IDA-Detwind, and TRNSYS-ULg are shown in Figures 11.5a to 11.5e, respectively. Two plots are contained in each figure. Table 11.8

contains average overall and 10 most influential input uncertainties that impacted the cooling power predictions taken from the n-way factorial analysis. A summary of the statistical comparisons is contained in Table 11.9.

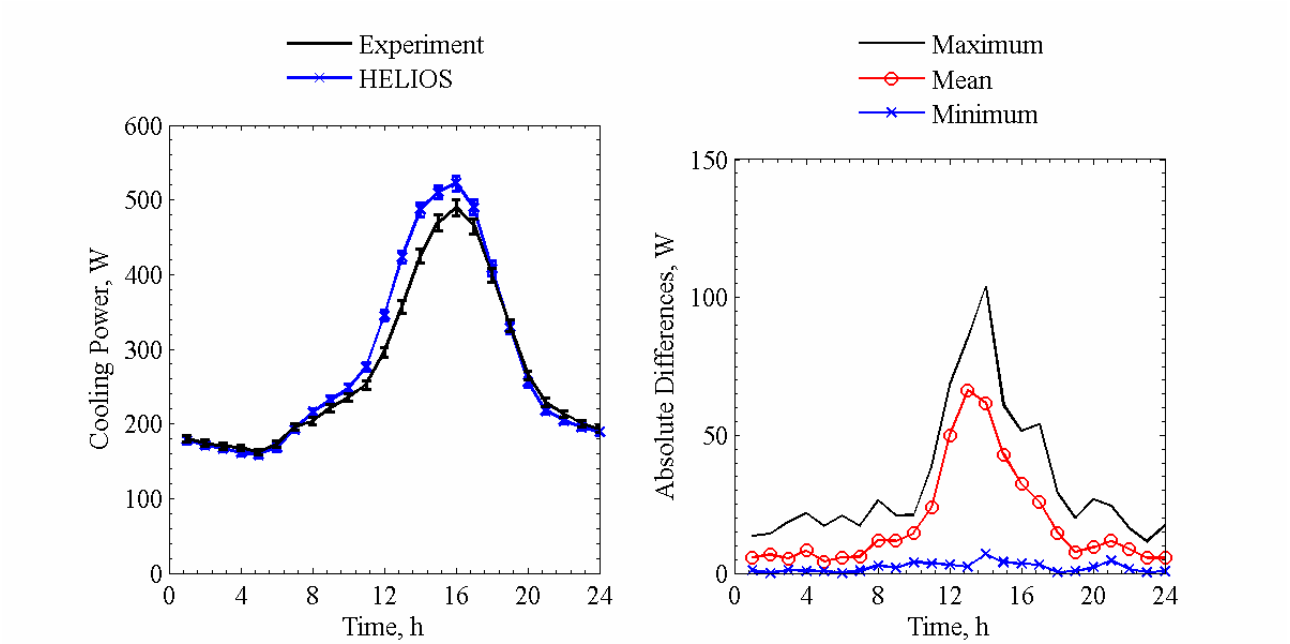

Figure 11.5a. Cooling power comparisons for HELIOS averaged over each given hour of the day (left) and absolute maximum, mean, and minimum differences for a given hour of the day (right).

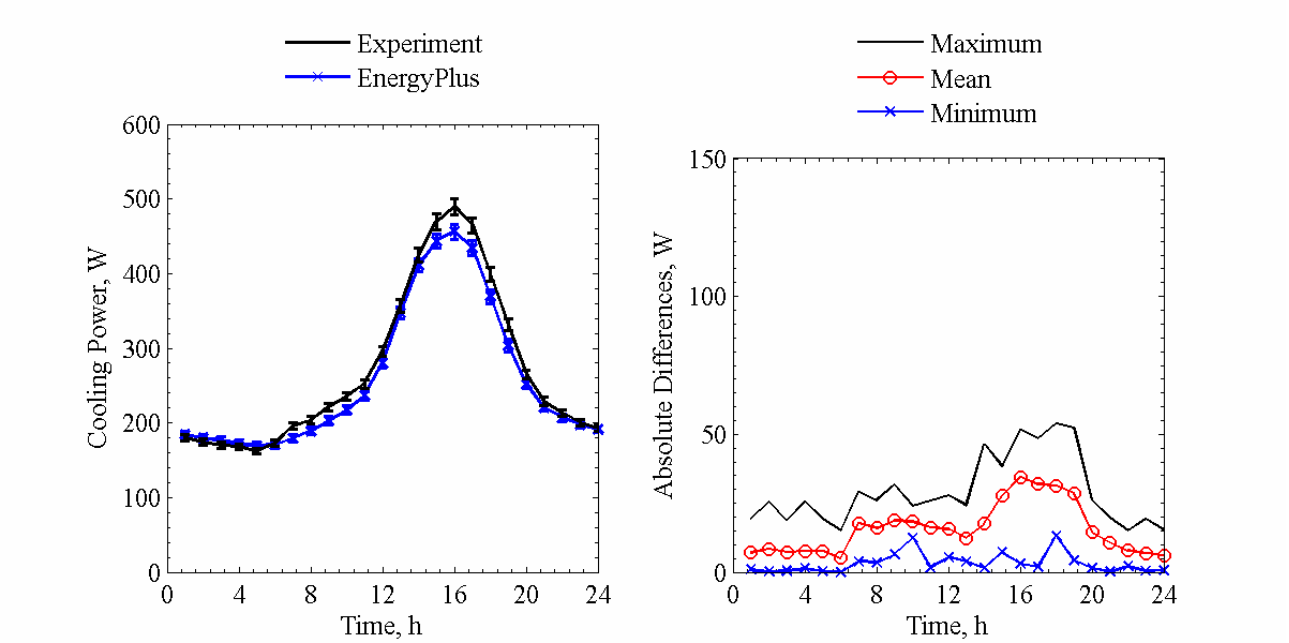

Figure 11.5b. Cooling power comparisons for EnergyPlus averaged over each given hour of the day (left) and absolute maximum, mean, and minimum differences for a given hour of the day (right).

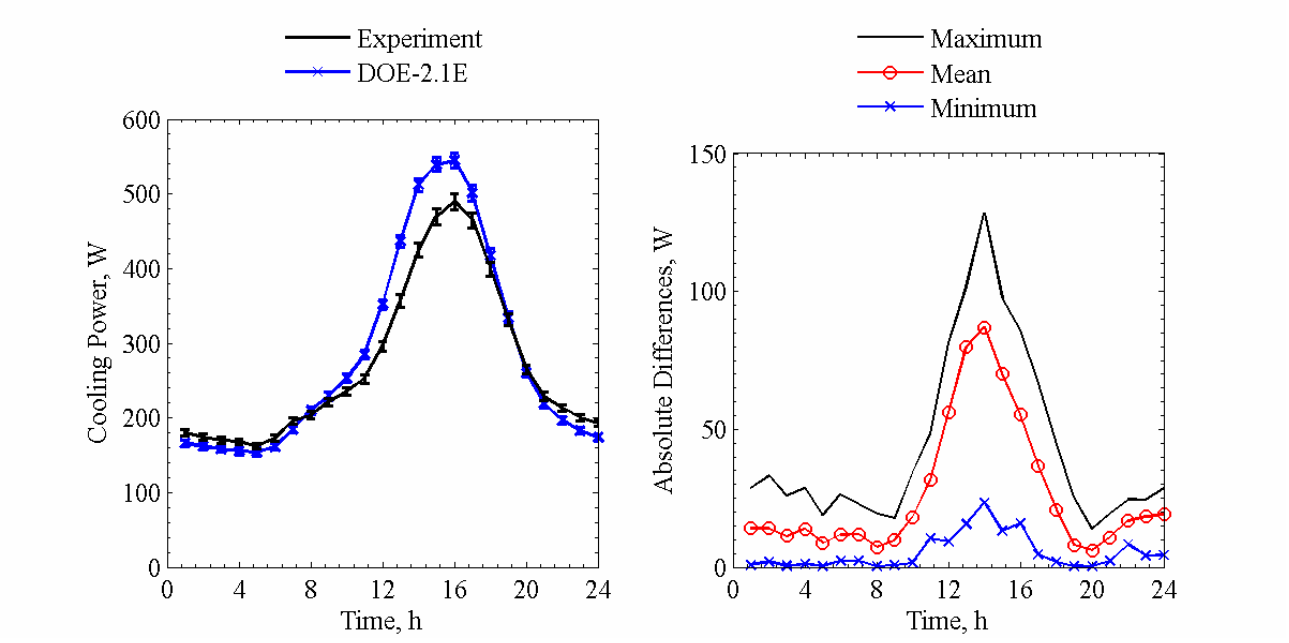

Figure 11.5c. Cooling power comparisons for DOE-2.1E averaged over each given hour of the day (left) and absolute maximum, mean, and minimum differences for a given hour of the day (right).

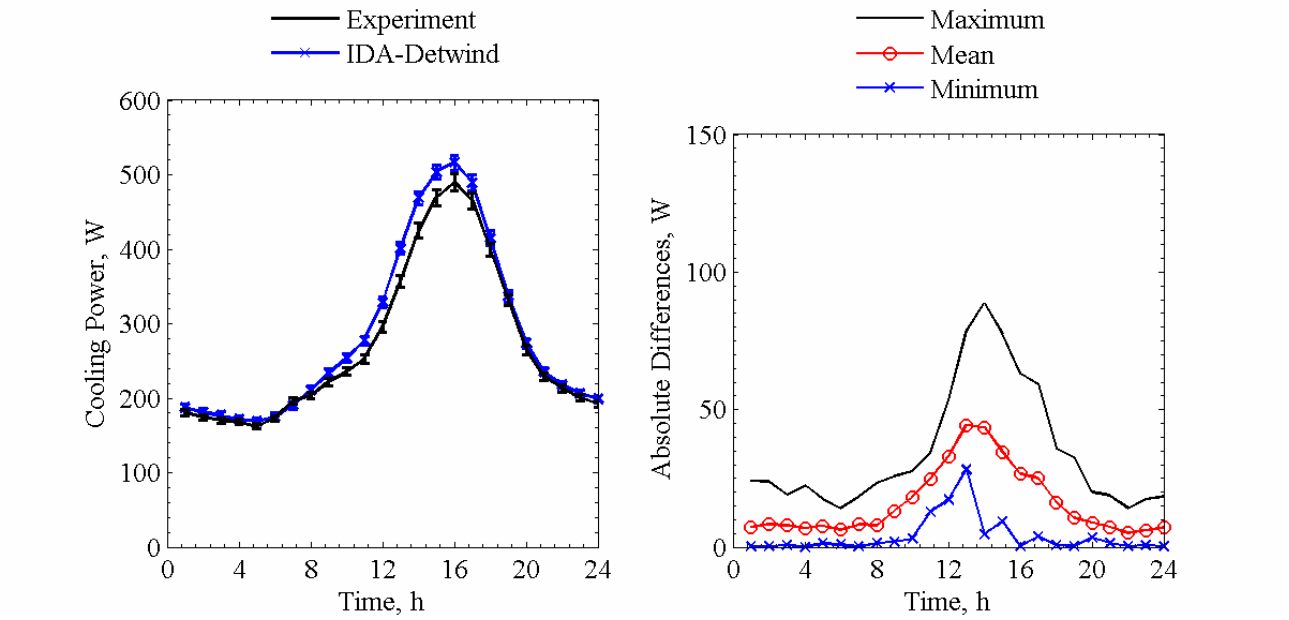

Figure 11.5d. Cooling power comparisons for IDA-Detwind averaged over each given hour of the day (left) and absolute maximum, mean, and minimum differences for a given hour of the day (right).

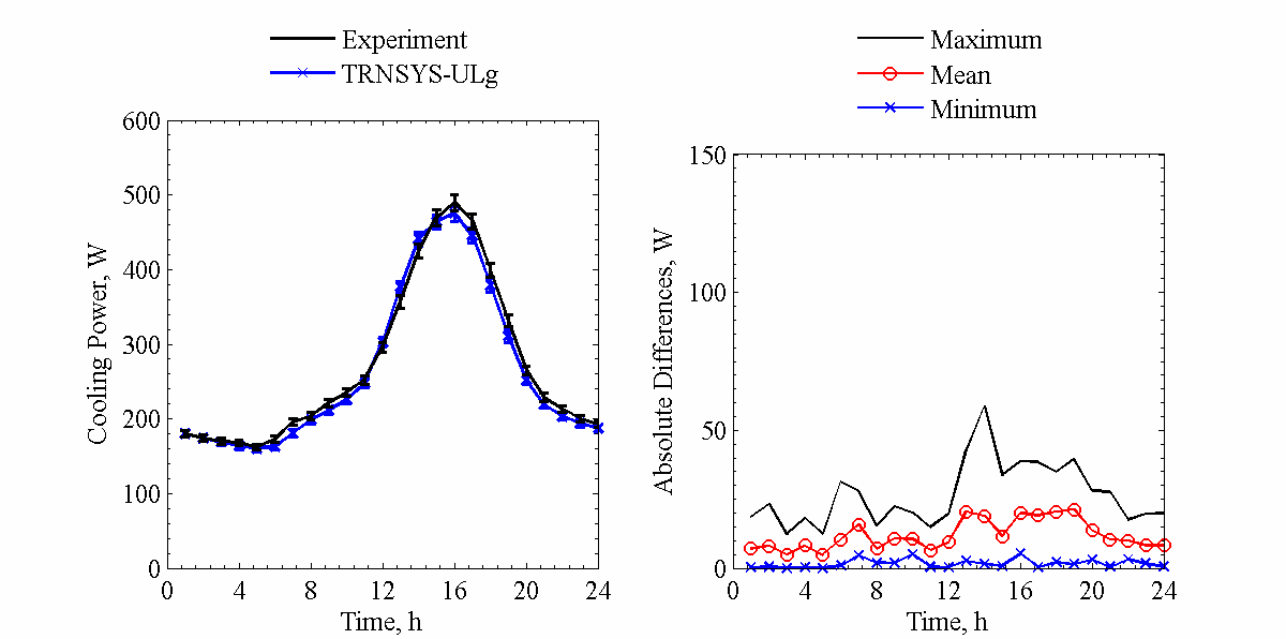

Figure 11.5e. Cooling power comparisons for IDA-Detwind averaged over each given hour of the day (left) and absolute maximum, mean, and minimum differences for a given hour of the day (right).

Table 11.8. Average overall uncertainty and 10 most influential input parameters from the n-way factorial analyses in Watts.

Parameter	**Forward**	**Backward**
Overall uncertainty	3.39	3.40
Average air temperature	-1.88	1.88
Fan power	1.04	-1.04
West wall surface temperature	0.79	-0.79
Ceiling surface temperature	0.73	-0.73
North wall surface temperature	0.69	-0.69
East wall surface temperature	0.56	-0.56
Outside air temperature	0.56	-0.56
Direct-normal solar irradiance	0.55	-0.56
Diffuse horizontal solar irradiance	0.47	-0.50
Front reflectance of inner glass pane	-0.43	0.42

Table 11.9. Statistical comparisons for cooling power in Exercise 8.

Parameter	Experiment	HELIOS	EnergyPlus	DOE-2.1E	IDA-Detwind	TRNSYS-ULg
$\bar{x}$	269.5 W	281.2 W	257.8 W	282.8 W	284.1 W	263.5 W
s	112.8 W	130.8 W	101.4 W	141.5 W	121.0 W	111.9 W
x_{max}	576.2 W	614.4 W	524.5 W	637.0 W	585.0 W	541.0 W
x_{min}	133.1 W	145.3 W	158.0 W	143.0 W	155.5 W	145.7 W
$\overline{D}$	-	11.6 W	-11.7 W	13.3 W	14.5 W	-6.1 W
$\overline{\lvert D \rvert}$	-	18.6 W	15.7 W	26.6 W	16.0 W	11.9 W
$\lvert D_{max} \rvert$	-	103.9 W	54.0 W	128.4 W	88.5 W	58.8 W
$\lvert D_{min} \rvert$	-	0.0 W	0.0 W	0.2 W	0.0 W	0.0 W
D_{rms}	-	27.9 W	19.7 W	37.7 W	22.5 W	15.1 W
$\lvert D \rvert_{95\%}$	-	69.7 W	40.8 W	88.0 W	52.1 W	31.3 W
$\overline{OU}$	6.1 W	-	6.3 W	-	-	-
$\overline{UR}$	-	1.3	1.2	1.9	1.2	1.0
UR_{max}	-	5.4	3.4	6.6	6.1	3.4
UR_{min}	-	0.0	0.0	0.0	0.0	0.0
$\overline{\lvert D \rvert} / \bar{x} \times 100\%$	-	6.9%	5.8%	9.9%	6.0%	4.4%
$\overline{D} / \bar{x} \times 100\%$	-	4.3%	-4.3%	4.9%	5.4%	-2.3%

Figure 11.6 contains a plot of the transmitted solar power for each given hour of the day through the glazing unit and interior shading screen for all programs.

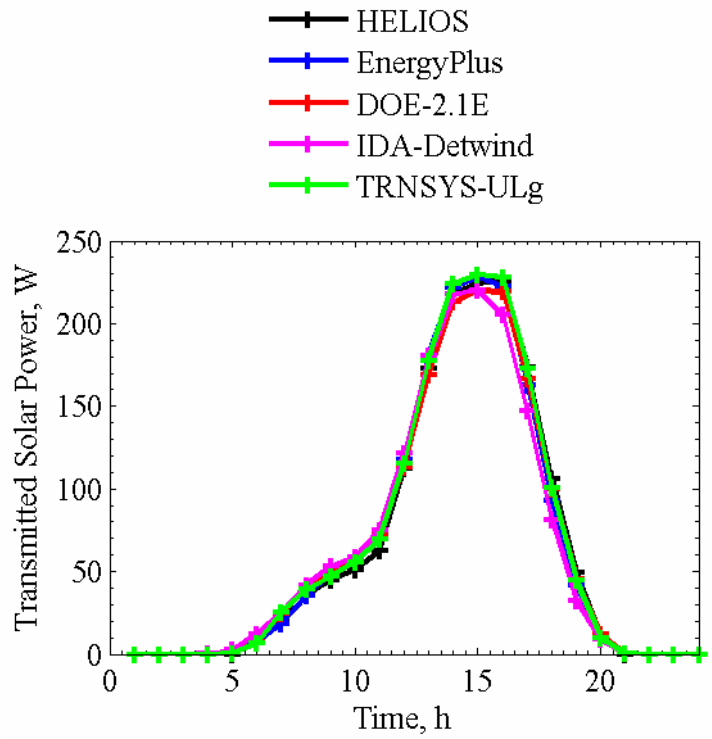

Figure 11.6. Transmitted solar power averaged over each given hour of the day.

Like in the glazing only exercise, the optical models used to simulating the glazing were very similar. Additional challenges were addressed in the building energy simulation programs

concerning properly accounting for the thermal bridges due to the mounting, spacer, and window frame.

CHAPTER 12: EMPA MODELERS' REPORTS

For each exercise, the modelers performing the simulation were requested to provide a brief summary of methodologies employed for modeling the experiments. During the course of the exercise, test specifications and inputs were provided to modelers and results were submitted for blind exercise; the data were then provided to the participants for identifying errors in program inputs. These errors and the associated changes were also documented by the modelers to provide guidance on common mishaps that can be made when simulating a building.

12.1. HELIOS

Name and Institution: Stephan Carl, Swiss Federal Laboratories for Materials Testing and Research (EMPA), Laboratory for Building Technologies

Building Energy Simulation Software and Version: HELIOS XP

12.1.1. General Information

HELIOS was developed at EMPA from 1982-1992 and is currently sold in Switzerland and Germany. A new initiative was started in 2004 to update software algorithms and develop a user-friendly interface for use with the Microsoft Windows operating system. The latest version of the program, called HELIOS XP, was released in November 2006. The software is now only available in German; however, an English version of the software is currently under development.

12.1.2. Transient Experiment Modeling (Exercise 1)

This exercise was simulated assuming constant convective heat transfer coefficients for each construction element as a function of surface orientation; these values were specified according to EN/ISO 6946 [19], and radiative heat transfer was neglected. For all simulations exercises, hourly outside surface temperatures and power inputs were scheduled into the program. The thermal bridges were accounted for with a fictitious wall of the same construction as the ceiling and interior walls and an equivalent area that corresponded to the overall thermal bridge conductance. The thermal mass inside the test cell was simulated as an internal construction element made of thin steel and appropriate dimensions were chosen to match the estimated thermal mass from specifications in the experiments.

12.1.3. Evaluation of Irradiation Models on Tilted Surfaces (Exercise 2)

HELIOS uses a Perez 1987 model [20] to estimate radiation on a tilted facade. When implementing this model, the program accounted for elliptical orbit of the earth when computing extraterrestrial radiation. For this exercise and the subsequent solar gain exercises, global and diffuse horizontal solar irradiances were used as inputs to the program.

12.1.4. Glazing Only Experiment (Exercise 3)

A glazing unit was added to exterior wall to the model from Exercise 1**.** The external thermal bridge was then included with the linear thermal transmittance from the spacer. The emittance of glazing unit was adjusted in HELIOS to match the measured center-pane thermal transmittance. The solar normal transmittances and reflectances for each pane of glass and measured emittance were input into the program and an angular-dependent model described in the Window 4.1 manual [21] was employed to calculate optical properties of the glazing unit. Radiative heat transfer was accounted for in the test cell by using simulated average interior surface construction element temperatures and emittances to calculate a radiative heat transfer coefficient according to EN/ISO 6946. This methodology linked the construction element surface temperatures to the interior test cell air node; convection was specified in the same manner as in Exercise 1.

No changes were made to the blind results.

12.1.5. Exterior and Interior Shading Screens (Exercises 4 and 5)

Exercises 4 and 5 used the same model as in Exercise 3 with the addition of shading screens. The exterior and interior shading screens were modeled as additional sheets of thin glass with inputs of normal solar reflectance and transmittance. The air gap calculations between the shading screens and the glazing unit were made according to an algorithm developed by Chauval and Millet [22]. The hemispherical emittances of the shading screens were estimated as 90%.

No changes were made to the blind results.

12.1.6. Exterior Venetian Blind and Internal Mini-Blind Assemblies (Exercises 6 and 7)

Exercises 6 and 7 used the same model as in Exercise 3 with the addition of interior and exterior blind assemblies. The blind model in HELIOS calculates two-dimension diffuse geometric viewfactors that account for curvature in the blind slat. The input optical properties were normal solar reflectance and hemispherical emittance. The underlying theory concerning the blind model is given by Simmler [23].The air gaps between the blind assemblies and the glazing unit were modeled like in Exercises 4 and 5.

No changes were made to the blind results.

12.1.7. Window (Exercise 8)

Exercise 8 was simulated in the same manner as Exercise 3. The addition of the frame was accounted for by adding a thermal bridge that accounted for spacer, mounting, and window frame transmittances. In this version of HELIOS, energy absorbed by the window frame via longwave and/or solar radiation is neglected.

No changes were made to the blind results.

12.1.8. Discussion of Results

HELIOS was used to simulate all exercises. For the eight exercises, the results for predicted cooling power were within 95% credible limits four times. HELIOS performed best for the glazing unit only and interior shading screen exercises.

12.1.9. Validation Impact

Numerous changes to HELIOS were made as a result of this validation effort. The tilted radiation model of the façade was changed from an Isotropic model to a Perez 1987 model and ground reflectance was made a user input. A new angular-dependent optical model was added for simulation of glazing units, and a blind assembly algorithm was implemented into the program. Changes were also implemented into the program to accommodate hourly schedules for internal loads and inside air and outer surface temperatures.

An error was discovered in the course of these validations in the thermal transmittance of the glazing unit. In the calculation, the thermal conductivities of the glass panes were neglected when computing the center-pane thermal transmittance.

12.2. EnergyPlus

Modeler and Institution: Peter Loutzenhiser, Swiss Federal Laboratories for Materials Testing and Research (EMPA), Laboratory for Building Technologies

Building Energy Simulation Software and Versions:

Exercise 1: EnergyPlus Version 1.2.0.029
Exercise 2-3: EnergyPlus Version 1.2.2.030
Exercise 4-8: EnergyPlus Version 1.2.3.023

12.2.1. General Information

The development of EnergyPlus began in 1996 as an initiative by the US Department of Energy; the first version of the software was released to the public in Spring 1998. Detailed information concerning the concept and development of the program is described in detail by Crawley et al. [24].

12.2.2. Transient Experiment Modeling (Exercise 1)

Exercise 1 was simulated using specifications and fixed thermophysical properties (as were subsequent exercises). Measured hourly outer surface temperatures and internal loads were used as program inputs. The thermal bridges were simulated in EnergyPlus by adding non-radiating surfaces to the back of the space with a constant outer cell surface temperature of 23.22 °C, which was the time-averaged outer cell surface temperature during the transient experiment. Because EnergyPlus calculates the radiative heat transfer using view factors and assuming gray and diffuse surfaces, six additional surfaces that faced each other were added to the model. The convective heat transfer coefficients for these surfaces were fixed and an equivalent area based on the thermophysical properties of the thermal bridge construction elements and was used to compute an equivalent area that accounted for total steady-state thermal bridge transmittance. For the other surfaces, a detailed approach was used to compute the convective heat transfer coefficient as a function of temperature difference between surface and cell air and surface orientation.

12.2.3. Evaluation of Irradiation Models on Tilted Facades (Exercise 2)

In EnergyPlus, a Perez 1990 model [25] was used to predict tilted surface solar irradiance using direct-normal and diffuse horizontal solar irradiances. The exercise was performed using weather data in 10 minute time intervals. In the EnergyPlus Perez 1990 algorithm, a constant averaged extra-terrestrial radiation is assumed for the whole year that does not account for the elliptical orbit of the earth around the sun.

12.2.4. Glazing Only Experiment (Exercise 3)

Exercise 3 was simulated by adding a glazing unit to the exterior façade of the model used in Exercise 1. Hourly internal loads, outer surface temperatures for the internal construction elements, and average air temperatures were scheduled into the program. For both panes of glass, reflectances and transmittances at near-normal incident angle in the wavelength interval between 250 and 2500 nm were used as inputs for EnergyPlus so that angular dependent calculations similar to those found in Window 5.2 could be made. The edge effects were modeled by modifying the "Ratio of Frame-Edge Glass Conductance" field. In EnergyPlus, the edge is defined as a 63.5 mm distance from the frame; therefore, an additional simulation was run in BISCO [13] software applying the same procedure described above to calculate a new center-of-glazing thermal transmittance using this definition. The impact of thermal bridges at the external wall edges was accounted for by adding additional thermal transmittance to the glazing edge calculation. Because EnergyPlus employs an algorithm for equivalent thermal conductivity of the glazing cavity that provides slightly higher values than those calculated above, the thermal conductivities of the glass

panes were reduced accordingly. A general overview for modeling windows in EnergyPlus is provided by Winkelmann [26]. Six hourly time steps were used with weather data at 10-minute intervals.

No changes were made from the blind to the non-blind exercise.

12.2.5. Exterior and Interior Shading Screen (Exercises 4 and 5)

The same model from Exercise 3 was used with the addition of exterior (Exercise 4) and interior (Exercise 5) shading screens. In the EnergyPlus optical model, all window layers such as glass panes and shading device(s), are assumed to be flat, parallel, and infinite. System reflectances and transmittances are computed based on a ray tracing technique. Spectral optical properties can be used for determining glazing reflectance and transmittance. The shading screen is, however, modeled using only a non-spectral method. The integral solar transmittances and reflectances of the screen based on measurements were used as program inputs. The ratios of the open sides as well as the openness factors of the shading devices were calculated and entered into the program. The screen thickness was assumed to be 0.5 mm and estimates for screen thermal conductivities (0.9 $Wm^{-1}K^{-1}$) were taken from ASHRAE Fundamentals [27]; these parameters were of very minor importance. The methodology employed to calculate the total heat transfer between the shade and the window in the program was taken from EN ISO 15099 [28], which factored in surface temperatures of the glazing and the screens to calculate the heat transfer through the air gap at each time step. According to a methodology proposed by [29], the emittances of the shading screens were assumed to be the product 0.9/(1-openness factor). The calculation performed in EnergyPlus assumed buoyancy driven flow. Weather data measured in 10 minute intervals were input into the program as boundary conditions.

No changes were made from the blind to the non-blind exercises.

12.2.6. Exterior Venetian Blind and Interior Mini-Blind Assemblies (Exercises 6 and 7)

The same model from Exercise 3 was used with the addition of exterior (Exercise 6) and interior (Exercise 7) shading screens. EnergyPlus contains a blind model that assumes flat diffuse slats [29] similar to the model proposed in prEN 13363-2 [30]. The slat's normal solar reflectance, hemispherical emittance, width, thickness, distance from the outer pane of glass (measured from the center of the blind slats), and distance between individual slats were entered into the program. The heat transfer between the window and the shading devices was calculated using ISO 15099 [28] assuming natural buoyancy; this was performed as an iterative procedure in the program.

No changes were made from the blind to the non-blind exercises.

12.2.7. Window (Exercise 8)

A window was specified in the exterior façade using the model from Exercise 1. Measured reflectances and transmittances for each pane of glass from 250 nm or 2500 nm were input in EnergyPlus as well as emittance. The thermal conductivities of the glass panes were reduced to match the thermal conductance measured from the hotbox due to the same constraints discussed in Exercise 3. The linear thermal transmittance due to the mounting was included in the overall window frame conductance as well as the external wall thermal bridge. The spacer effects were computed using the definition of edge-effects (Section 12.2.4) for EnergyPlus.

No changes were made from the blind to non-blind exercises.

12.2.8. Discussion of Results

EnergyPlus was used to simulate every exercise. For this suite of experiments, EnergyPlus was within the overlapping 95% credible limits described by the uncertainty ratio for Exercises 1,4,6,

and 7 and outside 95% credible limits for the other exercises. The program performed best when simulating blind assemblies (both interior and exterior).

12.2.9. Validation Impact

During these validation exercises, it was discovered that blind schedule inputs for specifying changing blind slat angles was expected in radians but prescribed in degrees; this problem was fixed in Version 1.2.3.023.

12.3. DOE-2.1E

Modeler and Institution: Peter Loutzenhiser, Swiss Federal Laboratories for Materials Testing and Research, Laboratory for Building Technologies

Building Energy Simulation Software and Versions: DOE-2.1E Version-119

12.3.1. General Information

The original version of DOE-2.1E was released in November 1993 from Lawrence Berkley National Laboratories. DOE-2 was developed by Lawrence Berkeley National Laboratory, Hirsch & Associates, Consultants Computation Bureau, Los Alamos National Laboratory, Argonne National Laboratory and University of Paris. Major support was provided by the U.S. Department of Energy; additional support was provided by the Gas Research Institute, Pacific Gas & Electric Company, Southern California Edison Company, Electric Power Research Institute, California Energy Commission and others [31].

12.3.2. Transient Experiment Modeling (Exercise 1)

Exercise 1 was simulated using specifications and fixed thermophysical properties (as were subsequent exercises). To use the outer surface temperatures as boundary conditions, adjacent zones were created with a single zone air conditioner for each test cell surface. The zone temperature was scheduled as the outer cell surface temperature. The inside film resistance for these zones was specified as zero, thus making the adjacent zone temperature and the outer cell surface temperature equal. Because the inside surface temperatures of the construction elements were nearly the same the effect of radiative heat transfer between the surfaces was neglected. The inside film coefficients for the walls, ceiling and floor were specified according to EN ISO 6946 [19] considering only convective heat transfer. The thermal mass inside the cell was modeled as a steel sheet.

12.3.3. Evaluation of Irradiation Models on Tilted Facades (Exercise 2)

In DOE-2.1E, a Perez 1990 model [20] was used predict tilted surface solar irradiance using direct-normal and global horizontal solar irradiances. The exercise was performed using weather data in one hour time intervals. In the DOE-2.1E Perez 1990 algorithm, a constant averaged extra-terrestrial radiation is assumed for the whole year that does not account for the elliptical orbit of the earth around the sun.

12.3.4. Glazing Only Experiment (Exercise 3)

Exercise 3 was simulated by adding a glazing unit to the exterior façade of the model used in Exercise 1. For DOE-2.1E, the glazing unit was modeled using Window 5.2 [32] coupled with wavelength-dependent near-normal optical measurements from a custom database file from Optics5 (Rubin et al. [33]). Background information for this type of modeling is provided by Reilly et al. [34]. Because there was no quantitative input for edge effects in DOE-2.1E (there were spacer types), a 3.0 cm window frame was modeled with an equivalent thermal conductivity to account for the edge effects, exterior thermal bridges, one-dimensional heat transfer of the construction

displaced by the frame, and two-dimensional heat transfer. The thermal transmittance from the Window 5.2/DOE-2 output file was modified to reflect the center-of-glazing thermal transmittance calculated above with adjustments made to account for different heat transfer coefficients. Hourly weather data were put into TMY2 weather format and read into the program; the outputs were verified with the measured data. In TMY2 weather format, the horizontal infrared irradiance is not explicitly described; therefore, the opaque sky cover quantity from the weather inputs (including the infrared irradiance) was calculated by reversing the algorithm used to calculate infrared irradiance in the program (Walton [35]; Clark and Allen [36]). Measured direct-normal and global horizontal solar irradiance were used as inputs for the calculations of the global vertical solar irradiance on the external façades. Combined constant heat transfer coefficients that factored in the impact of radiation and convection as a function of surface orientation using design standards were taken from 2001 ASHRAE Handbook, Fundamentals [27].

No changes were made from the blind to the non-blind exercise.

12.3.5. Exterior and Interior Shading Screen (Exercises 4 and 5)

The same model for Exercise 3 was used for these experiments with the addition of shading devices. The optical model of DOE-2.1E is much simpler than the EnergyPlus model. The transmitted solar energy through the glazing unit is reduced by the integral solar transmittance of the shading screen (i.e., no solar radiation reflected from the glazing and then back-reflected into the room is taken into account). Because the outer surface temperature of the glazing unit and the screen were not known, a less robust method was used to account for the heat transfer in the gap between the shade and the window. The amount of additional heat transfer through the gap between the glazing and the shading screen was calculated assuming the same screen properties used for EnergyPlus and the thermal resistance for a well-ventilated air layer using EN ISO 6946 [19].

No changes were made from the blind to the non-blind exercises.

12.3.6. Window (Exercise 8)

A window was specified in the exterior façade using the model from Exercise 1. Measured reflectances and transmittances for each pane of glass from 250 nm or 2500 nm were input in DOE-2.1E using Optics and Window 5.2 output file. The linear thermal transmittances due to the spacer and mounting and the external wall thermal bridge were included in the overall window frame conductance.

No changes were made from the blind to non-blind exercises.

12.3.7. Discussion of Results

DOE-2.1 was used to simulate Exercises 1-5 and 8. Currently, DOE-2.1E or subsidiary software do not contain algorithms necessary for simulated complex window shading devices like Venetian blinds and mini-blinds. For this suite of experiments, DOE-2.1E was within the overlapping 95% credible limits described by the uncertainty ratio for Exercises 1 and 4 and outside 95% credible limits for the other exercises; however, the results were comparable with other programs with more advanced shading and heat transfer algorithms.

12.4. ESP-r

Name and Institution: Paul Strachan, Department of Mechanical Engineering, University of Strathclyde

Building Energy Simulation Software and Version: ESP-r Version 10.12

12.4.1. General Information

ESP-r is an open source program developed by the Energy Systems Research Unit at the University of Strathclyde with input from many other organizations. It has been developed over a 28 year period. Full details of the underlying theory can be found in [37].

12.4.2. Transient Experiment Modeling (Exercise 1)

Because ESP-r requires a fully bounded zone, it was not possible to simulate the thermal bridges by simply adding additional surfaces connecting the internal air temperature with the external environment to represent the thermal bridges. Different approaches for modelling edge effects were tried, but the one giving the best agreement with measured data was the use of a ‘‘fin’’ added to the back of the test cell with a total surface area equivalent to that used in the other simulation programs. This allowed the edge losses to be modelled without affecting the convective and radiative heat transfer from the 1-D heat transfer surfaces. Boundary temperatures were modelled by creating additional zones and imposing the measured temperatures. Several different convective regimes can be modelled by ESP-r, but the results presented here were based on the same convective coefficients as fixed according to EN ISO 6946 [19]. The thermal mass in the test cell was modelled as steel sheets in the room of appropriate dimensions.

12.4.3. Evaluation of irradiation models on tilted facades (Exercise 2)

ESP-r has the Perez 1990 [25] model as its default, but other models are available to the user, namely the Isotropic [38], Klucher [39], Muneer [40] and Perez 1987 [20] models. Measured 6 minute averaged data were input to the program. The program also takes into account variations in the extraterrestrial radiation in the Perez and Muneer models. It is also possible to use direct-normal plus diffuse horizontal solar irradiances, or global horizontal plus diffuse horizontal solar irradiances as inputs to ESP-r; for this study, only the direct normal and diffuse horizontal inputs were used.

12.4.4. Glazing Only Experiment (Exercise 3)

For ESP-r, the glazing unit was modelled using WIS [41] software. The inputs were the optical and emittance values at normal incidence for the two panes of glass. The calculated angular dependent transmission and absorption properties over the solar spectrum were then used in the ESP-r model. The glazing thermal bridge was modelled by adding a window frame with an equivalent thermal conductivity to account for the thermal bridges and the one-dimensional heat transfer of the construction displaced by the frame. The thermal transmittance from the WIS output for the centre-of-glazing thermal transmittance was used to calculate an equivalent air gap resistance of the argon-filled glazing cavity. Simulations were undertaken with six-minute climate data, using the measured direct normal and diffuse horizontal irradiances. The internal convection was modelled using the buoyancy correlations reported by Alamdari and Hammond [42] for vertical and horizontal surfaces, which take into account direction of heat flow, surface dimensions, and temperature differences.

12.4.5. Exterior and Interior Shading Screens (Exercises 4 and 5)

The two situations of external and internal free-hanging shading screens required the modelling of ventilation between the screen and the glazing. This was accomplished in ESP-r by modelling the gap between the shading screen and the glazing as a thermal zone. The advantage of modelling the air gap as a thermal zone is that the heat transfer processes of long-wave radiant exchange, surface convection and solar transmission, reflection, and absorption can be fully modeled. A network air-flow model was defined to predict the airflow due to buoyancy in the case of the internal shading screen, and due to both buoyancy and wind pressure in the case of the external shading screen. There were uncertainties regarding suitable boundary pressure coefficients for the edge of the external blind, but the results were found to be not particularly sensitive to the chosen values. For the external shading screen, the thermal zone representing the air gap between the screen and the win-

dow was modelled with the shading screen material on the external surface. The glazing unit separated the two thermal zones representing the test cell and the air gap. This was reversed for the internal shading screen, with the shading screen material separating the two thermal zones. The optical properties of the window (without shading screens) were obtained using the software WIS, given the optical properties at normal incidence for the two panes of glass. The calculated angular dependent transmission and absorption properties over the solar spectrum were then used in the ESP-r model. The thermophysical properties of the shading screens were assumed in a similar way to those described above for EnergyPlus (Section 12.2). Simulations were undertaken with 6 minute climatic data, using the measured direct-normal and diffuse horizontal irradiances. Measured temperatures from the test cell guard spaces were input as boundary conditions, together with the measured average test cell air temperature and internal fan power. The internal convection for all internal test cell surfaces, including those for the internal shading screen, was modelled using the buoyancy correlations reported by [42] for vertical and horizontal surfaces which take into account direction of heat flow, surface dimensions and temperature differences. Cooling power and internal surface temperatures were also predicted.

12.4.6.. Discussion of Results

ESP-r was used to simulate Exercises 1 to 5. For this suite of experiments, ESP-r was within the overlapping 95% credible limits described by the uncertainty ratio for Exercises 1 (UR=0.4) and 5 (UR=0.9), but outside 95% credible limits for Exercises 3 (UR=1.6), and 4 (UR=1.1). In the case of Exercise 2, concerned with predicting the incident radiation, the Perez 1990 anisotropic sky model gave the best agreement with experiment (UR=1.2).

12.4.7. Validation Impact

ESP-r has a number of anisotropic sky models for diffuse radiation. In May 2005, the Perez 1990 model was made the default rather than the Perez 1987 model which had been the default up to that time. The empirical data from this IEA work (and other tests) were used to justify this change. At the same time other minor enhancements were made in solar processing, with more recent algorithms for extraterrestrial radiation and air mass calculations.

12.5. TRNSYS-TUD

Name and Institution: Clemens Felsmann, Technical University of Dresden (TUD), Institute of Thermodynamics and Building Systems Engineering

Building Energy Simulation Software and Version: Technical University of Dresden research code based on the frame of TRNSYS 14.2

12.5.1. General Information

The software tool, TRNSYS-TUD, is a research code that was developed at the Institute of Thermodynamics and Building Systems Engineering at Technical University of Dresden and is based on the frame of the TRNSYS version 14.2. Modifications and developments from the original source code were necessary to stabilize calculation processes, improve user-friendliness and handling of the software, and to extend fields of software application. In this context, some new features have been added relating to the building model, detailed longwave radiation exchange, underfloor heating and thermally activated layers, detailed solar distribution, internal windows, simple daylighting, etc.. The ability to run simulations at smaller time steps (seconds) was also implemented. The realization of some of these features was initialized by the IEA Task34/Annex43 software validation tests.

12.5.2. Transient Experiment Modeling (Exercise 1)

The TRNSYS-TUD model was constructed using convective heat transfer coefficients that were

functions of the differences between the air temperature and the surface temperature and the orientation of the construction elements. The heat losses due to thermal bridges in the envelope of the test cell were simulated using an infiltration model. The steady-state heat loss coefficients of the thermal bridges were converted into a fictitious air change rate. The radiative heat transfer was calculated assuming gray diffuse surfaces using view factors. The temperature dependent thermophysical properties were fixed using an average mean envelope temperature of 29.00°C.

12.5.3. Evaluation of irradiation models on tilted facades (Exercise 2)

TRNSYS-TUD allows the user to select from four models and various inputs for solar irradiance. For these experiments, the Isotropic [38], Hay–Davies [43], Reindl [44], and Perez 1990 [25] model were used with inputs of measured direct-normal and global horizontal irradiances; the inputs to the models were in one hour timesteps. The extraterrestrial irradiation was varied to account for the elliptical orbit of the sun for the Perez, Reindl, and Hay–Davies models.

12.5.4. Glazing Only Experiment (Exercise 3)

In Exercise 3, the optical properties of the glazing unit were precalculated using WINDOW 5 [32] and OPTICS 5 [33] programs (software distributed by LBNL) based on given spectral optical data for the different glass panes. The calculated angular-dependent solar heat gain coefficients were then used by TRNSYS-TUD for the load calculations. An equivalent thermal conductivity of the glazing cavity was calculated according to EN ISO 15099 [28] and temperature-dependent internal and external heat transfer coefficients were used. Although edge effects were almost negligible, they were taken into account by a modified steady-state heat loss coefficient of the 6.0 cm window frame. The heat loss was calculated based on the given two-dimensional heat transfer data. The thermal bridges for both exterior surfaces and surfaces adjacent to the guard zone were modeled in the envelope of the test cell using an infiltration model; the steady-state heat loss coefficient for the thermal bridges was converted into two fictitious air change rates. A detailed algorithm was used to calculate the convective heat transfer coefficients as functions of temperature differences (average surface and air temperatures) and surface orientation. The radiative heat transfer was calculated assuming gray diffuse surfaces using view factors. Simulations were performed using measured hourly weather data in one-hour time steps. Measured diffuse and global horizontal irradiance were employed as inputs to calculate the global vertical irradiance on the exterior façade.

There were no changes made from the blind to the non-blind exercise.

12.5.5. Exterior and Internal Shading Screen (Exercises 4 and 5)

The model from the glazing only exercise was used with the addition of internal and external shading screens. The TRNSYS-TUD window model consisted of a thermal and optical calculation algorithm. For the external shading device case, the only coupling between both algorithms was the solar absorptance of the glass panes that leads to heat sources in the panes. Interior and exterior shading devices were treated as additional heat transfer resistances. The model accounted for re-reflections between window, shading device, and inside wall surfaces.

If there was an internal shading device, then a convective component that represented solar radiation absorbed at the internal shading was directly linked to the air temperature node. The outside shading device consisted only of a transmittance shield that reduced irradiation at the outside surface of the window. There was no algorithm implemented that calculates the impact of the air flow between window and shading devices or the heat transfer coefficients.

Due to poor predictions, a model that accounted for the re-reflections between window and shading screens was added to the standard TRNSYS simulation tool.

12.5.6. Exterior Venetian Blind Assembly (Exercise 6)

For the TRNSYS-TUD model, diffuse and global horizontal irradiance were used as inputs in one hour intervals. This version of TRNSYS does not contain a tool for explicitly modeling exterior Venetian blinds. For that reason, the blind slats were modeled as small overhangs related to the

window sub-surfaces. Therefore the standard component of TRNSYS (Type34) was used, which was modified to also allow the simulation of tilted overhangs. The depth of slat overhang was 0.1031m and they extend glazing width at both sides by 0.0375m. The results of the standard overhang model have been corrected using a fin factor that should account for blind slat thickness. The fin factor was calculated according to Equation 12.1.

$$f_{\text{fin}} = 1 - \frac{0.0131\,\text{m}}{0.062\,\text{m}} = 0.789 \qquad (12.1)$$

The dimension of a single window sub-surface that corresponds to a single slat (representing the overhang) was (0.0131-0.062) m X 1.29 m. Optical properties of the slats or any re-reflection effects between slats were not taken into consideration for the simulation.

12.5.7. Discussion of Results

The TRNSYS-TUD software showed excellent agreement in the first validation exercise The accuracy of predicting solar irradiation on a tilted facade depended on the algorithm used by the solar processor shown in the second exercise. A comparison of Exercises 3 to 5 shows that installation of shading devices (exterior or interior) reduce the errors in the predicted building loads. Based on this information, both the basic algorithms for modeling solar radiation passing through unshaded window as well as solar distribution in the room need to be analyzed more carefully Exercise 6 shows that it was not possible to model detailed shading devices (for instance Venetian blinds) with simple standard shading models without taking into account some a-priori knowledge from the experiments concerning solar gain functionality.

12.5.8. Validation Impact

All of these validation exercises were very useful in assessing whether the software handles the impact of solar radiation on the thermal building performance correctly. One assumption that was found was that TRNSYS-TUD does account for re-reflections into the spaces between the window panes and shading devices. This prompted modifications to the TRNSYS TUD source code.

Furthermore, Exercise 2 provided valuable insight to the user regarding differences in models for calculating solar irradiation on tilted façade and was useful for emphasizing the importance of model selection.

12.6. IDA-ICE

Name and Institution: Sven Moosberger, University of Applied Science of Central Switzerland (HTAL), Forschungsbereich Architektur+Technologie (A+T)

Building Energy Simulation Software and Version: IDA-ICE 3.0 Build 14

12.6.1. General Information

IDA is a simulation environment developed at the Royal Institute of Technology (KTH) in Stockholm, Sweden. Today it is maintained and supported commercially by EQUA SA in Stockholm. One application of IDA is IDA-ICE designed for thermal building simulations. IDA-ICE dynamically simulates room air temperatures, mean radiant temperatures at any point in a room, air humidity, and CO_2 concentrations and employs an adaptive time step. The distribution of incoming solar and longwave radiation to all room surfaces are calculated using a view factor method. Both IDA simulation environments and IDA-ICE employ various user levels which include:

- IDA room level for very simple simulations that are restricted to one room (web based freeware)
- IDA-ICE standard level with a graphical user interface for multiple zone buildings with HVAC System

- IDA-ICE advanced level for detailed model building, free variable linking, and reporting
- IDA-ICE modeler level for simple model changes

In the next version of IDA-ICE, a new detailed window model is planned. This model, called "Detwind", is under development and was used for Exercises 3 and 8 of this empirical validation.

12.6.2. Transient Experiment Modeling (Exercise 1)

The thermal bridges inputs were modeled at the standard level and linked in the advanced level to the outer floor surface temperature. Hourly outer surface temperatures and internal loads were scheduled into the program at the advanced level. The longwave radiative heat transfer was simulated using view factors. A dynamic convective heat transfer coefficient algorithm that accounted the construction element length, orientation, and air and surface temperature differences was used. The thermal mass inside the test cell was modeled by increasing the mass of the air.

12.6.3. Evaluation of Irradiation Models on Tilted Facades (Exercise 2)

IDA-ICE currently has three models used for predicting tilted surface radiation, including: ASHRAE [45], Kondratjev [46], and Perez 1990 [25]. From this exercise, the Perez 1990 model was chosen to model subsequent solar gain experiments because the results corresponded best with measured global vertical irradiance on the southwest façade. Hourly direct-normal and diffuse horizontal solar irradiances were the inputs into the program. A model called the "climate processor" was used to calculate the sun position; these pre-calculations were then used in conjunction with the selected diffuse tilted surface radiation model.

12.6.4. Glazing Only Experiment (Exercise 3)

The model from Exercise 1 was used with the addition of a glazing unit in the external construction element. The thermophysical properties were modified to account for changing mean building element temperatures; these modifications were also made in all subsequent exercises as well.

Three window models were used to simulate the glazing only experiment. The existing model in IDA-ICE can take inputs that include: solar heat gain coefficient and solar transmittance and compute shading coefficients; however for this exercise the center-pane thermal transmittance, and inner and outer emittance were inputs and the shading coefficients for radiation (Sc) and solar radiation (Ssc) were computed using two different methods, including: 1) a manual calculation performed using SIA rules and 2) in a subsidiary software called PARASOL [47]. The computed Sc and Ssc using SIA rules were 0.5336 and 0.4730, respectively, and from PARASOL were 0.5563 and 0.4931, respectively. The program then adjusted the shading coefficients to account for angular dependent optical properties of the glazing unit. The new Detwind model used ISO-15099 [28] to compute radiative heat transfer and all window parameters.

For the glazing only experiment and subsequent solar gain experiments with the glazing unit, the thermal bridge between the test cell and the guard zones was set at 4.526 W/K, and the thermal bridge to the outside was 0.5010 W/K. The outside thermal bridge included: the linear thermal transmittance of the glazing and the external thermal bridges.

To maintain the air temperature in the test cell, a terminal heating/cooling unit was added to the model to that supplied and exhausted conditioned air to and from the space. The mass flow rate of the supply air was fixed at 1 kg/s and the supply air temperature was controlled by a PI controller; the fan for the unit was always turned off, and hourly test cell air temperatures were scheduled into the program.

No changes were made to the model from the blind to the non-blind exercise.

12.6.5. Exterior and Interior Shading Screens (Exercises 4 and 5)

The same model was used as in Exercise 3 with the addition of exterior and interior shading screens. The Detwind window model currently does not support window shading devices so these

exercises were performed using the existing model and the SIA rules. The SIA rules generated for the Sc and Ssc values were 0.255 and 0.238, respectively, for the exterior shading screen and were 0.655 and 0.337, respectively, for the interior shading screen. No changes were made in the software to account for the additional thermal resistant of the shading screen and the air gap.

No changes were made in the models from the blind to the non-blind exercises.

12.6.6. Window (Exercise 8)

This exercise was only simulated using the new Detwind model. The parameters for the window panes and gas filling were determined using the provided window properties. The thermal bridges due to frame mounting were added to the thermal transmittance of the window frame.

12.6.7. Discussion of Results

All simulation results corresponded well with the experimental data. The existing IDA-ICE model was limited in accuracy while the new Detwind model required detailed knowledge of the window composition. Both models still cannot simulate blind assemblies. Current plans include the implementation of a blind assembly algorithm into the Detwind model.

12.6.8. Validation Impact

The accuracy of the existing window model was quantified. For most of the simulation cases, the accuracies were within the uncertainties of the window parameters. The new Detwind model provides better simulation performance in cases where there is detailed knowledge of the window parameters requiring access to an extensive window database. Plans are now in place for the development and refinement of a detailed window model (Detwind). An additional change that was made in IDA-ICE because of this validation exercise was that Perez 1990 model was made the default tilted surface radiation model in IDA-ICE.

12.7. TRNSYS-ULg

Names and Institution: L'HOEST Julien, ANDRE Philippe, ADAM Christophe, Department of Environmental Science and Management, University of Liège

Building Energy Simulation Software and Version: TRNSYS 16.00.0038 developed by the Solar Energy Laboratory (University of Wisconsin-Madison) in Madison, Wisconsin USA.

12.7.1. General Information

TRNSYS ("Transient System Simulation") is a transient system simulation program with a modular structure. The modular nature of TRNSYS gives the program tremendous flexibility and facilitates additions to the program of mathematical models not included in the standard TRNSYS library. TRNSYS is well-suited for detailed analyses of systems whose behavior is time-dependent.

The building model used in this work was Type 56 developed by TRANSSOLAR Energietechnik GmbH in Stuttgart, Germany. Type 56 is the version which is includes in the TRNSYS 16.00.0038 version; TRNFLOW was not used.

12.7.2. Transient Experiment Modeling (Exercise 1)

From the characteristics of the wall given in the experiment setup, modeling of the walls in TRNSYS Type 56 was straightforward. Fixed thermophysical properties were used and measured hourly outer surface temperatures and internal loads were program inputs.

Thermal bridges were modeled by introducing, for each test cell wall, an additional massless wall. The thermal conductance of the guard zone cold bridges was equally spread out over the additional surfaces. The thermal transmittance (calculated by TRISCO software: 12.21 W/ K) was divided into the internal heat convection resistance, the wall heat conduction resistance and the external heat convection resistance. Giving standard value for convection coefficients, the wall transmittance was estimated as 11.78 W/ K-m². The cold bridge for the south wall was neglected.

Type 56 can calculate the convective heat transfer coefficients for each internal surface but not for the surfaces connected to the ambient or to boundary conditions. Variable convective heat transfer coefficients are calculated according to Equation 12.2.

$$h = a\left(T_{surf} - T_{air}\right)^{b} \qquad (12.2)$$

where

h is the convection coefficient,
T_{surf} is the internal wall surface temperature,
T_{air} is the internal air temperature, and
a and b are empirically derived coefficients.

The following assumptions were developed to simulate the test cell:

- in order to take into account the equipment thermal mass, a 200 KJ/K thermal mass internal wall was added, and the air capacitance was multiplied by a factor 5 to account for convection mechanisms and the fact that the air is not isotherm in the room, and
- the emissivity of the surfaces was fixed by the software as follows:
  - internal surface of walls: ε = 1.00 (black bodies), and
  - external surface of walls: ε = 1.00 (black bodies).

All the heat sources (fans and pseudo-random heat source) were defined in the zone as a thermal gain. These thermal gains were considered purely convective.

12.7.3. Evaluation of irradiation models on tilted facades (Exercise 2)

Five horizontal radiation modes are available with TRNSYS Type 16, depending on the available information:

- Type 16a: Mode 1 = only the global horizontal radiation is known,
- Type 16c: Mode 2 = the global horizontal radiation, the ambient temperature and the relative humidity are known,
- Type 16e: Mode 3 = the beam normal and the diffuse radiations are known,
- Type 16g: Mode 4 = the global horizontal and beam normal radiations are known, and
- Type 16i: Mode 5 = the global horizontal and diffuse radiations are known.

Horizontal Radiation Modes 1 and 2 are based on the relationships developed by Reindl (9a). Both modes provide estimates of the diffuse fraction of the total horizontal radiation (Id/I). Mode 1 is a reduced form of the full correlation given in Mode 2. Mode 1 uses the clearness index and the solar altitude angle to estimate the diffuse components. Horizontal Radiation Mode 2 estimates the diffuse fraction as a function of the clearness index, solar altitude angle, ambient temperature, and relative humidity.

In Horizontal Radiation Mode 3, beam and diffuse radiation on a horizontal surface are input directly. For Horizontal Radiation Mode 4, total horizontal and direct normal radiation are inputs and Horizontal Radiation Mode 5 has inputs of total and diffuse radiation on a horizontal surface.

The four tilted surface radiation models available include:

- Tilted Surface Radiation Mode 1 that uses the isotropic sky model [38]. This is the model that has been used by default in previous versions of TRNSYS. The isotropic sky model assumes that the diffuse radiation is uniformly distributed over the complete sky dome,
- Tilted Surface Radiation Mode 2 that uses a model developed by Hay and Davies [43]. The Hay and Davies model accounts for both circumsolar and isotropic diffuse radiation. Under clear sky conditions, there is an increased intensity of diffuse radiation in the area around the sun (circumsolar diffuse). The Hay and Davies model weights the amount of circumsolar diffuse by using an anisotropy index. The anisotropy index defines a portion of the diffuse radiation to be treated as circumsolar with the remaining portion of diffuse radiation

considered isotropic,

- Tilted Surface Radiation Mode 3 that uses a model developed by Reindl [44] based on the work of several previous authors. This model adds a horizon brightening diffuse term to the Hay and Davies model. The horizon brightening is lumped in with the isotropic diffuse term and its magnitude is controlled by a modulating factor, and
- Tilted Surface Radiation Mode 4 that uses a version of the tilted surface model developed by Perez, et al [20]. This model accounts for circumsolar, horizon brightening, and isotropic diffuse radiation by empirically derived "reduced brightness coefficients". The reduced brightness coefficients are functions of sky clearness and sky brightness parameters.

In general, the solar processors Type 16a, Type 16c, Type 16e, Type 16g and Type 16i are equivalent and produce more or less the same results for horizontal radiations. The choice of the solar processor mode should be done only on the basis of available information and the quality of measurements. The measurement of the global horizontal radiation permits generation of incidental radiation for any orientation. More precision will be realized if outside temperature and the relative humidity of the air are added.

When two following solar radiations parameters are measured:

- the direct horizontal and diffuse radiations,
- the global horizontal and direct normal radiations, or
- the global horizontal and diffuse radiations.

It is necessary to use the solar processor. The influence of the "tilted surface radiation mode", was different. Changing from mode 1, 2, 3 and 4 continually increased the tilted surface radiation predictions. Each increase corresponded to accounting for increasingly complex model of calculation of the diffuse radiation. By default, TRNSYS uses Mode 3. For the solar gain experiments, the Type16g was used with tilted Mode 4 which provided the closest estimates of global vertical radiation.

12.7.4. Glazing Only Experiment (Exercise 3)

The optical properties of the window were recalculated from the spectral data using OPTICS 5.1 [33] and WINDOW 5.2 [32] softwares. A small vinyl frame was specified in the library file but was not used in the simulation and the properties were calculated according to European Standard EN 410 [7]. The same optical properties were found for the outer and the inner panes as specified.

The calculated center-pane thermal transmittance was 1.32 W/m²-K instead of 1.144 W/m²-K (+15 %). The thermal conductivity for the two panes was 1 W/m-K. The thickness of the two panes is 6 mm each. Between the glass panes a mixed gas is present (Air 10% - Argon 90%). Its thermal conductivity was 0.017063 W/m-K. The total thickness of the two panes and the gap was 28 mm. The total thermal conductivity of those three elements was equal to 1.05 W/m²-K.

12.7.5. Exterior Shading Screen (Exercise 4)

The same model from Exercise 3 was used with the addition of an exterior shading screen. In TRNSYS, external shading devices reduce the incoming solar radiation on the glazing area of the external window by a factor given in the building description. The solar transmittance of the external shade was introduced as a Type 56 property. The air gap was not taken into account.

12.7.6. Interior Shading Screen (Exercise 5)

An internal shading device was specified giving the reduction of the transmitted solar radiation, a reflection coefficient for solar radiation for both faces of the shading device and a parameter defining the degree of additional convection to the air node of the zone. The Type 56 model takes into account multiple reflections between the internal shading device and the window panes and calculates the absorption of reflected solar radiation from the internal shading on the different window panes.

12.7.7. Exterior Venetian Blind Assembly (Exercise 6)

TRNSYS Type 56 does not include complex blind models; therefore a model was implemented outside of the building model. The first model used in Exercise 6 was a geometric model which calculated the entering solar gains with respect to the sun position in the sky. However, the results were unsatisfactory so the measurements were used to define an equation which would be able to express solar gains with respect to direct solar radiation and total vertical solar radiation. A logarithmical regression was used to determine a horizontal slat equation. For inclined slats, the solar gains were found to be proportional to total vertical incident radiation with a factor of 0.82.

12.7.8. Interior Mini-Blind Assembly (Exercise 7)

In order to model an interior mini-blind assembly, the same function as the one presented in Exercise 6 was used. Since blind modeling is not possible in TRNSYS, the opaque view factor was evaluated by the equations found in the previous exercise.

12.7.9. Window (Exercise 8)

The window was modeled using OPTICS and WINDOW softwares as explained in Experiment 3. Optical properties of the inner pane and outer pane were recalculated with OPTICS 5.2 from the data supplied in the Excel file (Experiment 8.xls). OPTICS 5.2 only allows user to introduce wavelength values from 300 nm, then the first 50 values provided (from 250 to 299) were not used. The calculated center-pane thermal transmittance was 1.14 W/m^2-K.

A window frame was defined in the WINDOW 5.2 software with a thermal conductance of 1.643 W/m^2-K. The correlation was used to determine edge of glass thermal transmittance assuming a stainless steel/dual seal one spacer. The material absorbance of the window frame was set to the default value (0.9) in the absence of information.

The overall window thermal transmittance was 1.556 W/m^2-K. This window was added to the library file to be used in TRNSYS. The linear transmittance for the spacer and the mounting were accounted for by adding equivalent thermal bridges spread out over the total window area

12.7.10. Discussion of Results

The completion of these experiments and the result quality show the TRNSYS software quality for shading and load interaction simulation. There were, however, some limitations that the results permitted us to identify:

- the solar gain repartition calculation and
- the external shading device simulation (involving multiple reflections)

The building model reproduced accurately the steady-state and the transient heat transfers of the test cell.

12.7.11. Validation Impact

An error was discovered and fixed in the plugin of the Type 14 (time-dependent forcing function).

CHAPTER 13: DESCRIPTION OF THE ERS

The ERS is located on the Des Moines Area Community College campus in Ankeny, Iowa USA. The building is uniquely equipped for high-quality data sets and is, therefore, useful for empirical validations. The structure is comprised of eight test rooms, a computer room, offices, two classrooms and other rooms necessary for the support and operation of the facility. A photograph of the building is shown in Figure 13.1. The test rooms were constructed in symmetrical pairs to provide side-by-side testing with exposures to nearly identical outside thermal loads; three pairs of test rooms are located at the perimeter of the building (east, south, and west) and the other two test rooms are situated inside the facility. There are three air-handling units (AHU's) in the facility. Test rooms denoted as A and B are served by different two nearly identical AHU's; the other AHU serves the rest of the facility. The building also contains a weather station, pyranometer, pyrheliometer, precision infrared radiometer, and numerous exterior light sensors. Detailed information instrumentation and uncertainties, material construction (thermophysical properties and dimensions), and facility layout of the building is provided by [48]; architectural drawings of the facility were used for modeling the building and can be made available upon request. The following sections contain a general description of the setup and location of the building, input and output files, and a description of the results.

Figure 13.1. Photograph of the ERS.

13.1. Building Location

The ERS is oriented for a true north/south alignment. A description of the location of the building is given in Table 13.1. For both ERS experiments, the data and results were reported in Central Standard Local time (GMT -6h).

Table 13.1. Location of the ERS.

Degrees of longitude	93.61° West
Degrees of latitude	41.71° North
Altitude above sea-level	285.9 m
Time zone	Central Standard Time (GMT – 6 h)

13.2. Experimental Setup

Both experiments were run for seven days during the summer. This section provides a generic overview of the following:

- test room windows and exterior shading fins,
- daylight reference point locations and surface optical properties,
- test room set points, and
- system set points.

Information pertaining to materials, schedules, and lighting and illuminance measurements is given in the chapters with ERS results.

13.2.1. Test Room Windows and Exterior Shading Fins

Three types of windows were used during the course of this project and are described in Table 13.2.

Table 13.2. Test room windows and properties.

Window type	**25.2 mm LOW-E #3**	**25.2 mm LOW-E #2**	**25.2 mm Clear Glass**
Makeup	**6 mm Clear (103)[1] 13.2 mm air gap 6 mm Lof Pyro Low-E #3 (9924)[1]**	**6 mm VE3-55 #2 (6059)[1] 13.2 mm airs gap 6 mm Clear (103)[1]**	**6 mm Clear (103)[1] 13.2 mm air gap 6 mm Clear (103)[1]**
Visible transmittance	73%	23%	79%
Solar transmittance	52%	14%	61%
Visible light-exterior reflectance	17%	6%	14%
Visible light-interior reflectance	16%	15%	14%
Solar exterior reflectance	15%	10%	11%
ASHRAE u-value Winter nighttime	1.87 W/m^2-K	1.76 W/m^2-K	2.68 W/m^2-K
ASHRAE u-value summer daytime	2.0 W/m^2-K	1.87 W/m^2-K	2.81 W/m^2-K
Shading coefficient	0.79	0.26	0.81
Solar factor (SHGC)	0.66	0.22	0.70

[1]Correspond the number listed in the Window 5.2 glazing database

Exterior shading fins were installed over the east test room windows for Experiment 1 and the south test room windows for Experiment 2. The exterior fins were constructed out of a dark brown polymeric material to minimize reflection from the fins through the windows to the space. Figure 13.2 contains a drawing with dimensions of the exterior fins.

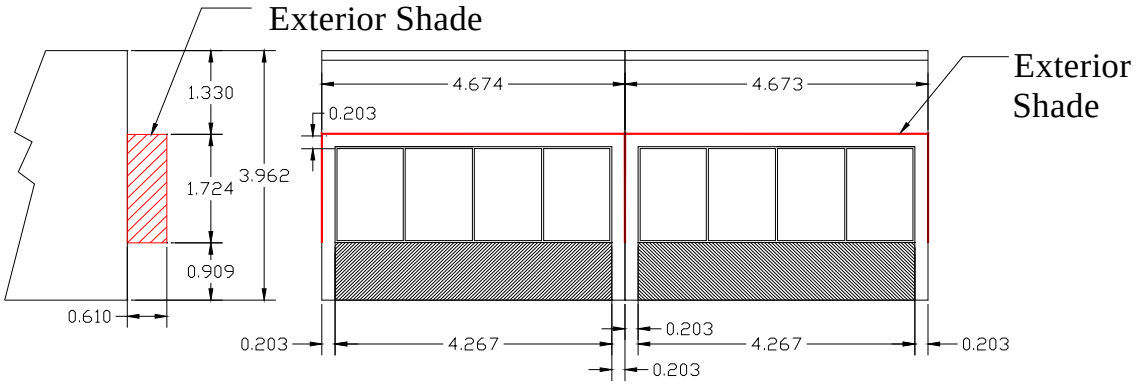

Figure 13.2. Drawing and dimensions in meters of the exterior fins for west test rooms.

13.2.2. Daylight Reference Point Locations and Surface Optical Properties

The light sensors used to control the dimmable ballasts to given light levels were installed on a table in the middle of each test room. The location of the light sensor is provided in Figure 13.3.

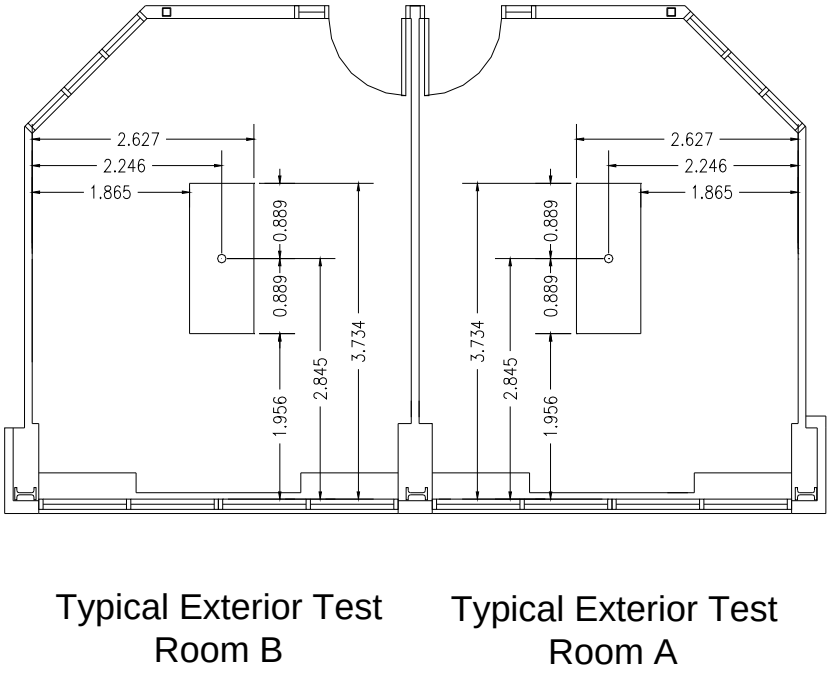

Figure 13.3. Light sensor reference point dimensioned in meters (the sensor height is 0.7239 m from the floor).

Optical measurements were taken on the interior walls, ceiling, and floor of the test rooms were taken from samples and measured from 250 nm to 2500 nm. The integral properties were computed according to European Standard EN 410 [7] using Glad software [8] and visible and solar reflectances of the interior surfaces of the test room are given in Table 13.2.

Table 13.3 Optical properties for the interior surfaces.

Surface	**Solar reflectance, %**	**Visible reflectance, %**
Ceiling	49.8	55.7
Walls	78.8	83.6
Floor	26.4	10.3

13.2.3. Test Room Setup

The test rooms were setup to use variable-air-volume boxes with electric reheat coils. The minimum and maximum airflow rates for the interior and exterior test rooms are provided in Table 13.3. The thermostats were configured so that the heating and cooling set points were 22°C and 23°C, respectively. The return air path was through the return air plenum. Spaces adjacent to the test rooms were maintained at nearly the same temperatures as the test rooms to eliminate heat transfer through the interior construction elements. During both experiments, one stage of electric baseboard heat with a heating capacity of ~890 W was turned on in all test rooms. In the exterior test rooms, box fans were also hung from the ceiling to reduce temperature stratification within the test cell. Power measurements revealed that the box fans added an additional internal load of ~125 W.

Table 13.3. Test room airflow rate set points.

Airflow rate set point	Airflow rate set points, m^3/h
Maximum airflow rate in the exterior test rooms	1000
Minimum airflow rate in the exterior test rooms	800
Maximum airflow rate in the interior test rooms	700
Minimum airflow rate in the interior test rooms	425

13.2.4. System Set Points

Both systems serving the test rooms were configured to supply air at 13°C to the test rooms. For both experiments, 100% re-circulated air was used and duct air losses were negligible. The heat duct gains were, on average, 0.6 K. The supply and return fans from the AHU's were on all the time and the static pressure set points of the supply fans were 348.4 Pa. The supply fans were draw-through and the fan motors were in the airflow stream. Because of the relatively high airflow rates, the fan powers for both systems during both experiments were nearly constant and were averaged over the experiment; these quantities are given in Table 13.4.

Table 13.4. Measured supply fan powers.

Supply fan	Measured fan power, W	
	Experiment 1	Experiment 2
System A	1,143	1,070
System B	1,096	1,144

13.3. Explanation of Experimental Data

For each experiment, the weather data in one minute intervals are contained in files described in Appendix B. Additional files that contain hourly results from the experiments and 95% credible limits from the MCA are also described in Appendix B. The Excel files can be used in conjunction with this document for assessing the capabilities of building energy simulation programs.

CHAPTER 14: ERS DAYLIGHTING EXPERIMENT 1

An experiment was performed at the ERS for a seven-day period from July 1 to July 7, 2005 to evaluate the performances of building energy simulation programs for daylighting with different combinations of windows and shading devices. Dimmable ballasts were used in the exterior test rooms to reduce the illuminance in rooms based on available daylight and maintain illuminances of 645 Lux in the East and West Test Rooms and 700 Lux in the South Test Rooms. A control scheme was implemented that turned off the lamps when the illuminance at the reference point was at minimum capacity and the light level exceeded the set point; the lights were turned back on when the light level was 108 Lux below the set point. A general description of the window/shading combinations is given in Chapter 2 (Table 2.1); however, additional information about the interior shading devices, light schedules, light versus illuminance measurements are provided. Results that focus on exterior test room comparisons are also provided. Weather data, exterior illuminance measurements, and adjacent space temperatures are given in "ERS Experiment 1.xls" in one-minute intervals. Additional information is contained in the subsequent sections concerning:

- interior shading devices,
- lighting schedules, sources and corresponding illuminance, and
- results.

14.1. Interior Shading Devices

Two types of interior shading devices were used in this experiment including: mini-blinds and Nysan shading screens. A description of the properties and mounting are described in this section.

14.1.1. Mini-blinds

Interior blinds were mounted inside the east test rooms for this experiment configured in two different ways. Figure 14.1 gives the dimension of the blind blades and the spacing. In the morning, the blind assemblies in the East A test room were setup to adjust to block out beam irradiance entering the space. In the afternoon, the blinds slats were controlled to the horizontal position and then closed at 16:00 Central Standard Time (GMT-6h). The blind assemblies in the South B and East B test rooms were set in a horizontal position. The fixed-angle and motorized mini-blinds were mounted 76.2 mm and 38.1 mm, respectively, from the tip of the blade nearest the inner pane to the window in the horizontal position. Optical measurements were taken on a blade from a blind unit similar to the one installed in the east test rooms and are reported in Table 14.1

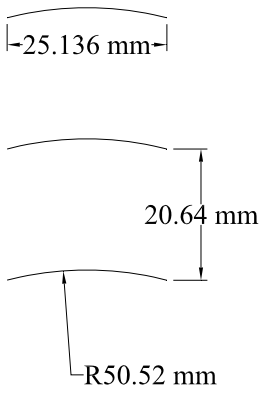

Mini blinds are nominall 25.4 mm wide aluminum sheet metal
which are formed to produce a curved blade with a 50.52 mm radius.
The cord length of the blade is 25.136 mm
The aluminum sheet thickness is 0.248 mm.
Blades are spaced 20.64 mm apart.

Figure 14.1. Dimensioned drawing of the blades.

Table 14.1. Optical properties of the blind blades.

Property	Quantity
Solar reflectance, %	63.9
Visible reflectance, %	73.1
Hemispherical emittance, %	72.1

14.1.2. Interior Shading Screens

The shades installed South A and West A test rooms were Nysan Superweave 1000 (10% open) shading screens. The screens were mounted 108.0 mm from the glazing. The optical and solar properties measured at EMPA are shown in Table 14.2.

Table 14.2. Test room interior shade properties.

Type	Nysan Superweave 1000 (10% open) white fabric
Visible transmittance, %	30.5
Solar transmittance, %	30.4
Visible reflectance, %	67.3
Solar reflectance, %	59.4

14.2. Lighting Schedules, Sources, and Corresponding Illuminance

Four fluorescent lights were installed in each test room. Prior to running each experiment, detailed measurements were made to quantify the light power and illuminance at the daylight reference points. The maximum and minimum light power and along with illuminance with daylighting for the test rooms for this experiment are giving in Table 14.3; these measurements were taken during the night before the experiment.

Table 14.3. Maximum light power for each test room and minimum light power for the exterior test rooms during the experiment.

Test room	Maximum light power, W	Illuminance at maximum light power, lux	Minimum light power, W	Illuminance at minimum light power, lux
East A	356	645	86.1	21.8
East B	362	645	89.3	36.9
South A	364	700	88.1	31.9
South B	362	700	89.3	32.6
West A	362	645	88.4	32.3
West B	348	645	86.9	32.1
Interior A	359	-	-	-
Interior B	358	-	-	-

During the experiment, the lights were scheduled to come on one hour prior to sunrise and turn-off one hour after sunset. Table 14.4 contains the light schedule given in Central Standard Time (GMT-6h).

Table 14.4. Test room lighting schedule used during the test.

Time, h	Report schedule (Midnight to 1 AM = Hour 1)	Lights, On/Off
0:00	1	Off
1:00	2	Off
2:00	3	Off
3:00	4	Off
4:00	5	On
5:00	6	On
6:00	7	On
7:00	8	On
8:00	9	On
9:00	10	On
10:00	11	On
11:00	12	On
12:00	13	On
13:00	14	On
14:00	15	On
15:00	16	On
16:00	17	On
17:00	18	On
18:00	19	On
19:00	20	On
20:00	21	On
21:00	22	Off
22:00	23	Off
23:00	24	Off
24:00		Off

14.3. Results

Comparisons were made in the exterior test rooms between predicted results from the building energy simulation programs and measurands from the experiment. The comparisons along with statistical analyses for each zone included:

- reheat coil powers,
- airflow rates,
- air temperatures,
- reference point illuminances due to daylight, and
- light powers.

Figure 14.2 contains measured direct-normal and global horizontal solar irradiances. The global exterior illuminances on the test room façades (east, south, and west) and on the horizontal plane were measured during the experiment but were not required outputs for the building energy simulation program. From this information, hypotheses can be made to assess general trends expected with respect to daylight in the test rooms. The exterior global illuminances are plotted in Figure 14.3.

From these plots, there were initially two sunny days, following by two relatively cloudy days, and, finally, again three moderately sunny days. The global vertical illuminances provide information concerning the amount of visible light incident upon the outer windows (this is reduced for the west test rooms where exterior fins were installed). Because of the high path that the sun takes across the sky during a day in July, beam illuminances and solar irradiances were never incident upon the south windows but were incident in the morning and evenings on the east and west windows, respectively.

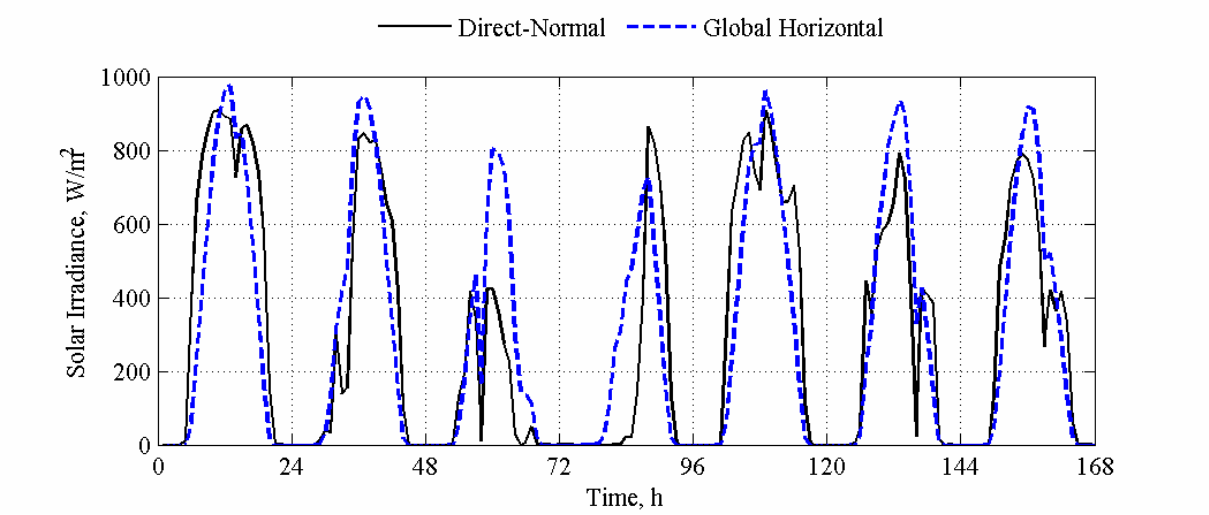

Figure 14.2. Direct-normal and global horizontal solar irradiance measurements during the experiment.

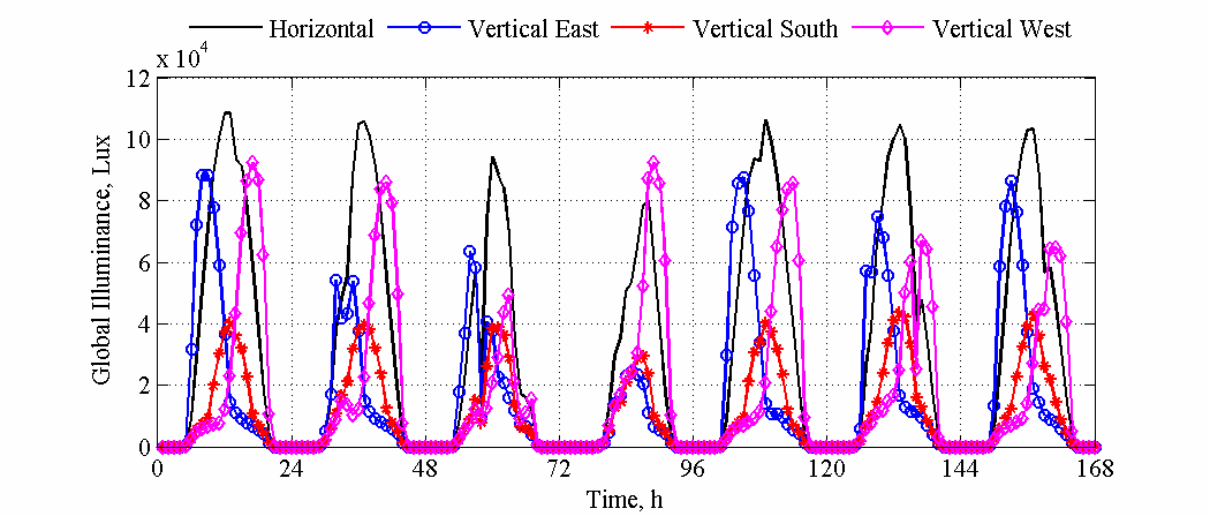

Figure 14.3. Horizontal and vertical global exterior illuminance.

14.3.1. Zone Reheat Coil Power

The electric reheat coil power for each zone was measured and compared with results from the building energy simulation programs. Plots of the reheat coil powers for the east, south, and west test rooms are contained in Figures 14.4 to 14.6, respectively, and statistical analyses are contained in Tables 14.5 to 14.7, respectively.

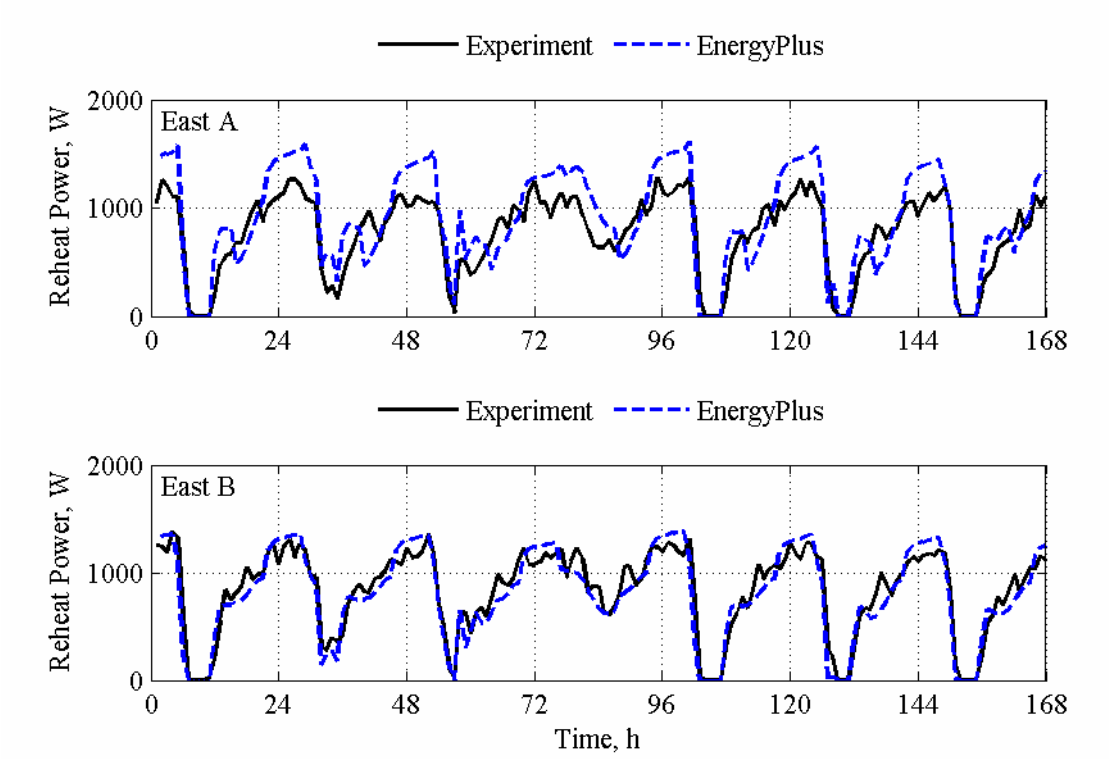

Figure 14.4. Reheat coil power comparisons for the east test rooms.

Table 14.5. Statistical analyses for reheat coil powers in the east test rooms.

	East A		**East B**	
	Experiment	**EnergyPlus**	**Experiment**	**EnergyPlus**
$\bar{x}$	809.1 W	948.7 W	864.7 W	843.1 W
s	337.4 W	433.5 W	360.8 W	399.3 W
x_{max}	1284.0 W	1611.0 W	1378.0 W	1385.2 W
x_{min}	3.0 W	0.0 W	2.0 W	0.0 W
$\overline{D}$	-	-139.7 W	-	21.7 W
$\overline{\lvert D \rvert}$	-	229.0 W	-	111.6 W
D_{max}	-	494.8 W	-	356.5 W
D_{min}	-	3.0 W	-	0.0 W
D_{rms}	-	262.0 W	-	136.8 W
$D_{95\%}$	-	419.5 W	-	253.7 W
$\overline{OU}$	1.8 W	90.3 W	2.0 W	87.5 W
$\overline{UR}$	-	2.5	-	1.2
UR_{max}	-	13.1	-	3.9
UR_{min}	-	0.0	-	0.0
$\overline{\lvert D \rvert} / \bar{x} \times 100\%$	-	28.3%	-	12.9%
$\overline{D} / \bar{x} \times 100\%$	-	-17.3%	-	2.5%
N	158	158	160	160

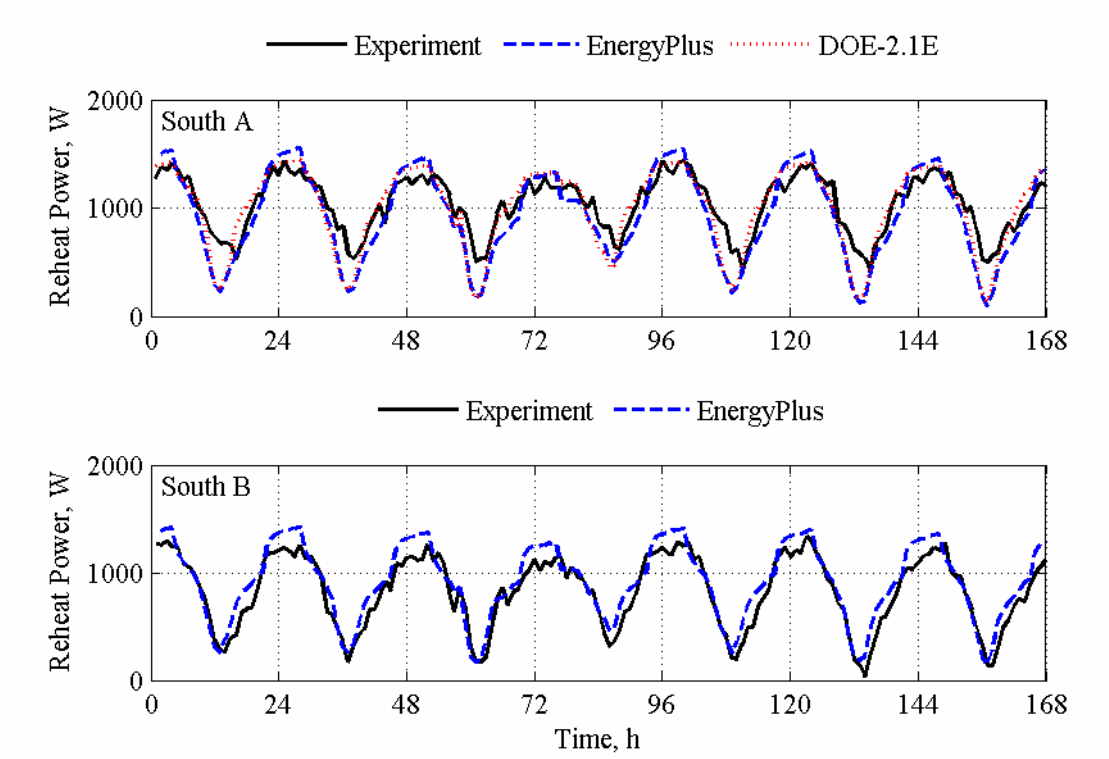

Figure 14.5. Reheat coil power comparisons for the south test rooms.

Table 14.6. Statistical analyses for reheat coil power in the south test rooms.

	South A			**South B**	
	Experiment	**EnergyPlus**	**DOE-2.1E**	**Experiment**	**EnergyPlus**
$\bar{x}$	1028.8 W	935.6 W	998.8 W	828.0 W	914.2 W
s	268.8 W	411.8 W	379.1 W	340.0 W	353.4 W
x_{max}	1433.0 W	1557.4 W	1439.4 W	1338.0 W	1425.6 W
x_{min}	410.0 W	96.0 W	133.7 W	31.0 W	138.4 W
$\overline{D}$	-	93.3 W	30.0 W	-	-86.3 W
$\overline{\lvert D \rvert}$	-	172.2 W	133.8 W	-	115.3 W
D_{max}	-	524.5 W	524.4 W	-	295.6 W
D_{min}	-	7.3 W	0.5 W	-	0.6 W
D_{rms}	-	205.3 W	178.8 W	-	136.6 W
$D_{95\%}$	-	413.6 W	377.5 W	-	234.5 W
$\overline{OU}$	2.3 W	87.9 W	-	1.9 W	87.6 W
$\overline{UR}$	-	1.9	1.5	-	1.3
UR_{max}	-	5.9	5.9	-	3.3
UR_{min}	-	0.1	0.0	-	0.0
$\overline{\lvert D \rvert} / \bar{x} \times 100\%$	-	16.7%	13.0%	-	13.9%
$\overline{D} / \bar{x} \times 100\%$	-	9.1%	2.9%	-	-10.4%
N	168	168	168	168	168

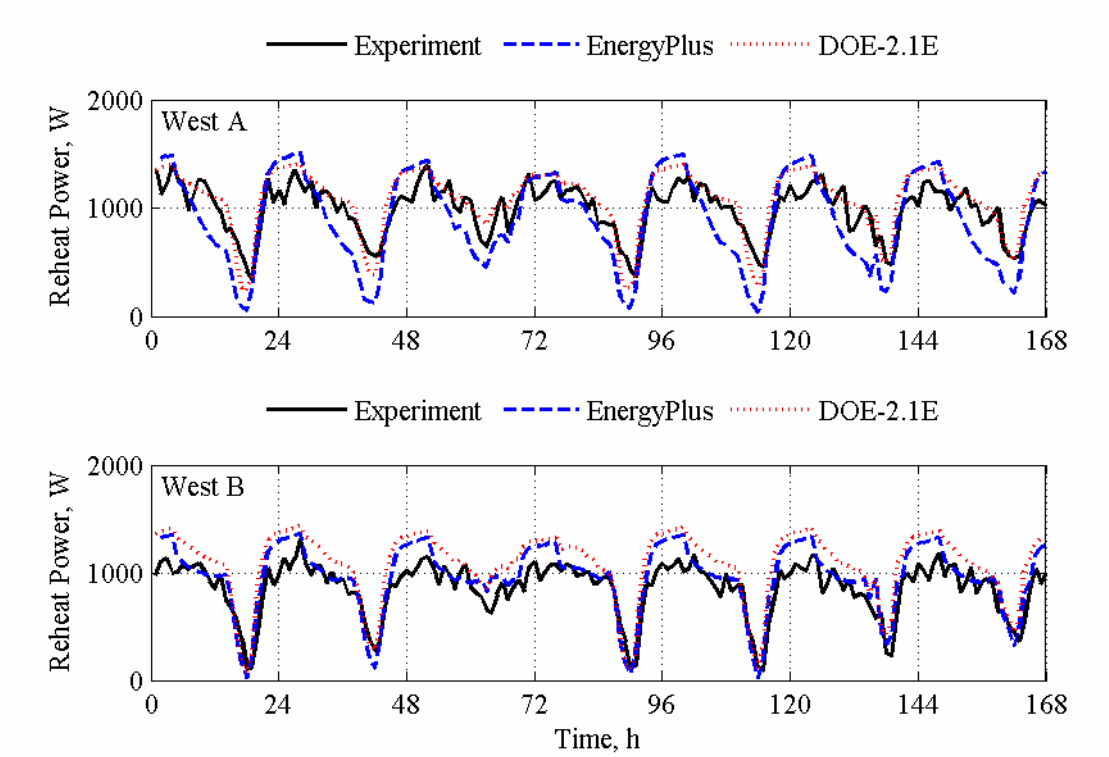

Figure 14.6. Reheat coil power comparisons for the west test rooms.

Table 14.7. Statistical analyses for reheat coil power in the west test rooms.

	West A			**West B**		
	Experiment	**EnergyPlus**	**DOE-2.1E**	**Experiment**	**EnergyPlus**	**DOE-2.1E**
$\bar{x}$	984.7 W	897.6 W	1075.5 W	876.6 W	983.7 W	1099.7 W
s	237.5 W	420.1 W	295.4 W	224.3 W	281.2 W	286.0 W
x_{max}	1390.0 W	1511.4 W	1413.5 W	1308.0 W	1358.5 W	1428.8 W
x_{min}	339.0 W	37.8 W	231.7 W	87.0 W	142.9 W	158.7 W
$\overline{D}$	-	87.1 W	-90.9 W	-	-107.1 W	-223.0 W
$\overline{\lvert D \rvert}$	-	232.6 W	137.5 W	-	142.9 W	236.1 W
D_{max}	-	555.8 W	414.6 W	-	376.5 W	510.5 W
D_{min}	-	0.1 W	0.5 W	-	1.7 W	3.2 W
D_{rms}	-	272.9 W	165.6 W	-	175.4 W	261.1 W
$D_{95\%}$	-	487.1 W	297.9 W	-	329.6 W	419.3 W
$\overline{OU}$	2.2 W	91.3 W	-	2.0 W	88.4 W	-
$\overline{UR}$	-	2.5	1.5	-	2.7	3.7
UR_{max}	-	6.8	4.6	-	98.9	89.7
UR_{min}	-	0.0	0.0	-	0.0	0.0
$\overline{\lvert D \rvert} / \bar{x} \times 100\%$	-	23.6%	14.0%	-	16.3%	26.9%
$\overline{D} / \bar{x} \times 100\%$	-	8.8%	-9.2%	-	-12.2%	-25.4%
N	168	168	168	163	163	163

14.3.2. Zone Airflow Rates

The zone airflow rates were measured and compared with results from the building energy simulation programs. Plots for the east, south, and west test rooms are contained in Figures 14.7 to 14.9, respectively, and statistical analyses are contained in Tables 14.8 to 14.10, respectively.

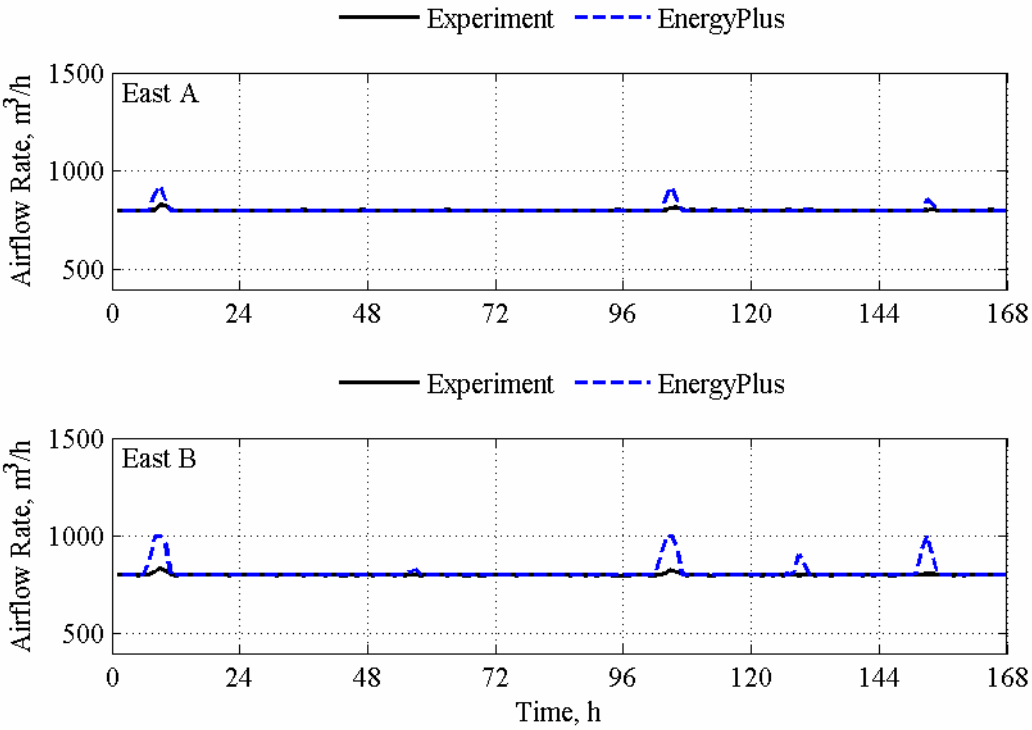

Figure 14.7. Airflow rate comparisons for the east test rooms.

Table 14.8. Statistical analyses for airflow rates in the east test rooms.

	East A		**East B**	
	Experiment	**EnergyPlus**	**Experiment**	**EnergyPlus**
$\bar{x}$	800.5 m^3/h	803.3 m^3/h	800.6 m^3/h	811.5 m^3/h
s	3.4 m^3/h	16.5 m^3/h	4.0 m^3/h	41.2 m^3/h
x_{max}	827.0 m^3/h	925.2 m^3/h	833.0 m^3/h	1000.0 m^3/h
x_{min}	799.0 m^3/h	800.0 m^3/h	798.0 m^3/h	800.0 m^3/h
$\overline{D}$	-	-2.9 m^3/h	-	-10.9 m^3/h
$\overline{\lvert D \rvert}$	-	3.0 m^3/h	-	11.1 m^3/h
D_{max}	-	105.5 m^3/h	-	193.9 m^3/h
D_{min}	-	0.0 m^3/h	-	0.0 m^3/h
D_{rms}	-	14.3 m^3/h	-	39.5 m^3/h
$D_{95\%}$	-	2.8 m^3/h	-	104.4 m^3/h
$\overline{OU}$	18.1 m^3/h	18.3 m^3/h	18.1 m^3/h	18.3 m^3/h
$\overline{UR}$	-	0.1	-	0.3
UR_{max}	-	2.9	-	5.3
UR_{min}	-	0.0	-	0.0
$\overline{\lvert D \rvert} / \bar{x} \times 100\%$	-	0.4%	-	1.4%
$\overline{D} / \bar{x} \times 100\%$	-	-0.4%	-	-1.4%
N	168	168	168	168

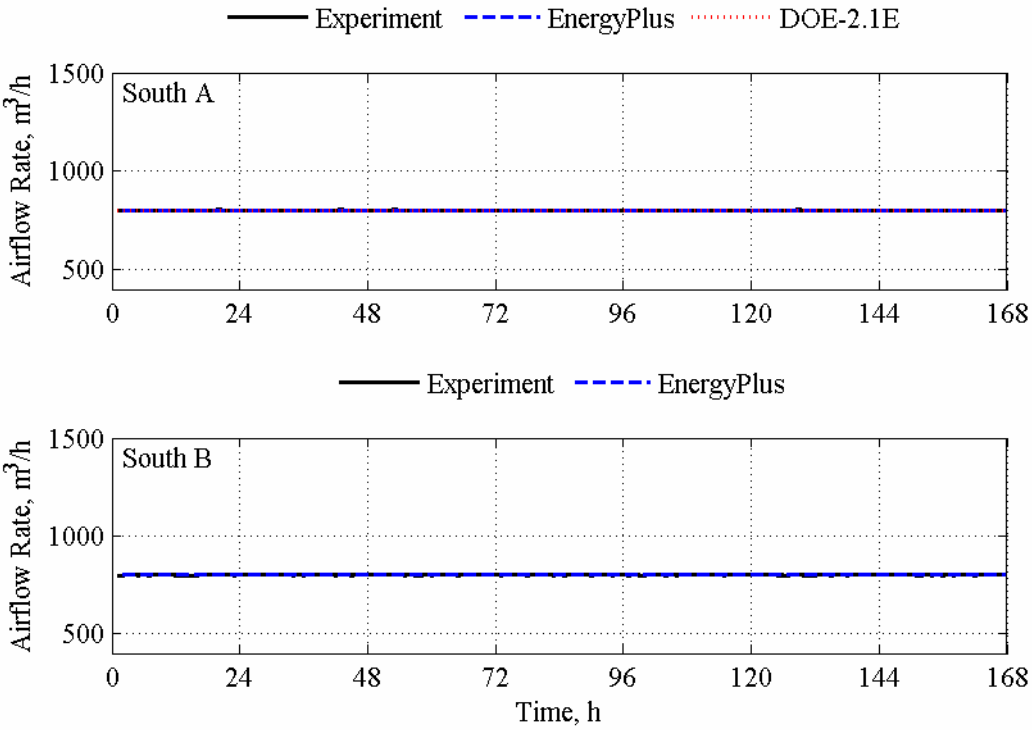

Figure 14.8. Airflow rate comparisons for the south test rooms.

Table 14.9. Statistical analyses for airflow rates in the south test rooms.

	South A			**South B**	
	Experiment	**EnergyPlus**	**DOE-2.1E**	**Experiment**	**EnergyPlus**
$\bar{x}$	799.8 m^3/h	800.0 m^3/h	800.0 m^3/h	799.9 m^3/h	800.0 m^3/h
s	0.5 m^3/h	0.0 m^3/h	0.0 m^3/h	0.6 m^3/h	0.0 m^3/h
x_{max}	801.0 m^3/h	800.0 m^3/h	800.0 m^3/h	802.0 m^3/h	800.0 m^3/h
x_{min}	799.0 m^3/h	800.0 m^3/h	800.0 m^3/h	798.0 m^3/h	800.0 m^3/h
$\overline{D}$	-	-0.2 m^3/h	-0.2 m^3/h	-	-0.1 m^3/h
$\overline{\lvert D \rvert}$	-	0.3 m^3/h	0.3 m^3/h	-	0.4 m^3/h
D_{max}	-	1.0 m^3/h	1.0 m^3/h	-	2.0 m^3/h
D_{min}	-	0.0 m^3/h	0.0 m^3/h	-	0.0 m^3/h
D_{rms}	-	0.5 m^3/h	0.5 m^3/h	-	0.7 m^3/h
$D_{95\%}$	-	1.0 m^3/h	1.0 m^3/h	-	1.0 m^3/h
$\overline{OU}$	18.1 m^3/h	18.3 m^3/h	-	18.1 m^3/h	18.3 m^3/h
$\overline{UR}$	-	0.0	0.0	-	0.0
UR_{max}	-	0.0	0.0	-	0.1
UR_{min}	-	0.0	0.0	-	0.0
$\overline{\lvert D \rvert} / \bar{x} \times 100\%$	-	0.0%	0.0%	-	0.1%
$\overline{D} / \bar{x} \times 100\%$	-	0.0%	0.0%	-	0.0%
N	168	168	168	168	168

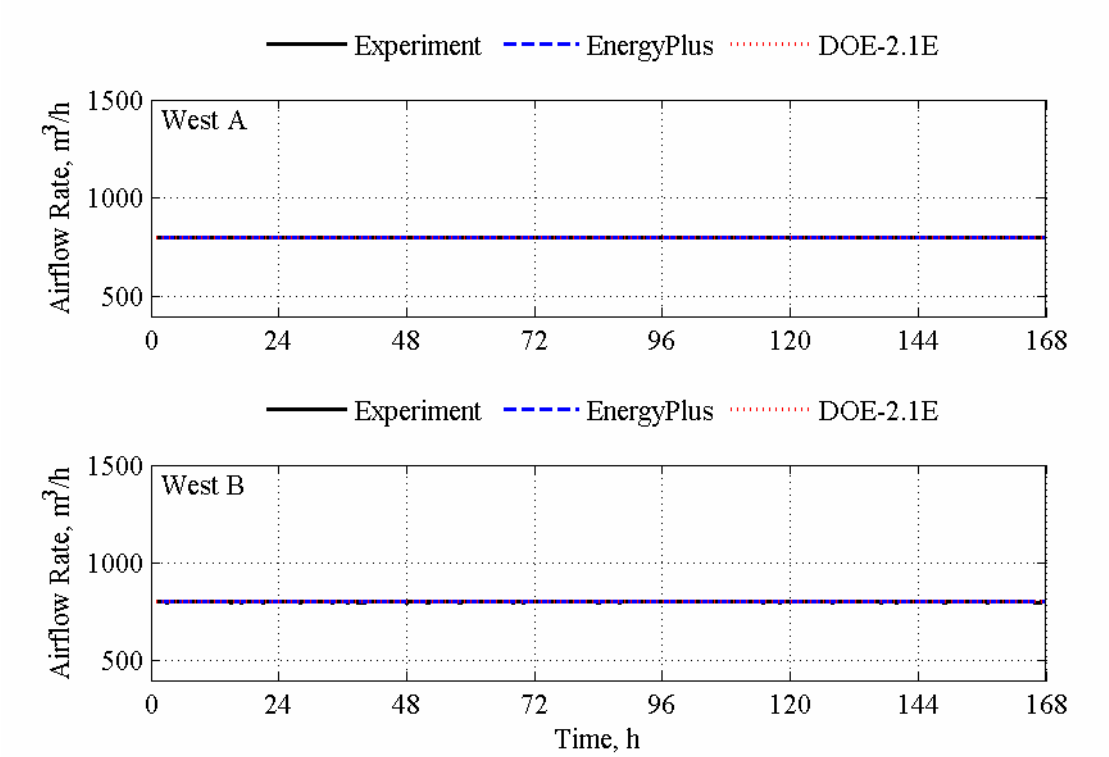

Figure 14.9. Airflow rate comparisons for the west test rooms.

Table 14.10. Statistical analyses for airflow rates in the west test rooms.

	West A			**West B**		
	Experiment	**EnergyPlus**	**DOE-2.1E**	**Experiment**	**EnergyPlus**	**DOE-2.1E**
$\bar{x}$	799.9 m^3/h	800.0 m^3/h	800.0 m^3/h	799.9 m^3/h	800.0 m^3/h	800.0 m^3/h
s	0.2 m^3/h	0.0 m^3/h	0.0 m^3/h	0.4 m^3/h	0.0 m^3/h	0.0 m^3/h
x_{max}	800.0 m^3/h	800.0 m^3/h	800.0 m^3/h	801.0 m^3/h	800.0 m^3/h	800.0 m^3/h
x_{min}	799.0 m^3/h	800.0 m^3/h	800.0 m^3/h	799.0 m^3/h	800.0 m^3/h	800.0 m^3/h
$\overline{D}$	-	-0.1 m^3/h	-0.1 m^3/h	-	-0.1 m^3/h	-0.1 m^3/h
$\overline{\lvert D \rvert}$	-	0.1 m^3/h	0.1 m^3/h	-	0.2 m^3/h	0.2 m^3/h
D_{max}	-	1.0 m^3/h	1.0 m^3/h	-	1.0 m^3/h	1.0 m^3/h
D_{min}	-	0.0 m^3/h	0.0 m^3/h	-	0.0 m^3/h	0.0 m^3/h
D_{rms}	-	0.3 m^3/h	0.3 m^3/h	-	0.4 m^3/h	0.4 m^3/h
$D_{95\%}$	-	1.0 m^3/h	1.0 m^3/h	-	1.0 m^3/h	1.0 m^3/h
$\overline{OU}$	18.1 m^3/h	18.3 m^3/h	-	18.1 m^3/h	18.3 m^3/h	-
$\overline{UR}$	-	0.0	0.0	-	0.0	0.0
UR_{max}	-	0.0	0.0	-	0.0	0.0
UR_{min}	-	0.0	0.0	-	0.0	0.0
$\overline{\lvert D \rvert} / \bar{x} \times 100\%$	-	0.0%	0.0%	-	0.0%	0.0%
$\overline{D} / \bar{x} \times 100\%$	-	0.0%	0.0%	-	0.0%	0.0%
N	168	168	168	168	168	168

14.3.3. Zone Air Temperatures

The zone air temperatures were measured and compared with results from the building energy simulation programs. Plots for the east, south, and west test rooms are contained in Figures 14.10 to 14.12, respectively, and statistical analyses are contained in Tables 14.11 to 14.13, respectively.

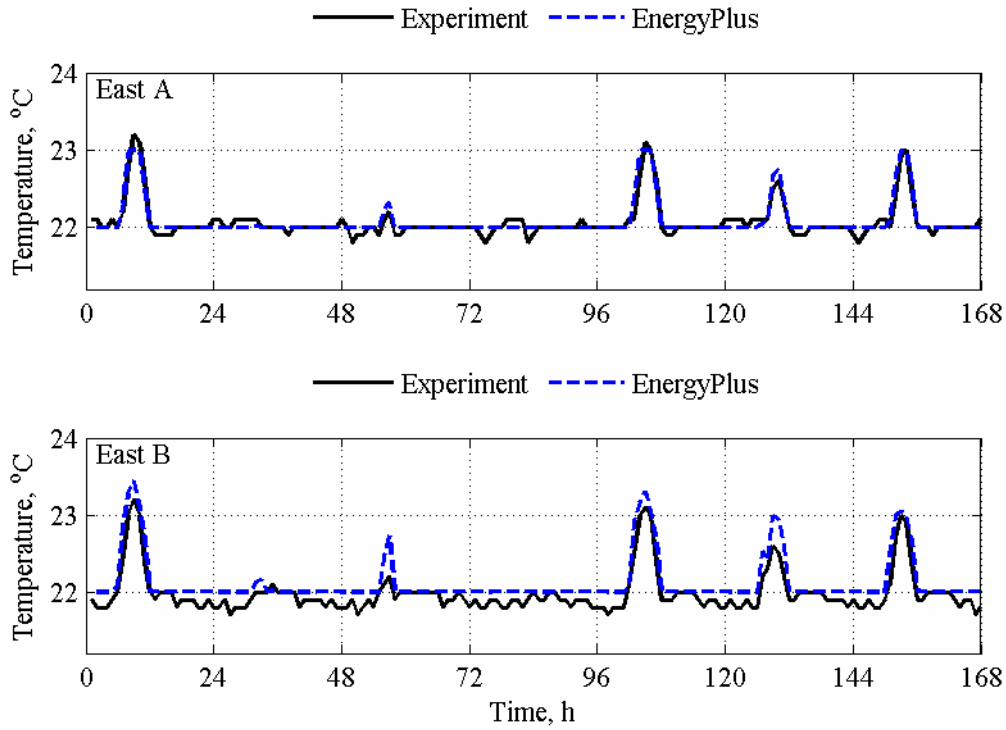

Figure 14.10.Air temperature comparisons for the east test rooms.

Table 14.11. Statistical analyses for air temperatures in the east test rooms.

	East A		**East B**	
	Experiment	**EnergyPlus**	**Experiment**	**EnergyPlus**
$\bar{x}$	22.1 °C	22.1 °C	22.0 °C	22.1 °C
s	0.2 °C	0.2 °C	0.3 °C	0.3 °C
x_{max}	23.2 °C	23.0 °C	23.2 °C	23.4 °C
x_{min}	21.8 °C	22.0 °C	21.7 °C	22.0 °C
$\overline{D}$	-	0.0 K	-	-0.1 K
$\overline{\lvert D \rvert}$	-	0.0 K	-	0.1 K
D_{max}	-	0.3 K	-	0.5 K
D_{min}	-	0.0 K	-	0.0 K
D_{rms}	-	0.1 K	-	0.2 K
$D_{95\%}$	-	0.2 K	-	0.3 K
$\overline{OU}$	0.2	0.2	0.2	0.2
$\overline{UR}$	-	0.2	-	0.4
UR_{max}	-	0.9	-	1.8
UR_{min}	-	0.0	-	0.0
$\overline{\lvert D \rvert} / \bar{x} \times 100\%$	-	0.2%	-	0.6%
$\overline{D} / \bar{x} \times 100\%$	-	0.0%	-	-0.6%
N	168	168	168	168

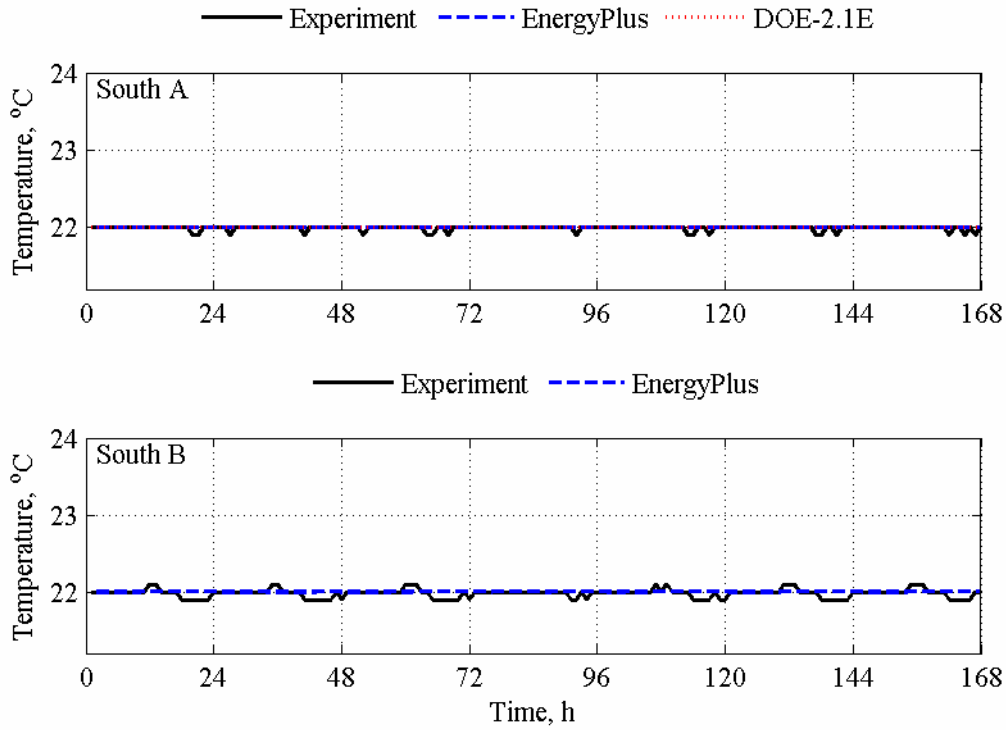

Figure 14.11. Air temperature comparisons for the south test rooms.

Table 14.12. Statistical analyses for air temperatures in the south test rooms.

	South A			**South B**	
	Experiment	**EnergyPlus**	**DOE-2.1E**	**Experiment**	**EnergyPlus**
$\bar{x}$	22.0 °C	22.0 °C	22.0 °C	22.0 °C	22.0 °C
s	0.0 °C	0.0 °C	0.0 °C	0.1 °C	0.0 °C
x_{max}	22.0 °C	22.0 °C	22.0 °C	22.1 °C	22.0 °C
x_{min}	21.9 °C	22.0 °C	22.0 °C	21.9 °C	22.0 °C
$\overline{D}$	-	0.0 K	0.0 K	-	0.0 K
$\overline{\lvert D \rvert}$	-	0.0 K	0.0 K	-	0.0 K
D_{max}	-	0.1 K	0.1 K	-	0.1 K
D_{min}	-	0.0 K	0.0 K	-	0.0 K
D_{rms}	-	0.0 K	0.0	-	0.1 K
$D_{95\%}$	-	0.1 K	0.1	-	0.1 K
$\overline{OU}$	0.2 K	0.2 K	-	0.2 K	0.2 K
$\overline{UR}$	-	0.0	0.0	-	0.1
UR_{max}	-	0.3	0.3	-	0.3
UR_{min}	-	0.0	0.0	-	0.0
$\overline{\lvert D \rvert} / \bar{x} \times 100\%$	-	0.0	0.0	-	0.1%
$\overline{D} / \bar{x} \times 100\%$	-	0.0	0.0	-	-0.1%
N	168	168	168	168	168

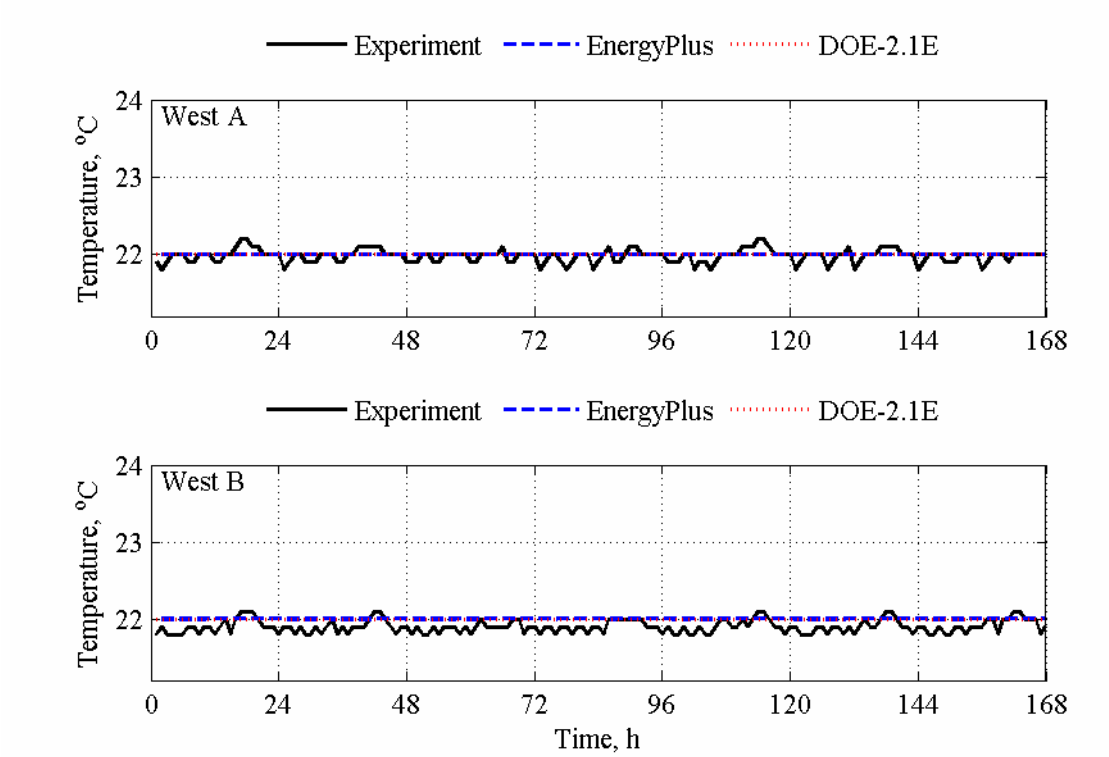

Figure 14.12. Air temperature comparisons for the west test rooms.

Table 14.13. Statistical analyses for air temperatures in the west test rooms.

	West A			**West B**		
	Experiment	**EnergyPlus**	**DOE-2.1E**	**Experiment**	**EnergyPlus**	**DOE-2.1E**
$\bar{x}$	22.0 °C	22.0 °C	22.0 °C	21.9 °C	22.0 °C	22.0 °C
s	0.1 °C	0.0 °C	0.0 °C	0.1 °C	0.0 °C	0.0 °C
x_{max}	22.2 °C	22.0 °C	22.0 °C	22.1 °C	22.0 °C	22.0 °C
x_{min}	21.8 °C	22.0 °C	22.0 °C	21.8 °C	22.0 °C	22.0 °C
$\overline{D}$	-	0.0 K	0.0 K	-	-0.1 K	-0.1 K
$\overline{\lvert D \rvert}$	-	0.1 K	0.1 K	-	0.1 K	0.1 K
D_{max}	-	0.2 K	0.2 K	-	0.2 K	0.2 K
D_{min}	-	0.0 K	0.0 K	-	0.0 K	0.0 K
D_{rms}	-	0.1 K	0.1 K	-	0.1 K	0.1 K
$D_{95\%}$	-	0.2 K	0.2 K	-	0.2 K	0.2 K
$\overline{OU}$	0.2 K	0.2 K	-	0.2 K	0.2 K	-
$\overline{UR}$	-	0.2	0.2	-	0.4	0.4
UR_{max}	-	0.6	0.6	-	0.6	0.6
UR_{min}	-	0.0	0.0	-	0.0	0.0
$\overline{\lvert D \rvert} / \bar{x} \times 100\%$	-	0.3%	0.3%	-	0.5%	0.5%
$\overline{D} / \bar{x} \times 100\%$	-	-0.1%	-0.1%	-	-0.4%	-0.4%
N	168	168	168	168	168	168

14.3.4. Reference Point Daylight Illuminance

The zone reference point daylight illuminances were measured and compared with results from the building energy simulation programs. Plots for the east, south, and west test rooms are contained in Figures 14.13 to 14.15, respectively, and statistical analyses are contained in Tables 14.14 to 14.16, respectively.

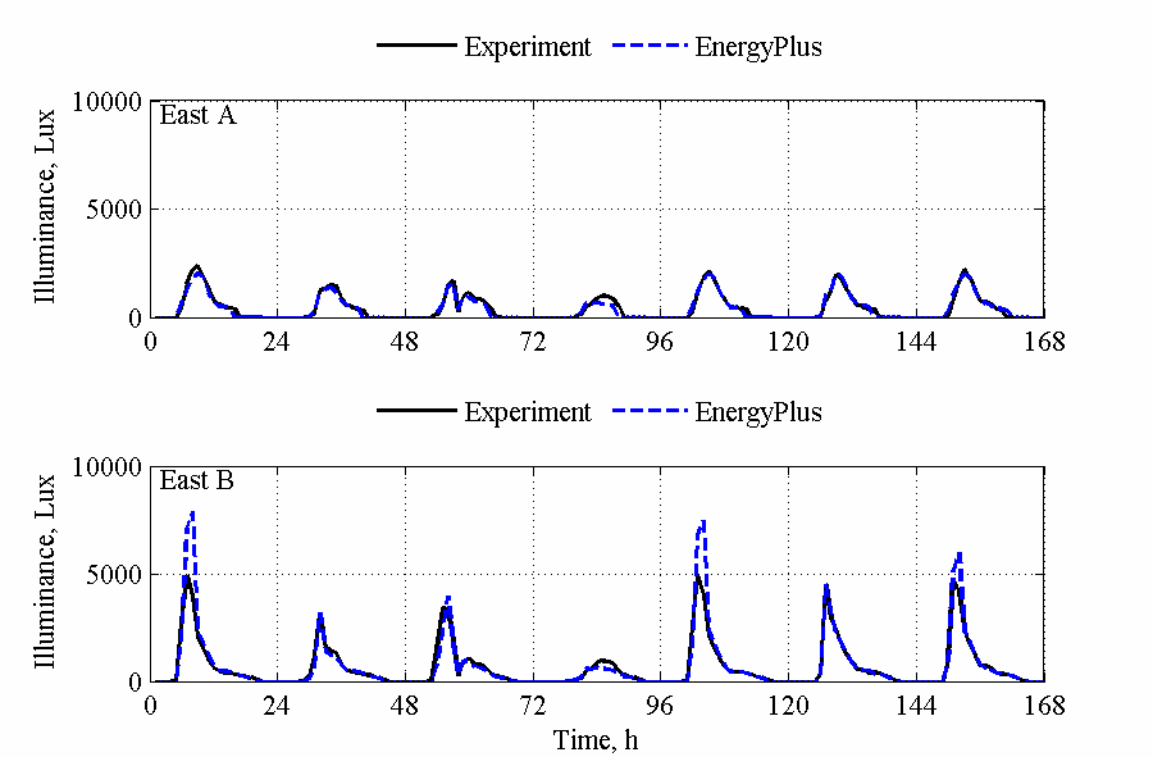

Figure 14.13. Zone reference point daylight illuminance comparisons for the east test rooms.

Table 14.14. Statistical analyses for reference point daylight illuminances in the east test rooms.

	East A		East B	
	Experiment	**EnergyPlus**	**Experiment**	**EnergyPlus**
$\bar{x}$	692.8 Lux	648.6 Lux	1050.3 Lux	1132.8 Lux
s	640.4 Lux	608.7 Lux	1214.5 Lux	1653.9 Lux
x_{max}	2375.0 Lux	2014.2 Lux	4937.0 Lux	7859.4 Lux
x_{min}	0.0 Lux	2.1 Lux	12.0 Lux	10.3 Lux
$\overline{D}$	-	44.1 Lux	-	-82.5 Lux
$\overline{\lvert D \rvert}$	-	109.2 Lux	-	259.0 Lux
D_{max}	-	550.6 Lux	-	3940.4 Lux
D_{min}	-	0.6 Lux	-	0.5 Lux
D_{rms}	-	167.4 Lux	-	661.4 Lux
$D_{95\%}$	-	374.4 Lux	-	1149.1 Lux
$\overline{OU}$	39.2 Lux	11.2 Lux	59.4 Lux	18.4 Lux
$\overline{UR}$	-	4.3	-	3.1
UR_{max}	-	60.7	-	20.5
UR_{min}	-	0.0	-	0.0
$\overline{\lvert D \rvert} / \bar{x} \times 100\%$	-	15.8%	-	24.7%
$\overline{D} / \bar{x} \times 100\%$	-	6.4%	-	-7.9%
N	95	95	102	102

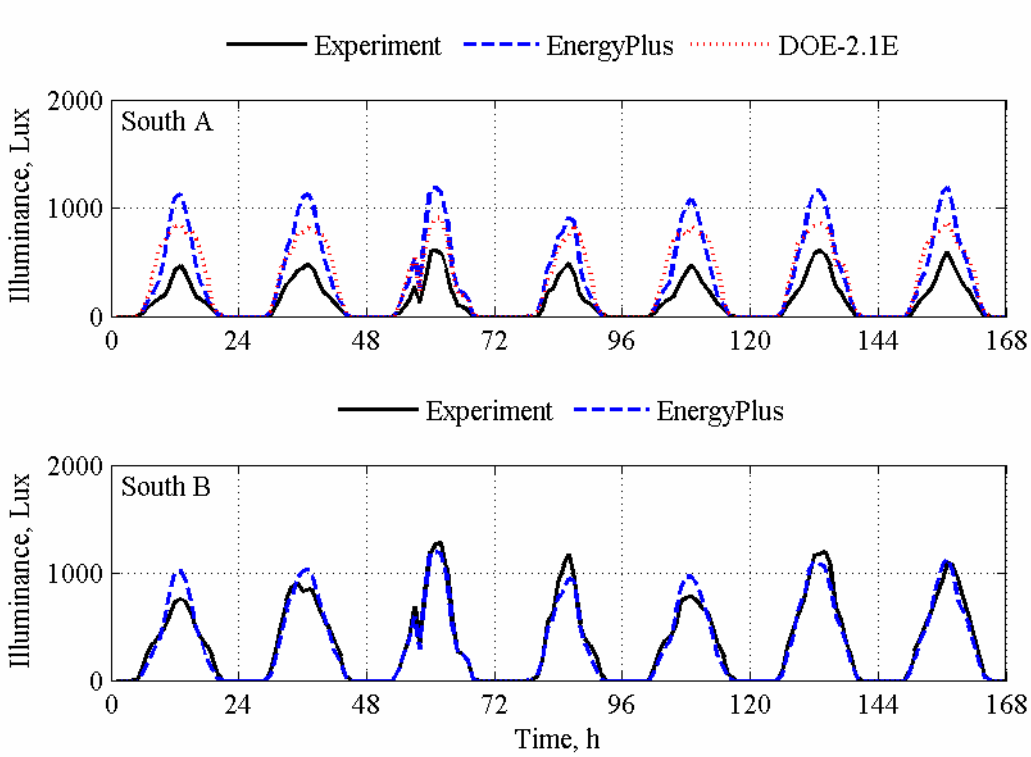

Figure 14.14. Zone reference point daylight illuminance comparisons for the south test rooms.

Table 14.15. Statistical analyses for reference point daylight illuminances in the south test rooms.

	South A			**South B**	
	Experiment	**EnergyPlus**	**DOE-2.1E**	**Experiment**	**EnergyPlus**
$\bar{x}$	248.1 Lux	543.7 Lux	531.1 Lux	545.5 Lux	524.8 Lux
s	167.9 Lux	365.8 Lux	264.5 Lux	334.1 Lux	355.5 Lux
x_{max}	609.0 Lux	1191.0 Lux	905.6 Lux	1272.0 Lux	1186.5 Lux
x_{min}	0.0 Lux	39.6 Lux	32.7 Lux	28.0 Lux	9.3 Lux
$\overline{D}$	-	-295.6 Lux	-283.0 Lux	-	20.8 Lux
$\overline{\lvert D \rvert}$	-	295.6 Lux	283.0 Lux	-	80.3 Lux
D_{max}	-	677.9 Lux	552.8 Lux	-	277.0 Lux
D_{min}	-	19.9 Lux	20.2 Lux	-	0.3 Lux
D_{rms}	-	359.1 Lux	317.1 Lux	-	101.4 Lux
$D_{95\%}$	-	618.2 Lux	503.4 Lux	-	205.8 Lux
$\overline{OU}$	14.0 Lux	16.5 Lux	-	30.9 Lux	19.2 Lux
$\overline{UR}$	-	9.9	12.0	-	2.5
UR_{max}	-	32.1	26.8	-	13.1
UR_{min}	-	4.5	3.5	-	0.0
$\overline{\lvert D \rvert} / \bar{x} \times 100\%$	-	119.2%	114.1%	-	14.7%
$\overline{D} / \bar{x} \times 100\%$	-	-119.2%	-114.1%	-	3.8%
N	96	96	96	102	102

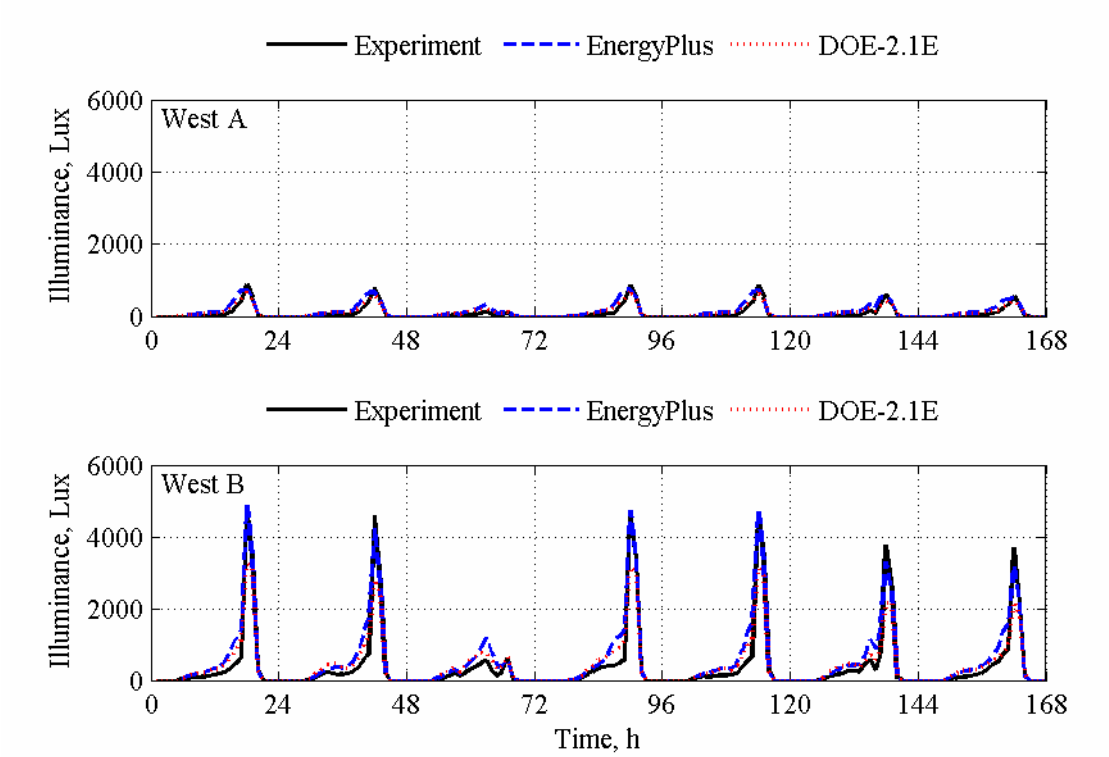

Figure 14.15. Zone reference point daylight illuminance comparisons for the west test rooms.

Table 14.16. Statistical analyses for reference point daylight illuminances in the west test rooms.

	West A			**West B**		
	Experiment	**EnergyPlus**	**DOE-2.1E**	**Experiment**	**EnergyPlus**	**DOE-2.1E**
$\bar{x}$	132.0 Lux	220.8 Lux	172.5 Lux	653.7 Lux	862.6 Lux	692.9 Lux
s	210.8 Lux	214.4 Lux	161.1 Lux	1140.1 Lux	1106.9 Lux	791.9 Lux
x_{max}	873.0 Lux	744.8 Lux	666.9 Lux	4593.0 Lux	4880.4 Lux	3238.7 Lux
x_{min}	0.0 Lux	10.5 Lux	11.6 Lux	0.0 Lux	32.1 Lux	30.9 Lux
$\overline{D}$	-	-88.8 Lux	-40.5 Lux	-	-208.9 Lux	-39.2 Lux
$\overline{\lvert D \rvert}$	-	100.9 Lux	70.2 Lux	-	246.0 Lux	265.4 Lux
D_{max}	-	305.9 Lux	224.9 Lux	-	939.5 Lux	1763.6 Lux
D_{min}	-	0.2 Lux	3.3 Lux	-	6.5 Lux	9.8 Lux
D_{rms}	-	127.4 Lux	81.3 Lux	-	343.8 Lux	430.1 Lux
$D_{95\%}$	-	278.6 Lux	130.8 Lux	-	754.8 Lux	1354.3 Lux
$\overline{OU}$	7.5 Lux	21.9 Lux	-	37.0 Lux	62.7 Lux	-
$\overline{UR}$	-	5.9	5.2	-	4.2	4.2
UR_{max}	-	10.4	12.7	-	13.7	12.8
UR_{min}	-	0.0	0.1	-	0.0	0.1
$\overline{\lvert D \rvert} / \bar{x} \times 100\%$	-	76.4%	53.2%	-	37.6%	40.6%
$\overline{D} / \bar{x} \times 100\%$	-	-67.2%	-30.7%	-	-32.0%	-6.0%
N	99	99	99	102	102	102

14.3.5. Light Power

The zone light powers were measured and compared with results from the building energy simulation programs. Plots for the east, south, and west test rooms are contained in Figures 14.16 to 14.18, respectively and statistical analyses are contained in Tables 14.17 to 14.19, respectively.

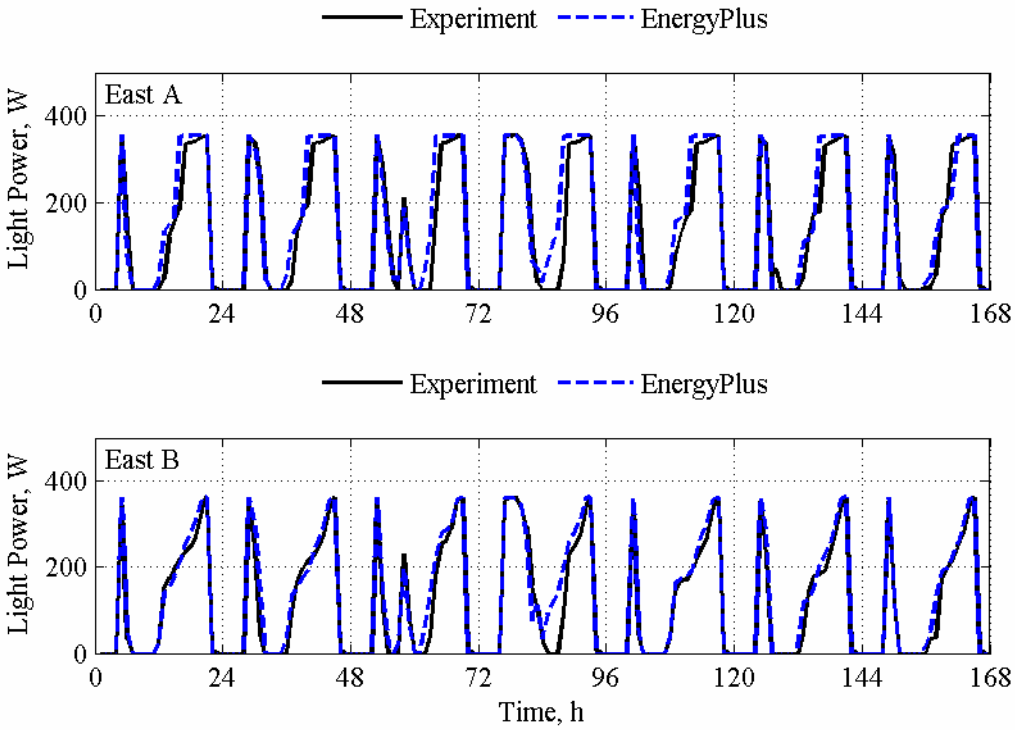

Figure 14.16. Light power comparisons for the east test rooms.

Table 14.17. Statistical analyses of light powers in the east test rooms.

	East A		**East B**	
	Experiment	**EnergyPlus**	**Experiment**	**EnergyPlus**
$\bar{x}$	177.4 W	195.0 W	167.8 W	183.7 W
s	153.0 W	152.6 W	134.4 W	133.3 W
x_{max}	356.0 W	356.0 W	362.0 W	362.0 W
x_{min}	0.0 W	0.0 W	0.0 W	0.0 W
$\overline{D}$	-	-17.6 W	-	-15.9 W
$\overline{\lvert D \rvert}$	-	29.8 W	-	21.8 W
D_{max}	-	284.8 W	-	139.3 W
D_{min}	-	0.0 W	-	0.0 W
D_{rms}	-	57.1 W	-	35.0 W
$D_{95\%}$	-	132.8 W	-	90.1 W
$\overline{OU}$	0.4 W	11.9 W	0.4 W	10.9 W
$\overline{UR}$	-	3.6	-	2.4
UR_{max}	-	36.7	-	15.4
UR_{min}	-	0.0	-	0.0
$\overline{\lvert D \rvert} / \bar{x} \times 100\%$	-	16.8%	-	13.0%
$\overline{D} / \bar{x} \times 100\%$	-	-9.9%	-	-9.5%
N	119	119	112	112

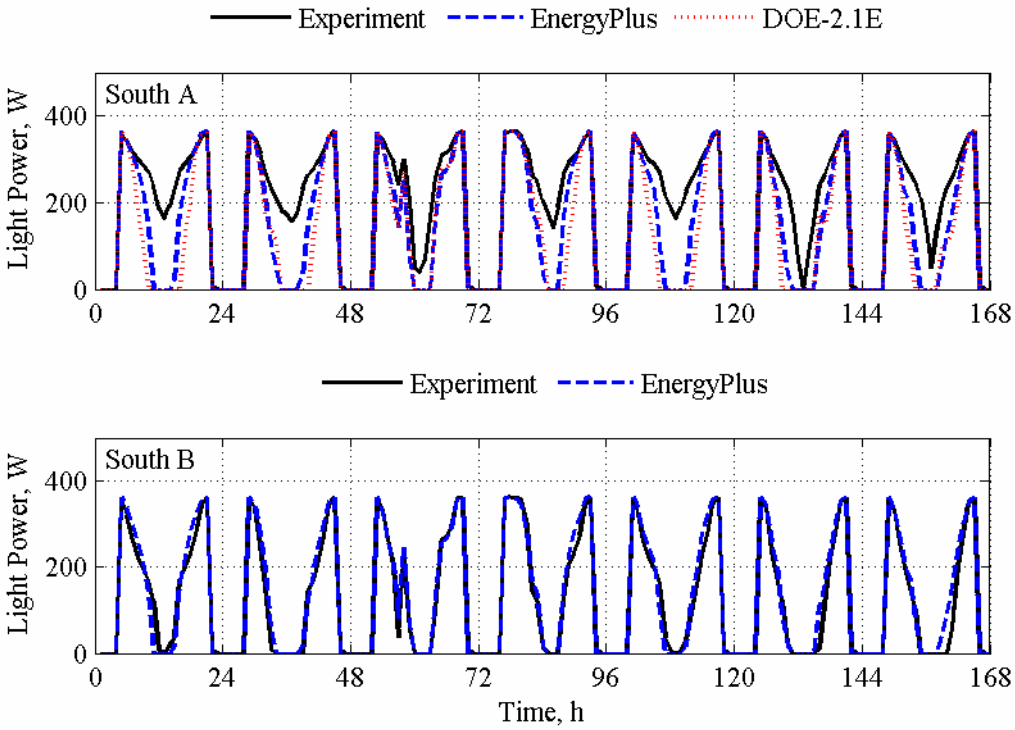

Figure 14.17. Light power comparisons for the south test rooms.

Table 14.18. Statistical analyses of light powers in the south test rooms.

	South A			**South B**	
	Experiment	**EnergyPlus**	**DOE-2.1E**	**Experiment**	**EnergyPlus**
$\bar{x}$	302.6 W	251.4 W	223.1 W	229.8 W	245.2 W
s	47.7 W	106.7 W	127.2 W	113.8 W	108.0 W
x_{max}	364.0 W	364.0 W	364.0 W	362.0 W	362.0 W
x_{min}	191.0 W	0.0 W	0.0 W	0.0 W	16.0 W
$\overline{D}$	-	51.2 W	79.5 W	-	-15.4 W
$\overline{\lvert D \rvert}$	-	53.4 W	81.2 W	-	21.3 W
D_{max}	-	215.8 W	276.0 W	-	100.6 W
D_{min}	-	0.0 W	0.0 W	-	0.0 W
D_{rms}	-	79.6 W	117.9 W	-	30.0 W
$D_{95\%}$	-	171.9 W	255.0 W	-	53.4 W
$\overline{OU}$	0.7 W	11.6 W	-	0.5 W	12.8 W
$\overline{UR}$	-	3.8	6.2	-	1.6
UR_{max}	-	33.6	27.1	-	6.4
UR_{min}	-	0.0	0.0	-	0.0
$\overline{\lvert D \rvert} / \bar{x} \times 100\%$	-	17.6%	26.8%	-	9.3%
$\overline{D} / \bar{x} \times 100\%$	-	16.9%	26.3%	-	-6.7%
N	92	92	92	90	90

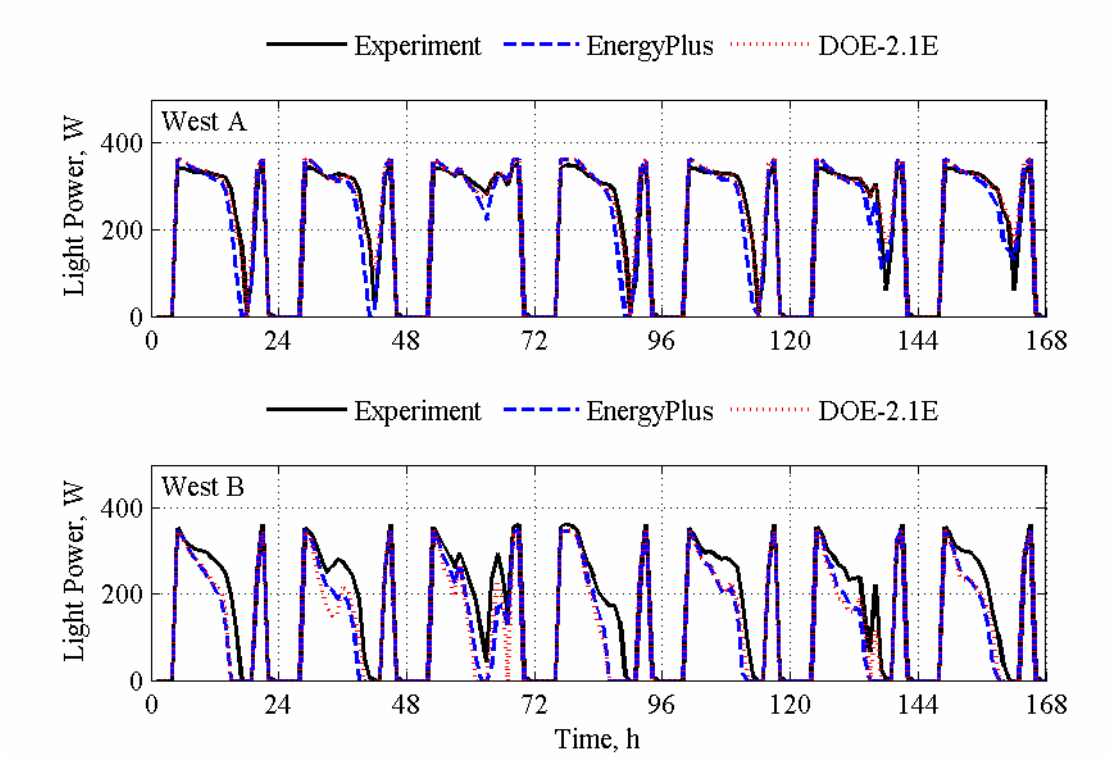

Figure 14.18. Light power comparisons for the west test rooms.

Table 14.19. Statistical analyses of light powers in the west test rooms.

	West A			**West B**		
	Experiment	**EnergyPlus**	**DOE-2.1E**	**Experiment**	**EnergyPlus**	**DOE-2.1E**
$\bar{x}$	324.4 W	325.6 W	330.9 W	318.2 W	304.4 W	297.3 W
s	29.0 W	39.4 W	28.9 W	43.3 W	46.4 W	61.2 W
x_{max}	348.0 W	362.0 W	362.0 W	362.0 W	348.0 W	348.0 W
x_{min}	160.0 W	111.1 W	212.8 W	144.0 W	124.1 W	0.0 W
$\overline{D}$	-	-1.1 W	-6.4 W	-	13.8 W	20.9 W
$\overline{\lvert D \rvert}$	-	14.2 W	11.2 W	-	16.4 W	24.7 W
D_{max}	-	81.9 W	52.8 W	-	52.2 W	144.0 W
D_{min}	-	0.3 W	0.0 W	-	1.7 W	4.2 W
D_{rms}	-	17.7 W	14.6 W	-	19.5 W	34.7 W
$D_{95\%}$	-	28.3 W	29.3 W	-	36.7 W	66.2 W
$\overline{OU}$	0.7 W	11.2 W	-	0.7 W	11.0 W	-
$\overline{UR}$	-	1.5	1.2	-	1.8	3.2
UR_{max}	-	29.1	12.5	-	13.8	31.7
UR_{min}	-	0.0	0.0	-	0.2	0.5
$\overline{\lvert D \rvert} / \bar{x} \times 100\%$	-	4.4%	3.5%	-	5.2%	7.8%
$\overline{D} / \bar{x} \times 100\%$	-	-0.3%	-2.0%	-	4.3%	6.6%
N	91	91	91	48	48	48

14.4. Discussion

Due to high ventilation loads caused by high minimum airflow rate set points and low supply air temperatures, the electric reheat coils were nearly always energized despite a large internal load from the baseboard heaters. However, the reheat coil power was decreased during the day when

higher outdoor air temperatures and solar gains increased the cooling load. For a few hours in some exterior test rooms, the solar gains increased the cooling loads so that no reheat coil power was required and the VAV damper modulated from its minimum position to overcome the thermal load in the zone. For several hours, it was not possible, even at the maximum airflow rate, to maintain the air temperature at the cooling set point temperature, and the temperature floated above the cooling set point.

During the experiments, the lights in the exterior test rooms modulated to provide adequate illuminance at the zone reference points. For several hours in specific test rooms, the daylight entering the space provided enough illuminance to maintain the prescribed light level at the references points when the light fixtures were turned off.

The various permutations of shading and window combinations allowed for careful assessment of overall building energy simulation performances and are useful for empirical validations. In-depth analyses and discussion of these results are provided by Loutzenhiser et al. [49].

CHAPTER 15: ERS DAYLIGHTING EXPERIMENT 2

The second ERS daylighting experiment was performed over a seven-day period from June 4 to June 10, 2006. This experiment was simpler than the first experiment using only two types of windows in combination with interior shading screens and exterior shading fins given in Chapter 2 (Table 2.2). The control scheme for the dimmable ballasts from ERS Experiment 1 was also used for this experiment; however the illuminance set points in all the exterior test rooms were fixed at 645 Lux. Additional information is contained in this chapter concerning:

- interior shading screens,
- lighting schedules and corresponding illuminance, and
- results.

15.1. Interior Shading Screens

While Nysan Superweave 1000 shading screens and white muslin cloth were installed over the windows in the exterior A and B test rooms, respectively. Both shading devices were mounted 152.2 mm from the inner glass pane of the window. The optical properties for the Nysan Superweave 1000 are given in Chapter 14 (Table 14.2), and the optical properties of the white muslin cloth are given in Table 15.1. These properties were measured from 250 nm to 2500 nm at EMPA and the integral properties were computed according to European Standard EN 410 [7] using Glad Software [8].

Table 15.1. Optical properties of the white muslin cloth.

Type	White Muslin Cloth
Visible transmittance, %	38.8
Solar transmittance, %	38.4
Visible reflectance, %	60.5
Solar reflectance, %	58.8

15.2. Lighting Schedules, Sources, and Corresponding Illuminance

The same lighting configuration as in ERS Experiment 1 was used for this experiment. The maximum and minimum light power and along with illuminance with daylighting for the test rooms for this experiment are giving in Table 15.2; these measurements were taken during the night before the experiment.

Table 15.2. Maximum light power for each test room and minimum light power for the exterior test rooms during the experiment.

Test room	Maximum light power, W	Illuminance at maximum light power, Lux	Minimum light power, W	Illuminance at minimum light power, Lux
East A	349	645	89.7	22.1
East B	356	645	91.3	29.2
South A	344	645	88.9	29.4
South B	361	645	90.7	27.2
West A	345	645	90.2	29.8
West B	353	645	88.2	26.7
Interior A	359	-	-	-
Interior B	359	-	-	-

During the experiment, the lights were scheduled to come on one hour prior to sunrise and turn-off one hour after sunset. Table 15.3 contains the light schedule given in Central Standard Time (GMT-6h).

Table 15.3. Test room lighting schedule used during the test.

Time, h	Report schedule (Midnight to 1 AM = 1)	Lights, On/Off
0:00	1	Off
1:00	2	Off
2:00	3	Off
3:00	4	Off
4:00	5	On
5:00	6	On
6:00	7	On
7:00	8	On
8:00	9	On
9:00	10	On
10:00	11	On
11:00	12	On
12:00	13	On
13:00	14	On
14:00	15	On
15:00	16	On
16:00	17	On
17:00	18	On
18:00	19	On
19:00	20	On
20:00	21	On
21:00	22	Off
22:00	23	Off
23:00	24	Off
24:00		Off

15.3. Results

The same comparisons and statistical analyses were performed for each zone as in ERS Experiment 1 (Chapter 14). Figure 15.1 contains measured direct-normal and global horizontal solar irradiances. The global exterior illuminances on the test room façades (east, south, and west) and on the horizontal plane were measured during the experiment. The exterior global illuminances are plotted in Figure 15.2.

From these plots, there were initially two partly cloudy days, following by two sunny days, two partly cloudy days, and followed by one cloudy day. The global vertical illuminances provide information concerning the amount of visible light incident upon the windows and the potential daylighting to the space. During June, the sun takes a high path across the sky and during the day, with the installation of exterior fins, beam illuminances and solar irradiances were never incident upon the south windows. However, direct sunlight was incident in the morning and evenings on the east and west windows, respectively.

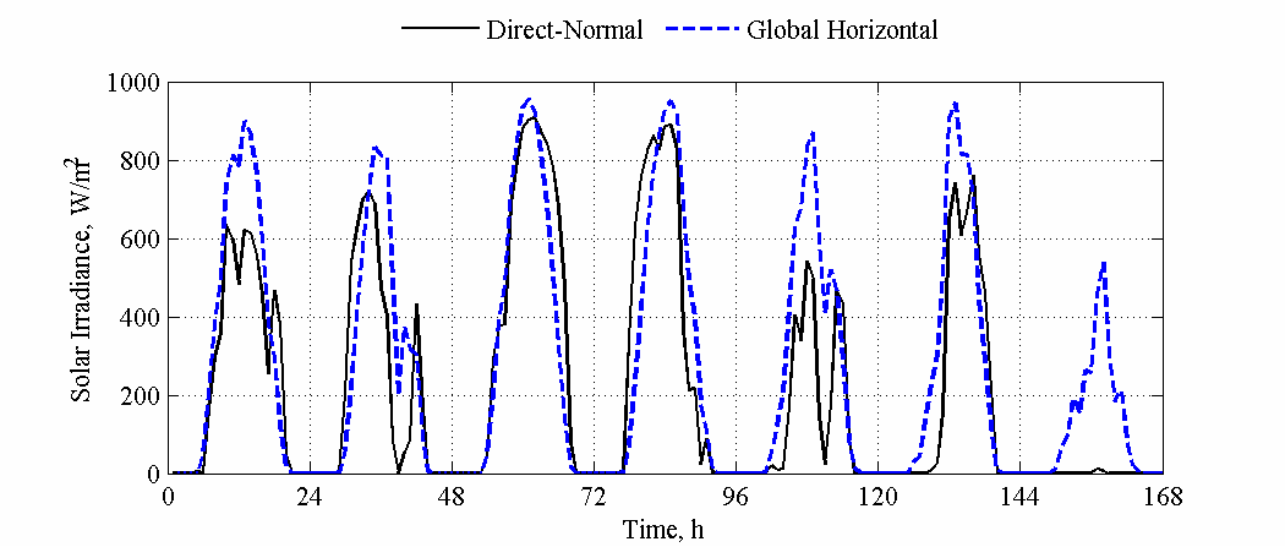

Figure 15.1. Direct-normal and global horizontal solar irradiance measurements during the experiment.

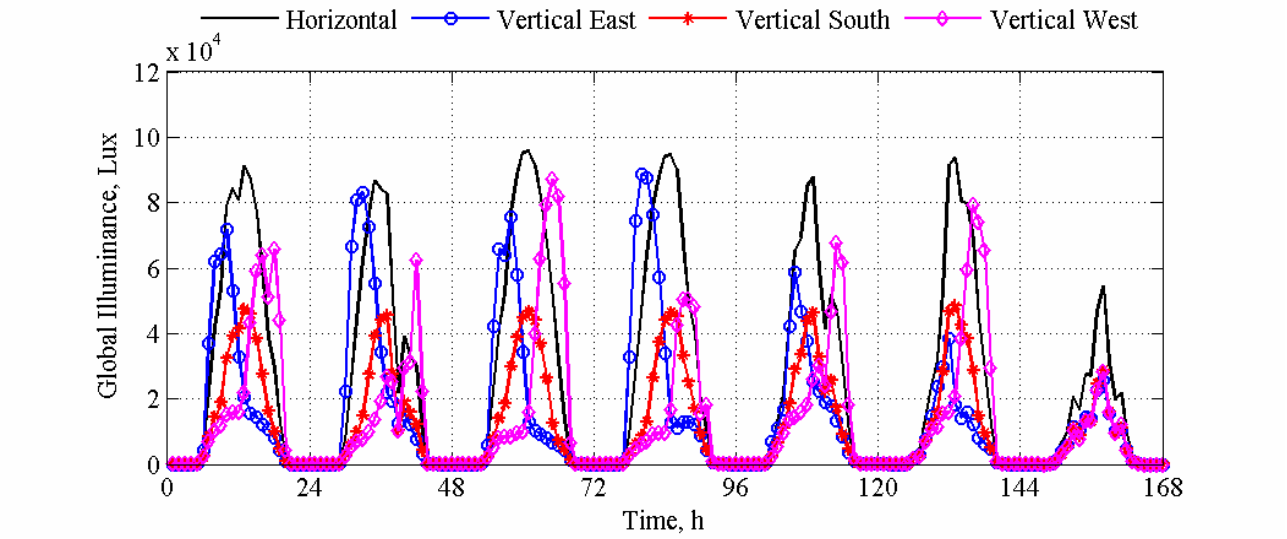

Figure 15.2. Horizontal and vertical global exterior illuminance.

15.3.1. Zone Reheat Coil Power

The electric reheat coil power for each zone was measured and compared with results from the building energy simulation programs. Plots of the reheat coil power for the east, south, and west test rooms are contained in Figures 15.1 to 15.3, respectively, and statistical analyses are found in Tables 15.4 to 15.6, respectively.

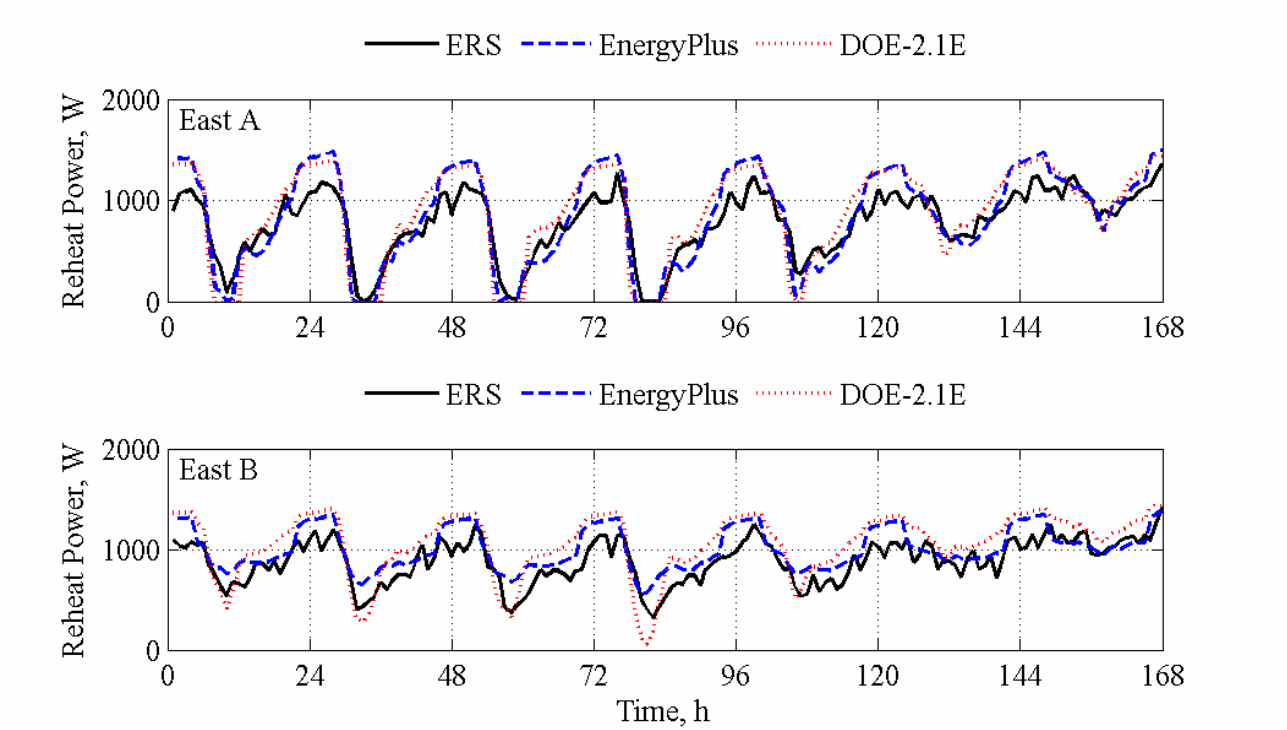

Figure 15.3. Reheat coil power comparisons for the east test rooms.

Table 15.4. Statistical analyses of reheat coil powers in the east test rooms.

	East A			East B		
	Experiment	**EnergyPlus**	**DOE-2.1E**	**Experiment**	**EnergyPlus**	**DOE-2.1E**
$\bar{x}$	781.0 W	855.1 W	888.0 W	879.2 W	1002.8 W	1056.0 W
s	322.6 W	464.2 W	461.0 W	219.0 W	206.9 W	304.9 W
x_{max}	1357.0 W	1492.9 W	1455.8 W	1418.0 W	1371.9 W	1446.2 W
x_{min}	3.0 W	0.0 W	0.0 W	318.0 W	553.0 W	57.7 W
$\overline{D}$	-	-74.1 W	-106.9 W	-	-123.6 W	-176.8 W
$\overline{\lvert D \rvert}$	-	171.7 W	202.7 W	-	145.3 W	213.0 W
D_{max}	-	519.2 W	647.3 W	-	379.1 W	455.7 W
D_{min}	-	0.3 W	0.4 W	-	1.8 W	5.5 W
D_{rms}	-	214.1 W	239.2 W	-	174.6 W	236.8 W
$D_{95\%}$	-	409.3 W	410.3 W	-	312.4 W	385.8 W
$\overline{OU}$	1.8 W	78.3 W	-	2.0 W	78.3 W	-
$\overline{UR}$	-	2.2	2.5	-	1.8	2.7
UR_{max}	-	7.7	7.7	-	4.7	5.7
UR_{min}	-	0.0	0.0	-	0.0	0.1
$\overline{\lvert D \rvert} / \bar{x} \times 100\%$	-	22.0%	25.9%	-	16.5%	24.2%
$\overline{D} / \bar{x} \times 100\%$	-	-9.5%	-13.7%	-	-14.1%	-20.1%
N	166	166	166	168	168	168

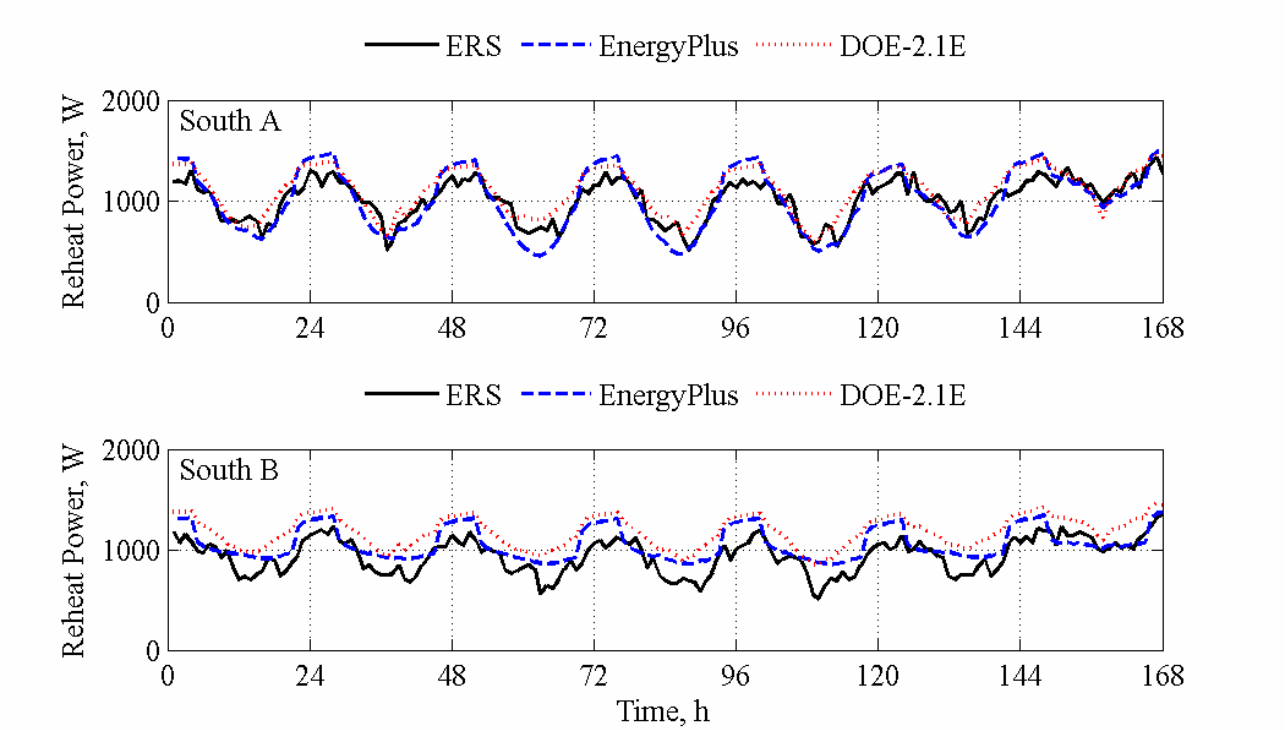

Figure 15.4. Reheat coil power comparisons for the south test rooms.

Table 15.5. Statistical analyses of reheat coil powers in the south test rooms.

	South A			**South B**		
	Experiment	**EnergyPlus**	**DOE-2.1E**	**Experiment**	**EnergyPlus**	**DOE-2.1E**
$\bar{x}$	1006.4 W	1009.7 W	1096.6 W	933.4 W	1052.9 W	1173.8 W
s	210.7 W	306.9 W	225.4 W	176.3 W	158.9 W	154.9 W
x_{max}	1432.0 W	1492.6 W	1457.7 W	1357.0 W	1369.6 W	1461.5 W
x_{min}	513.0 W	460.5 W	598.1 W	507.0 W	850.9 W	848.1 W
$\overline{D}$	-	-3.3 W	-90.2 W	-	-119.5 W	-240.3 W
$\overline{\lvert D \rvert}$	-	120.1 W	116.1 W	-	136.1 W	240.3 W
D_{max}	-	335.8 W	286.0 W	-	361.3 W	429.5 W
D_{min}	-	0.9 W	2.2 W	-	0.8 W	65.3 W
D_{rms}	-	146.5 W	135.5 W	-	161.5 W	252.9 W
$D_{95\%}$	-	261.1 W	242.0 W	-	276.2 W	382.3 W
$\overline{OU}$	2.3 W	79.5 W	-	2.1 W	78.3 W	-
$\overline{UR}$	-	1.5	1.4	-	1.7	3.0
UR_{max}	-	4.1	3.5	-	4.5	5.4
UR_{min}	-	0.0	0.0	-	0.0	0.8
$\overline{\lvert D \rvert} / \bar{x} \times 100\%$	-	11.9%	11.5%	-	14.6%	25.7%
$\overline{D} / \bar{x} \times 100\%$	-	-0.3%	-9.0%	-	-12.8%	-25.7%
N	168	168	168	168	168	168

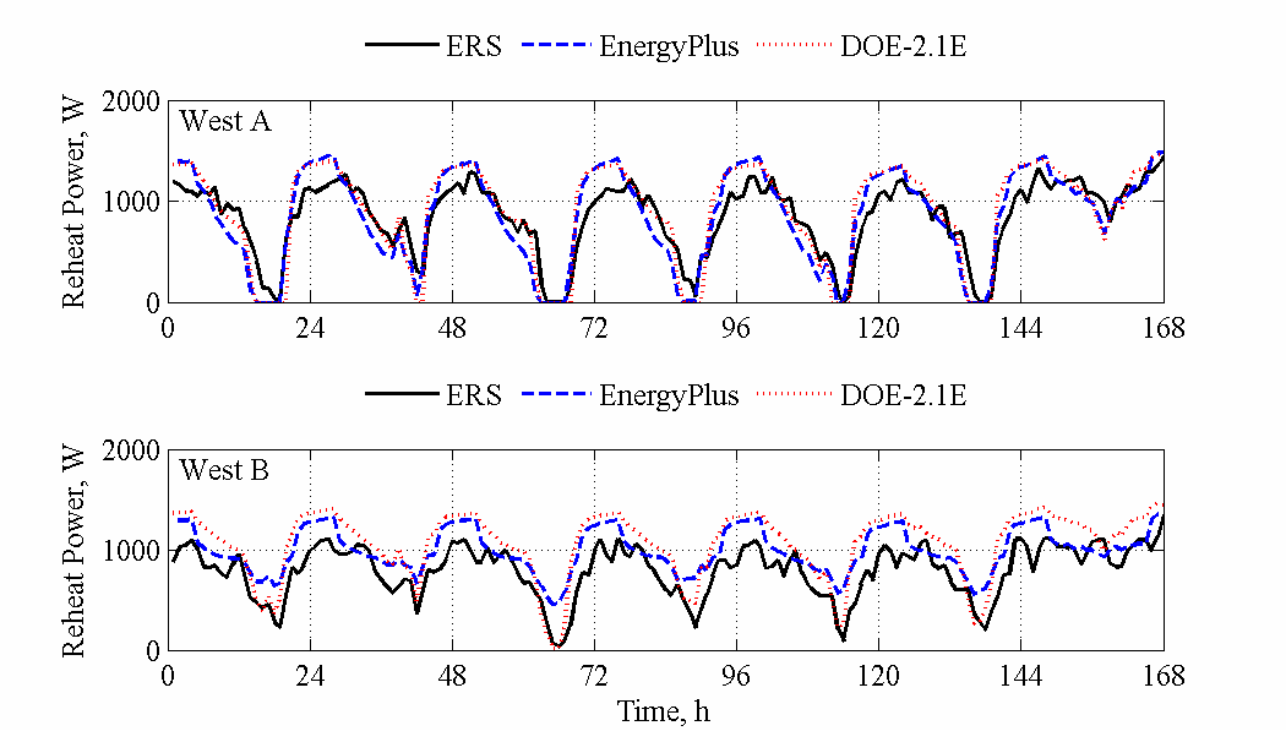

Figure 15.5. Reheat coil power comparisons for the west test rooms.

Table 15.6. Statistical analyses of reheat coil powers in the west test rooms.

	West A			**West B**		
	Experiment	**EnergyPlus**	**DOE-2.1E**	**Experiment**	**EnergyPlus**	**DOE-2.1E**
$\bar{x}$	858.7 W	869.0 W	919.8 W	790.2 W	991.2 W	1058.8 W
s	346.6 W	456.7 W	465.8 W	262.3 W	217.5 W	328.1 W
x_{max}	1433.0 W	1483.3 W	1458.7 W	1339.0 W	1362.3 W	1462.5 W
x_{min}	3.0 W	0.0 W	0.0 W	31.0 W	457.2 W	14.4 W
$\overline{D}$	-	-10.3 W	-61.1 W	-	-201.0 W	-268.6 W
$\overline{\lvert D \rvert}$	-	181.7 W	178.8 W	-	215.9 W	277.2 W
D_{max}	-	626.1 W	637.0 W	-	538.7 W	619.6 W
D_{min}	-	2.3 W	0.1 W	-	3.5 W	2.4 W
D_{rms}	-	218.3 W	225.3 W	-	252.7 W	311.9 W
$D_{95\%}$	-	378.6 W	430.7 W	-	442.9 W	519.5 W
$\overline{OU}$	1.9 W	77.3 W	-	1.8 W	78.8 W	-
$\overline{UR}$	-	2.3	2.3	-	2.7	3.4
UR_{max}	-	7.5	7.9	-	6.7	7.6
UR_{min}	-	0.0	0.0	-	0.0	0.0
$\overline{\lvert D \rvert} / \bar{x} \times 100\%$	-	21.2%	20.8%	-	27.3%	35.1%
$\overline{D} / \bar{x} \times 100\%$	-	-1.2%	-7.1%	-	-25.4%	-34.0%
N	164	164	164	168	168	168

15.3.2. Zone Airflow Rates

The zone airflow rates were measured and compared with results from the building energy simulation programs. Plots for the east, south, and west test rooms are contained in Figures 15.6 to 15.8, respectively and statistical analyses are contained in Tables 15.7 to 15.9, respectively.

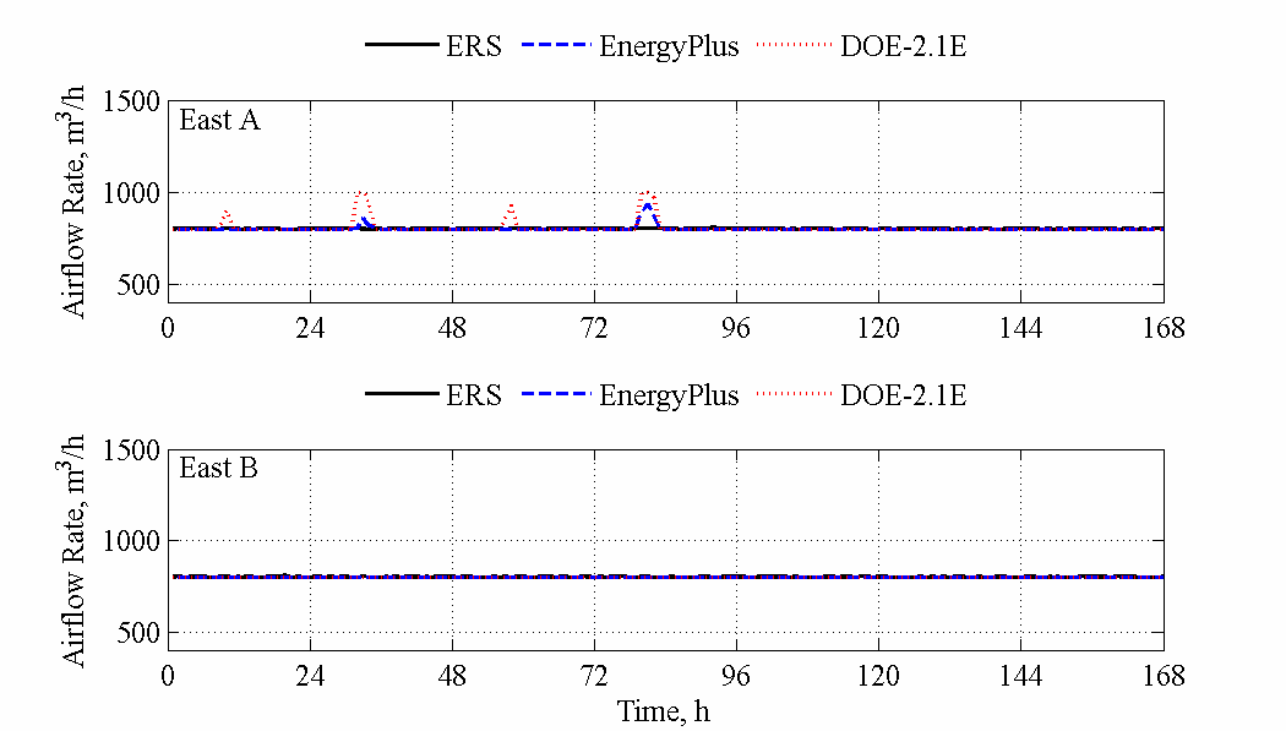

Figure 15.6. Airflow rate comparisons for the east test rooms.

Table 15.7. Statistical analyses of airflow rates in the east test rooms.

	East A			East B		
	Experiment	**EnergyPlus**	**DOE-2.1E**	**Experiment**	**EnergyPlus**	**DOE-2.1E**
$\bar{x}$	799.8 m^3/h	802.1 m^3/h	808.2 m^3/h	799.7 m^3/h	800.0 m^3/h	800.0 m^3/h
s	1.4 m^3/h	13.6 m^3/h	36.3 m^3/h	1.9 m^3/h	0.0 m^3/h	0.0 m^3/h
x_{max}	804.0 m^3/h	930.9 m^3/h	1000.0 m^3/h	806.0 m^3/h	800.0 m^3/h	800.0 m^3/h
x_{min}	795.0 m^3/h	800.0 m^3/h	800.0 m^3/h	796.0 m^3/h	800.0 m^3/h	800.0 m^3/h
$\bar{D}$	-	-2.3 m^3/h	-8.4 m^3/h	-	-0.3 m^3/h	-0.3 m^3/h
$\overline{\lvert D \rvert}$	-	3.1 m^3/h	9.3 m^3/h	-	1.5 m^3/h	1.5 m^3/h
D_{max}	-	128.9 m^3/h	201.0 m^3/h	-	6.0 m^3/h	6.0 m^3/h
D_{min}	-	0.0 m^3/h	0.0 m^3/h	-	0.0 m^3/h	0.0 m^3/h
D_{rms}	-	13.7 m^3/h	37.1 m^3/h	-	1.9 m^3/h	1.9 m^3/h
$D_{95\%}$	-	3.0 m^3/h	57.9 m^3/h	-	4.0 m^3/h	4.0 m^3/h
$\overline{OU}$	18.1 m^3/h	18.4 m^3/h	-	18.1 m^3/h	18.3 m^3/h	-
$\overline{UR}$	-	0.1	0.2	-	0.0	0.0
UR_{max}	-	3.0	5.2	-	0.2	0.2
UR_{min}	-	0.0	0.0	-	0.0	0.0
$\overline{\lvert D \rvert} / \bar{x} \times 100\%$	-	0.4%	1.2%	-	0.2%	0.2%
$\bar{D} / \bar{x} \times 100\%$	-	-0.3%	-1.1%	-	0.0%	0.0%
N	168	168	168	168	168	168

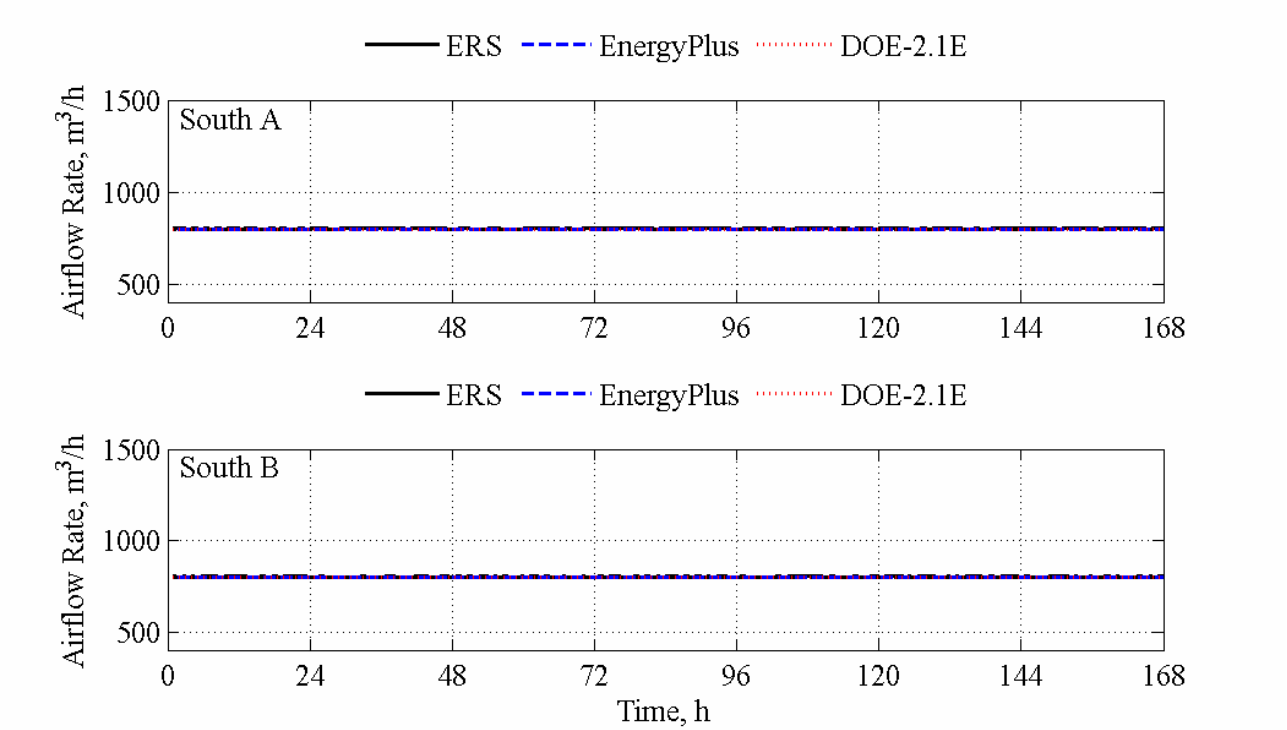

Figure 15.7. Zone airflow rate comparisons for the south test rooms.

Table 15.8. Statistical analyses of airflow rates in the south test rooms.

	South A			**South B**		
	Experiment	**EnergyPlus**	**DOE-2.1E**	**Experiment**	**EnergyPlus**	**DOE-2.1E**
$\bar{x}$	799.9 m^3/h	800.0 m^3/h	800.0 m^3/h	799.9 m^3/h	800.0 m^3/h	800.0 m^3/h
s	1.0 m^3/h	0.0 m^3/h	0.0 m^3/h	1.2 m^3/h	0.0 m^3/h	0.0 m^3/h
x_{max}	802.0 m^3/h	800.0 m^3/h	800.0 m^3/h	803.0 m^3/h	800.0 m^3/h	800.0 m^3/h
x_{min}	797.0 m^3/h	800.0 m^3/h	800.0 m^3/h	797.0 m^3/h	800.0 m^3/h	800.0 m^3/h
$\bar{D}$	-	-0.1 m^3/h	-0.1 m^3/h	-	-0.1 m^3/h	-0.1 m^3/h
$\overline{\lvert D \rvert}$	-	0.7 m^3/h	0.7 m^3/h	-	1.0 m^3/h	1.0 m^3/h
D_{max}	-	3.0 m^3/h	3.0 m^3/h	-	3.0 m^3/h	3.0 m^3/h
D_{min}	-	0.0 m^3/h	0.0 m^3/h	-	0.0 m^3/h	0.0 m^3/h
D_{rms}	-	1.0 m^3/h	1.0 m^3/h	-	1.2 m^3/h	1.2 m^3/h
$D_{95\%}$	-	2.0 m^3/h	2.0 m^3/h	-	2.0 m^3/h	2.0 m^3/h
$\overline{OU}$	18.1 m^3/h	18.3 m^3/h	-	18.1 m^3/h	18.3 m^3/h	-
$\overline{UR}$	-	0.0	0.0	-	0.0	0.0
UR_{max}	-	0.1	0.1	-	0.1	0.1
UR_{min}	-	0.0	0.0	-	0.0	0.0
$\overline{\lvert D \rvert} / \bar{x} \times 100\%$	-	0.1%	0.1%	-	0.1%	0.1%
$\bar{D} / \bar{x} \times 100\%$	-	0.0%	0.0%	-	0.0%	0.0%
N	168	168	168	168	168	168

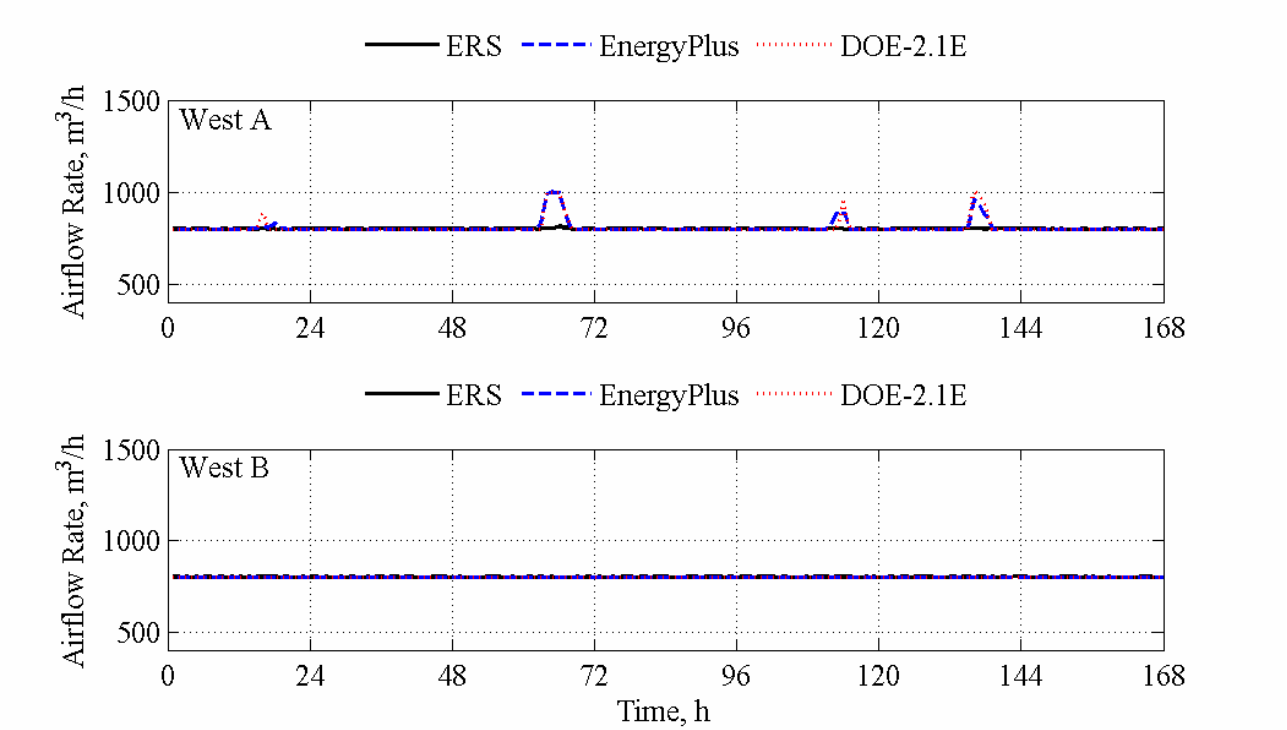

Figure 15.8. Airflow rate comparisons for the west test rooms.

Table 15.9. Statistical analyses of airflow rates in the west test rooms.

	West A			**West B**		
	Experiment	**EnergyPlus**	**DOE-2.1E**	**Experiment**	**EnergyPlus**	**DOE-2.1E**
$\bar{x}$	799.8 m^3/h	807.8 m^3/h	808.4 m^3/h	800.0 m^3/h	800.0 m^3/h	800.0 m^3/h
s	1.7 m^3/h	32.4 m^3/h	37.1 m^3/h	1.1 m^3/h	0.0 m^3/h	0.0 m^3/h
x_{max}	811.0 m^3/h	1000.0 m^3/h	1000. 0 m^3/h	803.0 m^3/h	800.0 m^3/h	800.0 m^3/h
x_{min}	796.0 m^3/h	800.0 m^3/h	800.0 m^3/h	797.0 m^3/h	800.0 m^3/h	800.0 m^3/h
$\overline{D}$	-	-8.0 m^3/h	-8.6 m^3/h	-	0.0 m^3/h	0.0 m^3/h
$\overline{\lvert D \rvert}$	-	8.6 m^3/h	9.3 m^3/h	-	0.7 m^3/h	0.7 m^3/h
D_{max}	-	199.0 m^3/h	200.0 m^3/h	-	3.0 m^3/h	3.0 m^3/h
D_{min}	-	0.0 m^3/h	0.0 m^3/h	-	0.0 m^3/h	0.0 m^3/h
D_{rms}	-	32.6 m^3/h	37.4 m^3/h	-	1.1 m^3/h	1.1 m^3/h
$D_{95\%}$	-	72.6 m^3/h	83.6 m^3/h	-	2.0 m^3/h	2.0 m^3/h
$\overline{OU}$	18.1 m^3/h	18.3 m^3/h	-	18.1 m^3/h	18.3 m^3/h	-
$\overline{UR}$	-	0.2	0.2	-	0.0	0.0
UR_{max}	-	4.5	4.6	-	0.1	0.1
UR_{min}	-	0.0	0.0	-	0.0	0.0
$\overline{\lvert D \rvert} / \bar{x} \times 100\%$	-	1.1%	1.2%	-	0.1%	0.1%
$\overline{D} / \bar{x} \times 100\%$	-	-1.0%	-1.1%	-	0.0%	0.0%
N	168	168	168	168	168	168

15.3.3. Zone Air Temperatures

The zone air temperatures were measured and compared with results from the building energy simulation programs. Plots for the east, south, and west test rooms are contained in Figures 15.9 to 15.11, respectively and statistical analyses are contained in Tables 15.10 to 15.12, respectively.

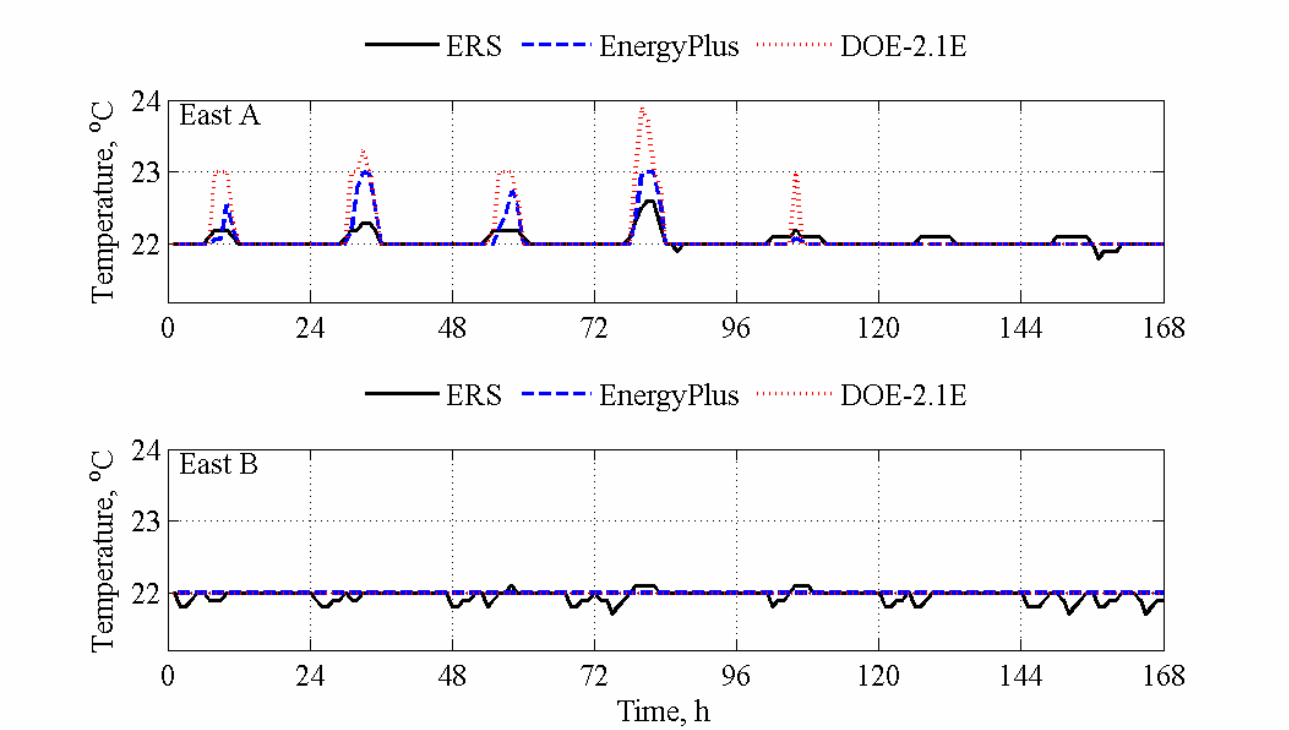

Figure 15.9. Air temperature comparisons for the east test rooms.

Table 15.10. Statistical analyses of air temperatures in the west test rooms.

	East A			**East B**		
	Experiment	**EnergyPlus**	**DOE-2.1E**	**Experiment**	**EnergyPlus**	**DOE-2.1E**
$\bar{x}$	22.0 °C	22.1 °C	22.1 °C	22.0 °C	22.0 °C	22.0 °C
s	0.1 °C	0.2 °C	0.3 °C	0.1 °C	0.0 °C	0.0 °C
x_{max}	22.6 °C	23.0 °C	23.9 °C	22.1 °C	22.0 °C	22.0 °C
x_{min}	21.8 °C	22.0 °C	22.0 °C	21.7 °C	22.0 °C	22.0 °C
$\overline{D}$	-	0.0 K	-0.1	-	0.0 K	0.0 K
$\overline{\lvert D \rvert}$	-	0.1 K	0.1	-	0.1 K	0.1 K
D_{max}	-	0.7 K	1.4	-	0.3 K	0.3 K
D_{min}	-	0.0 K	0.0	-	0.0 K	0.0 K
D_{rms}	-	0.1 K	0.3	-	0.1 K	0.1 K
$D_{95\%}$	-	0.3 K	0.8	-	0.2 K	0.2 K
$\overline{OU}$	0.2 K	0.2 K	-	0.2 K	0.2 K	-
$\overline{UR}$	-	0.2	0.3	-	0.2	0.2
UR_{max}	-	2.2	4.4	-	0.9	0.9
UR_{min}	-	0.0	0.0	-	0.0	0.0
$\overline{\lvert D \rvert} / \bar{x} \times 100\%$	-	0.2%	0.5%	-	0.2%	0.2%
$\overline{D} / \bar{x} \times 100\%$	-	-0.1%	-0.3%	-	-0.2%	-0.2%
N	168	168	168	168	168	168

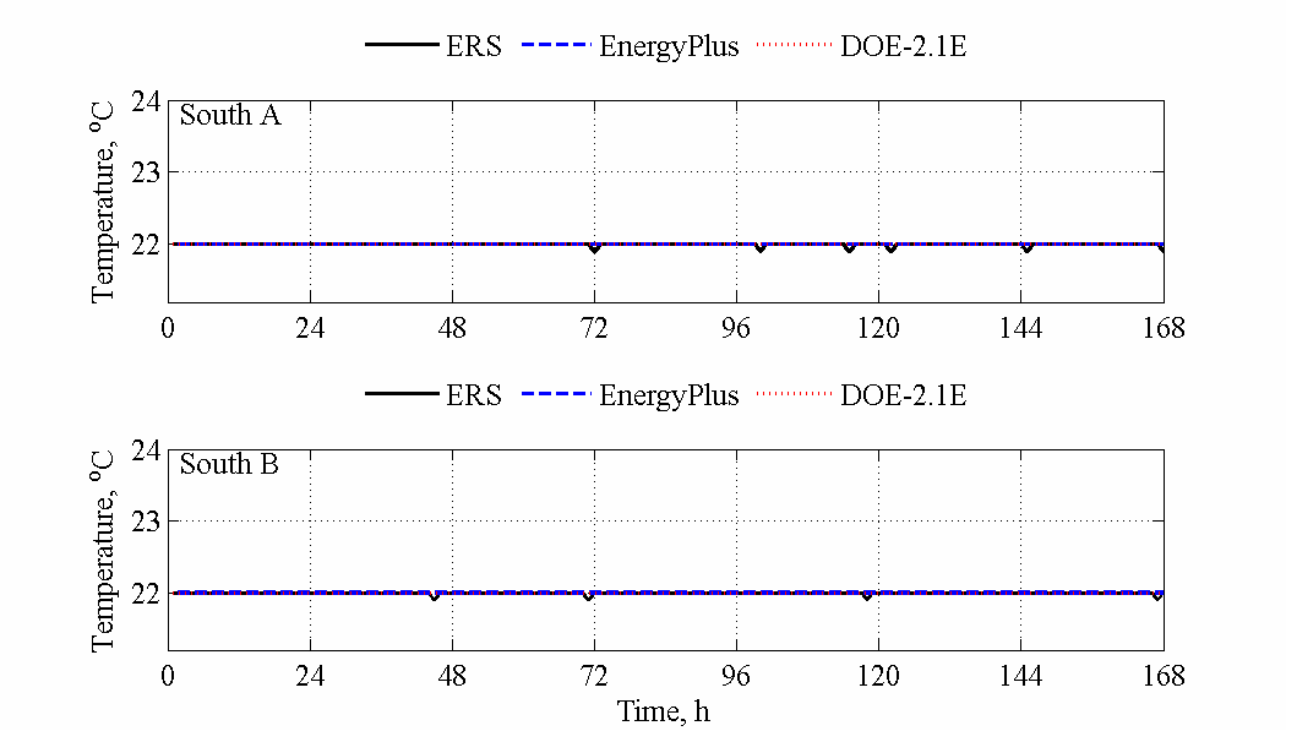

Figure 15.10. Air temperature comparisons for the south test rooms.

Table 15.11. Statistical analyses of air temperatures in the south test rooms.

	South A			**South B**		
	Experiment	**EnergyPlus**	**DOE-2.1E**	**Experiment**	**EnergyPlus**	**DOE-2.1E**
$\bar{x}$	22.0 °C	22.0 °C	22.0 °C	22.0 °C	22.0 °C	22.0 °C
s	0.0 °C	0.0 °C	0.0 °C	0.0 °C	0.0 °C	0.0 °C
x_{max}	22.0 °C	22.0 °C	22.0 °C	22.0 °C	22.0 °C	22.0 °C
x_{min}	21.9 °C	22.0 °C	22.0 °C	21.9 °C	22.0 °C	22.0 °C
$\overline{D}$	-	0.0 K	0.0 K	-	0.0 K	0.0 K
$\overline{\lvert D \rvert}$	-	0.0 K	0.0 K	-	0.0 K	0.0 K
D_{max}	-	0.1 K	0.1 K	-	0.1 K	0.1 K
D_{min}	-	0.0 K	0.0 K	-	0.0 K	0.0 K
D_{rms}	-	0.0 K	0.0 K	-	0.0 K	0.0 K
$D_{95\%}$	-	0.0 K	0.0 K	-	0.0 K	0.0 K
$\overline{OU}$	0.2 K	0.2 K	-	0.2 K	0.2 K	-
$\overline{UR}$	-	0.0	0.0	-	0.0	0.0
UR_{max}	-	0.3	0.3	-	0.3	0.3
UR_{min}	-	0.0	0.0	-	0.0	0.0
$\overline{\lvert D \rvert} / \bar{x} \times 100\%$	-	0.0%	0.0%	-	0.0%	0.0%
$\overline{D} / \bar{x} \times 100\%$	-	0.0%	0.0%	-	0.0%	0.0%
N	168	168	168	168	168	168

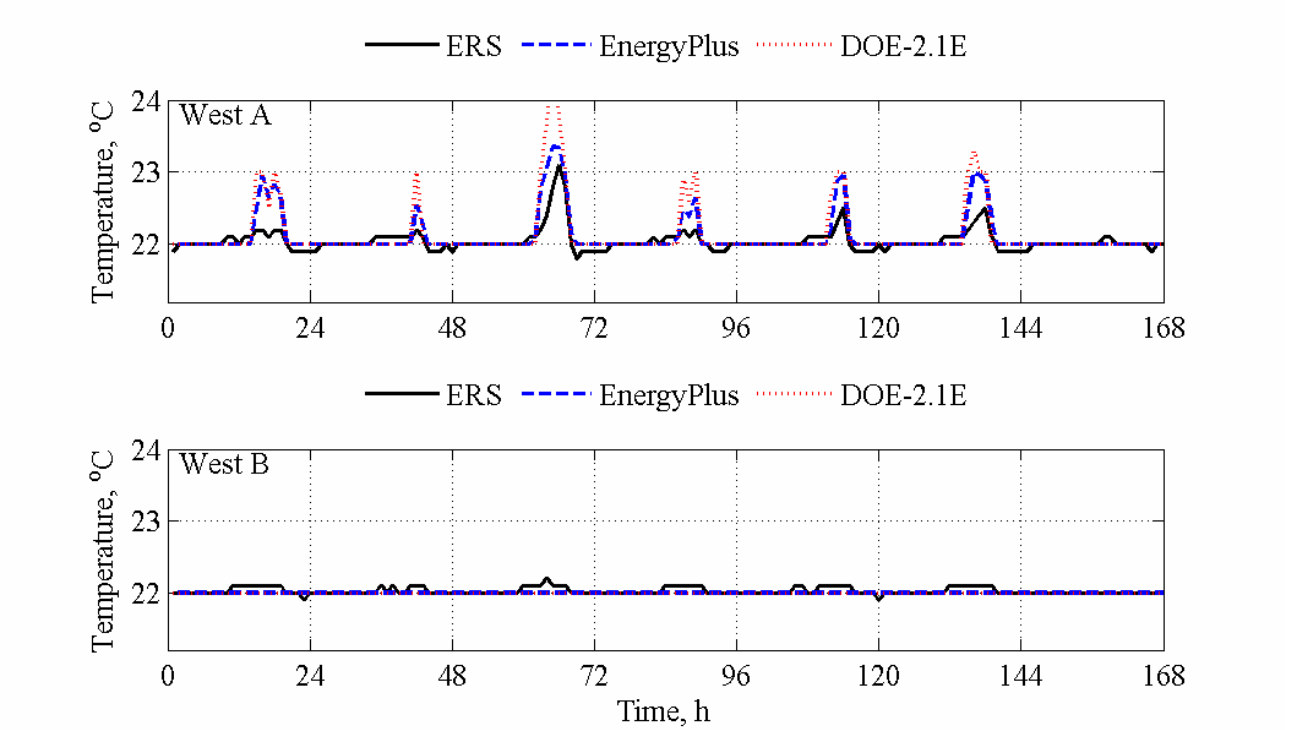

Figure 15.11. Zone air temperature comparisons for the west test rooms.

Table 15.12. Statistical analyses of air temperatures in the west test rooms.

	West A			**West B**		
	Experiment	**EnergyPlus**	**DOE-2.1E**	**Experiment**	**EnergyPlus**	**DOE-2.1E**
$\bar{x}$	22.0 °C	22.1 °C	22.1 °C	22.0 °C	22.0 °C	22.0 °C
s	0.2 °C	0.3 °C	0.4 °C	0.0 °C	0.0 °C	0.0 °C
x_{max}	23.1 °C	23.4 °C	24.4 °C	22.2 °C	22.0 °C	22.0 °C
x_{min}	21.8 °C	22.0 °C	22.0 °C	21.9 °C	22.0 °C	22.0 °C
$\overline{D}$	-	-0.1 K	-0.1 K	-	0.0 K	0.0 K
$\overline{\lvert D \rvert}$	-	0.1 K	0.1 K	-	0.0 K	0.0 K
D_{max}	-	0.8 K	1.6 K	-	0.2 K	0.2 K
D_{min}	-	0.0 K	0.0 K	-	0.0 K	0.0 K
D_{rms}	-	0.2 K	0.3 K	-	0.1 K	0.1 K
$D_{95\%}$	-	0.6 K	0.8 K	-	0.1 K	0.1 K
$\overline{OU}$	0.2 K	0.2 K	-	0.2 K	0.2 K	-
$\overline{UR}$	-	0.3	0.4	-	0.1	0.1
UR_{max}	-	2.4	5.1	-	0.6	0.6
UR_{min}	-	0.0	0.0	-	0.0	0.0
$\overline{\lvert D \rvert} / \bar{x} \times 100\%$	-	0.4%	0.6%	-	0.1%	0.1%
$\overline{D} / \bar{x} \times 100\%$	-	-0.3%	-0.4%	-	0.1%	0.1%
N	168	168	168	168	168	168

15.3.4. Reference Point Daylight Illuminance

The zone reference point daylight illuminances were measured and compared with results from the building energy simulation programs. Plots for the east, south, and west test rooms are contained in Figures 15.12 to 15.14, respectively, and statistical analyses are contained in Tables 15.13 to 15.15, respectively.

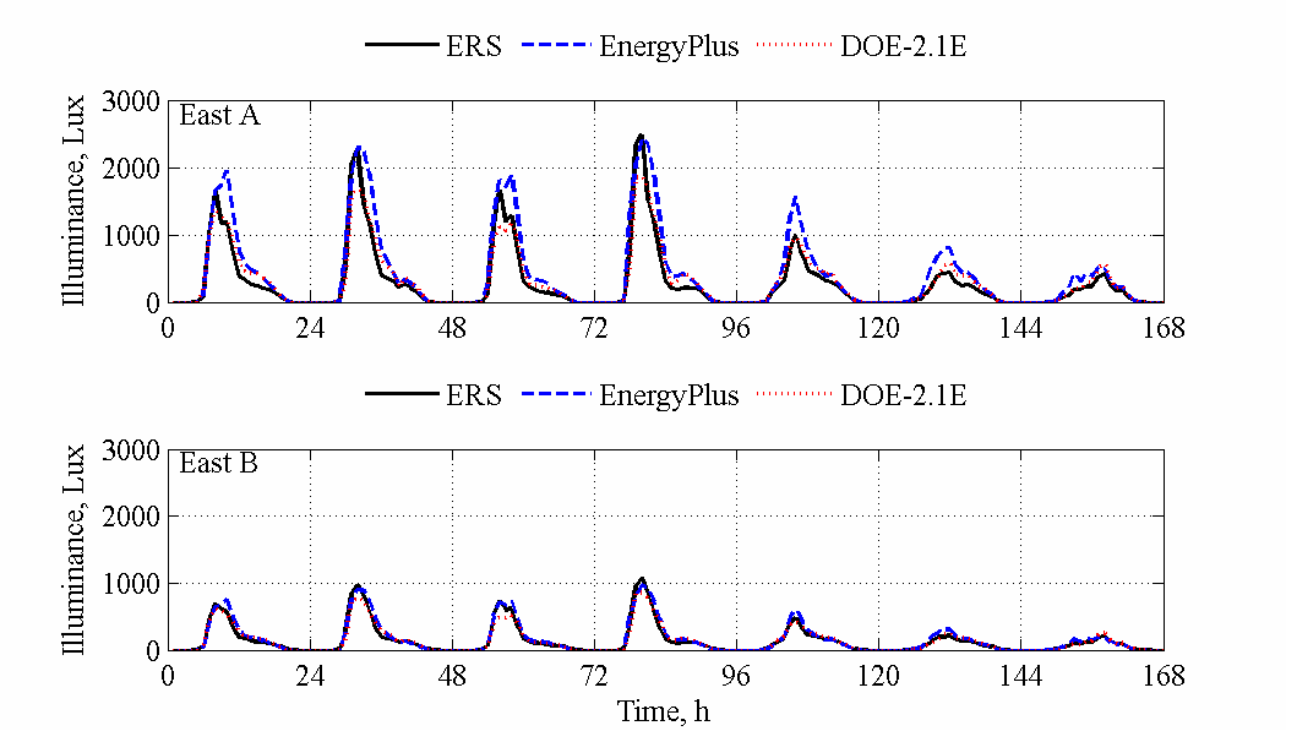

Figure 15.12. Reference point daylight illuminance comparisons for the east test rooms.

Table 15.13. Statistical analyses of reference point daylight illuminances in the east test rooms.

	East A			**East B**		
	Experiment	**EnergyPlus**	**DOE-2.1E**	**Experiment**	**EnergyPlus**	**DOE-2.1E**
$\bar{x}$	461.2 Lux	650.4 Lux	495.3 Lux	217.9 Lux	246.0 Lux	217.2 Lux
s	539.5 Lux	639.1 Lux	451.1 Lux	239.8 Lux	249.2 Lux	205.1 Lux
x_{max}	2489.0 Lux	2441.4 Lux	1858.3 Lux	1075.0 Lux	965.7 Lux	855.7 Lux
x_{min}	14.0 Lux	11.9 Lux	14.5 Lux	13.0 Lux	1.7 Lux	3.6 Lux
$\overline{D}$	-	-189.3 Lux	-34.2 Lux	-	-28.0 Lux	0.8 Lux
$\overline{\lvert D \rvert}$	-	200.4 Lux	115.0 Lux	-	43.9 Lux	39.5 Lux
D_{max}	-	840.4 Lux	630.7 Lux	-	191.6 Lux	229.5 Lux
D_{min}	-	1.6 Lux	0.5 Lux	-	0.1 Lux	0.6 Lux
D_{rms}	-	287.2 Lux	165.3 Lux	-	64.2 Lux	60.1 Lux
$D_{95\%}$	-	597.6 Lux	292.4 Lux	-	147.5 Lux	124.1 Lux
$\overline{OU}$	26.1 Lux	13.5 Lux	-	12.3 Lux	36.1 Lux	-
$\overline{UR}$	-	6.0	3.6	-	1.4	1.2
UR_{max}	-	13.1	10.4	-	11.9	10.0
UR_{min}	-	0.0	0.2	-	0.0	0.0
$\overline{\lvert D \rvert} / \bar{x} \times 100\%$	-	43.5%	24.9%	-	20.2%	18.1%
$\overline{D} / \bar{x} \times 100\%$	-	-41.0%	-7.4%	-	-12.9%	0.4%
N	102	102	102	105	105	105

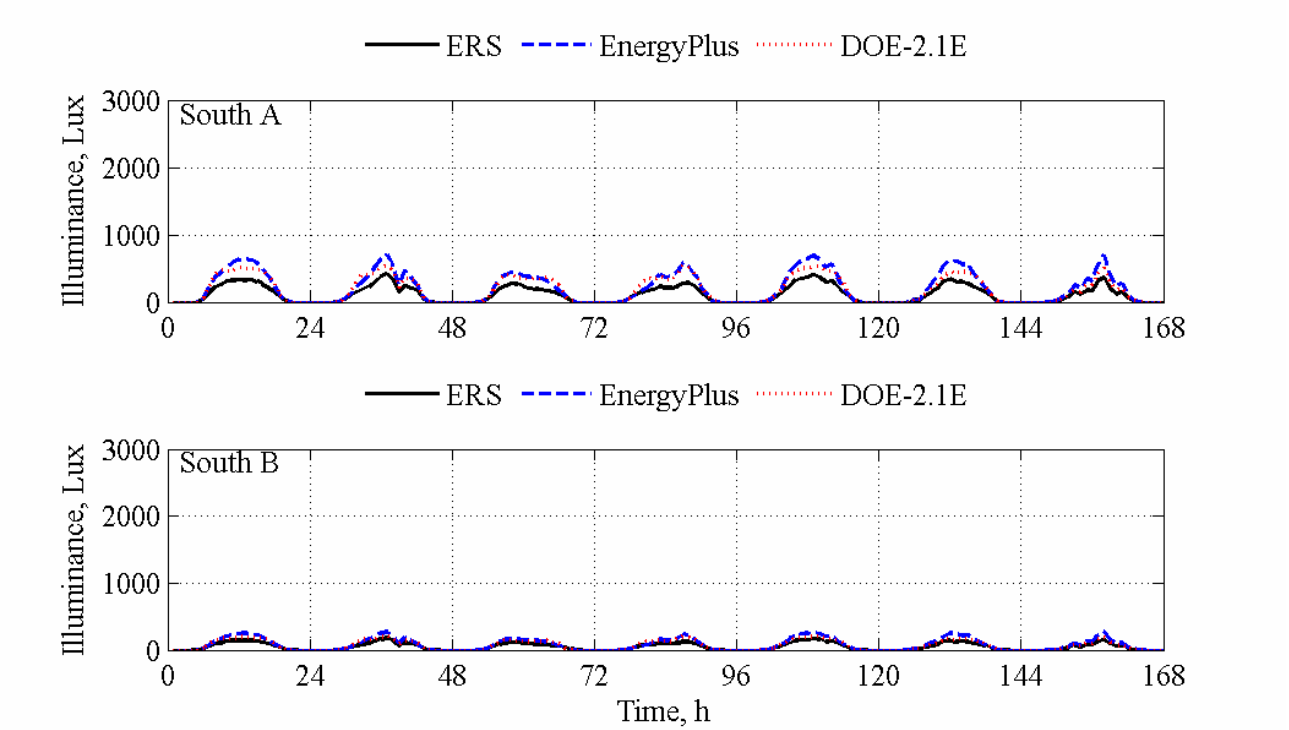

Figure 15.13. Reference point daylight illuminance comparisons for the south test rooms.

Table 15.14. Statistical analyses of reference point daylight illuminances in the south test rooms.

	South A			**South B**		
	Experiment	**EnergyPlus**	**DOE-2.1E**	**Experiment**	**EnergyPlus**	**DOE-2.1E**
$\bar{x}$	194.5 Lux	337.7 Lux	303.7 Lux	84.3 Lux	130.5 Lux	113.5 Lux
s	103.9 Lux	197.4 Lux	157.5 Lux	43.8 Lux	77.7 Lux	60.1 Lux
x_{max}	414.0 Lux	702.2 Lux	566.8 Lux	175.0 Lux	274.3 Lux	214.1 Lux
x_{min}	12.0 Lux	11.3 Lux	16.0 Lux	6.0 Lux	4.4 Lux	4.8 Lux
$\overline{D}$	-	-143.2 Lux	-109.2 Lux	-	-46.2 Lux	-29.2 Lux
$\overline{\lvert D \rvert}$	-	143.5 Lux	109.3 Lux	-	46.7 Lux	29.8 Lux
D_{max}	-	330.5 Lux	290.8 Lux	-	117.7 Lux	93.1 Lux
D_{min}	-	0.2 Lux	0.2 Lux	-	0.0 Lux	0.4 Lux
D_{rms}	-	172.4 Lux	127.2 Lux	-	58.0 Lux	36.1 Lux
$D_{95\%}$	-	300.0 Lux	198.8 Lux	-	104.8 Lux	60.2 Lux
$\overline{OU}$	11.0 Lux	7.1 Lux	-	4.8 Lux	19.1 Lux	-
$\overline{UR}$	-	7.2	6.0	-	1.7	1.3
UR_{max}	-	11.9	13.1	-	4.3	3.2
UR_{min}	-	0.0	0.1	-	0.0	0.1
$\overline{\lvert D \rvert} / \bar{x} \times 100\%$	-	73.8%	56.2%	-	55.5%	35.3%
$\overline{D} / \bar{x} \times 100\%$	-	-73.6%	-56.2%	-	-54.8%	-34.6%
N	100	100	100	101	101	101

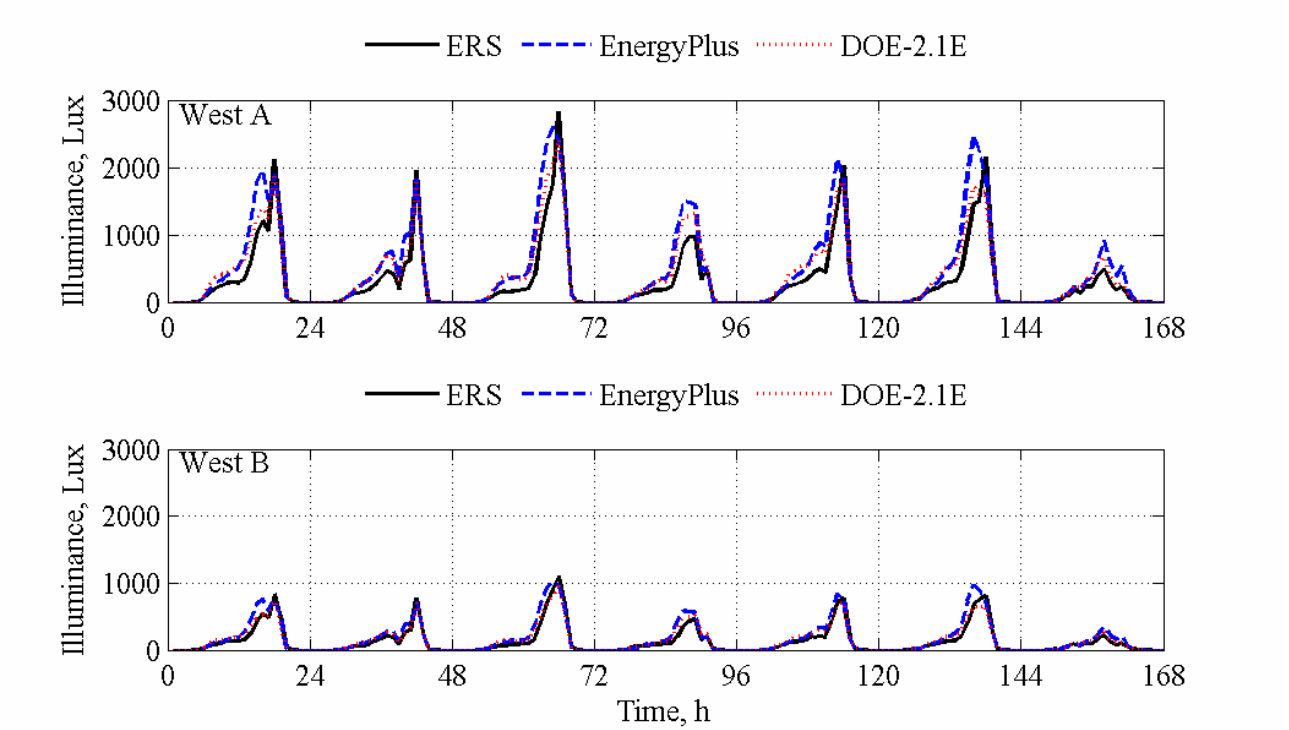

Figure 15.14. Reference point daylight illuminance comparisons for the west test rooms.

Table 15.15. Statistical analyses of reference point daylight illuminances in the west test rooms.

	West A			**West B**		
	Experiment	**EnergyPlus**	**DOE-2.1E**	**Experiment**	**EnergyPlus**	**DOE-2.1E**
$\bar{x}$	484.2 Lux	693.9 Lux	604.5 Lux	214.1 Lux	269.6 Lux	235.5 Lux
s	560.4 Lux	674.5 Lux	536.9 Lux	237.2 Lux	264.5 Lux	210.9 Lux
x_{max}	2836.0 Lux	2597.7 Lux	2406.4 Lux	1099.0 Lux	1024.3 Lux	956.8 Lux
x_{min}	13.0 Lux	9.7 Lux	17.0 Lux	10.0 Lux	3.7 Lux	6.6 Lux
$\overline{D}$	-	-209.6 Lux	-120.2 Lux	-	-55.5 Lux	-21.4 Lux
$\overline{\lvert D \rvert}$	-	237.2 Lux	161.8 Lux	-	68.7 Lux	46.5 Lux
D_{max}	-	1013.3 Lux	507.1 Lux	-	324.8 Lux	166.3 Lux
D_{min}	-	1.1 Lux	2.8 Lux	-	0.1 Lux	0.1 Lux
D_{rms}	-	345.6 Lux	200.3 Lux	-	100.8 Lux	61.2 Lux
$D_{95\%}$	-	786.1 Lux	417.2 Lux	-	220.9 Lux	133.0 Lux
$\overline{OU}$	27.4 Lux	14.4 Lux	-	12.1 Lux	39.5 Lux	-
$\overline{UR}$	-	6.2	5.6	-	1.5	1.2
UR_{max}	-	14.4	15.6	-	6.7	3.6
UR_{min}	-	0.1	0.5	-	0.0	0.0
$\overline{\lvert D \rvert} / \bar{x} \times 100\%$	-	49.0%	33.4%	-	32.1%	21.7%
$\overline{D} / \bar{x} \times 100\%$	-	-43.3%	-24.8%	-	-25.9%	-10.0%
N	103	103	103	103	103	103

15.3.5. Light Power

The zone light powers were measured and compared with results from the building energy simulation programs. Plots for the east, south, and west test rooms are contained in Figures 15.15 to 15.17, respectively and statistical analyses are contained in Tables 15.16 to 15.18, respectively.

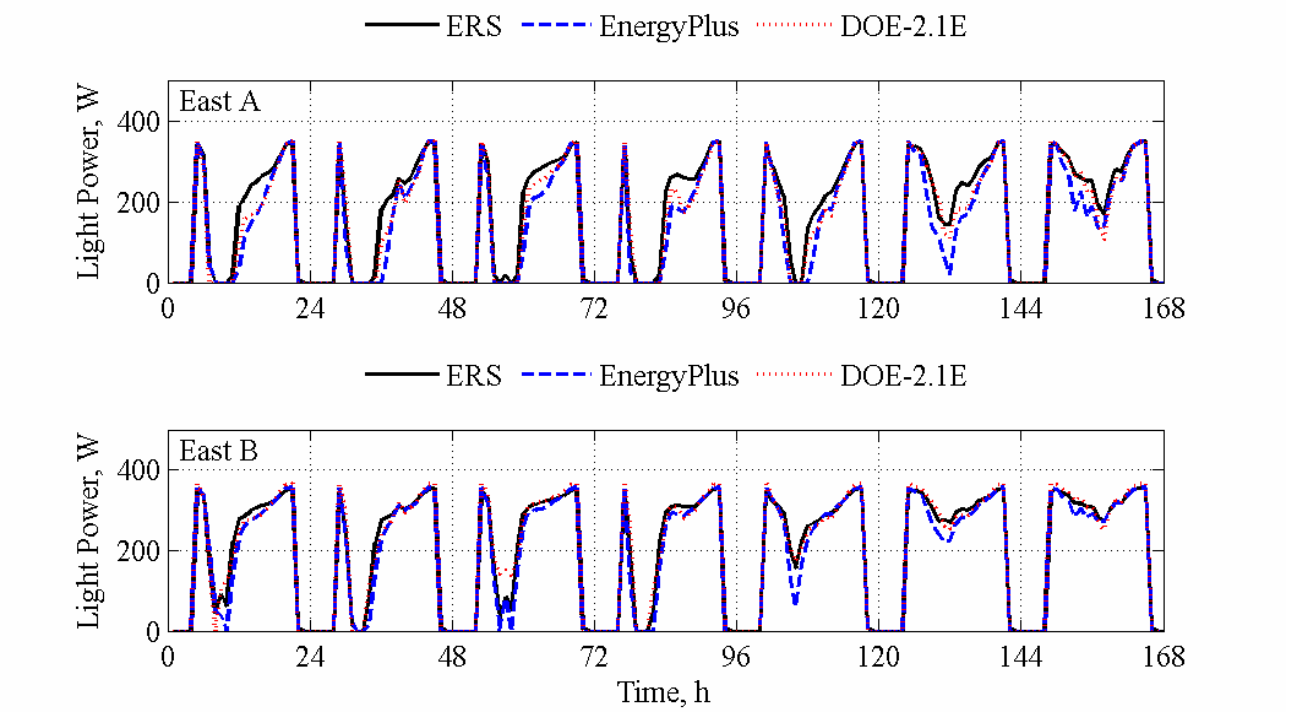

Figure 15.15. Light power comparisons for the east test rooms.

Table 15.16. Statistical analyses of light powers in the east test rooms.

	East A			**East B**		
	Experiment	**EnergyPlus**	**DOE-2.1E**	**Experiment**	**EnergyPlus**	**DOE-2.1E**
$\bar{x}$	230.1 W	194.2 W	209.6 W	320.9 W	314.4 W	325.2 W
s	113.0 W	124.0 W	117.8 W	31.4 W	40.2 W	35.8 W
x_{max}	349.0 W	349.0 W	349.0 W	356.0 W	356.0 W	366.0 W
x_{min}	0.0 W	0.0 W	0.0 W	176.0 W	117.6 W	171.2 W
$\overline{D}$	-	35.9 W	20.4 W	-	6.5 W	-4.3 W
$\overline{\lvert D \rvert}$	-	37.1 W	25.3 W	-	9.7 W	11.4 W
D_{max}	-	180.0 W	90.9 W	-	76.4 W	70.0 W
D_{min}	-	0.0 W	0.0 W	-	0.0 W	0.0 W
D_{rms}	-	55.6 W	35.6 W	-	15.3 W	15.2 W
$D_{95\%}$	-	125.5 W	73.0 W	-	32.8 W	22.6 W
$\overline{OU}$	0.5 W	10.6 W	-	0.7 W	13.4 W	-
$\overline{UR}$	-	3.9 W	2.7	-	0.9	1.1
UR_{max}	-	16.2	10.2	-	7.3	5.6
UR_{min}	-	0.0	0.0	-	0.0	0.0
$\overline{\lvert D \rvert} / \bar{x} \times 100\%$	-	16.1%	11.0%	-	3.0%	3.5%
$\overline{D} / \bar{x} \times 100\%$	-	15.6%	8.9%	-	2.0%	-1.3%
N	115	115	115	86	86	86

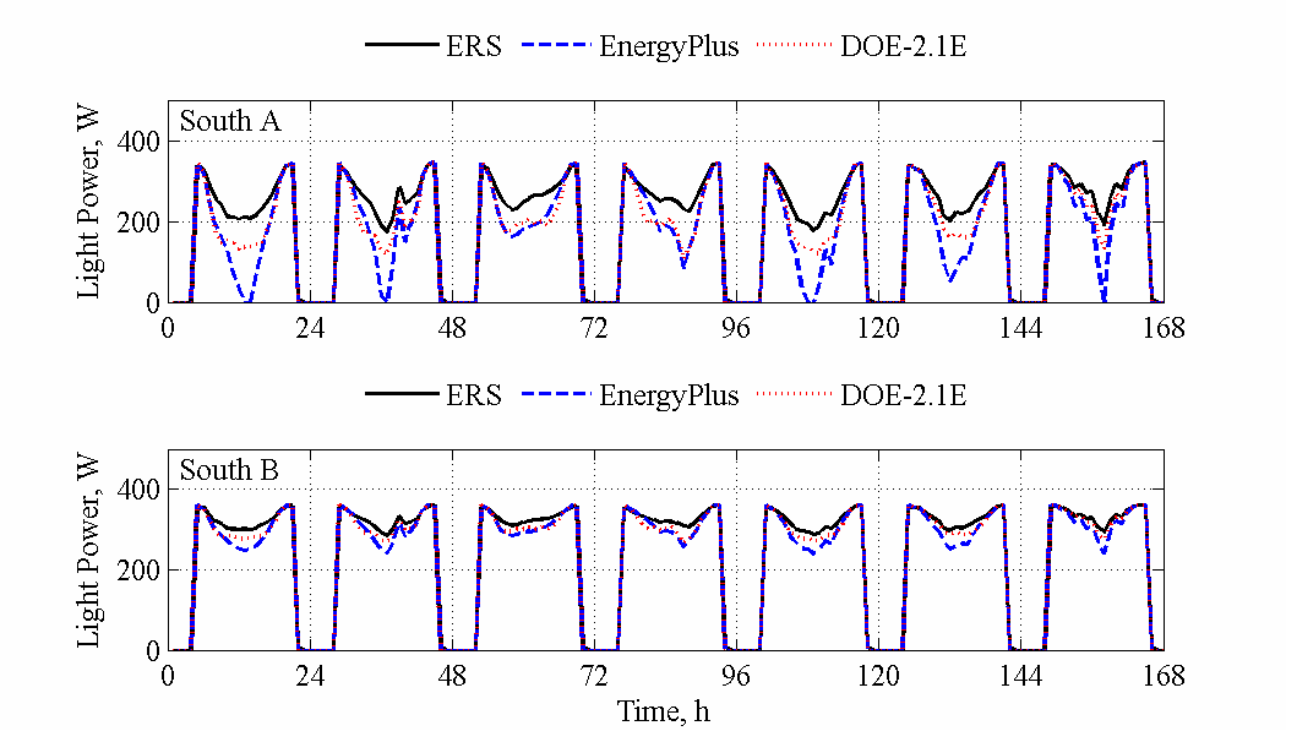

Figure 15.16. Zone light power comparisons for the south test rooms.

Table 15.17. Statistical analyses of light powers in the south test rooms.

	South A			**South B**		
	Experiment	**EnergyPlus**	**DOE-2.1E**	**Experiment**	**EnergyPlus**	**DOE-2.1E**
$\bar{x}$	274.8 W	218.6 W	237.3 W	336.5 W	325.2 W	327.6 W
s	48.5 W	102.9 W	76.1 W	16.8 W	28.9 W	26.4 W
x_{max}	344.0 W	344.0 W	344.0 W	361.0 W	361.0 W	361.0 W
x_{min}	172.0 W	0.0 W	107.1 W	302.0 W	263.4 W	276.3 W
$\overline{D}$	-	56.1 W	37.5 W	-	11.3 W	9.0 W
$\overline{\lvert D \rvert}$	-	57.2 W	38.6 W	-	12.7 W	10.5 W
D_{max}	-	210.0 W	121.9 W	-	41.6 W	32.5 W
D_{min}	-	0.0 W	0.0 W	-	0.0 W	0.0 W
D_{rms}	-	79.3 W	48.7 W	-	16.9 W	13.9 W
$D_{95\%}$	-	173.0 W	81.9 W	-	32.9 W	26.5 W
$\overline{OU}$	0.6 W	8.5 W	-	0.8 W	15.0 W	-
$\overline{UR}$	-	6.0	4.2	-	1.0	0.8
UR_{max}	-	20.1	12.0	-	14.3	5.9
UR_{min}	-	0.0	0.0	-	0.0	0.0
$\overline{\lvert D \rvert} / \bar{x} \times 100\%$	-	20.8	14.0	-	3.8%	3.1%
$\overline{D} / \bar{x} \times 100\%$	-	20.4	13.6	-	3.4%	2.7%
N	119	119	119	96	96	96

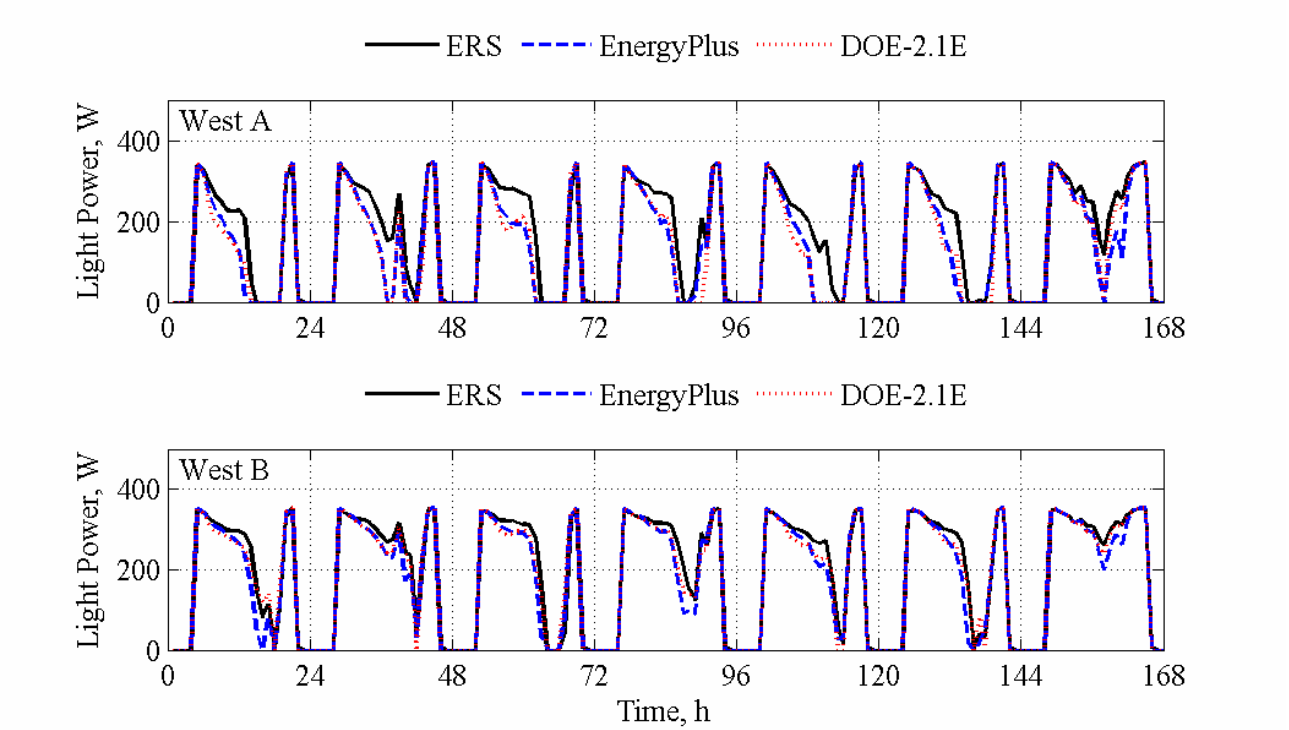

Figure 15.17. Light power comparisons for the west test rooms.

Table 15.18. Statistical analyses of light powers in the west test rooms.

	West A			**West B**		
	Experiment	**EnergyPlus**	**DOE-2.1E**	**Experiment**	**EnergyPlus**	**DOE-2.1E**
$\bar{x}$	222.5 W	182.6 W	180.2 W	323.9 W	317.2 W	317.3 W
s	114.1 W	129.8 W	130.3 W	27.8 W	33.7 W	31.4 W
x_{max}	345.0 W	345.0 W	345.0 W	353.0 W	353.0 W	353.0 W
x_{min}	0.0 W	0.0 W	0.0 W	194.0 W	198.8 W	232.2 W
$\overline{D}$	-	39.9 W	42.3 W	-	6.7 W	6.7 W
$\overline{\lvert D \rvert}$	-	42.1 W	44.4 W	-	10.3 W	10.8 W
D_{max}	-	193.3 W	209.0 W	-	48.1 W	38.2 W
D_{min}	-	0.0 W	0.0 W	-	0.0 W	0.0 W
D_{rms}	-	64.3 W	64.2 W	-	15.0 W	14.8 W
$D_{95\%}$	-	151.0 W	124.0 W	-	32.4 W	32.5 W
$\overline{OU}$	0.5 W	10.5 W	-	0.7 W	11.9 W	-
$\overline{UR}$	-	4.4	4.7	-	1.0	1.0
UR_{max}	-	18.9	23.4	-	9.2	10.7
UR_{min}	-	0.0	0.0	-	0.0	0.0
$\overline{\lvert D \rvert} / \bar{x} \times 100\%$	-	18.9%	19.9%	-	3.2%	3.3%
$\overline{D} / \bar{x} \times 100\%$	-	18.0%	19.0%	-	2.1%	2.1%
N	115	115	115	78	78	78

15.4. Discussion

This experiment was much simpler than the first experiment performed at the ERS (Chapter 14). The simpler shading/window combinations made it possible for the exercise to be modeled and simulated in all programs used for this validation.

Many of the same phenomena that were seen in the first experiment concerning high ventilation

loads, VAV box damper modulation, zone air temperatures above the cooling set point temperatures, and lights fixture dimming due to daylight were also seen in this experiment. However, much simpler shading devices used in conjunction with different window combinations also provided good insight about building energy simulation program performances in addressing issues pertaining to daylighting, transient thermal load calculations, and solar gains.

CHAPTER 16: ERS MODELERS' REPORTS

For both experiments, the modelers performing the simulation were requested to provide a brief summary of methodology employed for modeling the experiments. The modelers were provided with the results but requested to document changes made from initial to final models. For both models, the ground temperature was computed using a subsidiary program from EnergyPlus for computing ground temperatures in conjunction with a TMY2 weather file for Des Moines, IA USA. The perimeters ground temperatures for Experiments 1 and 2 were 19.30°C and 19.42°C, respectively, and the ground reflectance estimated using measurements from [49] was approximated as 15%.

16.1. EnergyPlus

Modeler and Institution: Peter Loutzenhiser, Swiss Federal Laboratories for Materials Testing and Research (EMPA), Laboratory for Building Technologies

Building Energy Simulation Software and Versions: EnergyPlus 1.4.0.025

16.1.1. General Information

The development of EnergyPlus began in 1996 as an initiative by the US Department of Energy; the first version of the software was released to the public in Spring 1998. Detailed information concerning the concept and development of the program is described in detail by Crawley et al. [24].

16.1.2. Facility Modeling

A simulation model of the facility was constructed in EnergyPlus. The construction elements adjacent to occupied zones in the building were modeled as adiabatic boundaries. The internal heat loads in the test rooms were considered purely sensible 97% convective loads and the light fixtures were modeled as recessed fluorescent lamps. Weather data measured at the facility were averaged in 10 minute intervals and used as boundary conditions. Because diffuse global solar irradiance was not measured at the facility but is a required input, it was computed using the solar altitude angles calculated from EnergyPlus (to ensure the same solar angle algorithm was used) and direct-normal and global horizontal solar irradiances measured with the solar instruments.

The "DAYLIGHTING: DETAILED" model in EnergyPlus was used because of its configuration closely matched the provided inputs compared with the other two available models in EnergyPlus. The inputs required for this model included: maximum and minimum light powers and corresponding illuminances (input as ratios), a daylight reference point(s) (a maximum of two), and illuminance set points. This model is similar to the daylighting model used in DOE-2.1E with two additional sky luminance distributions [29]. The vertical solar irradiances and illuminances on the exterior façades were computed in the program using a Perez 1990 [25] model and solar irradiance inputs.

The windows were modeled in Window 5.2a [32] and an output file was used that accounted for angular dependent properties. The window spacer and frame were modeled as a generic aluminum spacers and aluminum frames, respectively. The shading screens were modeled as diffuse transmitters. The shading screens were described in the program using normal visible and solar transmittances and reflectance described in Chapters 14 and 15 and accounted for re-reflections into the space from the window screen using a ray tracing method that assumed infinitely flat plates. EnergyPlus contains a blind model used to estimate the visible and solar transmittance of the blind assemblies. This model assumes that the blinds are perfectly flat diffuse reflectors which are infinitely long. Cross-strings for two-dimensional configuration factor calculations were used for blind slats and the window described by [29]. The heat transfer between the window and the shading devices was calculated using ISO 15099 [28] assuming natural buoyancy; this was

performed as an iterative procedure in the program. The exterior fins were modeled as opaque non-reflecting fins around the west windows. The HVAC equipment was auto-sized in the program and zone heating and cooling set points for temperatures and maximum and minimum airflow rates were fixed in the model.

A detailed algorithm as a function of surface orientation and surface temperatures was used to quantify convective heat transfer and approximate geometric view factors in the program were employed to calculate the radiative heat exchange between interior surfaces.

16.1.3. Discussion of Simulation Results

The results in general provide accurate assessments of the power and reliability of EnergyPlus. However for these analyses, only the zone temperatures and airflow rates were within 95% credible limits for both experiments in all exterior test rooms.

In the first experiment, reheat coil power predictions in the exterior test rooms where mini-blinds with the slat blades fixed in the horizontal positions in East B and South B test rooms performed best when comparing uncertainty ratios. The daylight reference point illuminance reference point predictions were also best when comparing uncertainty ratios in the East B and South B test rooms. These predictions resulted in good light power predictions in these test rooms. However when using the uncertainty ratio, the light power predictions in the West A test room where interior shading screens were installed in conjunction with exterior fins.

In the second experiment, the reheat coil power predictions when examining uncertainty ratios were best in the south test rooms where only diffuse sunlight was incident upon the outer glass of the windows. The daylight illuminance predictions at the references points were generally much better in the B test rooms where the tighter weave white muslin fabric covered the windows. Good illuminance predictions in the B test rooms correlated to good light power predictions. Both the East B and South B test rooms were within 95% credible limits for the experiment.

16.1.4. Validation Impact and Modeling Challenges

While performing these validations in a previous version of EnergyPlus (Version 1.3.0.018), it was discovered that at the minimum airflow rate the heating coil will not energize when heat is required until the next timestep (in this case 10 minutes) and the temperature was allowed to float below the heating set point; therefore, the solution oscillated between these states. This problem was fixed in the version of EnergyPlus used to perform these validations.

An additionally finding that resulted in a correction was with respect to scheduling blind slat angles. In versions of EnergyPlus prior to version 1.3.0.018, the blind slat angles needed to be specified in radians instead of degrees as specified by the users' manual. This also resulted in a change.

16.2. DOE-2.1E

Modeler and Institution: Peter Loutzenhiser, Swiss Federal Laboratories for Materials Testing and Research, Laboratory for Building Technologies

Building Energy Simulation Software and Versions: DOE-2.1E Version-119

16.2.1. General Information

The original version of DOE-2.1E was released in November 1993 from Lawrence Berkley National Laboratories. DOE-2 was developed by Lawrence Berkeley National Laboratory, Hirsch & Associates, Consultants Computation Bureau, Los Alamos National Laboratory, Argonne National Laboratory and University of Paris. Major support was provided by the U.S. Department of Energy; additional support was provided by the Gas Research Institute, Pacific Gas & Electric Company, Southern California Edison Company, Electric Power Research Institute, California

Energy Commission and others [31].

16.2.2. Facility Modeling

In the DOE-2.1E model, the test rooms were modeled as cuboids with room widths and heights that corresponded with the actual dimensions of the space and an equivalent room length corresponding to the room volume was implemented. Custom weighting factors were used in the program to account for transient heat transfer of the building elements. The test rooms' internal loads were considered sensible and 97% convective and recessed light fixture models were employed. The interior walls adjacent to occupied areas were modeled as adiabatic boundaries. The daylighting model in DOE-2.1E is described in detail by [51]. Hourly averaged weather data measured at the facility were put into TMY2 weather format and used as inputs into the program. Measured global horizontal and direct-normal solar irradiances were used to calculate the global vertical irradiances and illuminances on the east, south, and west façades using the Perez 1990 model using the same ground reflectance as in EnergyPlus. In TMY2 weather files, it is impossible to input global horizontal infrared irradiance; therefore the opaque sky cover was calculated by reversing the code algorithm for calculating infrared global horizontal irradiance used in the TMY2 weather file.

The windows were modeled in Window 5.2a, which accounted for angular dependent properties. Generic aluminum spacers and frames were used. Integral solar and visible shading transmittances were employed for simulating the shading screens. The DOE-2.1E did not account for reflected light back into the space from the shading screens. Because surface temperatures of the inner glass panes and the shading screen, and the air temperatures in the gap were not known, the heat transfer in the air gap between the inner glazing and shading screen was estimated using EN ISO 6946 [19] for an unventilated air layer. The exterior fins over the east windows were described in the input file as opaque non-reflecting surfaces. Currently, DOE-2.1E does not have an algorithm to model mini-blinds and there are no subsidiary softwares designed to be used in conjunction with this building energy simulation program; therefore, comparisons for the test rooms with mini-blinds did not include results from DOE-2.1E.

Combined design heat transfer coefficients that accounted for construction element orientations were taken from [52] for all construction elements (floor, ceiling, and walls) to estimated total impact of convective and radiative heat transfer for the interior surfaces. This was done because construction element surface temperatures in the program were not known.

16.2.3. Discussion of Simulation Results

The comparisons made using DOE-2.1E were limited to zones where the mini-blinds were not installed. Therefore the results provided an overall assessment of DOE-2.1E when evaluating windows in combination with or without shading screens and exterior fins. For these experiments, only the zone temperatures and airflow rates were within 95% credible limits for both experiments in all exterior test rooms; however, when the cooling load in the zone could not be overcome at the maximum airflow rates, the predicted air temperatures in the zones floated well above the measured air temperatures.

In the first experiment, reheat coil power predictions for those zones compared were not within 95% credible limits according to the uncertainty ratios. However, all of the uncertainty ratios were between 1 and 2. The daylight reference point illuminance predictions were comparable to the other program used in the validation, despite the fact that the shading screen model did not account for re-reflections and the room geometry was not as precise. The best correlation to the experiment for light power was in the West A test room where exterior fins and interior shading screens were installed with high efficient windows.

In the second experiment, the reheat coil power predictions when examining uncertainty ratios were best in the south test rooms where only diffuse sunlight was incident upon the outer glass of the windows. Like EnergyPlus, the daylight illuminance predictions at the references points were

generally much better in the B test rooms, although still outside 95% credible limits. Good reference point illuminance predictions did translate to you light power predictions in the B test rooms, especially in the South B test room where the results were within 95% credible limits for the experiment.

CHAPTER 17: DISCUSSION AND CONCLUSIONS

Empirical validations of building energy simulation programs are intensive undertakings that require well-instrumented facilities, experienced staff, and extensive collaboration between the people designing and running the experiments and modelers. While programs are being continually improved to better simulate reality, the experimental design and data sets from these studies are available for evaluating and improving building energy simulation programs and algorithms and can be a lasting contribution for continued improvements in the area of building energy simulation.

The focus of empirical validations was to evaluate the performance within the constraints of the programs. Therefore, it was impossible to use an occupied building with changing internal loads, infiltration between zones, changing shading conditions, and other parameters that are varied by occupants. In such cases, the uncertainties associated with these predictions would make it impossible to assess the performance of programs. For this research, nearly every facet of the experiments was controlled.

Particular emphasis was placed on ensuring that the inputs to the building energy simulation programs were well-described.

17.1. EMPA Experiments

For the series of experiments performed at EMPA, the optical properties of the glass panes, shading devices and interior surfaces over the entire solar spectrum, thermal conductivities of the construction materials, two and three-dimensional heat transfer simulation programs, and well-described boundary conditions (outside surface temperatures for construction elements adjacent to the guard zone, measured internal loads, and accurate weather inputs) were measured or simulated for use in evaluating building energy simulation programs. While this level of detail could not be attained in when using building energy simulation programs for designing actual buildings, the precise determination in the study allowed for careful assessments and comparisons; in many cases, quantifying the input properties, particularly the thermal bridges, required calorimetric hotbox experiments and software calculations that were much more computationally intensive than what is currently found in building energy simulation programs. But from these comparisons, conclusions were drawn concerning heat transfer coefficients, transmitted solar energy, radiative heat exchange, heat transfer in the air gap between shading devices and window panes, tilted radiation models, and many more topics.

The order of experiments from simple to complex provided clear levels for identifying specific problems within the various models. This step-by-step methodology allowed for accurate diagnosis of potential deviations and a determination of the how the discrepancies in the models propagated through the various experiments. The list below identifies some of these items.

- The transient characterization experiment provided evidence that the thermophysical properties and thermal bridges within the test cell were well-described and could accurately characterize the test cell in the programs for subsequent experiments.
- An evaluation of tilted radiation models prior to evaluating solar gains through the glazing unit revealed differences associated with incident radiation on the exterior wall and glazing unit, which impacted the solar gain models. This study also identified differences between the components of solar irradiances (direct-normal, diffuse horizontal, and global horizontal). The predictions were compared and the most reliable tilted radiation models for this region were used for remaining experiments.
- The glazing unit experiment provided reliable information concerning the quantifying and modeling the thermal bridges associated with the glazing unit spacer and mounting. The experiment also offered insight into the performance of algorithms for modeling angular dependent window properties.
- Diffuse interior and exterior shading screens were the simplest of all shading devices used in this study. The two experiments revealed discrepancies and shortcomings in

various programs' abilities to account for transmissions through the screens and model the heat transfer in the air gap between the shading device and the glazing unit.

- The outside Venetian blind and inside mini-blind assemblies were much more complicated shading device that could not be simulated by all building energy simulation programs. But the study revealed that there were models specifically designed to address these issues and implemented in some building energy simulation programs.
- The window experiment revealed the complexities associated with the mounting, frame, and spacer; however, when these quantities were properly specified by combining hotbox measurements with two-dimensional heat transfer simulations, the results were accurate simulation of the test cell in the building energy simulation programs.

In some instances, some of the effects in the glazing unit experiment did not affect the shading experiments. For example, the magnitude of the transmitted solar power to the test cell impacted the convective heat transfer coefficient algorithms which altered the time constant of the test cell in some programs; this was somewhat mitigated in several building energy simulation programs by the installation of shading devices where mostly diffuse radiation entered the test cell.

But for all the planning and preparation that went into the experiments, there were some issues that could not be addressed within this study and will be discussed.

17.2. ERS Experiments

The experiments performed at the ERS were well-documented and designed for assessing the performance of daylighting algorithms and their implementations within the building energy simulation programs. While analyses of thermophysical properties and thermal bridges were not as extensive as that done at EMPA, high airflow rates into the test rooms offset many of these uncertainties. Inputs that pertained to daylighting like optical properties of the shading screens, blinds slats, and interior surfaces were measured over the entire solar spectrum and integrated over both the solar and visible spectrums. The windows were simulated using software and an international database of glass spectral data. Light power versus illuminance measurements accurately describe of the daylighting input for the building energy simulation programs, and the reference point was fixed on the table with a light sensor that controlled the dimming of the lights.

While many of the inputs and control strategies used for this exercise would not be known or used by design engineers, they do provide for a comprehensive evaluation of the daylighting algorithms. The comparisons between the different test rooms oriented in different direction and combinations of windows and shading devices provided a unique assessment about the performance of building energy simulation programs.

17.3. Overall Assessments

Many things can be taken from this study and used in future empirical validation efforts. The reasons for the relative success of the project was due to careful examination of the literature prior to initiating the endeavor, thoughtful design of the experimental setup using simulation tools, vigilant monitoring of the data, emphasis on thoroughly quantifying input parameters, careful consideration of uncertainties, collaboration with IEA Task 34/Annex 43 Project C, and a cohesive set of statistical parameters used for assessing the performance of the programs. While in retrospect, it is always possible to improve the experiments, this study was one of the most detailed empirical validations for building energy simulation programs ever performed.

17.4. Validation Impact

The impact of these studies were realized in numerous changes and updates to the programs to reflect more accurate accountings of actual buildings. Table 17.1 contains a summary of these changes and updates described more thoroughly in the modelers' reports.

Table 17.1. A list of updates and changes in each program resulting from this validation effort.

Program	Description of the problem and action taken
HELIOS XP	Addition of the Perez 1987 tilted surface radiation model.
	Ground reflectance was made a user input.
	Angular-dependent optical model for glazing unit simulation.
	Hourly schedules for outer construction element surface temperatures.
	An error was fixed in the center-pane thermal transmittance calculation.
	An optical model to account for blind assemblies was implemented.
EnergyPlus	An error was discovered and corrected blind slat angle inputs.
	An error was discovered and fixed when pertaining to the VAV systems at minimum airflow rate. The heating coil did not energize when heat was required until the next timestep (in this case 10 minutes) and the temperature was allowed to float below the heating set point; therefore, the solution oscillated between these states. This problem was fixed in the version of EnergyPlus used to perform these validations.
ESP-r	The Perez 1990 model was made the default tilted surface radiation model.
	Minor enhancements were made in the solar processing, updating the solar mass and extraterrestrial radiation calculations.
TRNSYS-TUD	The code was modified to account for reflections between shading screens and glazing units.
IDA-ICE	Plans are now in place to upgrade the window model.
	The Perez 1990 tilted surface radiation model was made the default model.
TRNSYS-ULg	An error was discovered and fixed in the plugin of the Type 14 (time-dependent forcing function).

CHAPTER 18: RECOMMENDATION FOR FUTURE WORK

This research provides a solid foundation for future work in this field. Validation of building energy simulation programs is an ongoing task continually evolving to address changes in technology and building energy simulation programs. The research focused on very simple models of glazing units, shading devices, and daylighting that can be expanded upon to evaluate more complex cases described in the subsequent sections.

18.1. Glazing Units

For this research, typical glazing units were used for empirical validation. Additional validation could assess the simulation of switchable glazing units that change optical characteristics to address different levels of light entering the zone. As glazing technology continues to improve, so-called smart glazing units will become more important in building construction, and, thus, the need for reliable predictions will become necessary.

18.2. Window Shading Devices

The shading devices investigated in this study were very simple and the optical properties were nearly independent of wavelength over the solar spectrum. This allowed the use of integral transmittance and reflectance in the building energy simulation programs that were reasonably precise. The accuracy of this method for shading devices with wavelength selective properties in the solar spectrum coupled with wavelength selective glazing units should be studied in future work to investigate the viability of this assumption made in some building energy simulation programs with respect to optical properties of shading devices.

18.3. Daylighting

The most fundamental component of daylight controls were investigated in this study. But there are many additional facets of daylighting including: light shelves, light well, dome fenestration, and double skin facades that need to be validated, and should be the topic of future studies.

REFERENCES

[1] Judkoff RD. Validation of Building Energy Analysis Simulation Programs at the Solar Energy Research Institute, Energy and Buildings, 10 (1998) 221-239

[2] Loutzenhiser PG, H Manz, C Felsmann, PA Strachan, T Frank, and GM Maxwell. Empirical validation of models to compute solar irradiance on inclined surfaces for building energy simulation. Solar Energy 81, 2 (2007) 254-267

[3] Strachan P, Model Validation using the PASSYS Test Cells, Building and Environment 28 (1993) 153-165

[4] Moinard S and G Guyon. Empirical Validation of EDF ETNA and GENEC Test-Cell Models, A Report of Task 22, Project A.3 Empirical Validation, International Energy Agency (1999)

[5] TRISCO Version 10.0w. A computer program to calculate 3D steady-state heat transfer, Physibel, Heirweg 21, B-9990 Maldegem, Belgium (2002)

[6] prEN ISO 10077 - 2 Thermal performance of windows, doors and shutters -Calculation of thermal transmittance - Part 2: Numerical method for frames (Final Draft), European Committee for Standardization, Brussels (2003)

[7] European Standard EN 410. Glass in building – Determination of luminous and solar characteristics of glazing. European Committee for Standardization, Brussels, Belgium, (1998)

[8] GLAD Software. Swiss Federal Laboratories for Materials Testing and Research (EMPA). Duebendorf, Switzerland (2002)

[9] Duffie, JA and WA Beckman. Solar Engineering and Thermal Processes 2nd Edition, John Wiley and Sons Inc., New York, Chichester, Brisbane, Toronto, Singapore (1991)

[10] Modest M. Radiative Heat Transfer 2nd Edition, Academic Press, Amsterdam, Boston, London, New York, Oxford, Paris, San Diego, San Francisco, Singapore, Sydney, Tokyo (2003)

[11] Klein, SA. Engineering Equation Solver (EES) Software, Department of Mechanical Engineering, University of Wisconsin—Madison (2004)

[12] Manz H, P Loutzenhiser, T Frank, PA Strachan, R Bundi, and G Maxwell. 2006. Series of experiments for empirical validation of solar gain modeling in building energy simulation codes—Experimental setup, test cell characterization, specifications and uncertainty analysis. Building and Environment 41,12 (2006) 1784-1797

[13] BISCO Version 7.0w. A computer program to calculate 2D steady-state heat transfer, Physibel, Heirweg 21, B-9990, Maldegem, Belgium (2004)

[14] Nussbaumer T and T Frank. Bestimmung des Wärmedurchgangskoeffizien-ten U_g einer 2-fach Isolierverglasung, Nr. 880´097, STS-Nr. 086, EMPA, Duebendorf, Switzerland (Nov. 30, 2004) In German

[15] Loutzenhiser PG, H Manz, PA Strachan, C Felsmann, T Frank, GM Maxwell, and P Oelhafen. An empirical validation of modeling solar gains through a glazing unit using building energy simulation programs. HVAC & R Research 12, 4 (2006) 1097-1116

[16] Loutzenhiser PG, H Manz, C Felsmann, PA Strachan, and GM Maxwell. An empirical validation of modeling solar gain through a glazing unit with external and internal shading screens. Applied Thermal Engineering 27 (2007) 528-538

[17] Loutzenhiser PG, H Manz, S Carl, H Simmler, and GM Maxwell. Empirical validations of solar gain models for a glazing unit with exterior and interior blind assemblies. Energy and

Buildings (2007), doi:10.1016/j.enbuild.2007.02.034

[18] Carl S and H Simmler. Bestimmung des Wärmedurchgangskoeffizien-ten U_w, Nr. 880´097, STS-Nr. 086, EMPA, Duebendorf, Switzerland (March 6, 2006) In German

[19] EN ISO 6945, Building components and building elements—Thermal resistance and thermal transmittance—Calculation methods, Draft Revision, ISO (2004)

[20] Perez, R., Seals, R., Ineichen, P., Stewart, R., Menicucci, D. A new simplified version of the Perez diffuse irradiance model for tilted surfaces. Solar Energy 39, 3 (1987) 221–232

[21] Finelayson, EU, DK Arasteh, C Huizenga, MD Rubin, MS Reilly. Window 4.0: Documentation of Calculation Procedures, Lawrence Berkley Laboratory Report LBL-33946 University of California Report UC-350 (July 1993)

[22] Chauvel P and J Millet. L'appreciation des caracteristiques des pretections solaires des bais, Centre Scientifique et Technique du Batiment, Department de l'Energetique et de la Productique GEC/DAC-90.115R (October 1991)

[23] Simmler H and B Binder. Testing and modelling of angular-dependent solar heat gain of glazing with venetian shading DYNASTEE Conference 2005, 12-14 (October 2005) Athens

[24] Crawey DB, LK Lawrie, FC Winkelmann, WF Buhl, YJ Huang, COPedersen, RK Strand, R.J. Liesen, DE Fisher, MJ Witte, and J Glazer. EnergyPlus: creating a new-generation building energy simulation program, Energy and Buildings 33 (2001) 319-331

[25] Perez R, P Ineichen, R Seals, J Michalsky, and R Stewart. Modeling daylight availability and irradiance components from direct and global irradiance. Solar Energy 44, 5 (1990) 271-289

[26] Winkelmann FC. Modeling windows in EnergyPlus. Proceedings IBPSA Building Simulation 2001, Rio de Janeiro (listed as LBNL Report 47972) (2001)

[27] ASHRAE. ASHRAE Fundamentals 2001 SI Edition, American Society of Heating, Refrigeration and Air-Condition Engineers, Inc, Atlanta, GA. (2001)

[28] ISO/FDIS 15099: 2003(E), Thermal performances of windows, doors, and shading devices—Detailed calculations (2003)

[29] EnergyPlus, Input Output Reference, Board of Trustees of University of Illinois and the University of California through Orlando Lawrence Berkley Laboratories (October 11, 2005)

[30] prEN 13363-2 (Final Draft), Solar protection devices combined with glazing - Calculation of total solar energy transmittance and light transmittance - Part 2: Detailed calculation method (English Version) (October 2004)

[31] DOE-2.1E Documentation. http://gundog.lbl.gov (2006)

[32] Windows 5.2 Version 5.2.17a.. Code to calculate window properties, LBL, http://windows.lbl.gov/software/window/window.html (2005)

[33] Rubin M., K Von Rottkay, and R Powles. Window Optics. Solar Energy, 65, 3 (1998) 149-161

[34] Reilly MS, FC Winkelmann, DK Arasteh, and WL Carrol. Modeling windows in DOE-2.1E. Energy and Buildings 22 (1995) 59-66

[35] Walton GN. Thermal Analysis Research Program Reference Manual. NBSIR 83-2655, March 1983 (1983) 21

[36] Clark G and C Allen. The Estimation of Atmospheric Radiation for Clear and Cloudy Skies. Proc. 2nd National Passive Solar Conference (AS/ISES) (1978) 675-678

[37] Clarke JA. Energy simulation in building design. Oxford: Butterworth Heinemann (2001)

[38] Liu BYH and RC Jordan. The interrelationship and characteristic distribution of direct, diffuse, and total solar radiation. Solar Energy 4, 3 (1960) 1–19

[39] Klucher TM. Evaluation of models to predict insolation on tilted surfaces. Solar Energy 23, 2 (1979) 111–114.

[40] Muneer T. Solar Radiation and Daylight Models for the Energy Efficient Design of Buildings. Architectural Press, Oxford (1997)

[41] WIS. Window Information System. http://windat.ucd.ie/wis/html/index.html. 2004

[42] Alamdari F and GP Hammond. Improved data correlation for buoyancy-driven convection in rooms. Building Services Engineering Research and Technology 4 (1983) 106–112

[43] Hay JE and JA Davies. Calculations of the solar radiation incident on an inclined surface, Proc. of First Canadian Solar Radiation Data Workshop (Eds: J.E. Hay and T.K. Won), Ministry of Supply and Services Canada, (1980) 59

[44] Reindl, DT, WA Beckmann, and JA Duffie. Evaluation of hourly tilted surface radiation models. Solar Energy 45, 1 (1990) 9-17

[45] ASHRAE. ASHRAE Fundamentals 1997 SI Edition, American Society of Heating, Refrigeration and Air-Condition Engineers, Inc, Atlanta, GA (1997)

[46] Kondratjev K. Radiation Regime of Inclined Surfaces. WMO Technical Note 152. Geneva. (1977)

[47] Parasol Software Version 2.2. A window simulation program. www.parasol.se (2006)

[48] Price BA and TF Smith, Description of the Iowa Energy Center Energy Resource Station: Facility Update III, University of Iowa, Iowa City, IA (2000)

[49] Loutzenhiser PG, GM Maxwell, and H Manz. Empirical validation of the daylighting algorithms and associated interactions in building energy simulation programs using various shading devices and windows. Energy 32, 10 (2007) 1855-1870

[50] Ineichen P, R Perez, and R Seals. The importance of correct albedo determination for adequately modeling energy received by a tilted surface. Solar Energy 39, 4 (1987) 301-305

[51] Winkelmann FC and S Selkowitz. Daylighting simulation in DOE-2 building energy analysis program. Energy and Building 8 (1985) 271-286

[52] Winkelmann FC, BE Birdsall, WF Buhl, KL Ellington, AE Erdem, JJ Hirsch, S Gates. DOE-2 Supplement Version 2.1E. LBL-34947 (November 1993)

APPENDIX A: DESCRIPTION OF ASSOCIATED FILES FROM THE EMPA FACILITY

For the exercises performed at the EMPA facility, measurements necessary for simulation and comparisons of the various parameters were collected and put into Excel files. The first two exercises were non-blind exercises and so the results were provided along with the input data. Subsequent experiments were blind exercises; for the first iteration of simulations; for the next iteration, the results were provided to the participants. A compact disc contains all the files necessary for simulating and comparing output, and the data are also available for download at www.empa.ch/ieatask34; with these files, it is possible to repeat the exercises described in the report and make comparisons. This section contains a list of files and tables that describe the file headers. Table A.1 contains a list of file names and the corresponding Excel files associated with each exercise.

Table A.1. Exercises and associated files.

Exercise	**Associated file(s)**
Exercise 1	Experiment 2.xls
Exercise 2	Experiment 3 Weather Data.xls
Exercise 3	Experiment 3.xls
	Experiment 3 Subhourly Data.xls
	Experiment 3 Validations.xls
Exercise 4	Experiment 4.xls
	Experiment 4 Subhourly Data.xls
	Experiment 4 Validations.xls
Exercise 5	Experiment 5.xls
	Experiment 5 Subhourly Data.xls
	Experiment 5 Validations.xls
Exercise 6	Experiment 6.xls
	Experiment 6 Subhourly Data.xls
	Experiment 6a Validations.xls
	Experiment 6b Validations.xls
Exercise 7	Experiment 7a.xls
	Experiment 7b.xls
	Experiment 7a Subhourly Data.xls
	Experiment 7b Subhourly Data.xls
	Experiment 7a Validations.xls
	Experiment 7b Validations.xls
Exercise 8	Experiment 8.xls
	Experiment 8 Subhourly Data.xls
	Experiment 8 Validations.xls

A.1. Exercise 1

All the input information necessary for simulating Exercise 1 is contained in an Excel file entitled “Experiment 2.xls”. Table A.2 contains a list and description of column headers in the file. The measurements for this experiment were averaged over one hour increments. During this experiment, none of the construction elements were exposed to the outside environment; therefore, measured weather data were not required.

Table A.2. Description of column header from “Experiment 2.xls”.

Column header names		Description
	Time	Specific time of the experiment in h
	Internal Load	Measured internal heat load in W
Outside Surface	T_floor_out	Average outer surface temperature of the floor in °C
	T_ceiling_out	Average outer surface temperature of the ceiling in °C
	T_south_out	Average outer surface temperature of the south wall in °C
	T_west_out	Average outer surface temperature of the west wall in °C
	T_north_out	Average outer surface temperature of the north wall in °C
	T_east_out	Average outer surface temperature of the east wall in °C
Inside Surface Temperatures	T_floor_in	Average inner surface temperature of the floor in °C
	T_ceiling_in	Average inner surface temperature of the ceiling in °C
	T_south_in	Average inner surface temperature of the south wall in °C
	T_west_in	Average inner surface temperature of the west wall in °C
	T_north_in	Average inner surface temperature of the north wall in °C
	T_east_in	Average inner surface temperature of the east wall in °C
Zone Air Temperatures	T_mean_cell_air	Average air temperature inside the test cell in °C
	T_mean_cell_air_unc	Average air temperature 95% credible limits from the experiment in K
	T_mean_cell_air_unc_MCA	Average air temperature 95% credible limits from the MCA in K
	T_cell_air_1	Air temperature measured at Thermocouple 1 in °C
	T_cell_air_2	Air temperature measured at Thermocouple 2 in °C
	T_cell_air_3	Air temperature measured at Thermocouple 3 in °C
	T_cell_air_4	Air temperature measured at Thermocouple 4 in °C
	T_cell_air_5	Air temperature measured at Thermocouple 5 in °C
	T_cell_air_6	Air temperature measured at Thermocouple 6 in °C
	T_cell_air_7	Air temperature measured at Thermocouple 7 in °C
	T_cell_air_8	Air temperature measured at Thermocouple 8 in °C

A.2. Exercise 2

All the information required for simulating Exercise 2 is contained in an Excel file entitled “Experiment 3 Weather Data.xls”. This file contains two Excel worksheets. The first worksheet entitled “Weather” contains weather data for the experiment and second worksheet entitled “Artificial Turf” contains measured reflectance of the artificial turf as a function of wavelength. The headers for the “Weather” and “Artificial Turf” worksheets are contained in Tables A.3 and A.4, respectively.

Table A.3. Description of column header from "Weather" worksheet in the "Experiment 3 Weather Data.xls" workbook.

Column header names		**Description**
	Date and Time	Time and date of the experiment for the central European time zone (GMT+1h) average over the previous hour (note: 01:00 corresponds to 00:01 to 01:00)
Weather	Outside Air Temperature	Measured outside air temperature in °C
	Relative Humidity	Measured outdoor relative humidity in %
	Barometric Pressure	Measured atmospheric pressure in hPa
	Dew Point Temperature	Computed dew point temperature using EES in °C
	Horizontal Wind Speed	Measured horizontal wind speed in m/s
	Vertical Wind Speed	Measured vertical wind speed in m/s
	Horizontal Wind Direction	Measured horizontal wind direction in degrees
Solar Irradiance	Global Horizontal Irradiance	Measured global horizontal solar irradiance in W/m^2
	Global Vertical Irradiance (29° West of South)	Measured global vertical solar irradiance on the exterior façade in W/m^2
	Global Vertical Irradiance Experimental Uncertainty	Computed global vertical solar irradiance 95% credible limits from the experiment on the exterior façade in W/m^2
	Global Vertical Irradiance MCA Uncertainty	Computed global vertical solar irradiance 95% credible limits from the MCA on the exterior façade in W/m^2
	Direct-Normal Irradiance	Measured direct-normal solar irradiance in W/m^2
	Diffuse Horizontal Irradiance	Measured diffuse horizontal solar irradiance in W/m^2
Infrared Irradiance	Global Horizontal Infrared Irradiance	Measured global horizontal infrared irradiance in W/m^2
	Global Vertical Infrared Irradiance (29° West of South)	Measured global vertical infrared irradiance on the exterior façade in W/m^2
Solar Angle	Elevation or Solar Altitude	Computed solar altitude in degrees
	Azimuth	Computed solar azimuth in degrees

Table A.4. Description of column header from "Artificial Turf" worksheet in the "Experiment 3 Weather Data.xls" workbook.

Column header names	**Description**
Wavelength	Wavelength in nm
Direct-Hemispherical Reflectance	Measured direct to hemispherical reflectance of the artificial turf in nm

Because some building energy simulation programs can use weather data in subhourly timesteps. Weather data were made available in 6, 10, and 12 minute intervals. These data are contained in an Excel file entitled "Experiment 3 Subhourly Data.xls". Table A.5 contains a list of column header names for all the worksheets contained in "Experiment 3 Subhourly Data.xls".

Table A.5. Description of the column headers in the “Experiment 3 Subhourly Data.xls”.

Column header names	**Description**
Date and Time	Time and date of the experiment for the central European time zone (GMT+1h) average over the previous hour time period
Drybulb Temperature	Measured outside air temperature in °C
Relative Humidity	Measured outdoor relative humidity in %
Pressure	Measured atmospheric pressure in hPa
Dew Point Temperature	Computed dew point temperature using EES in °C
Wind Speed	Measured wind speed in m/s
Wind Direction	Measured wind direction in degrees
Global Horizontal Irradiance	Measured global horizontal solar irradiance in W/m^2
Direct-Normal Irradiance	Measured direct-normal solar irradiance in W/m^2
Diffuse Horizontal Irradiance	Measured diffuse horizontal solar irradiance in W/m^2
Global Vertical Irradiance (29° W of S)	Measured global vertical solar irradiance on the outside façade in W/m^2
Global Horizontal Infrared Irradiance	Measured global horizontal infrared irradiance in W/m^2
Global Vertical Infrared Irradiance	Measured global vertical infrared irradiance on the exterior façade in W/m^2

A.3. Exercise 3

All the inputs required for simulating Exercise 3 is contained in an Excel file entitled “Experiment 3.xls”. The workbook consists of four worksheets that contain various measurements required for input including: “Weather”, “Temp BC and Internal Load”, “Glazing Measurements”, and “Individual Cell Air Temps”. Table A.6 contains column header for the worksheet entitled “Weather”.

Table A.6. Description of column header from “Weather” worksheet in the “Experiment 3.xls” workbook.

Column header names		**Description**
	Date and Time	Time and date of the experiment for the central European time zone (GMT+1h) average over the previous hour (note: 01:00 corresponds to 00:01 to 01:00)
Weather	Outside Temperature	Measured outside air temperature in °C
	Relative Humidity	Measured relative humidity in °C
	Barometric Pressure	Measured atmospheric pressure in hPa
	Dew Point Temperature	Computed dew point temperature with EES in °C
	Horizontal Wind Speed	Measured horizontal wind speed in m/s
	Vertical Wind Speed	Measured vertical wind speed in m/s
	Horizontal Wind Direction	Measured horizontal wind direction in degrees
Solar Irradiance	Global Horizontal Irradiance	Measured global horizontal solar irradiance in W/m^2
	Global Vertical Irradiance (29° West of South)	Measured global vertical solar irradiance on the exterior façade in W/m^2
	Direct-Normal Irradiance	Measured direct-normal solar irradiance in W/m^2
	Diffuse Horizontal Irradiance	Measured diffuse horizontal solar irradiance in W/m^2
Infrared Irradiance	Global Horizontal Infrared Irradiance	Measured global horizontal infrared irradiance in W/m^2
	Global Vertical Infrared Irradiance (29° West of South)	Measured global vertical irradiance on the exterior façade in W/m^2
Solar Angles	Elevation or Solar Altitude	Computed solar altitude in degrees
	Azimuth	Computed solar azimuth of the exterior façade in degrees

The boundary conditions for the experiment included hourly outer surface temperatures of all construction elements adjacent to guard zones, average test cell air temperatures, and internal loads. This information is contained in a worksheet entitled “Temp BC and Internal Load”; the column headers for this worksheet are given in Table A.7. An additional worksheet entitled “Individual Cell Air Temps” contains a drawing and individual hourly measured air temperatures shown in Table A.8.

Table A.7. Column headers for “Temp BC and Internal Load” worksheet.

Column header names		**Description**
	Date and Time	Time and date of the experiment for the central European time zone (GMT+1h) average over the previous hour (note: 01:00 corresponds to 00:01 to 01:00)
Cell Air	Average Temp	Average air temperature of the test cell in °C
Average Outside Surface Temperatures	Floor Temp	Average outside surface temperature of the floor in °C
	Ceiling Temp	Average outside surface temperature of the ceiling in °C
	West Wall Temp	Average outside surface temperature of the west wall in °C
	North Wall Temp	Average outside surface temperature of the north wall in °C
	East Wall Temp	Average outside surface temperature of the north wall in °C
	Internal Heat Gains	Measured internal gains inside the test cell in W

Table A.8. Column headers for “Glazing Measurements” worksheet.

Column header names		**Description**
	Wavelength	Wavelength in nm
Outer Glazing	Transmittance	Measured transmittance of the outer glazing in %
	Reflectance (front)	Measured front reflectance of the outer glazing in %
	Reflectance (back)	Measured back reflectance of the outer glazing in %
Inner Glazing	Transmittance	Measured transmittance of the inner glazing in %
	Reflectance (front)	Measured front reflectance of the inner glazing in %
	Reflectance (back)	Measured back reflectance of the outer glazing in %

Due to the preconditioning phase, the first 120 h of the experiment were used as a warm-up period for all of the simulations; therefore comparisons with experimental data were only made with the last 480 h of the experiment. The measured data from the experiment used for comparison is provided in an Excel file entitled “Experiment 3 Validations.xls”. Two worksheets are contained in this file: 1) “Experiment” and 2) “Uncertainties”. The column headers for these worksheets are contained in Tables A.9 and A.10, respectively.

Table A.9. Column headers for the "Experiment" worksheet.

Column header names		Description
	Date and Time	Time and date of the experiment for the central European time zone (GMT+1h) average over the previous hour (note: 01:00 corresponds to 00:01 to 01:00)
	Cooling Power	Measured cooling power in W
Surface Temperatures	Outer Glazing Unit	Average outer surface temperature of the glazing unit in °C
	Inside Glazing Unit	Average inner surface temperature of the glazing unit in °C
	West Inside Wall	Average inner surface temperature of the west wall in °C
	North Inside Wall	Average inner surface temperature of the north wall in °C
	East Inside Wall	Average inner surface temperature of the east wall in °C
	Ceiling Inside	Average inner surface temperature of the ceiling in °C
	Floor Inside	Average inner surface temperature of the floor in °C

Table A.10. Column headers for the "Uncertainties" worksheet.

Column header names		Description
	Date and Time	Time and date of the experiment for the central European time zone (GMT+1h) average over the previous hour (note: 01:00 corresponds to 00:01 to 01:00)
95% Credible Limits of Cooling Power	Experiment	Computed 95% credible limits for the measured cooling power in W
	Monte Carlo Analysis	Computed 95% credible limits from MCA for the cooling power in W

A.4. Exercises 4 and 5

Files with the same worksheets and column headers were produced for Exercises 4 and 5; one exception is that the worksheet entitled "Glazing Measurements" from "Experiment 3.xls" was replaced in "Experiment 4.xls" and "Experiment 5.xls" workbooks with worksheets named "Shade Properties"; a description of the column headers for this worksheet is contained Table A.11.

Table A.11. Column headers for the "Shade Properties" worksheet.

Column header names	Description
Wavelength	The wavelength in nm
Transmittance	Measured transmittance as a function of wavelength in %
Reflectance	Measured reflectance as a function of wavelength in %

A.5. Exercises 6 and 7

Files with the same worksheets and column headers as in Exercise 4 were produced for Exercises 6 and 7; one exception is that the worksheet entitled "Shade Properties" was replaced by worksheets called "Blind Slat Properties"; a description of the column headers is shown in Table A.12. For the blind assembly experiments, results from two blind slat positions were assessed. In Exercise 6, the second experiment was performed immediately after the first experiment (i.e. there is only one input file and two output files). For the two output files, the horizontally and 45° downward tilting experiments were differentiated with "a" and "b", respectively. For Exercise 7, the experiments were run and different times of the year and therefore there are two input and output files using the same distinction for blind slat positions as in Exercise 6.

Table A.12. Column headers for the “Blind Slat Properties” worksheet.

Column header names	Description
Wavelength	The wavelength in nm
Reflectance	Measured reflectance as a function of wavelength in %

A.6. Exercises 8

For Exercise 8, input and output files were generated that contain the same headers as in Exercise 3.

APPENDIX B: DESCRIPTION OF ASSOCIATED FILES FROM THE ERS FACILITY

For the ERS experiments, the files necessary for simulated the exercise and comparing the results were collected into Excel files. A list of the experiments and corresponding workbooks are contained in Table B.1.

Table B.1. List and description of ERS files.

Experiment	Files
Experiment 1	Experiment 1 Inputs.xls
	Experiment 1 Comparisons.xls
	Experiment 1 Experimental Error.xls
	Experiment 1 MCA.xls
Experiment 2	Experiment 2 Inputs.xls
	Experiment 2 Comparisons.xls
	Experiment 2 Experimental Error.xls
	Experiment 2 MCA.xls

Additional information specific to the files is contained in subsequent sections.

B.1. Input Files

The input files for Experiments 1 and 2 are “Experiment 1 Input.xls” and “Experiment 2 Input.xls”, respectively, and contain identical worksheets entitled “Weather”, “Outside Illuminance”, and “Adjacent Temperatures”. Lists and Descriptions of the column headers in the “Weather”, “Outside Illuminance”, and “Adjacent Temperatures” worksheets are given in Tables B.2 to B.4, respectively.

Table B.2. Column headers for the “Weather” worksheets.

Column header names	Description
Date and Time	Date and time of each row of data given in Central Time (GMT-6h)
Outside Air Temperature	Measured outside air temperature in °C
Dew Point Temperature	Computed dewpoint temperature in °C
Relative Humidy	Measured relative humidity in %
Barometric Pressure	Measured barometric pressure in Pa
Wind Speed	Measured wind speed in m/s
Wind Direction	Measured wind direction in °
Direct-Normal Irradiance	Measured direct-normal solar irradiance in W/m^2
Global Horizontal Irradiance	Measured global horizontal solar irradiance in W/m^2
Infrared Global Horizontal Irradiance	Measured global horizontal infrared irradiance in W/m^2

Table B.3. Column header and descriptions for the “Outside Illuminance” worksheets.

Column header names	Description
Date and Time	Date and time of each row of data given in Central Time (GMT-6h)
Global Horizontal Illuminance	Measured global horizontal illuminance in Lux
East Global Vertical Illumiance	Measured global vertical illuminance on the east façade in Lux
South Global Vertical Illuminance,	Measured global vertical illuminance on the east façade in Lux
West Global Vertical Illuminance	Measured global vertical illuminance on the east façade in Lux

Table B.4. Column header and descriptions for the “Adjacent Temperatures” worksheets.

Column header names	Description
Date and Time	Date and time of each row of data given in Central Time (GMT-6h)
Break Room Temperature	Measured air temperature in the break room in °C
Computer Center Temperature	Measured air temperature in the computer center in °C
Display Room Temperature	Measured air temperature in the display room in °C
East Vestibule	Measured air temperature in the east vestibule in °C
Mechanical Room	Measured air temperature in the mechanical room in °C
Northeast Plenum	Measured air temperature in the northeast plenum in °C
Media Center Temperature	Measured air temperature in the media center in °C
Office Temperature	Measured air temperature in the office in °C
Reception Temperature	Measured air temperature in the reception room in °C
Southwest Plenum Temperature	Measured air temperature in the southwest plenum in °C
Southwest Media Center Temperature	Measured air temperature in the southwest media center in °C
West Vestibule Temperature	Measured air temperature in the west vestibule in °C

B.2. Output Data

The measurands used for comparisons were taken in one minute increments and then averaged over each hour for Experiments 1 in “Experiment 1 Output .xls” and for Experiment 2 in “Experiment 2 Output.xls”. Table B.5 contains a list and descriptions of the worksheets in the workbook.

Table B.5. Name and description of output file worksheets.

Worksheet names	Description
East A	Measurands from the East A test room
East B	Measurands from the East B test room
South A	Measurands from the South A test room
South B	Measurands from the South B test room
West A	Measurands from the West A test room
West B	Measurands from the West B test room
Interior A	Measurands from the Interior A test room
Interior B	Measurands from the Interior B test room

The experiment comparisons parameters for each room were the same (for interior test rooms, the reference point daylight illuminances were zero). A list and description of the column headers are given in Table B.6.

Table B.6. Name and description of worksheet column headers.

Column header	Description
Month	Month of the year given in Central Standard Time (GMT–6h)
Day	Day of the month given in Central Standard Time (GMT–6h)
Hour	Hour of the day given in Central Standard Time (GMT–6h) (where hour 1 is 00:01 to 01:00)
Zn-temp	Measured zone temperature in °C
Zn-flow	Measured zone airflow rate in m^3/h
Htg-power	Measured electric reheat coil power in W
Lt-elec	Measured light power (including ballasts) in W
Dayl-ill	Computed from measurement daylight illuminance at the reference point in Lux

B.3. Uncertainties

The uncertainties associated with the instruments used at the facility were incorporated into the statistical analyses for each parameter using manufacturers’ information. Ninety-five percent

experimental credible limits were computed for both experiments and are contained in “Experiment 1 Experimental Error.xls” and “Experiment 2 Experimental Error.xls”. The workbook contains worksheets described in Table B.5 and with column headers from Table B.6; however, the results are hourly 95% experimental credible limits

Additional analyses were performed to quantify the how uncertainties in input parameters to the building energy simulation programs propagated through the programs and impacted output parameters. Ninety-five percent credible limits were computed using and MCA and are give for both experiments in “Experiment 1 MCA.xls” and “Experiment 2 MCA.xls”. The workbook contains worksheets described in Table B.5 and with column headers from Table B.6; however, the results are hourly 95% credible limits from the MCA.